ESA-SCI-DIR-RP-001
April 26th, 2022

Comet Interceptor

Visiting a pristine comet

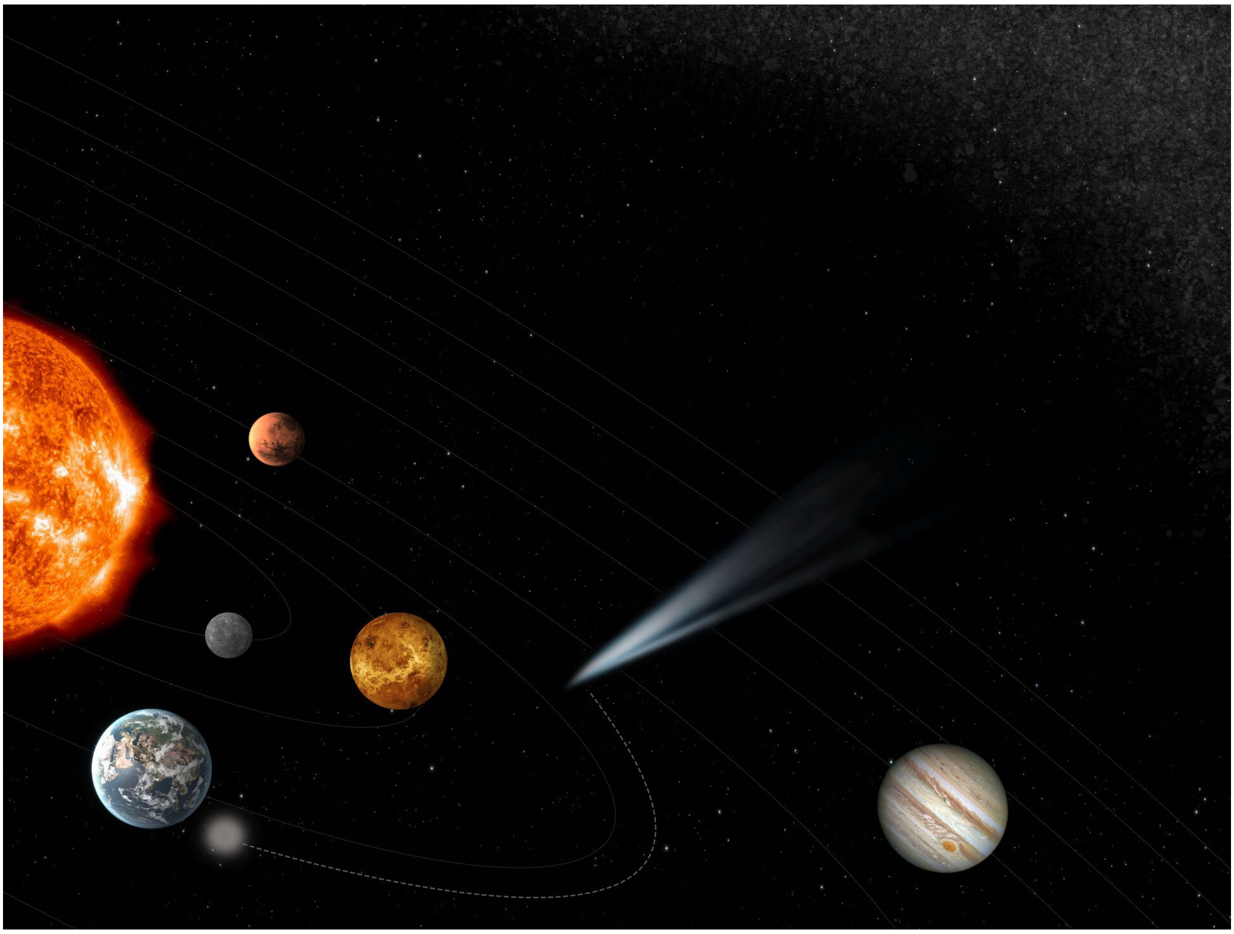

Definition Study Report

European Space Agency

The front page shows a simplified graphic (not to scale) representing how the *Comet Interceptor* mission will wait at the Sun-Earth Lagrange point L2, 1.5 million km anti-sunward of the Earth. Once a target has been identified, the spacecraft will embark on an intercept trajectory to fly past the comet, performing multi-point measurements of the cometary atmosphere and nucleus (Credit: ESA).

Comet Interceptor Definition Study – Mission Summary	
Cosmic Vision Themes	What are the conditions for planet formation and the emergence of life? How does the solar system work?
Key scientific goals	The primary goals of the mission are to provide the first-ever in-situ (as opposed to ground-based observation) characterisation of a long period comet, which could be a dynamically-new comet or an interstellar object, and to perform the first simultaneous multi-point exploration of a cometary coma and nucleus.
Top level science questions	• Comet Nucleus Science - What is the surface composition, shape, morphology, and structure of the target object? • Comet Environment Science - What is the composition of the coma, its connection to the nucleus (activity) and the nature of its interaction with the solar wind?
Payload	**Spacecraft A:** • CoCa: Comet Camera • MANiaC: Mass Analyzer for Neutrals in a Coma • MIRMIS: Modular InfraRed Molecules and Ices Sensor • DFP: Dust, Fields, and Plasma **Probe B1:** • HI: Hydrogen Imager • NAC: Narrow Angle Camera • WAC: Wide Angle Camera • PS: Plasma Suite **Probe B2:** • OPIC: Optical Periscope for Comets • EnVisS: Entire Visible Sky • DFP: Dust, Fields, and Plasma
Description of Spacecraft	Attitude control: S/C A and probe B1 - 3-axis stabilised. Probe B2 - spin stabilised. Propulsion (S/C A): chemical (no propulsion onboard probe B1 and B2). Communication: S-band (Inter Satellite Link) and X-band (communication with Earth). Data volume from fly-by: ~ 200 Gbits Probe B1 mass: 35 kg Probe B2 mass: 35 kg Total CI spacecraft mass (dry): ~ 700 kg Total CI spacecraft mass (with propellant): ~ 975 kg Dimensions (stowed, appendages excluded): ~ 2.0 m x 2.0 m x 2.5 m Deployable Probes Intersatellite Link
Mission Profile	Launch: by 2029, direct injection to SE-L2; to wait at L2 until a suitable target comet is identified. S/C A will then inject into an intercept trajectory, deploying the probes shortly before closest approach. Launcher: Ariane 62 (shared launch with ARIEL). Mission duration: 6 years maximum
Programmatic	ESA is mission architect, responsible for: procurement of spacecraft A and probe B2 and for their integration with the spacecraft AIV, launcher, ground stations, mission, and science operations. Instruments on Spacecraft A and probe B2 are provided by the ESA Member States, as well as contributions to science operations. JAXA/ISAS is responsible for the probe B1 platform and instruments, spacecraft testing and related AIV.

Foreword

Comets are the surviving remnants of the original building blocks of the solar system. A significant amount of pristine material from the formation of the solar system survives in the Oort Cloud, which extends out to at least 1 light year from the Sun, unmodified or barely modified since the earliest days of the solar system. All other material to which we have access – asteroids, meteorites, lunar and planetary surface samples and atmospheres – has been significantly or heavily modified, both physically and chemically since its formation. While multiple comets have been studied *in situ*, all, with the exception of 1P/Halley, have been low-activity, short-period, highly-evolved comets, which have changed radically since their formation, having spent considerable time in the inner solar system. Even Comet Halley, with its longer period and high activity is thought to have made several thousand returns to perihelion. Such objects are highly depleted in volatiles, particularly low-temperature volatiles, at least in their outer layers. While all the comets studied *in situ* to date share certain characteristics (e.g., low albedo, jet activity, …), the observed nucleus morphology shows considerable differences between objects, suggesting that they have experienced radically different evolutionary processes, possibly due, at least in part, to their orbital instability that leads to considerable variations of perihelion distance and thus insolation over timescales of decades and centuries. These highly evolved objects also show significant morphological differences with the only small Kuiper-Belt object to be observed to date, 2014 MU_{69} (Arrokoth), studied by the *New Horizons* mission in a fly-by similar to the proposed *Comet Interceptor* encounter. *Comet Interceptor* follows the successful history of European exploration of comets, following in the footsteps of ESA's *Giotto* and *Rosetta* missions, as well as the substantial contribution of scientists from European countries to the two Soviet-led *VEGA* missions.

Dynamically new comets arriving from the Oort Cloud have never visited the inner solar system before. They are expected to be rich in the low-temperature volatiles retained from their formation and close to their pristine state, particularly in the case of a pre-perihelion encounter. Given the long lead-up times required to plan and launch a space mission, it has been impossible prior to *Comet Interceptor* to contemplate encounter missions with such objects. The opportunity to observe, *in situ*, a dynamically new comet that is entering the inner solar system for the first time will allow the data from previous comet encounter missions and from ground-based campaigns to be placed in its proper context, observing a pristine, or minimally evolved nucleus and study its morphology, its activity, and its interactions with the interplanetary medium. Such an encounter will allow the composition, both chemical and isotopic, of the protosolar nebula to be studied for the first time. This will offer valuable insights into the chemical and isotopic evolution of the solar system since its formation.

It has been known for many years that there is a population of dynamically new objects that are lost to the solar system. These objects' paths are perturbed in the inner solar system into hyperbolic orbits and, thus, escape solar influence. It has long been assumed that there is a similar population of objects external to the solar system that enter it from interstellar space: these objects have been expelled from the solar system where they formed and thus present the opportunity of sampling primordial material formed around other stars, in different conditions to the formation of our solar system. Such an interstellar wanderer manifests itself by having a sufficiently large hyperbolic excess of velocity to demonstrate that it could not have originated in the Oort Cloud. Two such objects are now known: 1I/'Oumuamua and 2I/Borisov, discovered in 2017 and 2019 respectively. While the probability of detecting such an interstellar object that satisfies the targeting conditions for *Comet Interceptor* is low, it is non-zero: such an object would be potentially an extremely high-value target scientifically. It is expected that the Vera C. Rubin Observatory's Legacy Survey of Space and Time (LSST) will increase considerably the detection capability, not just of dynamically new objects, but also of this population of interstellar comets.

Comet Interceptor was selected as ESA's first F-Class mission in its Cosmic Vision Programme, following a call for missions in July 2018. Selected in Summer 2019, Phase A started in 2020, with two parallel industrial studies. In April 2021 *Comet Interceptor* moved into Phase B1. Presently, phase B2 is nearing completion. During Phase A and B1, the Science Study Team (SST) and Science Steering Committee with its working group studied and validated the science case, supported by the ESA study team. This report summarizes the definition study of *Comet Interceptor*, describing the mission architecture, including space and ground elements, that fulfils the science requirements.

Authorship, acknowledgements

This report has been prepared by members of the Comet Interceptor science study team and Instrument Lead Scientists listed below.

Comet Interceptor SST		
Name	*Affiliation*	*City, Country*
Geraint Jones	University College London	London, United Kingdom
Hideyo Kawakita	Kyoto Sangyo University	Kyoto, Japan
Luisa Lara	IAA/CSIC	Granada, Spain
Colin Snodgrass	University of Edinburgh	Edinburgh, United Kingdom
Cecilia Tubiana	INAF/IAPS	Rome, Italy
Comet Interceptor Lead Scientists		
Neil Bowles (MIRMIS Lead Scientist)	University of Oxford	Oxford, United Kingdom
Vania Da Deppo (EnVisS Lead Scientist)	CNR-Institute for Photonics and Nanotechnologies	Padova, Italy
Ryu Funase (Probe B1 Lead Scientist)	University of Tokyo	Tokyo, Japan
Satoshi Kasahara (PS Lead Scientist)	University of Tokyo	Tokyo, Japan
Mihkel Pajusalu (OPIC Lead Scientist)	University of Tartu	Tartu, Estonia
Hanna Rotkaehl (DFP Lead Scientist)	Space Research Centre	Warsaw, Poland
Martin Rubin (MANiaC Lead Scientist)	University of Bern	Bern, Switzerland
Naoya Sakatani (WAC/NAC Lead Scientist)	Rikkyo University	Tokyo, Japan
Nicolas Thomas (CoCa Lead Scientist)	University of Bern	Bern, Switzerland
Kazuo Yoshioka (HI Lead Scientist)	University of Tokyo	Tokyo, Japan

The ESA team supporting the activities is composed of:

ESA study team		
Nicola Rando (Study manager)	ESTEC	Noordwijk, The Netherlands
Carlos Corral van Damme (System Engineer)		
Francesco Ratti (Payload Manager)		
Annamarija Stankov (Payload Engineer)		
Arno Wilders (Payload Engineer)		
Joel Asquier (Platform Engineer)		
Romain Peyrou-Lauga (Thermal Engineer)		
Malgorzata Solyga (Thermal Engineer)		
Veronique Agnolon (PRODEX Officer)		
Kristin Wirth (PRODEX Officer)		

Michael Küppers (Study Scientist)	ESAC	Villanueva de la Cañada, Spain
Mark Kidger (Deputy Study Scientist)		
Andrea Accomazzo (MOC)	ESOC	Darmstadt, Germany
Ana Piris Nino (MOC)		
José Manuel Sánchez Pérez (Mission Analysis)		
ESA Coordination Office		
Luigi Colangeli	ESTEC	Noordwijk, The Netherlands

We also acknowledge the contribution of (in alphabetical order):

Jessica Agarwal; Bhaskar Shrikant Agarwal; Clémence Agrapart; Yuki Akizuki; Altti Akujärvi; Vesa Alatalo; Konrad Aleksiejuk; Miguel Almeida; Felix Althaus; Fernando Alvarez; Gerecs Andras; Nicolas André; István Apáthy; Timothy Arnold; Kazushi Asamura; Shahid Aslam; Barbara Atamaniuk; Nicholas Attree; Uli Auster; Stefano Bagnulo; Michele Bannister; Stas Barabash; Jędrzej Baran; Anna Baranyai; Tomasz Barciński; Tamas Barczy; Jose Barros; Rituparna Baruah; Pascal Barzin; Thomas Beck; Thomas Behnke; Alessandra Beni; Gerhard Berghofer; Martin Berglund; Ivano Bertini; Arnaud Beth; Umesh Anilchandra Bhat; Marcin Bieda; Viktoriia Biliaieva; Steffen Blum; Sandra Bordon; Jean-Christophe Bouquier; Mathias Brändli; Simon Brönnimann; Martin-Diego Busch; Andrei Cacovean; Andrea Calabrese; Simon Calcutt; Maria Teresa Capria†; Chris Carr; Antonio Casciello; José María Castro Marín; Olivier Chassela; Paolo Chioetto; Agata Chuchra Konrad; Maria Ciarka; Andrew Coates; Lorenzo Cocola; Fabrice Colin; François Corthay; Chiaki Crews; Victoria Cripps; Emanuele Cupido; Rowan Curtis; Alberto Dassatti; Johan De Keyser; Thierry De Roche; Simone Del Togno; Vincenzo Della Corte; Thomas Dias; Federico Di Paolo; Kjetil Dohlen; Kerri Donaldson-Hanna; Frederik Dhooghe; Niklas Edberg; Andreas Edström; Mohamed Ramy El-Maarry; Anders Eriksson; Rory Evans; Sara Faggi; Andrey Fedorov; Gianpaolo Ferraioli; David Fischer; Richárd Flonta; Johan Floriot; Fabio Frassetto; Jesper Fredriksson; Francis Froborg; Lucas Froissart; Marco Fulle; Patrick Gailly; Marina Galand; Philippe Garnier; Stéphane Gauffre; Martin Gäumann; Dorota Gawel; Richard Gendur; Karl-Heinz Glaßmeier; Lillia Gnojczak; Juan-Carlos Gómez; Charlotte Götz; Ben Greenhagen; Alexander Grigoriev; Benjamin Grison; Péter Gross; Olivier Groussin; Aurélie Guilbert-Lepoutre; Daniel Guirado; Gergely Gutay; Pedro J. Gutiérrez; Tedjani Hachemi; Christian Hagen; Yuki Harada; Johann Hasiba; Nico Haslebacher; Sébastien Hayoz; Pierre Henri; Miguel Luis Herranz De La Revilla; Laszlo Hevesi; Tilak Hewagama; Markus Hiltunen; Andrew Holland; Florian Hostetter; Chris Howe; Dimce Iliev; Laura Inno; Jemej Irmgard; Patrick Irwin; Yukihiro Ishibashi; Jérôme Jacobs; Jiri Jansky; Don Jennings; Irmgard Jernej; Harald Jeszenszky; Jaime Jimenéz; Laurent Jorda; Leif Kalla; Shingo Kameda; Grzegorz Kasprowicz; Sylvain Keller; Máté Kerényi; Akos Kereszturi; Christian Kintziger; Matthew Knight; Joerg Knollenberg; Tomáš Kohout; Hirotsugu Kojima; Alexander Kokka; Rosita Kokotanekova; Ivana Kolmasova; Konrad Kossacki; Zsolt Kovács; Tomasz Kowalski; Pawel Kowalczyk; Karin Kruuse; Máté Krisztián Kubi; Ekkehard Kührt; Masaki Kuwabara; Yuna Kwon; Fiorangela La Forgia; Robert Labudda; Michal Ladno; Gunter Laky; Etienne Lallemand; Helmut Lammer; Radek Lan; Benoit Lavraud; Eric Le Comte; Olivier Le Duff; Bao Long Le Van; Qiu-Mei Lee; Zoe Lee-Payne; Stefan Leitner; Anny-Chantal Levasseur-Regourd; Jan Ligus; Hannah Lindberg; Manuela Lippi; Andrea Longobardo; Jeroen Maes; Werner Magnes; Hunor Makkai; Iljadin Manurung; Raphael Marschall; Ignacio Martinez Navajas; Morad Masaoudi; Valentina Mascheroni; Romain Mathon; Barbara Matyjasiak; Ayako Matsuoka; Alexandra Mazzoli; Neville Mehta; Mirko Meier; Harald Michaelis; Alessandra Migliorini; Aude-Lyse Millet; Yasuyuki Miyazaki; Marek Morawski; Fernando Moreno; Alankrita Mrigakshi; Daniel Müller; Olga Muñoz; Go Murakami; Naofumi Murata; Kamil Myszka; Shintaro Nakajima; Antti Näsilä; Artiom Nikolajev; Hans Nilsson; Simone Nordera; Keith Nowicki; Stuart Ogborne; Dan Ohlsson; Magnus Oja; Aire Olesk; Jonas Olsen; Dan Olsson; Cyrielle Opitom; Jaime Jiménez Ortega; Harald Ottacher; Rikard Ottemark; Naoya Ozaki; Silvia Pagnoni; Karin Pai; Alessandro Pasetti; Martin Patak; Aditya Savio Paul; Daniel Pelikan; Emmanuel Penou; Antti Penttilä; Claudio Pernechele; Boris Pestoni; Joakim Peterson; Enrico Petraglio; Daniele Piazza; David Pisa; Ferdinand Plaschke; Jean-Yves Plesseria; Szymon Polak; Antoine Pommerol; Michał Porębski; Jaan Praks; Lubomir Prech; Silvia Protopapa; Walter Puccio; Gergo Rakosi; Sylvain Ranvier; Tristan Renon; Ingo Richter; Martin Rieder; Roberto Rigamonti; Julio Rodrigo; Alessandra Rotundi; Irene Ruiz Rodriguez; Yoshifumi Saito; Marianne Salo; Leevi Salonen; Ondrej Santolik; Takahiro Sasaki; Yasutaka Satoh; Rolf Schrödter; Leonhard Schulz; Stefan Schulze-Walewski; Gabriel Jörg Schwarzkopf; Henry Claude Séran; Richard Sherwood; Manabu Shimoyama; Yoshiharu Shinnaka; Iku Shinohara; Katherine Shirley; Cyril Simon Wedlund; Atakan Sirin; Andris Slavinskis; Alessandra Slemer; Balint Sodor; Matthew Soman; Reimo Soosaar; Jan Soucek; Robert Spry; Manfred Steller; Linus Stöckli; Marina Studniarek; Seiji Sugita; Guido

† deceased

Sutter; Paweł Szewczyk; Makoto Taguchi; Swati Thirumangalath; Stephen Tiller; Imre Toth; Gabor Troznai; Pascal Truchelut; Heinz Tschumi; Ludek Uhlir; David Upton; Naoto Usami; Timo Väisänen; Aris Valavanoglou; Jakub Vaverka; Christophe Verdeil; Kai Viherkanto; Geronimo Villanueva; Jean-Baptiste Vincent; Martin Volwerk; Wei Wang; Tris Warren; Gaëtan Wattieaux; Thomas Weigel; Belinda Wendler; Martin Wieser; Sebastian Wolf; Peter Wurz; Hajime Yano; Shoichiro Yokota; Ichiro Yoshikawa; Balazs Zabori; Tomasz Zawistowski; Christoph Zimmermann; Claudio Zimmermann; Paola Zuppella.

Table of contents

1 Executive summary

The huge scientific returns of *Giotto*, *Rosetta*, and other comet missions are unquestioned. So far, ten missions have encountered eight individual comets. However, these ground-breaking endeavours have all explored short-period comets that have approached the Sun many times, and thus undergone surface compositional and morphological modification, and blanketing of the nucleus by thick layers of dust. Even 1P/Halley, more active than any other comet visited by space probes by at least an order of magnitude, has, as estimated from its meteoroid stream, made already several thousand passes through perihelion.

As of April 2022, 801 short-period comets[1] are known, of which 440 are numbered (i.e., have been observed at a minimum of two passes through perihelion), with an average of over forty new ones discovered each year in the last five years. However, these new discoveries are limited to the lowest-activity end of the population distribution: the high-activity end of the population is essentially complete. In contrast, more than three thousand Long-Period Comets (LPCs) have been observed in history, many of them are dynamically new: they have made just one pass through the inner solar system and retain many or all of their initial characteristics, yet no LPC, let al.one Dynamically New Comet (DNC), has been encountered by a space mission.

Although LPCs outnumber by a considerable factor the short-period Jupiter family comets observed in the inner solar system, they have rarely even been studied in detail with modern instrumentation due to the unpredictability of their appearance, which makes intensive coordinated observing campaigns difficult to organise. Without a good understanding of the properties of LPCs and particularly of DNCs we are missing key information to understand the formation and evolution of the early solar system. Among the many issues that are currently debated is the exact role of cometary bombardment in the development of the volatile inventory of the Earth and the role of cometary material in the appearance of life on Earth. In particular, to what extent was cometary bombardment in the early solar system responsible for the delivery of the water that formed the Earth's oceans, offering an ecosystem propitious for the development of the first life forms? No less important is that question of to what extent the emergence of the first organisms on Earth was aided by the organic material supplied in the early cometary bombardment of Earth. To answer these questions, we require information on the volatile inventory of the early solar system that we can only obtain through the study of the pristine, or near pristine material in LPCs and, especially, in the DNCs that still retain the majority of their original volatiles. Isotope abundances and, especially, the D/H ratio will be key information to be obtained. Similarly, *Comet Interceptor* will obtain an inventory of (complex) organic molecules and other species possibly relevant in pre-biotic chemistry that will assist in answering questions about how comets may have contributed to the surprisingly rapid emergence of life on Earth after our planet's formation.

The biggest impediment to obtaining such information is the fact that LPCs from the Oort Cloud have historically been discovered only months (or, in exceptional cases, a few years) before they pass perihelion and initiate their return to the distant reaches of the outer Solar System. Given the long lead-up times required in planning, this is clearly too little time to launch a space mission to an LPC. For this reason, it has been impossible to date even to contemplate encounter missions with dynamically new objects.

Thanks to the ESA F-Mission programme, for the first time it is possible to resolve these issues of lead-up times. Here we describe a novel, multi-point mission, called *Comet Interceptor*, dedicated to the exploration of a little-processed LPC, possibly entering the inner Solar System for the first time, or, even, to encounter an interstellar object originating at another star. The mission concept is similar in some ways to the NASA *ICE* mission. In 1985, after several years at Earth-Sun L1, *ICE* (previously named *ISEE-3*) was directed to encounter successfully Comet 21P/Giacobini-Zinner. *Comet Interceptor* resolves the lead-up time issue by proposing, instead of a direct launch to a designated target, a flexible spacecraft that is designed to encounter an as-yet unknown target at an unknown future time. It will take advantage of the opportunity presented by the F-Class Call – a launch to a halo orbit around the Sun-Earth L2 point – to wait for the discovery of a suitable comet reachable with its Delta-V capability. The timing of the F-Class Call, allied to advancements in ground-based astronomy, enables this approach. As development of *Comet Interceptor* progresses, major new survey

[1] Defined as having a calculated period shorter than 200 years.

telescope facilities (especially the Vera C. Rubin Observatory's Legacy Survey of Space and Time (LSST), currently under construction in Chile) will, in the years before launch, greatly increase the distance at which comets are discovered in-bound towards perihelion. The expectation is that many comets will be found through routine observations outside the orbit of Uranus, giving at last five years lead-up time before perihelion. As each new discovery is made and announced, its orbit will be analysed to see if it is a feasible potential encounter candidate for *Comet Interceptor* (ecliptic crossing between ~0.9 and 1.2 AU) and, if the comet passes this initial selection, will be studied in detail to analyse its encounter potential.

Once a target is found, a detailed trajectory analysis will determine the exact departure burn and encounter circumstances once the target is selected and a decision to encounter is made. This wait phase at L2 will be followed by a cruise phase, potentially with an encounter of a Near-Earth Asteroid on the way to the target (if a suitable candidate is found) and comet fly-by within a total mission length of maximum 6 years.

Comet Interceptor will be unique in encountering and studying, at a nominal closest approach distance of 1000 km, a comet that represents a near-pristine sample of material from the formation of the solar system. It will also add a capability that no previous cometary mission has had, which is to deploy two sub-probes – B1 and B2 – that will follow different trajectories through the coma. While *Rosetta* was able to manoeuvre within the inner coma of Comet 67P/Churyumov-Gerasimenko and thus sample different regions of the comet, there was an inevitable time difference between the sampling at these different points that causes difficulty in interpreting the results in terms of 3-dimensional structure within the coma, given that cometary activity is characterised by its time variability. While the main probe passes at 1000 km distance (this is scaled to a 10 km nucleus size thus, for a larger nucleus, the distance would be greater), Probe B1 and B2 will follow different chords through the coma at distances of 850 km and 400 km, respectively. The result will be unique, simultaneous, spatially resolved information of the 3-dimensional properties of the target comet. As such, *Comet Interceptor* addresses very clearly two of the themes of the ESA Cosmic Vision 2015-2025 programme, namely:

- **Theme 1**: What are the conditions for planet formation and the emergence of life? And
- **Theme 2**: How does the Solar System work?
  - Particularly, sub-theme 2.3: Asteroids and Small Bodies.

The in-situ sampling and remote observation with proven instrumentation of gas and dust from a volatile-rich small body provides a cost-effective means of determining the nature and composition of this key body type. *Comet Interceptor* will study the target's macroscopic structure, characterising this type of body for the first time. The investigation of the solar wind and its interaction with the target al.so addresses sub-theme 2.1:

  - From the Sun to the edge of the Solar System.

Prime Science Questions:

The principal objective of the *Comet Interceptor* mission is to characterise an LPC, with the highest targeting priority to be given to a DNC, or an Interstellar Object (ISO). This will broaden our understanding of comet morphology, composition, and plasma environment. Most importantly, such a comet would offer a unique new viewpoint along the evolutionary path of comets from their formation to migration into the inner Solar System, as a relatively unprocessed object that will have been active for only the past few years or less, rather than a returning comet that has experienced many thousands of close approaches to the Sun. Should no suitable ISO or DNC be discovered, the best available LPC would be targeted, allowing most of the principal science goals to be achieved. Finally, if no suitable LPC is discovered either, the mission would be targeted to one of a list of Jupiter Family comets that serve as back-up targets.

Mission Profile:

Launch is planned for the end of 2029 as the upper passenger on an Ariane 62, with ARIEL as the prime payload. *Comet Interceptor* will enter a parking orbit around L2 where it will await target designation and transfer orbit injection. Depending on the possible need for gravity assist manoeuvres using the Earth and/or the Moon, transfer phase could last between a few months and 3-4 years. This phase will end with the acquisition of the final NAVCAM images for trajectory determination. In the last few days before closest approach, a series of trajectory corrections will be made before release of probes B1 and B2 to appropriate encounter distance. The encounter velocity itself is most likely to be in the range from 40-70 km/s, although lower velocities are possible. There will be a six-month, post-encounter phase, for data transmission to Earth, followed by de-commissioning and post-Operations.

Payload:

The mission will consist of a main spacecraft (S/C A), developed by ESA, plus two sub-probes: Probe B1 (developed by JAXA) and Probe B2 (also developed by ESA). Each will carry a suite of instrumentation. The payload for S/C A consists of: High resolution camera (CoCa) + Rotating Mirror Assembly (RMA); Mass spectrometer (MANiaC); Dust Field & Plasma instrument suite (DFP-A); IR multi-spectral imager (MIRMIS). Probe B1 will have a payload of a Hydrogen Imager (HI); Narrow Angle Camera (NAC), Wide Angle Camera (WAC) and Plasma Suite (PS). Probe B2 will have a payload of: Polarimetric camera (EnVisS); Low resolution camera (OPIC); Dust Field & Plasma instrument suite (DFP-B).

Spacecraft:

Two designs, developed by prime contractor industrial consortia led by OHB-IT and TAS-UK, are being studied, with the selection of Prime Contractor expected to be announced in Q3 of 2022. Both proposals feature a design with two deployable solar arrays, a fixed high-gain X-band antenna, AOGNC, chemical propulsion system and dust shield. Both sub-probes will be accommodated on the same face of S/C A.

Operations:

Comet Interceptor has four operational phases: LEOP and Commissioning Phase; parking orbit at L2, target identification and reaction; Encounter and post-Encounter; and Post-Operations. *Comet Interceptor* will be developed and operated under the responsibility of the ESA Future Missions Department at ESTEC until a Near-Earth Commissioning Review has been held successfully, at which point responsibility for operations will be transferred to the ESA Science and Operations Department at ESAC. ESA will maintain a low level of operational activity, mainly focussed on preparation for data reception and archiving, during the wait phase, parked at L2, until a target is identified, and the transfer manoeuvre is planned. During the cruise phase, final preparations will be made for encounter, including the detailed science operations plan (which will be heavily dependent on the target comet and its characteristics). Finally, in post-encounter, data will be transmitted to ground and distributed, while preparations are made for spacecraft de-commissioning. Operations end with spacecraft passivation, after which, in post-Operations, processed data is received and archived at ESAC.

Communication and Public Engagement:

A mission such as *Comet Interceptor* will have a very high public profile, mainly due to its novelty and to the fact that it will go, quite literally, where no one has gone before. While the highest media profile will, inevitably, be around the encounter, with its promise of unique images of the first space probe encounter with a non-periodic comet, there will be many more opportunities for outreach particularly as the search for a target comet progresses, a target is selected and characterised and approaches progressively perihelion. Previous missions such as *Giotto* and *Rosetta* have shown the high level of public interest in comets and the enormous potential for outreach and educational activities

2 Scientific objectives

2.1 Introduction

While the *Giotto* flyby of Halley was the first mission to provide good resolution images of a cometary nucleus, the *Rosetta* rendezvous was the first mission to monitor the changing activity of a cometary nucleus before and after perihelion. Both missions revolutionized cometary science. *Rosetta* showed that the composition of comet 67P/Churyumov-Gerasimenko (referred to as 67P) is rich in organics and has a different water isotope ratio to Earth's (Altwegg et al. 2015); that its surface structure and morphology (Sierks et al. 2015) are controlled by seasonal activity (Hässig et al. 2015), with starkly contrasting areas dominated by erosion and by dust fall-back (El Maarry et al. 2015, 2016); and that the comet's inner coma is highly dynamic, changing in time and space (e.g., Della Corte et al. 2015; Feldman et al. 2015; Lee et al. 2015).

Rosetta also raised important new questions:

- What properties are primordial, and reflect the process of comet formation, and what are evolutionary features?
- How do these properties control cometary activity?
- Are the differences in composition seen in the coma and solar wind interaction spatial or temporal in origin?

We detail these problems in the following sub-sections, divided into two themes that address Nucleus and Coma science, respectively, and present the *Comet Interceptor* mission to address them by making unique multi-point measurements (*Figure 1*) at a much more pristine type of comet. The exact sources and mechanisms driving activity in comets remain a puzzle after *Rosetta*. Due to the fly-by nature of the mission, *Comet Interceptor* will not be able to monitor changes in activity. However, detailed observations of the surface and the coma will be combined to address this point (i.e., potentially linking the coma structures to nucleus surface features). These are described within Section 2.3, in the Coma theme, below.

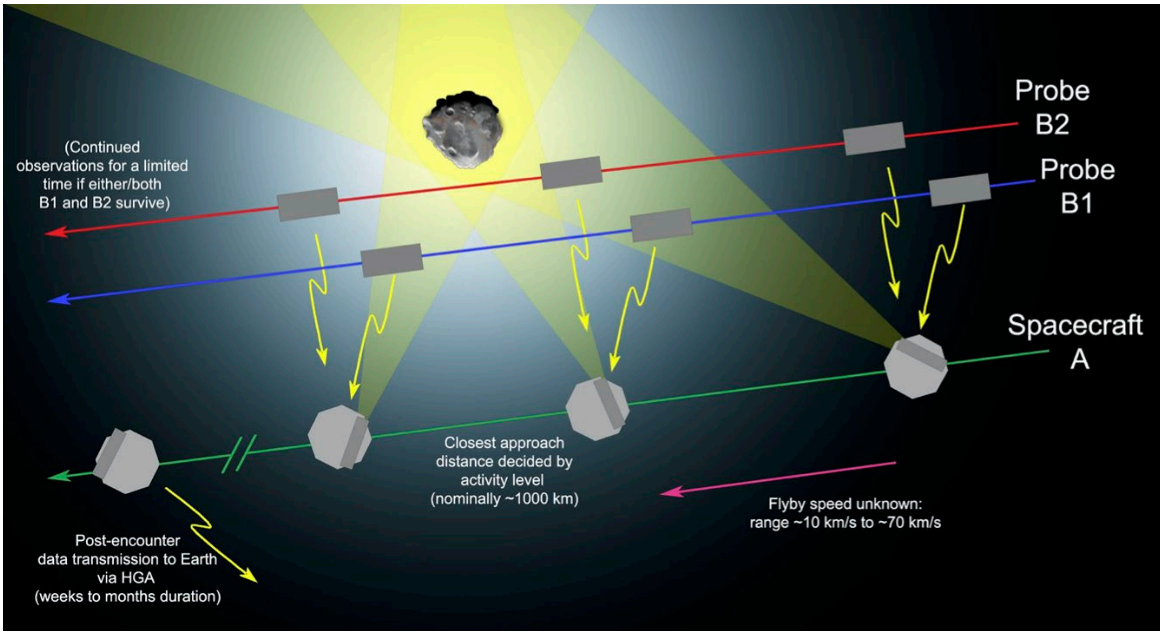

Figure 1: Sketch of the Comet Interceptor flyby, not to scale. Spacecraft A will pass furthest from the nucleus, with Probes B1 and B2 passing closer. Both probes will relay their data in real time to be stored on Spacecraft A.

2.2 Comet Nucleus Science

2.2.1 Introduction

This theme focuses on the nucleus, looking to answer the following questions. What are the:

- surface composition,
- shape,

- morphology, and
- structure

of the target object?

These questions can only be answered by *in situ* (as opposed to remote sensing from the Earth) measurements, in particular given the relative size of the nucleus with respect to the coma (the topic of Theme (2)) which hides the nucleus for observations from Earth and near-Earth based observatories. A comprehensive overview of the results of the nucleus of 1P/Halley (hereafter 1P) obtained by the *VEGA* and *Giotto* probes is given by Keller (1990), while a review, especially of the *VEGA* results, is provided by Toth (2017). The observational results of these missions confronted the model concepts developed over the previous decades with the reality and set the next step to our understanding of comets (see Chapters in Huebner 1990; Newburn et al. 1991; and recent overviews by Thomas et al. 2019; Keller and Kührt 2020). After the NASA's comet flyby missions *Deep Space 1* (2001) to 19P/Borrelly, *Stardust* (2004) to 81P/Wild 2, *Deep Impact* (2005) to 9P/Tempel 1, *EPOXI* (2010) to 103P/Hartley 2, and *Stardust-NExt* (2011) to 9P again, the next great milestone in comet exploration was ESA's *Rosetta* comet nucleus orbiter and lander mission. The results from this mission represent the state-of-the-art in cometary nucleus science, and are described in detail in the subsections below on the origin, bulk properties, morphology, composition, and evolution of nuclei.

Characterisation of the nucleus by *Comet Interceptor* will provide information on its bulk properties (shape, rotation rate, surface structure, etc.), which will in turn provide constraints for surface features' formation timescales. It is unknown whether there might be craters, depressions, layers, regolith, or boulders present – these could provide unique insights into early surface evolution. Do primordial small bodies display a singular primordial surface type, or do they show surface diversity at different size scales? Any impact crater population might provide an unmodified record of early bombardment in the Solar System, as few impacts are expected in the Oort Cloud (OC). This will give a unique insight into the early Solar System's accretion processes and the characteristics of primordial small planetesimals.

All comets already visited by spacecraft have undergone shape changes through sublimation and specific surface evolution processes during repeated perihelion passages. Recent results suggest that bi-lobate nuclei are common (e.g., *Giotto*, *Rosetta,* and other Jupiter Family Comet (JFC) missions). A comparison between an LPC and *New Horizons* studies of the 486958 Arrokoth will be particularly instructive. An LPC (and even more-so a DNC) would have experienced few changes due to insolation in recent times, when compared to JFCs, but could have had significant processing earlier in its lifetime. Characterisation of the difference and similarities will be invaluable, examining surface morphology and comparing to comets imaged by previous missions. In addition to this, composition measurements of a fresh surface, in comparison with *Rosetta* results, may tell us about chemical processing as comets evolve.

2.2.2 The origin of different classes of comet nuclei

Comets of all kinds formed in the outer part of the Solar System's protoplanetary disc, where ices could condense, and the giant planets also formed. As these planets settled into their final orbits, the small bodies in this region were scattered to form the various comet reservoirs that we know today: the Scattered Disc of the Kuiper Belt (KB), the source of low-inclination JFCs; the OC at the edge of the Solar System, which supplies the population of LPCs; and the recently identified probable reservoir of icy bodies in the main asteroid belt that occasionally show activity as Main Belt Comets. The taxonomy of Levison (1996) splits comets into low-inclination 'Ecliptic' comets from the KB, of which JFCs are the dominant subset, and 'Nearly Isotropic Comets' (NICs), which can have any inclination, including highly retrograde orbits, from the OC (*Figure* 2). NICs are subdivided into the LPCs (orbital periods > 200 years) and the Halley Type Comets (HTCs) with shorter periods. There is some debate on the origin of HTCs, with competing models suggesting that these can also come from the Scattered Disc, or from the OC (e.g., Levison et al. 2006, Wang & Brasser 2014, Fernández et al. 2016, and Nesvorny et al. 2017). LPCs can be further divided into DNCs and returning comets, depending on whether or not their previous perihelion distance was thought to be within the planetary region.

Planetary systems naturally scatter and eject most of the planetesimals that they form from their primordial discs of dust and gas. These planetesimals travel the Galaxy as ISOs. They preserve in their composition the record of the metallicity of their system's disc, and their size and shapes contain information on the planetesimal formation and evolution processes at stars other than the Sun. Each star is likely to contribute at least 10^{12} planetesimals to the Galaxy's drifting population of ISOs (Lintott et al., 2022), including earlier generations of stars that no longer exist, so the ISO population provides an overview of the properties of Galactic stellar and planetary formation through time. As ISOs can come from a range of locations across a disc's compositional gradients, the ones that will be sampled by the observable volume around the Sun could explore a wide compositional range. We can therefore anticipate potential upcoming ISO discoveries to span a volatile gradient. At one end are minimally volatile-emitting and silicate-rich bodies that either formed within a water ice line or were depleted of volatiles (cf. Damocloids, Manx comets, or D-type asteroids embedded during OC formation into the LPC population); 1I/'Oumuamua may be toward this end of the compositional range. At the other are volatile-rich objects that formed beyond their system's outer ice lines and were not heated prior to their ejections, and are thus equivalent to the dynamically new LPCs in our system. The latter type of ISO offers the chance to easily sample the volatiles of entirely chemically different disc compositions, as seen with the exceptionally CO-rich 2I/Borisov (Bodewits et al. 2020), which potentially came from an M-dwarf disk (Dybczynski et al., 2019).

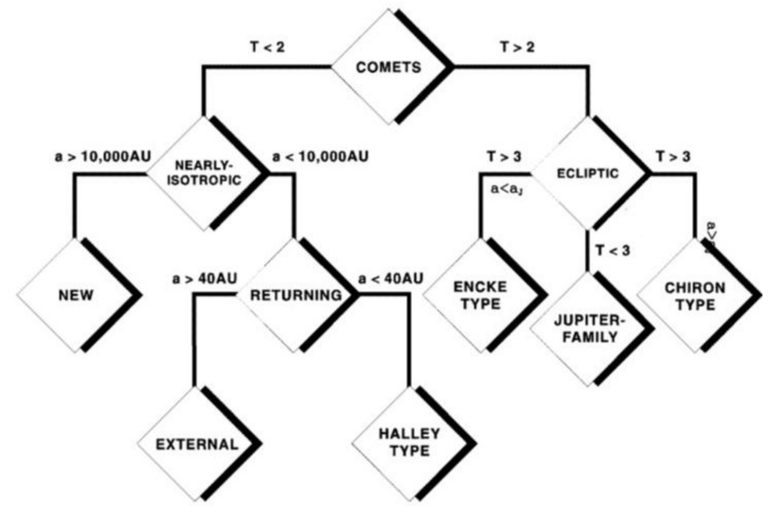

Figure 2: Classifications of comets by Levison (1996). T refers to the Tisserand parameter, whilst parameter a refers to orbital semi-major axis.

It was thought that the OC was primarily populated by bodies that formed near to Jupiter and Saturn, while the objects that would populate the KB formed more or less *in situ* at their current distances from the Sun (e.g., Dones et al. 2004, Duncan & Levison 1997), but modern thinking suggests a broader mixing of comets from different original locations in the protoplanetary disc being scattered to the various reservoirs (e.g., Dones et al. 2015). Results from the Stardust mission showed that material that must have formed in the warmer regions in the inner Solar System was incorporated into comets, suggesting widespread mixing within the disc (Brownlee 2014). It is therefore likely that all Solar System comets have broadly similar initial properties (although perhaps differing in composition, especially at an isotopic level, depending on where the majority of their component ices condensed from gas; see Section 2.2.4 and Rubin et al. 2020 for details). What we can expect to be different between JFCs (and perhaps HTCs) and LPCs is the degree to which they have subsequently evolved: the more distant OC stored comets in a colder environment (~10 K vs ~40 K in the KB; Weissman et al. 2020), and LPCs (and especially DNCs) enter the inner Solar System directly from this cold reservoir, while JFCs have evolved through a period (~10^4 years) in the Centaur region, with orbits between the giant planets, where significant activity can be expected to modify at least the surface layers. As such, even a 'new' JFC can be expected to be significantly modified from its primitive state, while LPCs should retain largely similar properties from the time that they were first ejected into the OC (discussed in more detail in Section 2.2.5). All previous spacecraft targets were JFCs or HTCs (Halley), and all are well known comets that have had many close perihelion passages and experienced further significant evolution as comets.

The motivation for a mission to a less evolved comet is clear – new comets retain, to some degree, the properties of the building blocks of planets, and are at least highly primitive bodies, unaltered since their ejection into their respective reservoirs. How much processing comets underwent during their formation in the disc, prior to ejection, is the subject of considerable debate (see, e.g., Weissman et al. 2020) and another reason to visit a comet from the OC, which retains the surface properties from the last interactions it had before ejection. There are two main theories of comet formation still under consideration following *Rosetta*, both of which are supported by evidence from the mission, but neither is entirely satisfactory. These are hierarchical accretion (e.g., Davidsson et al. 2016) and accretion of 'pebbles' by streaming instabilities (e.g., Blum et al. 2017). Both make predictions for the size scale of typical constituent building blocks of comets, and both sets of scale in features can be found in *Rosetta* data. Whether or not these features are primordial or evolutionary is the key question to advance this debate. There is also considerable interest in the question of how many collisions cometary nuclei have undergone, and the effects that these collisions would have on the properties of their ices, focussing on the period before the comets were ejected from the disc to their reservoirs. While the OC is so vast that collisions between bodies after ejection are virtually impossible, Jutzi et al. (2017) and Schwartz et al. (2018) both show that collisions large enough to alter the bulk shape of nuclei (perhaps forming the typical bilobed structure seen in many comets) were almost impossible to avoid in the disc prior to ejection. Again, investigating a comet that has not been significantly further altered since its last pre-ejection collision would be of great value to better constrain these models, and reveal how much these collisions locally alter material, compared with the (supposed) unaltered nucleus ices further from the collision site(s).

2.2.3 Bulk properties

The current understanding of the bulk properties of comet nuclei is a result of both remote telescope observations and spacecraft visits. Spacecraft in-situ observations provide precise measurements of the physical properties of individual nuclei. On the other hand, telescopes both in the optical and in the thermal infrared allow the coarse characterization of numerous nuclei, therefore enabling population studies. The presence of a coma surrounding the comet nuclei hinders direct telescope observations of comet nuclei. Hence, nucleus studies from the ground rely either on observations of the inactive nucleus near aphelion or on coma-subtraction models which allow the nucleus signal to be extracted; neither approach gives resolved images of the nucleus.

One of the easiest to constrain nucleus properties is size. Since the effective radius of comet nuclei (the radius of a sphere having the same volume as the comet nucleus) can in principle be derived from single-epoch observations, the sizes of over 200 comets have been determined (Knight et al. 2022). This large database reveals a broad diversity of comet sizes: from hundreds of metres to a few tens of km (see Figure 1) and has been used to derive the size-frequency distribution (SFD) of comets. The SFD of comet nuclei is believed to bear evidence of the processes involved in their formation and subsequent collisional and/or activity-driven evolution. De-biased Comet SFD studies show interesting trends indicating that the average size of LPCs is larger than that of JFCs (Bauer et al. 2017). Yet important questions such as whether there is a paucity of objects smaller than 2 km (see Bauer 2017) and whether comets are a collisionally evolved population (see Weissman et al. 2020) remain unresolved.

A great variety of surface properties can be revealed by spectrophotometric observations of the reflected light from the comet nucleus. Geometric albedo, defined as the ratio of the disk-integrated reflectance at opposition and the reflectance of a flat disk with the same size, is the most widely studied property. The geometric albedos of over 25 comets are known to this date (Knight et al. 2022). Most of them were derived from near-simultaneous observations of the comets' brightness in the visible and their near-IR flux. The geometric albedos of comet nuclei range from 0.02 (162P) to 0.06 (19P, 81P and 67P), distinguishing them as some of the darkest minor planet populations in the Solar System (see Knight et al. 2022).

The spectrophotometric properties of comet nuclei depend on the phase angle of the observations (the Sun-comet-observer angle, α). With the increase of α, the spectral slope increases (phase reddening) while the object's brightness decreases (phase darkening or phase function). These two parameters can be modelled to study the surface properties of minor planets - from the macroscopic properties of the surface regolith to the surface roughness and topography (see Verbiscer et al. 2013). So far, only the *Rosetta* measurements of 67P's nucleus have provided successful measurements of a comet's phase reddening (Ciarniello et al. 2015; Fornasier et al. 2015) and revealed a seasonal variation of decreasing phase reddening towards perihelion, followed by an increase along the outbound orbit (Fornasier et al. 2016). *Rosetta*'s observations were also the first to enable the characterization of 67P's opposition effect; the non-linear increase of its phase function close to α=0º (Fornasier 2015; Masoumzadeh et al. 2017; Hasselmann et al. 2017). Few of the other comets visited by spacecraft, or observed remotely from the ground, have been observed close to opposition and all other comet phase curves are well described by linear phase functions. It is possible that the phase function slope at moderate phase angles (α ~ 5-60º) can be used to reveal the level of erosion of the comet surface (see Longobardo et al. 2017, Kokotanekova et al. 2018, Vincent 2019). It remains to be seen if this also applies to LPCs, with very different surface evolutions, as all phase function data so far is on JFCs.

In the visible to near-IR, comet surface spectra are featureless and have spectral gradients up to 20% per 1000 Å (see Knight et al. 2022). Most spectra of comet nuclei have been obtained for weakly active comets observed from the ground and are similar to the spectra of primitive D-type asteroids, which have spectral slopes of 9.1 ± 1.1 % per 1000 Å (Fitzsimmons et al. 1994; Fornasier et al. 2007), as well as to those of moderately red Centaurs and TNOs (Fornasier et al. 2009). Since the spectra of comet nuclei, Centaurs, and TNOs are almost featureless in the visible, it is possible to compare them using parameters more widely available for remote observers, such as spectral slope and colour index (e.g., B-V, V-R, etc.). While a large fraction of the observed Centaurs and TNOs have very red surfaces with spectral slopes $S' > 25\%$ (Lacerda et al. 2014, and references therein) and $B - R > 1.5$ (see Peixinho et al. 2012; Wong and Brown 2017), all observed comet nuclei have less red surfaces with an average $B - R$ of 1.22 ± 0.03 and 1.37 ± 0.08

for LPC and JFC nuclei, respectively (Jewitt 2015). It is important to note that the average colours of JFCs, LPCs and dormant comets are indistinguishable within the uncertainties for each class (Jewitt 2015). Finally, *Rosetta* has revealed that the surface spectrum of 67P changes as the comet passes through perihelion due to the comet's seasonal water-ice cycle: the nucleus' mean spectral slope changed by ~30% or 50% (Fornasier et al. 2016; Filacchione et al. 2020).

Polarimetric studies of comet surfaces have not yet been performed during a spacecraft visit. There are only two JFCs for which polarisation studies from the ground have been published, 2P/Encke (Boehnhardt et al. 2008) and 209P/LINEAR (Kuroda et al. 2015). These data are too limited to extract any general conclusions about the bulk polarisation properties of comet nuclei besides pointing out the similarities of these two comets and known dark asteroids (Kiselev et al. 2015).

Compared to other parameters used to extract the physical properties of comet nuclei, rotation is relatively easy to obtain and has played a key role in revealing various physical properties of comets. The rotational state of a comet nucleus is described through rigid-body dynamics of a triaxial ellipsoid with principal axes $a \geq b \geq c$. The most stable and most commonly observed spin state of triaxial ellipsoids is the constant angular velocity rotation around the short principal axis (PA), but rotation around the two longer PA axes is also possible. Comets can also be in excited non-principal-axis (NPA) rotational states (e.g., tumbling). NPA rotation is, however, supposed to be short-lived due to the frictional loss of mechanical energy, which is eventually expected to bring the object back to the least-energetic state of PA rotation around the shortest axis (e.g., Jewitt, 1998). NPA spin states can be distinguished from PA rotation since NPA rotation states have two independent periods which can be detected with sufficiently detailed lightcurve observations. Only a few comets in an NPA state have been observed to date: e.g., comets 1P, 2P and 29P and 103P (see Knight et al., 2022, and references therein). *Rosetta* revealed that 67P was found to have PA rotation with a small precession of the pole (Jorda et al., 2016).

From the ground, the rotation period of a comet can be directly obtained by analysing the periodic variability of coma features of active comets, or of bare nuclei, (for an overview see Knight et al., 2022). In the rare cases when comets are observed with sufficient spatial resolution to extract the nucleus signal from that of the coma, it is also possible to determine the rotation rates of active comets (see Lamy et al., 2004). Space missions have allowed the rotation state of three comet nuclei to be characterized in greater detail: 9P (Chesley et al., 2013, and references therein), 103P (Belton et al., 2013, and references therein), and 67P (Jorda et al., 2016).

Rotation studies up to now have shown that comet nuclei typically have rotation rates ranging between ~6 and 70 hours (see *Figure 3*). About a dozen of the comets with known rotation periods have been observed to experience period changes ranging between seconds and hours (Knight et al. 2022 and references therein). The direct measurements of the spin changes of 67P during *Rosetta*'s observations were successfully reproduced by the numerical model of Keller et al. (2015) and provided clear evidence that the rotation periods of comets change mainly due to sublimation-induced jets from the cometary surface, which generate a net torque on the nucleus (see Knight et al. 2022).

Another parameter broadly used to analyse the formation and evolution of comet nuclei is shape. The shapes of six nuclei have been studied in detail from in-situ observations. The observations from the *Rosetta* mission to 67P stand out with their unprecedented resolution, which enabled a global 3D shape model with resolution down to metre scale (Preusker et al. 2017). In at least eight exceptional cases in which the comets approached the Earth sufficiently and could thus be observed by radar, shape models could be constructed (see Knight et al. 2022). For other comets, however, nucleus shapes can only be studied in terms of elongation. Measuring the peak-to-peak amplitude of the rotational lightcurve, Δm, provides a lower limit of the axial ratio of a/b of the comet nucleus. In principle it is possible to derive convex shape models of comet nuclei, provided that the comets are observed at a wide variety of different observing geometries, but this technique has so far only been applied to 67P in preparation for *Rosetta* (Lowry et al. 2012). Compiling elongation estimates from the different methods, Kokotanekova et al. (2017) determined a median axial ratio of $a/b = 1.5$ for JFCs, similar to the previous estimates from Lamy et al. (2004) and Snodgrass et al. (2011). As it can be seen in *Figure 3*, the measured minimum a/b spans a range of ~1.0 to > 3.0. The largest known axial ratio belongs to 103P (Thomas et al. 2013) which is one of the four comet nuclei visited by spacecraft that has a bilobate shape (the others are 1P (Keller et al. 1986), 19P (Britt et al. 2004; Oberst et al. 2004) and 67P (Sierks et al. 2015)). Moreover, the radar observations of 8P are also best modelled by assuming a contact binary shape (Harmon et al. 2010). This noticeable overabundance of highly elongated/bilobate objects in comparison to other small-body populations suggests some important difference in formation and/or evolutionary processes, which has not yet been fully explained. Whether or not the first LPC nucleus to be imaged *in situ* also shows a contact binary morphology will provide an important constraint on this question, and point to whether it is more likely attributable to a formation or an evolutionary process.

Comet nuclei have low density (480 ± 220 kg m^{-3}) and permittivity (1.9–2.0) which are consistent with a high porosity of 70–80% (Groussin et al. 2019). Before *Rosetta*'s direct measurements of the density and mass of 67P, various indirect methods were used to estimate the density of dozens of comets (see Groussin et al. 2019 for a review). Most of the density estimates were based on measuring the small orbital changes caused by non-gravitational forces (NGF) acting on the nucleus when outgassing occurs close to perihelion (Rickman 1986; Davidsson and Gutiérrez 2005, 2006; Sosa and Fernández 2009). Special circumstances were used to estimate the density of several other comets. For example, the density of comet Shoemaker-Levy 9 was derived by modelling its disruption on approach to Jupiter (Solem 1995; Asphaug and Benz 1996) – results that also confirmed that nuclei are strengthless on global scales (they can be thought of as 'rubble piles', held together by gravity alone). The densities of 9P (Richardson et al. 2007; Thomas et al. 2013a) and 103P (A'Hearn et al. 2011) were estimated to be ≤ 1000 kg m^{-3} from models of different observations enabled by the Deep Impact experiment and by the *EPOXI* fly-by. Lower limits on nucleus density can also be derived from the rotation rate and elongation determined from photometric observations: having these two parameters, nuclei are modelled as strengthless prolate ellipsoids, held together by gravity and requiring a minimum density to counteract the centrifugal force. Similarly to the analysis done on the asteroid spin barrier (Harris 1996; Pravec et al. 2002), the observed lack of comets requiring a minimum density ≥ 600 kg m^{-3} implies that this value corresponds to the average bulk density of comet nuclei (Lowry and Weissman 2003; Snodgrass et al. 2006; Kokotanekova et al. 2017). Interestingly, radar observations of a handful of comets have suggested densities between 500 and 1500 kg m^{-3} in the surface layers of comets (Harmon et al. 2004). These somewhat larger values can be explained with the possibility that the top layers of comet nuclei consist of denser, more consolidated material (see Davidsson et al. 2009; Groussin et al. 2019).

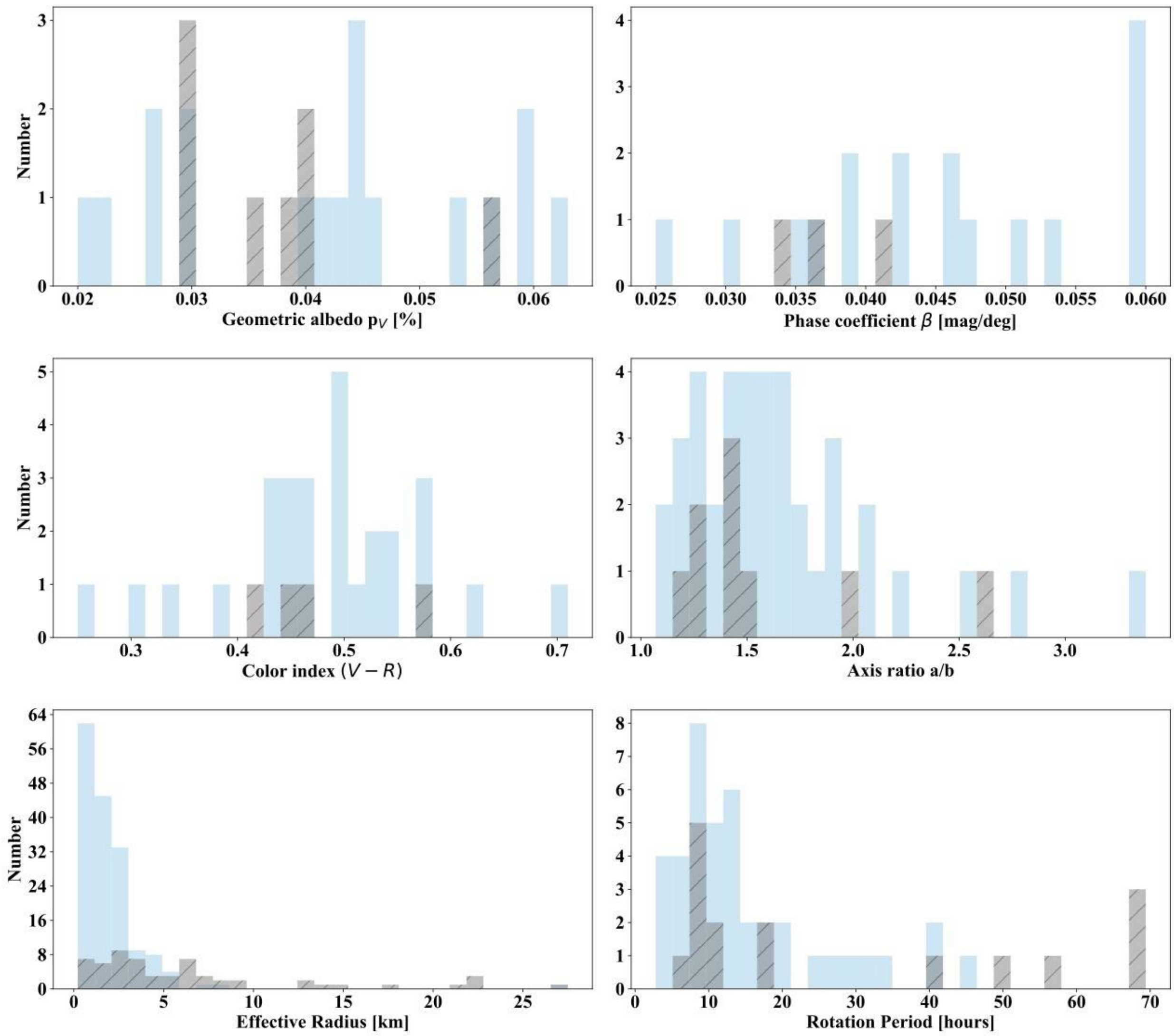

Figure 3: Histograms showing the range of observed comet properties (JFCs in blue and Halley-type/LPCs in grey hashing). The figure provides an overview of the range of measured values and the sample size of each parameter. In case a comet has multiple measurements of the same property, the most recently reported sufficiently precise measurement is displayed. The effective radius histogram is limited to thermal-IR measurements from Fernandez et al. (2013) and Bauer et al. (2017). The axis ratios plotted are lower limits for all comets except for these visited by spacecraft. Adapted from Knight et al. (2022).

Rosetta delivered unique direct measurements of 67P's mass, porosity, permittivity, and material strengths, largely confirming the predictions based on the previous body of work. *Rosetta* provided estimates for 67P's nucleus density of 532 ± 7 kg m^{-3} and porosity of 70–75% (Jorda et al. 2016). CONSERT, a bistatic radar on-board the *Rosetta* spacecraft and its *Philae* lander, was designed to probe the nucleus of 67P with radio waves at 90 MHz frequency. The relative permittivity of the materials is found to range from about 1.7 to 1.95 in the shallow subsurface (< 25 m) and about 1.2 to 1.32 in the interior (Kofman et al. 2020). These differences indicate different average densities between the shallow subsurface and the interior of comet. They can be explained by various physical phenomena such as different porosities, the possible compaction of surface materials, or even perhaps different proportions of the same materials. This strongly suggests that the less dense interior has kept its pristine nature. This is compatible with a proposed model that predicts very high porosities (> 70%) for the nucleus (Blum et al. 2017). *Philae* made a 0.25-metre-deep impression in the boulder ice, providing *in situ* measurements confirming that primitive ice has a very low compressive strength (less than 12 Pa, softer than freshly fallen light snow) and allowing a key estimate to be made of the porosity (75 ± 7 %) of the boulders' icy interiors (O'Rourke, et al. 2020). Generally low bulk tensile strengths of only a few Pascals were confirmed by measurements of terrain features (Attree et al. 2018) and the *Philae* lander's interactions with the surface (O'Rourke et al. 2020), although significantly stronger layers or local enhancements may exist (see summary by Groussin et al. 2019). Extremely weak cometary material has implications for the activity and formation mechanisms and may be supportive of 'pebble' formation models.

Thermal properties dictate the temperature distribution throughout the nucleus, and are thus key to describe physical and chemical processes occurring in response to solar illumination. The thermal inertia of a comet nucleus, for instance, drives its ability to adapt its temperature to a change in local insolation. A material with a large thermal inertia takes longer to adapt its temperature to changing illumination conditions compared to a material with low thermal inertia. Low thermal inertia - and therefore low thermal conductivity - means that the interior of nuclei remains cold when the surface is heated by the Sun, and can therefore retain more volatile ices (i.e., can be more 'pristine'). Estimates for comets made from spatially unresolved observations of the nucleus allowed a value lower than 50 J K^{-1} m^{-2} $s^{-1/2}$ to be derived. Owing to spacecraft flybys in the 2000 s, thermal inertia has since been derived from radiance measurements, from which temperature can be inferred, on the surface with spatially resolved maps of comets 9P, 103P and 67P. They point toward a low thermal inertia, between 50 and 200 J K^{-1} m^{-2} $s^{-1/2}$ for 9P (Davidsson et al. 2013), and less than 250 J K^{-1} m^{-2} $s^{-1/2}$ for 103P (Groussin et al. 2013). The suite of instruments on-board *Rosetta* indicates that 67P's thermal inertia is between 5 and 350 J K^{-1} m^{-2} $s^{-1/2}$ (Leyrat et al. 2015). It varies across the surface (Leyrat et al. 2015), perhaps due to variations in material properties such as density or porosity, between consolidated and unconsolidated terrains. Additional estimates in the near-subsurface were possible, down to 1 and 4 cm below the surface: they point to a thermal inertia of the order of 10 to 60 J K^{-1} m^{-2} $s^{-1/2}$, and lower than 80 J K^{-1} m^{-2} $s^{-1/2}$ (Gulkis et al. 2015; Choukroun et al. 2015; Schloerb et al. 2015; Marshall et al. 2018). Finally, the MUPUS measurement at the landing site of *Philae* suggests a local thermal inertia of the order of 120 J K^{-1} m^{-2} $s^{-1/2}$ (Groussin et al. 2019). These thermal inertia estimates depend strongly on the model used to derive them: they should be taken only as an indication that cometary material close to the surface has a low thermal inertia. Indeed, temperatures are not directly measured with remote sensing instruments, but rather the infrared or sub-mm flux is detected, or the brightness temperature is measured. The kinetic temperature, which gives information on thermal properties of a surface, must be retrieved through models. Measurements in the near infrared can be contaminated by reflected solar radiation (Keihm et al. 2012). Instruments detect a nonlinear average of potentially very different temperatures in the field of view, with large and small-scale topographic features and perhaps compositional heterogeneities. On *Rosetta*, MIRO measurements were affected by both the thermal and the optical properties of the material, which made the interpretation challenging. A yet larger caveat comes from the lack of a thermal infrared instrument on the *Rosetta* payload. Lower limits for the temperature derived from VIRTIS-M were effectively restricted to the dayside of the nucleus (Tosi et al. 2019). Kinetic temperatures over complete diurnal cycles and for the same layer could not be retrieved, and thermal inertia maps were derived with large error bars (Groussin et al. 2019). Resolved images of both the day and night sides in the thermal infrared are required to put stronger constraints on thermal models of cometary nuclei.

2.2.4 Morphology of nuclei

As cometary surfaces are almost impossible to resolve in Earth-based observations, our information about surface morphology of comets is based on flyby or orbital missions (with *Rosetta* currently the only mission to orbit around a comet for a prolonged amount of time). *Figure* 4 shows the shape and general morphology of all of the comets that have been imaged *in-situ*. It is useful to draw comparisons between the morphologies observed on comets (mostly JFCs) and Arrokoth, the cold classical KBO visited by NASA's *New Horizons* Mission in 2019. Whereas Arrokoth signifies a nearly primordial body characterised by low colour diversity, uniform textures, lack of topographical complexity, and a general lack of putative impact craters, circular features overall, or evidence of tectonics, comets that have spent a significant amount of their life in the inner solar system display clear evidence of surface evolution and overall weathering as is demonstrated by the higher degrees of surface roughness, topographical complexity, morphological diversity of terrains, and presence of smooth regions suggestive of weathered and eroded fine-scale materials (e.g., Keller et al. 1986; Britt et al. 2004; A'Hearn et al. 2005; A'Hearn et al. 2011; Veverka et al. 2013; Sierks et al. 2015; Thomas et al. 2015).

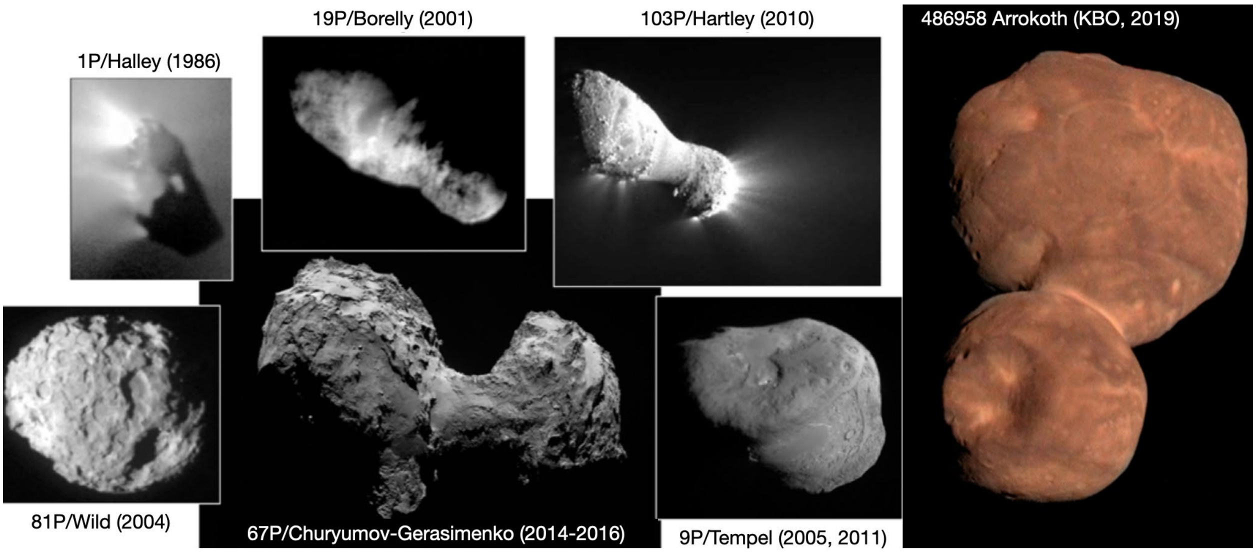

Figure 4: A subset of the cometary nuclei that have been visited by Spacecraft and on the right an image of Arrokoth, A Kuiper Belt Object. Objects are not shown to scale.

Rosetta demonstrated how activity caused by seasonal sublimation of volatiles (mostly water-ice but also other types of ice), as comets cross the snow-line during the perihelion part of their orbit, can account for various fine-scale morphology on cometary surfaces, with clear evidence of seasonal evolution (e.g., El-Maarry et al., 2017; 2019). However, it is unlikely that major landscape evolution occurs that way, at least on seasonal scales (El-Maarry et al., 2017): seasonal erosion causes changes on scales of order 1-10 m, while there are pits (*Figure* 5, left) approximately 100 m in diameter, and the cliff (*Figure 5*, right) above the 'neck' region between the two lobes of 67P is around a kilometre high.

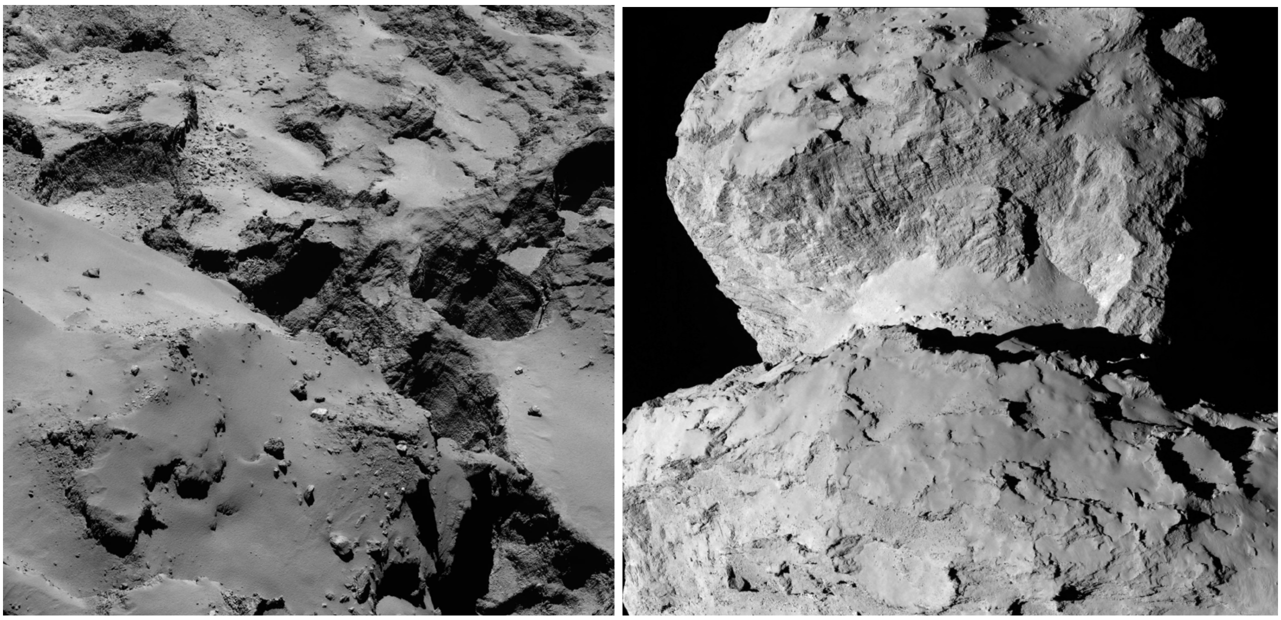

Figure 5: Pits on the surface of comet 67P/Churyumov-Gerasimenko (left). Hator cliff above the 'neck' region between the two lobes of 67P (right). ESA/Rosetta/MPS for OSIRIS Team MPS/UPD/LAM/IAA/SSO/INTA/UPM

Therefore, we can treat or consider JFCs, and KBOs such as Arrokoth, as two opposite end-member points in a spectrum of bodies in varying stages of evolution. Visiting a more pristine LPC would add a pivotal midpoint across that evolutionary path that can further explain how primordial KBOs transition to heavily evolved comets, and at which stage major landscape processes occur. JFCs go through a transitional "Centaur" phase as their orbits dynamically evolve to shorter orbits that place them in the inner Solar System. It is possible that comets undergo substantial changes during that time as hypervolatiles can sublimate beyond the water ice snowline. However, the degree of that change is currently unknown. A major question that can be answered by *Comet Interceptor* is where would LPCs, or generally comets that have not gone close to the Sun many times in their lifetime, place in that evolutionary path? Would they be closer in morphology to KBOs, or would they have developed some morphological and textural variety already during their early formation stages (see Section 2.2.6 below)? Do they show evidence for collisions before their ejection to the OC, and if so, what record do they retain of the primordial impactor population (e.g., crater size distribution)? Therefore, the possibility to encounter and investigate either an LPC, or especially a DNC, would offer more insights to the evolutionary path of comets and the conditions in the early Solar System more generally.

2.2.5 Composition of nuclei

Most of our knowledge on the composition of comets comes from measurements (either *in situ* by spacecraft, or remotely via spectroscopy) of the gas coma, which is discussed in detail in the coma science section below (see Section 2.3). Broadly, we understand the composition of nucleus ices indirectly, by working backwards from sublimated gasses in the coma, or from the products of further gas phase photochemistry. However, direct measurement of the nucleus composition is of great importance to comet science:

- to discover the starting point for these sublimation/chemistry models,
- to understand how (in)homogeneous the nucleus is,
- and to assess the composition of the original building blocks of comets (and planets) independent of our (lack of) understanding of evolution and activity processes.

We are limited to measurements of the surface composition as the only attempt to directly measure the interior composition of a comet nucleus, the SD2 drill on the *Philae* lander, failed to collect a sample (Boehnhardt et al. 2017). Mass spectroscopy results for surface dust returned by *Philae* were inconclusive, but did show a high proportion of organic compounds (Boehnhardt et al. 2017), consistent with remote sensing measurements. As discussed in Section 2.2.3 above, spectroscopy, both unresolved from telescopic observations and resolved from spacecraft encounters, reveals comet nuclei to be largely featureless in the visible and near infrared, with reddish slopes (but shallower than many KBOs) and very low albedo (e.g., Quirico et al. 2016). A broad 3.2-μm absorption was identified by the *Rosetta* VIRTIS instrument at 67P, which has been interpreted in a variety of ways, including salts, organic compounds, and/or silicates (Poch et al. 2020, Raponi et al. 2020, Mennella et al. 2020). Features due to water ice are, perhaps surprisingly, largely absent – they are only seen in *Rosetta* data in localised spots (Barucci et al. 2016), where fresh subsurface layers (e.g., *Figure 6*) have been uncovered (e.g., by cliff collapse; Filacchione et al. 2016), or as short-lived frosts deposited during the comet night time (De Sanctis et al. 2015). Nuclei are mostly too faint to be detected at shorter and longer wavelengths from Earth-based observations, but UV spectroscopy from the Alice instrument on-board *Rosetta* revealed a featureless blue slope (Feaga et al. 2015). At sub-mm wavelengths, *Rosetta*/MIRO could only constrain nucleus thermal emission, not give compositional information. Unresolved mid-infrared spectroscopy with the Spitzer space telescope shows broad features attributed to silicates, with similarities to D-type asteroids and Jupiter Trojans (Kelley et al. 2017). Spacecraft observations, made *in situ* at these wavelengths, have yet to be attempted, but are a promising direction to take. These wavelengths contain a wide array of features seen in common minerals and

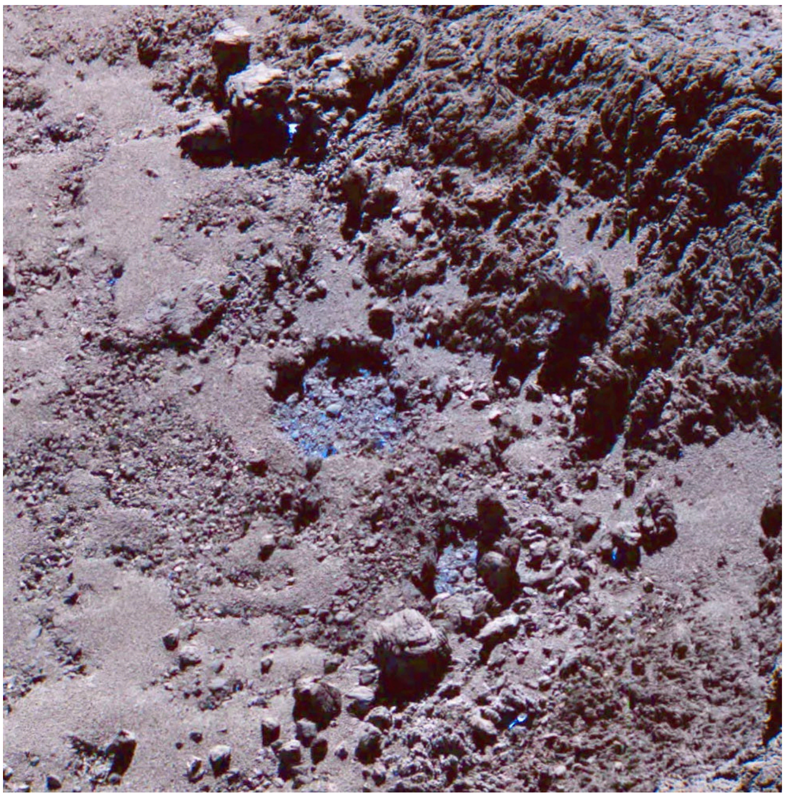

Figure 6: A water ice-filled depression on the surface of 67P's nucleus. This image is a false-colour composite, where the pale blue patches highlight the presence and location of water-ice. ESA/Rosetta/MPS for OSIRIS Team MPS/UPD/LAM/IAA/SSO/INTA/UPM/DASP/IDA.

organic ices, and could reveal both composition and its variation across the nucleus surface, in resolved spectroscopy and/or imaging.

2.2.6 Evolution of cometary nuclei

Both the mechanical and thermal processing of comet nuclei occur during distinct phases of a nucleus' life:

- during formation and early evolution in the protoplanetary disc.
- during the long period of storage in the comet reservoirs.
- and as an active comet upon return to the inner Solar System.

For JFCs, there is an additional, and significant, period of evolution during the slow evolution of their orbits through the Centaur phase (see below), while LPCs enter the inner Solar System directly from the OC. The results of thermophysical models described below show that significant composition changes can be expected in (at least) the outer layers of comets over their lifetimes, yet clearly comets do retain significant volatile ices to drive their observed activity, including some whose spectra are dominated by so-called super-volatiles (e.g., Paganini et al. 2012, Biver et al. 2018). There is still much to be understood about cometary activity and nucleus evolution, which is the primary motivation for visiting a less-evolved comet.

The active comet phase is the one that is best understood, following the results from *Rosetta*, as the evolution of the nucleus is driven entirely by the comet's activity and therefore by the energy it receives from the Sun. Erosion of the surface has long been understood as a consequence of sublimation of nucleus ices, with metres of the surface lost, on average, per perihelion passage (e.g., Whipple 1950; Britt et al. 2004; Veverka et al. 2013; Keller et al. 2015). However, a surprising result from the *Rosetta* mission was the importance of fall-back of material lifted into the inner coma, with some areas of the nucleus blanketed by deep layers of fine material (e.g., Thomas et al. 2015, Marschall et al. 2020, and Cambianica et al. 2021). In models of the nucleus consisting of pebbles, fall-back of decimetre-sized chunks leads to both surface morphology changes (*Figure* 7) and evolution of near-surface composition, as subsequent activity from the fall-back material is driven by water ice retained within these 'chunks', which have a lower abundance of the more volatile ices whose activity lifted the chunks from other areas in the first place (Fulle et al. 2020a). The many cycles of activity seen by short period comets mean that their surfaces have undergone significant evolution, while an LPC encountered at 1 AU will have relatively little recent evolution, depending on where exactly its activity began on the inbound leg (models range from 35 to 85 au; Jewitt et al. 2021, Fulle et al. 2020b), and on model-dependent levels of erosion and fall-back during this time.

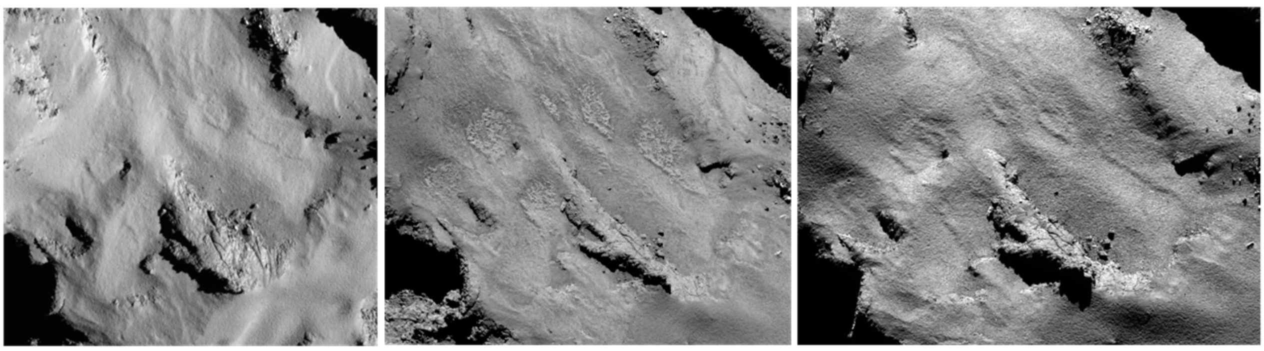

Figure 7 Surface morphology changes due to fall-back of dust on the surface of 67P/Churyumov-Gerasimenko. ESA/Rosetta/MPS for OSIRIS Team MPS/UPD/LAM/IAA/SSO/INTA/UPM.

The earliest phase in comet evolution, which the nuclei spent in their formation zone at 5-30 au, could last anywhere from 2.5 to several hundred million years (various models have different timing for the instabilities in the giant planet orbits that scattered comets into their reservoirs, e.g., Nesvorny et al. 2018, Morbidelli et al. 2018; Pirani et al. 2019, 2021). The OC could not have been populated while the Sun was still in its embedded star cluster phase – whose duration was perhaps a few Myr (e.g., Adams 2010, Pfalzner et al. 2020, Parker 2020) – because the Sun's tidal radius was too small (Tremaine 1993, Wyatt et al. 2017). When it comes to the survival of volatile species, this phase is significant: Davidsson (2021) reports that nuclei in the protoplanetary disc with diameters ranging from 4 to 200 km can lose all their condensed CO ice on short timescales (smaller than the minimum time to eject them in the reservoirs), through a combination of protosolar and long–lived radionuclide heating. This may have been avoided if cometesimals formed late enough (Davidsson et al. 2016), or in a region of the disc with relatively low abundance of radionuclides, which has been suggested by some observations (e.g., analysis of four Stardust samples indicate that 81P never contained any appreciable 26Al; Levasseur-Regourd et al. 2018). The drivers of evolution in this phase can also be expected to include collisions (Jutzi et al. 2017; Schwartz et al. 2018), although models of the timescales for CO-driven cometary activity suggest that erosion of ice-rich cometesimals in this early environment could dominate evolution over collisions (Fulle et al. 2020b).

Subsequently, and because the time of residence in the OC or the KB is very long, a significant fraction of the bulk of most comet nuclei can be affected by superficial heat sources, even if the thermal diffusivity is extremely low. Davidsson (2021) reports that, for objects large enough to have any pure condensed CO ice remaining in their bulk when they are ejected in their reservoirs, the long-term survival of supervolatile ices largely depends on whether nuclei are scattered in the OC, or in the KB. Indeed, objects reaching the OC could get subsurface temperatures low enough for CO gas, if diffusing from the deep interior, where it was heated due to radiogenic decay, to condense near the surface. In the KB, the equilibrium temperature ranges from 30 to 50 K, so that, for objects typically smaller than 4 km, all hypervolatiles initially present as pure ices should sublimate during the time of residence in this reservoir, even without any radiogenic heating (De Sanctis et al. 2001; Choi et al. 2002; Jewitt 2004; Davidsson 2021).

We emphasize again that, for OC comets, the thermal processing prior to the injection in this reservoir does not guarantee that a nucleus stored there can preserve a pristine inventory of hypervolatiles. In terms of internal structure expected for OC comets, Davidsson (2021) suggests that nuclei of any size exposed to the intense heating of the proto-Sun would lose not only hypervolatiles condensed as pure ices, but also CO_2, down to a depth of ~30 m. In addition, partial crystallization could occur in the upper ~200 m. As a consequence, the near-surface layers of a comet nucleus may be significantly processed: even DNCs cannot be completely pristine, and some might have lost a significant amount of hypervolatiles prior to their scattering into the OC. In addition, Stern and Shull (1988) suggest that up to 20% of comet nuclei stored in the OC could have been heated to at least 30 K down to several dozen metres below the surface, due to the passage of luminous stars during the history of the solar system. Most of them may have been heated to 45 K in the uppermost 1 m-layer due to stochastic supernovae events. This would lead to the formation of a surface layer depleted in hypervolatiles. Stern (2003) further reports that passing stars and supernovae heating events could modify the primordial composition of comet nuclei down to 5 to 50 m (for heating due to passing stars), and to 0.1 to 2 m (for heating due to supernovae events).

However, an extremely significant difference between JFCs and DNCs coming from the OC lies in their subsequent orbital evolution, which brings them to the orbit on which we observe them. Indeed, an intermediate evolution phase exists almost exclusively for Centaurs, of which a fraction become JFCs, during which comet nuclei are perturbed into their final orbit through a chaotic orbital evolution in the giant planet region. Processing during this phase intensifies, due to increasing equilibrium temperatures, and close passages to massive planets. Because the time spent in the giant planet region is significant (typically 10 Myr, Levison and Duncan 1997; Tiscareno and Malhotra 2003) the resulting processing is also substantial. This phase is non-existent for nuclei coming from the OC, which come from this reservoir to the inner solar system in a more rapid and direct pathway. Huebner et al. (2006) discussed the outcomes of such different injection types, which may result in extensive changes of the internal composition and structure of comets. Similarities between the structures resulting from the two types of orbital evolution are:

1- surface temperatures, driven by the heat balance at the surface, and

2- Water and CO_2 gas production, which are controlled by erosion, keeping both water and CO_2 ice close to the surface.

However, the significant differences resulting from the two orbital evolutions are mostly related to the location of the CO sublimation front (and hypervolatiles in general), and the amorphous/crystalline ice interface. The CO sublimation front for JFCs should be located hundreds of metres below the surface, while it remains very close to the surface for DNCs. In terms of activity, this is reflected in the fact that CO production is typically continuous for JFCs, or at least with a pattern which does not follow the water emission, and the production rate for the JFC nucleus is significantly smaller (ten times lower in their example) than for a DNC. Water and CO_2 sublimation remain, however, characterized by peak emissions towards the perihelion of each orbit. The simulations reported in Huebner et al. (2006) also showed the formation of a transient dust mantle, which was destroyed when the last orbital change occurred.

In conclusion, any comet nucleus coming from the OC would be significantly less altered and more informative of the processes that shaped the solar system in its early phases, when compared to the JFCs explored in space thus far.

2.3 Comet Environment Science

2.3.1 Introduction

This theme focuses on the coma, looking to answer the following questions:

- What is the composition of the gas and dust in the coma?
- How does it connect to the nucleus (i.e., how does cometary activity work)?
- What is the nature of its interaction with the solar wind?

These topics are addressed through observations of the gas, dust and plasma that are described in the subsections below. They are linked to each other, and also to the studies of the nucleus described in the previous section, through the processes of cometary activity; ices sublimating to gas, and lifting dust, followed by the decoupling of these and the photochemistry that generates the products we observe on large-scales. Data from telescopic observations and previous space missions have given us clues to understand all of these steps, but many puzzles remain. Measuring the composition and distribution of volatile species in the coma will help in understanding the activity processes of an LPC compared with the more evolved objects visited to date:

- What are the relative abundances of molecules of high volatility such as CH_4, CO and CO_2 with respect to water in an LPC versus JFCs (67P) and HTCs (1P) at similar heliocentric distances?
- Is there evidence for or against hyperactivity, i.e., significant activity being driven by sublimation from icy ‘chunks' in the coma, as seen at 103P by *EPOXI*?
- Are there differences in isotopic composition, e.g., in D/H, and other species if sufficiently abundant?

For each of these questions, *Comet Interceptor* will test whether or not the phenomenon is evolution-related, and will inform the interpretation of ground-based observations of other comets.

Comet Interceptor will also perform unique observations of the coma from three different positions simultaneously, due to its multi-spacecraft configuration. This will allow gas, dust, and plasma distributions or boundaries to be described in a 3-dimensional way. This was not possible with previous missions, which sampled only a single location at a time, and will allow separation of spatial and temporal variations. The multipoint in-situ plasma measurements will be complemented by Energetic Neutral Atom (ENA) observations, which may provide a more continuous observation of the variability of the solar wind, giving a clearer picture of which plasma variations are due to external influences.

2.3.2 Composition and Distribution of Gas and Dust

2.3.2.1 *Gas Coma*

The bulk of our knowledge of the composition of comets comes from studying the gas coma. Remote observations give a comparatively less detailed picture but of a larger number of comets, while *in-situ* measurements with mass spectrometers, in particular from *Rosetta*, have revealed a wealth of detail of just a few. Unfortunately, there have not been any good opportunities yet to link these approaches. Although a campaign of remote observations did support *Rosetta* (Snodgrass et al. 2017), 67P was not particularly bright around its 2015 perihelion and could not be studied with high resolution spectroscopy, for example. The comet al.so presented a poor observation geometry, being located on the other side of the Sun with respect to Earth. Much of our knowledge of comet composition (especially on an isotopic level) from telescopes is based on LPCs, which are often more active and brighter. A mission to a bright LPC would present an opportunity to compare high resolution spectroscopy at a range of wavelengths with *in-situ* mass spectrometry measurements, calibrating our understanding of the much wider observed population. Modern infrared and sub-mm facilities, such as the ESO Very Large Telescope and the other 8-10m class telescopes, and the Atacama Large Millimetre/submillimetre Array, which did not exist at the time of *Giotto*, are suitable for observing molecular species thought to be directly released from the nucleus.

2.3.2.2 *Bulk and isotopic composition of the neutral gas coma*

It is well established that within about 3AU from the Sun the main driver of cometary activity is the sublimation of water ice. At larger distances, more volatile species like CO or CO_2 are likely to play a major role (e.g., Meech et al.

2017). There remains a lot of uncertainty about where and how the transition between driving species takes place, and whether or not there are differences in this between new and returning comets. It has long been observed that DNCs tend to be brighter (more active) than periodic comets (the 'fading problem': Oort 1950; Dones et al. 2004); the most significant difference between DNCs and returning comets appears to be greater activity at larger distances in the former population, which implies different driving species (Meech & Svoren 2004). *Comet Interceptor* will measure the absolute and relative densities of the main neutral volatiles (H_2O, CO, and CO_2) along the fly-by trajectory, allowing us to derive production rates from these measurements, and show which is dominant in an LPC at ~1 au.

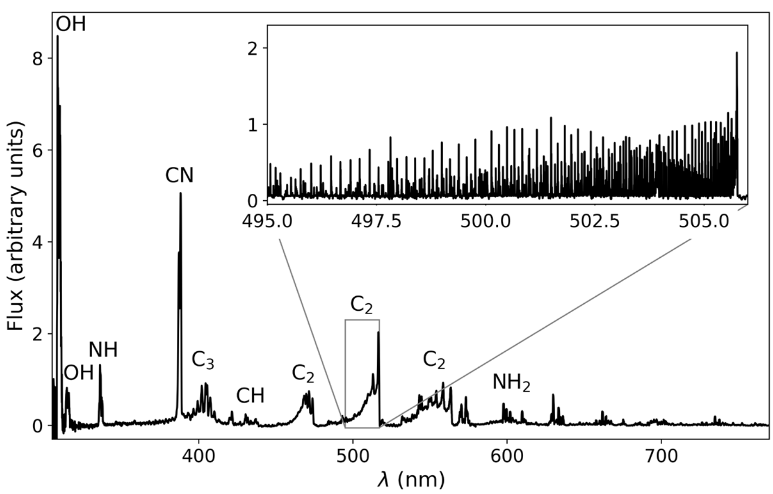

Figure 8: Typical comet spectrum from ground-based visible observations, with key emission features marked. Major components such as water or CO_2 are not observable and require space missions to characterise (Image courtesy of C. Opitom).

Although ground-based composition observations do not rival the comprehensive information that can be provided by *in situ* spacecraft measurements, remote observations still provide extremely valuable data on bulk composition (e.g., *Figure 8*). Differences of composition between JFCs and more pristine comets coming from the OC are starting to emerge from ground-based observations, with the most highly volatile species (such as CO, CH_4, C_2H_6, and C_2H_2) being depleted in JFCs compared to OCCs (Dello Russo et al. 2016). However, this has not been confirmed *in situ*. Ground-based observations of highly volatile molecules in infrared/radio domains are rarely simultaneous: for example, CO in the M-band and other organics in the L-band are not observed simultaneously, although most species are usually observed with H_2O, or its proxy OH, to derive mixing ratios with respect to H_2O. This makes the measurement and comparison of relative abundances difficult in some cases, especially for data taken by old-fashioned infrared spectrometers. A large dispersion of mixing ratios observed in ground-based observations might be partially explained by such non-simultaneous observations. *Comet Interceptor* will provide an unprecedented opportunity to measure gas composition *in situ* and compare the abundance of molecules of high volatility such as CO, CH_4, C_2H_6, and CO_2 with respect to water in a DNC versus JFCs (67P) and evolved LPCs (1P).

Aside from the volatiles mentioned above, *Comet Interceptor* will make detailed compositional measurements that are only possible *in-situ*. The *Rosetta* spacecraft revealed the presence of complex and diverse organic molecules in the coma of 67P, including key species for prebiotic chemistry, some being observed in the coma of a comet for the first time (see Altwegg et al. 2017a). These organics cannot be detected through ground-based observations with current technology, preventing us from assessing the variation of their abundances between comets and, in particular, between primitive DNCs and processed JFCs. Obtaining an inventory of (complex) organic molecules and other species important in prebiotic chemistry in a primitive LPC will delve further into the role of comets in transporting organic matter to the early Earth (Marty et al. 2016). A surprising result of *Rosetta* was the abundant molecular oxygen observed in the coma (Bieler et al. 2015a), while circumstantial evidence for O_2 was also found in comet 1P (Rubin et al. 2015). Several formation mechanisms have been discussed, from radiation of water ice and cold temperature chemistry in the ISM, to various *in situ* formation mechanisms. *Comet Interceptor* will assess how ubiquitous O_2 is in comets: a more pristine LPC or DNC target will narrow down possible formation mechanisms (c.f. Luspay-Kuti et al. 2018). Evidence of ammonium salts in 67P found by *Rosetta* (Altwegg et al. 2020) was also unexpected and may change the traditional view of species parentage and how molecules are stored in cometary ices; for example, NH_4CN (if present in the coma) can produce NH_3 and HCN, which were previously believed to be "parent" molecules released directly from the nucleus.

Isotopic ratios, being very sensitive to physico-chemical conditions, provide crucial information on the provenance of cometary material, and therefore provide information for comet and planet formation models. For instance, the D/H ratio in cometary water has been used to infer whether or not comets could be a source of the water on Earth (Hartogh et al. 2011). To date, all comets with known D/H either exhibit a terrestrial ratio or an elevated ratio (Altwegg et al. 2017b). A recent study suggests two distinct sources of water with different D/H: one source on the surface of the nucleus and the other in the form of sublimating icy grains in the coma (Lis et al. 2019). Fulle (2021) models these observations with 'pebbles' of different ice content. Depending on the type of the activity of the target comet, *Comet Interceptor* may obtain measurements of both reservoirs during the fly-by. The D/H ratio of a less evolved object may furthermore give some insight into outgassing-related fractionation processes. These measurements will also help in interpreting differences or similarities between remote and in- situ D/H measurements, in particular if simultaneous measurements can be made from the ground, which is likely to be the case if *Comet Interceptor*'s target is a relatively bright LPC, as expected. Measurement of the $^{18}O/^{16}O$ in H_2O by *Rosetta* revealed an enrichment in ^{18}O compared to the terrestrial value (Altwegg et al. 2019). Models of chemical evolution in the protoplanetary disc or natal molecular cloud of our Solar System do not yet explain these results, and demonstrate the value of isotopic measurements in furthering our understanding of the topic of planetary system formation in general (Hily-Blant et al. 2017; Wirstrom & Charnley 2018; Furuya & Aikawa 2018). Even though D/H is the primary objective, if the target is sufficiently active, *Comet Interceptor* will investigate isotopes in other species including, e.g.: $^{18}O/^{16}O$ in H_2O, $^{13}C/^{12}C$ in CO_2, and $^{34}S/^{32}S$ in OCS and CS_2.

Many pre-solar signatures have been observed in the isotopes of volatiles in 67P (Hoppe et al. 2018), while similar bulk abundances of volatile molecules were observed in Comet C/1995 O1 Hale-Bopp and 67P with in objects in the ISM (Bockelée-Morvan et al. 2000, Drozdovskaya et al. 2019). Detailed *in situ* measurement of an LPC or a DNC will probe the potential locations of origin of its ices at a molecular, elemental, and isotopic level.

2.3.2.3 *Spatial distribution and structures of the neutral gas coma*

The spatial distribution of volatiles in the coma is of particular interest as it can provide information on how the ices are distributed in the nucleus. However, this aspect is a difficult issue to address. Ground-based observations only allow mapping of the distribution of volatiles on very large scales, missing the crucial transition region between the nucleus and the inner coma. As *Rosetta* orbited the comet for an extended period, it built up maps of coma composition at much smaller scales above different areas (*Figure 9*). These revealed that the neck of the nucleus – the transition region between the head and the body parts of 67P – was the most active area, while minor activity was detectable from both lobes of the comet. *Rosetta* confirmed that comets have heterogeneous comas dominated by large fluctuations in composition, often linked to diurnal and seasonal variations in the major outgassing species such as H_2O, CO_2, and CO (e.g., Hässig et al. 2015). A general large-scale anticorrelation between H_2O and CO_2 was observed by *Rosetta* (e.g., Mall et al. 2016 & Migliorini et al. 2016). The gas density in the coma is strongly affected by nucleus concavities and sun illumination conditions, even when the distribution of ices on the nucleus surface is quite uniform (Bieler et al., 2015b).

Morphological features are observed for gas species in the coma of comets, in a similar way to the dust, both at very large scale from ground-based observations and at much smaller scales close to the nucleus. Narrow band images of neutral gas species acquired by *Rosetta* revealed plume-like morphology in some cases and more isotropic distribution in other cases (Bodewits et al., 2015). Although dust images revealed a variety of jets and collimated distributions, no narrow gas jets have been observed. Ground-based narrow-band gas observations of comets reveal that large-scale structures such as fans or spirals are common (e.g., Schleicher et al. 2004). Consequently, the features observed can be different for different species and often differ from dust species. Understanding how those features are produced and how they relate to the nucleus structure and homogeneity is a complex problem.

The existence of distributed sources of volatiles in the cometary coma has been the subject of debate for several decades now. Evidence suggests that, for some comets/species, mechanisms other than the sublimation of nucleus ices or the photo-dissociation of parent species are necessary to explain the spatial distribution of gas species in the coma. The thermal degradation of organic-rich or icy grains has been proposed as a potential distributed source to explain the spatial distribution of species like H_2CO, CO, HCN, CN, C_2 (Cottin et al. 2008). As mentioned above, recent evidence from *Rosetta* suggest that ammonium salts might play a role in the release of NH_3 or HCN in the coma. However, the existence of ammonium salt has never been confirmed in any comet other than 67P, so the ubiquity and significance of extended sources in the coma of comets remains unclear. As a consequence, the exact nature of extended sources is extremely difficult to assess from the ground and in-situ observations are thus critical to answer this question.

Long-term measurements of the distribution of species in the coma and its change with varying nucleus illumination and heliocentric distances will not be possible for a fly-by mission. Instead, separate but simultaneous measurements from spatially distributed sub-spacecraft will provide snapshots of different coma regions at the time of fly-by. This method actually has advantages over *Rosetta*'s approach, as it will allow, for the first time, separation of spatial and temporal variations. Interpretation of *Rosetta* results instead requires complex models to understand how the comet changed with time and space, because measurements of different coma areas were taken at different places and times along *Rosetta*'s orbit. The unique multi-spacecraft architecture of *Comet Interceptor* will allow the addressing of important questions on how dynamic effects in the coma relate to each other: Which are due to the changing position of the spacecraft relative to the nucleus, and which to the comet's time-varying behaviour? (c.f. Hansen et al. 2016) *Comet Interceptor* will be able to map the neutral gas coma and determine the distribution of H_2O, CO_2, and CO around the nucleus.

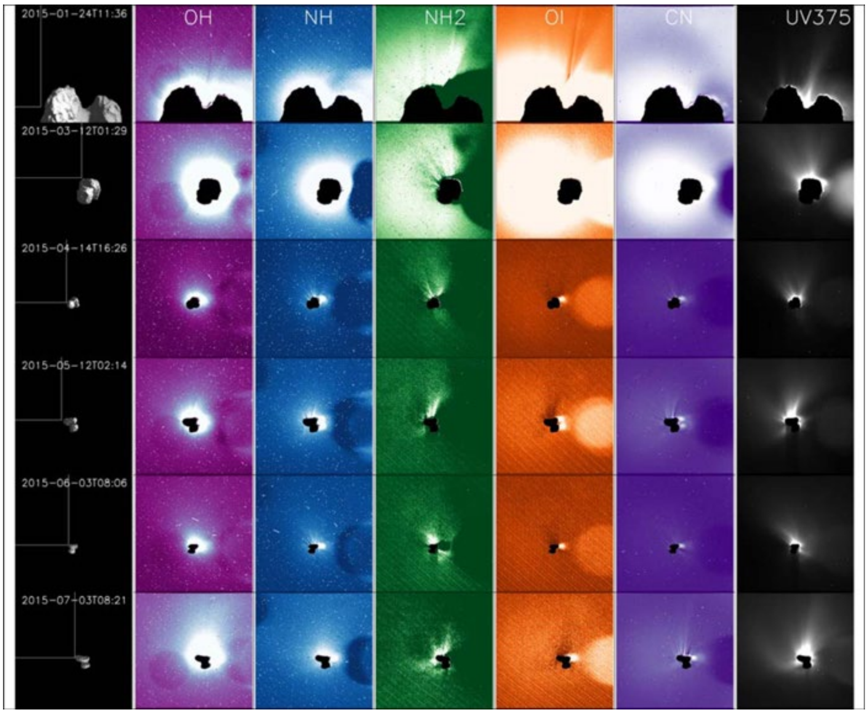

Figure 9: Images showing different morphology of gas jets of different species from Rosetta/OSIRIS (from Bodewits et al 2016).

2.3.2.4 *Dust Coma*

The refractory component of the comet coma is referred to as 'dust'. It is made up of minerals and organic components lifted from the surface with sizes ranging from sub-micron to metre-scale chunks. The properties of the dust are important to understanding comet composition and formation. For example, the similarity in size of the dominant particles in 67P's coma and those predicted to form planets via streaming instability was used to argue in favour of that model, assuming that particles reflect the original size distribution (Blum et al. 2017). Measuring the dust size distribution down to nm size in a DNC will test the universality of this assumption: if it is similar to JFCs it would imply a link with primordial dust distribution, and support streaming instability models, whereas a difference would imply that comet material has been processed at μm scales and that dust properties reveal evolutionary processes.

Whether or not solid material lifted from the comet's surface also contains ice is important for our understanding of activity processes, as sublimation from dust in the coma could form a distributed source of water or other gasses. *Rosetta* found that little water is provided by sublimation from particles beyond a few nucleus radii, so there is no significant distributed source for water at 67P. That does not preclude distributed sources for minor constituents: for instance, evidence has been found for a distributed source for the hydrogen halides (De Keyser et al. 2017) and some of the lesser volatiles including organics (Altwegg et al. 2016, 2017b). This is in stark contrast to the earlier *EPOXI* flyby of comet 103P (A'Hearn et al. 2011) and remote observations of the innermost coma of comet 73P/Schwassmann-Wachmann 3, where a significant fraction of the outgassing occurred from a distributed source of icy grains (Fougere et al. 2012, 2013). Still, assessing the existence of a distributed source is difficult, even during a fast flyby where one can consider gas and dust production to be basically constant: cometocentric longitude, latitude, and distance all change simultaneously, and therefore it is not straightforward to extract purely radial density profiles from which one can ascertain the existence of a distributed source. To detect and identify distributed sources, it is necessary to scan a very large range of radial distances and, simultaneously, to assess the dust and gas abundances at a minimum of two points in the coma: again, the multi-point architecture of *Comet Interceptor* will give it a unique advantage in addressing this question.

Constraining the dust-to-ice ratio in the coma (individually for icy particles, or in bulk by comparison of dust and gas production rates), and by inference in the nucleus, will also provide information for planet formation models. The question of how much ice is present in larger chunks in the coma is a critical parameter to understand the overall dust-to-ice ratio within a comet, which is a very important number to constrain the properties of the formation location of the comet, and one that is still the subject of intense debate following *Rosetta* (see, e.g., Fulle et al. 2019; Choukroun et al. 2020). Measurements at a less evolved LPC would be very valuable to understand this intrinsic ratio.

Comets are also a natural laboratory to study the poorly understood topic of dusty plasmas, important in many areas of astrophysics. GIADA, one of the three dust instruments on board *Rosetta*, measured the "electrical" interaction between the dust and the spacecraft. Dust particles, negatively charged by electrons sticking to their surfaces, interact with the spacecraft potential and fragmented before entering GIADA (Fulle et al. 2015). This is therefore important in interpreting showers of dust particles. Dust also influences plasma behaviour; electrons from the plasma sticking to the surface of a dust particle impart a negative charge, whereas photoemission of electrons from the particle leads to a positive charge. Charges bound to heavy dust particles give rise to new wave modes in the plasma (Barkan et al. 1995, Merlino et al. 1997); the detection of these waves provides an alternative measurement of the dust content.

2.3.2.5 *Dust reflectance properties*

Ground-based observations of the intensity, colour, and degree of linear polarisation of light scattered by cometary dust particles are used extensively for retrieving information on their physical properties, including their morphology and structure, as defined by Güttler et al. (2019). However, they are usually limited to certain observational geometries. Time variations of the brightness of the coma, as observed from Earth, are not only dependent on the phase angle, but also vary due to changes in the dust production rate. Due to these limitations, ground-based photometry and polarimetry often involves observations over multiple orbital periods of JFCs, or over a wide range in heliocentric distance for LPCs, so they may also be affected by possible changes with time in the particle properties. The most commonly used phase function for cometary dust, the Halley-Marcus function, is derived from a combination of models and observations of 1P over a wide range of phase angles during its 1980s return (Schleicher & Bair 2011). Its features reveal some characteristics of cometary dust: there is an opposition effect (brightening) at low phase angles and a much stronger upturn in the forward scattering regime, which are largely due to particle size. The colour of cometary dust – the ratio of reflectance at different wavelengths – also provides clues about particle size, due to differences in absorption and scattering of photons of different frequency. Colour observations have the advantage that they can be measured at a single time and geometry, but have the disadvantage that broadband photometry can also be influenced by emission from the gas coma. Finally, polarimetry is a remote sensing technique that is sensitive to the morphology, size distribution and composition of the dust particles and brings additional constraints compared to what can be obtained from intensity measurements alone.

Observations from spacecraft offer the opportunity to sample a wider range of geometries at a single time, from within the comet's coma. The analysis of the *Rosetta* dataset has exposed challenging contradictions between the properties of cometary dust as modelled from ground-based and from *in situ* observations. On the one hand, the OSIRIS camera system on-board the *Rosetta* spacecraft provided unique observations of the intensity of light scattered by dust within 67P's coma (Bertini et al. 2017). The observed phase functions show a peculiar U-shape with a minimum at a phase angle around 100° (compared with the minimum at ~55° in the Halley-Marcus function. Those data would indicate the presence of large grains. Further, ground-based observations of the degree of linear polarisation of 67P show a negative polarisation branch (NPB) at small phase angles and a maximum observed DLP (Degree of Linear Polarisation) of ~ 8% at a phase angle of 32° obtained after the 2015 perihelion (Myers & Nordsieck 1984; Chernova et al. 1993; Hadamcik et al. 2016). Micron-sized particles may reproduce the shape of the DLP curve, but certainly not the U-shaped OSIRIS phase function The major challenge is reconciling conclusions about the properties of cometary dust obtained from the analysis of both datasets, which demands a common framework to interpret consistently all the datasets available (Moreno et al. 2018; Markkanen et al. 2018; Levasseur-Regourd et al. 2019; Muñoz et al. 2020).

Rosetta did not provide *in situ* polarimetric observations, but these were obtained by *Giotto*'s HOPE (Halley Optical Probe Experiment) instrument, which took observations along the line-of-sight of the spinning spacecraft at different wavelengths free of gas-emission. These allowed an estimate to be made of the density of the cometary dust, which was found to be low (about 100 kg m^{-3}), and of its geometric albedo (0.04, matching that of the nucleus). It was found that the polarisation was highest when crossing dust jets and lower in the inner coma region. During the *Giotto Extended Mission* flyby of 26P/Grigg-Skjellerup, HOPE hinted at the presence of pebbles ejected from the nucleus. Since then, polarisation imaging of active comets, from both ground-based and satellite observatories, have confirmed the existence of lower polarisation in the innermost coma and increased polarisation along large-scale dust jets.

Interstellar comet 2I/Borisov presented unique polarimetric features: the observed polarisation was found to increase steeply with phase angle, reaching values substantially higher than typically measured in other small bodies of our Solar System (Bagnulo et al., 2021). These polarimetric properties distinguish 2I from dynamically evolved objects such as JFCs in our Solar System, and suggest that 2I was a highly pristine object, with a coma probably characterised by relatively small-sized aggregates. This also suggests that detailed *in situ* polarimetric observations at a DNC or LPC will be very valuable in revealing differences in dust properties between pristine and evolved comets.

2.3.2.6 *Dust structure and distribution*

Numerical simulations based on the reflectance properties described in the previous subsection conclude that dust particles are irregular, porous, built of smaller grains and are possibly fractal in nature. Additionally, experimental simulations under different conditions (including microgravity) suggest the presence of fluffy aggregates with comparable amounts of minerals and organics (Levasseur-Regourd et al. 2015). These conclusions agree with the results from *Rosetta*'s *in situ* sampling, in particular microscopic imaging of grains by the COSIMA (Langevin et al. 2020; Kimura et al. 2020) and MIDAS instruments (Mannel et al. 2019). *Rosetta* was unique in its ability to capture coma dust grains at low speed, due to the rendezvous nature of the mission, and this led to a great leap forward in understanding, with distinct categories of dust particle identified: Solid grains (that can be either round or irregular, or dense aggregates of these); 'fluffy' groups of fractal combinations of solid grains; porous agglomerations of individual grains, or groups of them (*Figure 10*; Güttler et al. 2019). The particles of different types have different effective porosities and densities, even if composed of the same minerals or ices; COSIMA was also able to probe particle composition. For instance, Gardner et al. (2020) detected phosphorus and fluorine in the solid particles collected from 67P's inner coma. Also, the cometary H/C elemental ratio measured by Isnard et al. (2019) is on average higher than the one found in the most primitive insoluble organic matter extracted from meteorites. The content of organic matter in the particles of 67P is approximately 50% in mass, mixed with mineral phases that are mostly anhydrous (Bardyn et al. 2017). Furthermore, the measured nitrogen-to-carbon (N/C) in 67P grains is compatible with the measurements of the particles of comet 1P/Halley and is in the lower range of the values measured in comet 81P/Wild 2 particles brought back to Earth by the Stardust mission (Fray et al. 2017).

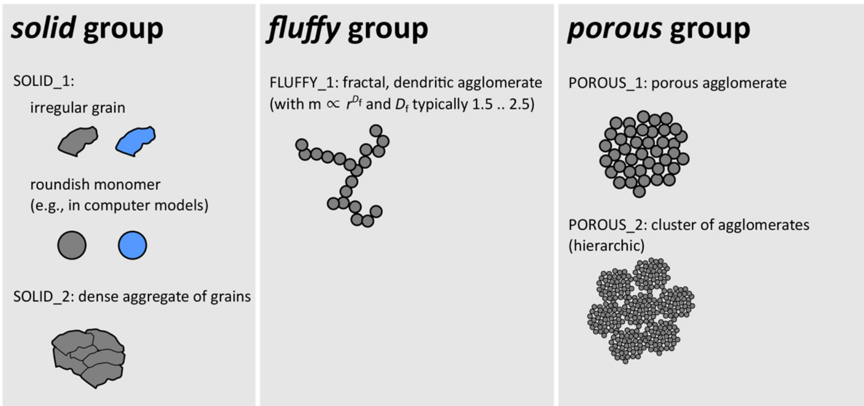

Figure 10: *Morphology of different types of dust particle, from summary by Güttler et al. (2019).*

This variation in different types of dust particle is important to consider in all other dust measurements. For example, the distribution of dust in the coma can be described in terms of size and/or spatial distribution. The size distribution of dust is challenging to estimate from ground-based images as models have many parameters (dust albedo, outflow speeds, etc.), while *in situ* measurements (typically measuring dust flux from momentum transferred in collisions with a target on the spacecraft) naturally sample only a single location in the coma at a time. *Rosetta*'s GIADA instrument combined a laser curtain with piezoelectric impact sensor to measure the cross-sectional area, velocity, and impact momentum of particles, and was therefore able to separate fluffy and compact particles. The instrument characterized the submicrometre - to micrometre-sized dust mass flux in 67P's coma, finding a differential size distribution index of ≈−3.0, which confirms that particles of size ≥0.1 mm dominate the dust coma cross-section during that comet's entire orbit (Della Corte et al. 2019). On flyby missions, the velocity of impacting particles is dominated by the relative spacecraft velocity to the comet, which is well known in all cases, so particle masses can be directly inferred from momentum sensors – this was achieved by *Giotto* and the NASA *Stardust* mission (the latter also collecting a sample of the more solid coma grains for return to Earth). *Comet Interceptor* will be the first mission to make such measurements at two locations in the coma simultaneously, which will be very important for understanding the evolution of particles (e.g., any evidence of fragmentation) as they flow away from the nucleus.

The spatial distribution of dust within the coma is important for understanding activity, i.e., how, and where the dust flows away from the nucleus (see next section), and can be divided into the inner coma, larger scale coma, and tails. Both remote sensing and *in situ* measurements reveal significant variation in the population of coma particles in different regions. There are broad outflows and more narrowly collimated jets, which appear to be controlled by nucleus topography in the inner coma, but are also visible on 1000s of km scales in ground-based imaging. The large-scale features have yet to be conclusively linked to the inner coma structures and the nucleus. At the very largest scales, dust is swept into the characteristic dust tail of the comet, where differences in acceleration due to solar radiation pressure differentiate the material largely by particle size – models of tail morphology can therefore be used to place constraints on particle properties. *Comet Interceptor* will produce a unique 3D portrait of the dust flows within the coma on all scales, via imaging from the cameras on all three spacecraft, including the all-sky scanning of EnVisS, and from *in situ* measurements from DFP.

The fast fly-by will provide an instantaneous snapshot of the nucleus and coma. However, depending on the spin state of the comet, pre- and post- closest approach observations will contribute additional information on the diurnal evolution of the near/far environment. Such observations, even with an unresolved nucleus, will be extremely valuable to characterize the gas and dust distribution around the nucleus, as well as the activity of different regions at multiple local times.

2.3.3 Activity

Cometary activity is a complex process: the exact sources and mechanisms driving activity in comets remain a puzzle. *Rosetta* revealed that cometary activity, jets, and outbursts (*Figure 11*) are linked to distinct morphological features observed on the nucleus of the comet (Vincent et al. 2015, 2016).

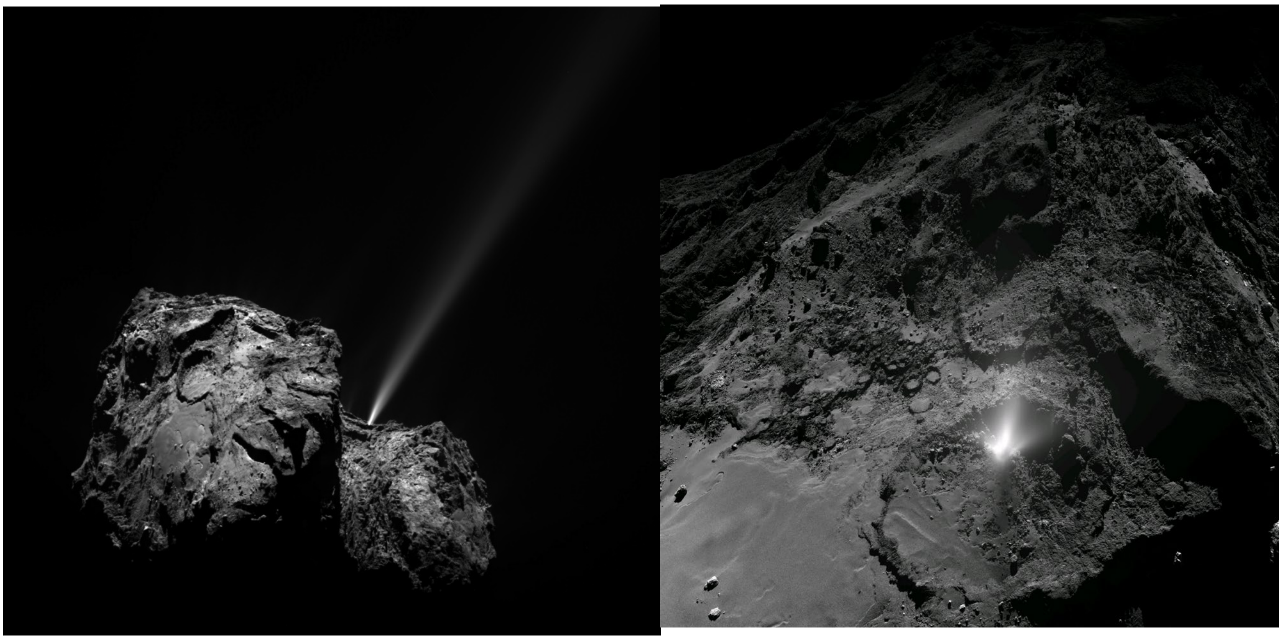

Figure 11: Outburst on the surface of 67P/Churyumov-Gerasimenko observed on 3 July 2016 (left) and on 29 July 2015 (right). ESA/Rosetta/MPS for OSIRIS Team MPS/UPD/LAM/IAA/SSO/INTA/UPM.

Working activity models have been recently provided in case of pebble-made nuclei (Fulle et al. 2020a, 2020b, Gundlach et al. 2020, Fulle 2021, Ciarniello et al. 2021, 2022). The pebble model is however debated in the community, as the existing data is not sufficient to fully assess its validity. By characterizing a DNC from a close distance, *Comet Interceptor* will obtain unique observations of dust and gas release from a type of object not studied before and provide a test case to evaluate all current cometary activity models. The surface of a DNC on its first approach to the Sun is expected to be little processed and *Comet Interceptor* will allow us to assess how this difference in surface properties impacts cometary activity. If activity can be attributed clearly to local areas in a DNC this would offer strong evidence that they are due to primordial shape or composition heterogeneities, and not evolution-driven features, as no processed surface crust is expected, unlike in previously visited comets. Evidence for or against hyperactivity – significant activity being driven by sublimation from icy 'chunks' in the coma (*Figure 12*) – would test also whether or not this phenomenon (seen in 103P but not in 67P) is evolution-related, and may be important in the interpretation of ground-based observations of other DNCs. Typically, the distribution of coma structures (gas and dust) in the near environment and their source locations on the nucleus are inferred from the spatial tracking of jet-like emissions across multiple images. The combined motion of the spacecraft and rotation of the nucleus usually provide sufficient geometric variation to reconstruct the three-dimensional shape of the jets. This method, however, assumes that tracked features do not evolve significantly in between images, which may not always be the case. By providing multiple views of the same features from different angles at the same time, *Comet Interceptor* observers (spacecraft A/B1/B2) remove this uncertainty and allow for a more precise mapping of apparent active regions.

The most obvious observational evidence of nuclear activity is the collimated jets of dust ejected from the surface. Less well collimated, and thus harder to detect, are neutral gas jets, previously discussed in Section 2.3.2.3. Exhaustive studies of the jets of 67P (e.g., Kramer & Noack 2016, Vincent et al. 2016) reveal that the structuring of these jets relate not only to some discrete active regions, but also to surface morphology, i.e., to the topography of the object. Such jets are also to be studied by *Comet Interceptor*.

Figure 12: Image from NASA's EPOXI mission shows part of the nucleus of Comet 103P/Hartley 2. The sun is illuminating the nucleus from the right. A distinct cloud of individual particles is visible, gas release from which is responsible for the high apparent activity level given this nucleus's size. Image Credit: NASA/JPL-Caltech/UMD.

There is strong complementarity between *in situ* and ground-based imaging of coma structures, as was shown in the case of 67P, where the analysis of ground based data revealed the presence of structures originating from certain latitude/longitudes on the nucleus surface (Vincent et al. 2010, 2013; Lara et al. 2011). This allowed the rotational period of the comet nucleus to be derived, based on previous apparitions, before the spacecraft arrived. These first results related to the spin period and activity of 67P were confirmed by *Rosetta*, although the mission's findings go beyond the classical view of active areas on a nucleus surface producing jet-like features. *Comet Interceptor*'s three spacecraft, with their cameras covering a wide range of different geometries and fields of view, will provide the data necessary to link nucleus surface activity and topography with the large dust structures in the cometary coma. Additionally, it is expected that ground-based observations monitoring the target activity should be plentiful and high signal-to-noise, for a relatively bright LPC target; these will complement and connect to the multi-point measurements of the coma by the three spacecraft.

2.3.4 Plasma Environment and Interactions

2.3.4.1 *Introduction*

This sub-section addresses the fascinating interplay and energy exchanges that occur between cometary material and the solar wind – the fast, continuous flow of positively and negatively electrically-charged particles that are ejected from the Sun. The neutral gas released from a comet's nucleus eventually becomes partially ionised through exposure to solar UV radiation, and/or through energetic particle impact bombardment. The ions born close to the nucleus interact with the cometary neutrals and, for a high enough outgassing, a rich range of chemical reactions can take place, producing new ion species (Beth et al. 2020). In addition, these fresh cometary ions come under the influence of the interplanetary heliospheric magnetic field, join, as pick-up ions, the flow of the solar wind through and past the comet, and are carried downstream of the nucleus, forming the visible ion or plasma tail.

Observations by several instruments on the mission's three platforms aim to characterise the comet's plasma environment. This includes the determination of the position and nature of the different plasma boundaries – regions where plasma or/and field parameters change abruptly (e.g., plasma density, speed, and temperature, magnetic field magnitude) – that form in the comet-solar wind interaction region. Simultaneous *in situ* observations at multiple locations will allow for the first time the assessment of the three-dimensional geometry of these boundaries and of the mass, energy, and momentum transfer in this fascinating environment. Models (Magnetohydrodynamic (MHD), hybrid, implicit Particle in Cell (iPiC)) show lots of detail, but it has not previously been possible to investigate and compare them with the global structure. Specifically, *Comet Interceptor* will include unprecedented simultaneous two-point measurements of the positive ion component of this region, as well as three-point measurements of the magnetic field vector. These *in situ* observations will remove the ambiguity in interpretation associated with single-point measurements by disentangling of spatial and temporal effects. Complementing the *in-situ* measurements of fields and particles, remote-sensing instrument observations will image the ion coma and tail, to capture the motion and evolution of features within them.

2.3.4.2 *Origin and Overall Structure of the Solar Wind interaction Region*

The ion cloud around a comet's nucleus presents an obstacle to the charged particles and the magnetic field of the solar wind (Alfvén 1957, Biermann et al. 1967). The plasma environment of a comet is heavily dependent on the number of cometary ions available in the coma, and therefore the gas production rate. As the cometary pick-up ions are incorporated into the solar wind – a process referred to as mass-loading – the flow around the comet changes and modifies the cometary and solar wind plasma. In the cometary reference frame, pickup ions are almost at rest, thus there is a large discrepancy in velocity between the two flows. Mass loading slows the solar wind while, at the same time, accelerating cometary ions. A bow shock forms, where the solar wind adjusts abruptly to the comet's presence. This has consequences for the magnetic field as well, as it is largely frozen into the flow, and starts to drape around the obstacle. If the magnetic field in the solar wind rotates, current sheets may form in the plasma, a process that results in an onion-like structure of magnetic field lines (Raeder et al. 1987; Volwerk et al. 2014).

2.3.4.3 *The value of multi-point measurements*

Comet Interceptor's multi-spacecraft comet encounter will provide a significant advantage over previous missions in that it will sample different paths through the comet-solar wind interaction region. This includes both the largest scales, beyond the cometocentric distances explored by *Rosetta* at closest approach and the smaller scales, nearer the nucleus. The *Rosetta* mission showed how strongly structured and dynamic the cometary plasma environment is, and how different processes affect different parts of the comet magnetosphere for different activity levels. Charge separation, shocks, and other boundaries, as well as excitation of waves and heating of plasma, all affect the exchange of energy, momentum, and mass on multiple scales simultaneously. This in turn is important for processes such as the sputtering of the nucleus surface and coma dust with energetic solar wind and cometary ions (Wurz et al. 2015), for the excitation of coma constituents and associated emissions (Galand et al. 2020), for coma chemistry, and for the formation of the comet ion tail and its rich structure. The *Rosetta* mission lacked a larger scale overview and understanding of the three-dimensional structure of the comet's induced magnetosphere and magnetosheath. Earlier flyby missions, such as *Giotto*, had the opposite issue: they provided measurements over very large scales, but only along a single path.

With *Comet Interceptor* we therefore expect to observe, along multiple chords through the coma (*Figure 13*), a shock, the diamagnetic cavity, strong electron heating, penetrating solar wind ions, energetic cometary ions moving towards the nucleus, and strong wave excitation. These measurements are needed to assess the relative importance of different mechanisms and to understand how the solar wind affects the comet environment for different types of objects and levels of comet activity. The three-dimensional picture is needed to distinguish between different physical models of the solar wind - coma interaction. This can only be properly investigated with a multi-spacecraft flyby mission, in order to reduce the spatio-temporal ambiguities introduced by potentially changing solar wind conditions during the flyby.

2.3.4.4 *Specific Features of Interest*

Bow shocks haves been observed in several active comets and modelled extensively (e.g., Koenders et al. 2013). In general, this shock moves outwards in the upstream solar wind, away from the nucleus, as the neutral gas production rate and hence the mass -loading increases, with standoff distances up to millions of km upstream of comets with high gas production rates (as for 1P). At low production rates, the critical point is never reached, and no bow shock forms. For example, *Giotto*'s 1992 flyby of 26P revealed a bow shock during the outbound trajectory, but no discernible bow shock inbound (Coates et al. 1997). Instead, it detected a bow wave (e.g., Scarf et al. 1986), a more gradual field increase rather than the jump-like classical shock. This was attributed to the low Mach number of the mass-loaded solar wind flow. At Halley, the bow shock was observed by *Giotto*; outbound, it was quasi-parallel (Neubauer et al. 1990). At 67P, *Rosetta*'s trajectory did not allow for detection of a bow shock or wave. At lower gas production rates, a feature interpreted as an infant bow shock, a highly asymmetric structure behaving like a shock and confined to one side of the interaction region (Gunell et al. 2018) was observed in the plasma environment. Spectral breaks in the pick-up ion energy distributions measured by *Rosetta* have furthermore been interpreted as indirect proof of the presence of a bow shock far upstream of the spacecraft's position (Alho et al. 2019, 2021). Modelling work has also revealed that solar wind charge exchange, as well as asymmetric neutral outgassing of the nucleus plays a major role in the dynamics, width, and extent of the shock structure (Simon Wedlund et al. 2017, Alho et al. 2021). As a consequence, measuring the specifics of the shock (or wave) at different locations, or finding that there is a shock-like feature at one spacecraft and a wave-like behaviour at another, brings invaluable information on the solar wind-comet interaction. Depending on the flyby velocity and sampling rate of measurements, unprecedented multi-point information could be obtained on the internal structure of the bow shock.

The magnetic field that is carried by the solar wind drapes around the outgassing comet, threading through the comet's coma and ion tail. This creates an *induced magnetosphere* around the cometary body similar in some ways to those seen around weakly magnetized or un-magnetised planets such as Mars and Venus. However, the solar wind magnetic field is not constant, varying in both strength and direction. Therefore, layers of magnetic field with different directions are embedded in the region surrounding the cometary nucleus - structuring referred to as "nested draping". This has been observed during the fast flybys of comet 1P, for which, a tentative model of how the magnetic field lines on either side of the nucleus are connected could be made (Raeder et al. 1987). Performing a flyby with magnetometers on three spacecraft at different distances will, for the first time, allow a reconstruction of the shape of the draped magnetic field. Three chords through the upstream induced magnetosphere will deliver three lines of magnetic field strength and direction that can be integrated into a whole, thus describing the field line draping structure of the induced magnetosphere. If the flyby is slow, dynamic draping can also be observed, first shown by *Rosetta* (Volwerk et al. 2019). When the convection velocity of the magnetic field towards the comet is faster than that of the spacecraft past the comet, then the time variation of the magnetic field between the spacecraft can show how the nested draping is moving towards the comet. It was also shown that the draping of the magnetic field is not confined to the solar wind magnetic field plane, but can be shifted (Koenders et al. 2016).

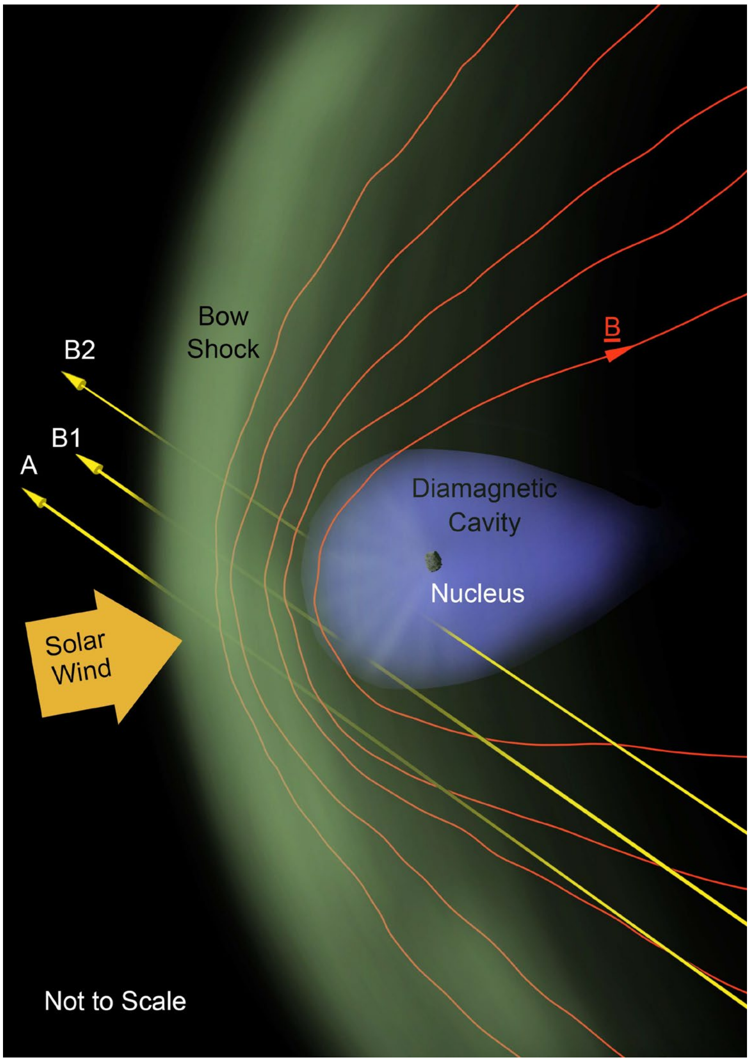

Figure 13: Multi-point measurements will determine the scale and shape of several structures in the comet-solar wind interaction. The time at which each of the three spacecraft/probes cross (or do not cross) the bow shock (green) and diamagnetic cavity (blue) will determine their shapes and scales. The magnetic field (red) will also be probed using magnetometers on all the three platforms.

In strongly outgassing comets, the solar wind-comet interaction forms a region immediately surrounding the nucleus called the diamagnetic cavity. This cavity is devoid of a magnetic field and prevents the solar wind's full penetration into the region closest to the nucleus. First observed in an artificial comet (through a barium release in the solar wind just outside the Earth's magnetosphere (Bernhardt et al. 1987), this cavity was also found in 1P by *Giotto*, extending up to 4,000 km from the nucleus. At 67P, *Rosetta* repeatedly detected the cavity, which extended only a few 10s to 100s km from the nucleus. The size of this magnetic field free region depends on the activity of the comet, and with 67P being much less active than 1P, the cavity size was accordingly much smaller. Due to the long residence time of *Rosetta* at 67P, it was found that the cavity boundary is very dynamic, moving in and out but, with only one spacecraft only limited information on the boundary could be obtained.

The exact mechanism that sustains the diamagnetic cavity is not understood and requires more measurements to determine which processes are responsible. The plasma in the cavity is much quieter than outside it and is much more dominated by cold electrons (Odelstad et al. 2018). The diamagnetic cavity boundary - observed only at 1P and 67P - seemed to be very unstable in both. The amplitude of this instability was thought to be small at 1P (Neubauer 1987), but large at 67P (Götz et al. 2016). At 1P the boundary thickness was determined to be 25 km, a value that also agreed with simulations for 67P at perihelion. With this assumption, Götz et al. (2016) found that the current density in the boundary was probably of the order of a few μA/m^2, although this could not be proven unambiguously with just single-point measurements. Only rough estimates of the boundary velocity could be derived.

The boundaries between different regions are asymmetric and highly variable in both space and time. They depend on both the activity of the comet and variations in the upstream solar wind conditions. Edberg et al. (2016a, b), Hajra et al. (2018), and Götz et al. (2018) showed that drastic changes occurred in the plasma at 67P, when interplanetary coronal mass ejections or co-rotating interaction regions passed the comet. To advance our understanding of the physics of these interactions, we need to go beyond what was possible with previous missions, all of which could only measure at one location at one time, by measuring at more than one position simultaneously, allowing spatial variations to be separated from temporal changes. Whether one, two, or all three of the *Comet Interceptor* platforms will enter the diamagnetic cavity, will on its own give information on the cavity's size and shape, as well as indications of its dynamics, and will be expanded upon by other measurements.

Solar wind charge exchange produces cometary ions as well as energetic neutral hydrogen and helium that can be observed remotely through ENA imaging (Simon Wedlund et al. 2016, 2017, Nilsson et al. 2017, Simon Wedlund et al. 2019a, b, c): their presence testifies to the efficiency of energy and momentum transfer between the solar wind and the cometary coma. Observations of ENAs are also useful to characterise plasma interactions in the region where the solar wind reaches deepest into the neutral atmosphere (Ekenbäck et al. 2008), possibly partaking in the sputtering of the cometary nucleus's surface (Nilsson et al. 2015). Ion chemistry within the coma also depends on neutral gas composition and, therefore, ion observations can shed light on the bulk composition of the nucleus, and the still poorly understood complex chemical and photo-ionisation reactions in the coma (Haeberli et al. 1995, Fuselier et al. 2016, Beth et al. 2017, Heritier et al. 2017).

Figure 14 The highly-structured ion tail of Comet C/2016 R2 (Pan-STARRS). Image: ESO, under licence Attribution 4.0 International (CC BY 4.0).

Waves take on an important role in the cometary plasma environment, transferring energy across boundaries and heating particle populations through wave-particle interactions. The plasma environment of a comet is a complex mix of ions of different species and origin and relative velocities, electrons of different temperatures, neutral molecules and dust particles of different sizes and charge states. Solar wind interactions with the cometary plasma gives rise to instabilities that drive waves of various kinds, including ion-cyclotron and/or mirror-mode waves (e.g., Mazelle et al. 1991), harmonic waves created by the ion-Weibel instability (the "singing comet" waves found by *Rosetta*; Weibel 1959, Richter et al. 2015, Meier et al. 2016, Glassmeier 2017), lower hybrid waves (e.g., Karlsson et al. 2017), and ion acoustic waves (e.g., Gunell et al. 2021). It is, however, not clear in which region of the coma these waves are present and how they depend on comet activity. Through multipoint measurements in the coma one can determine, in principle, the temporal and spatial development of the waves. Going from single spacecraft to multi-spacecraft observations thus enables new insights into both the physics of the waves themselves and how they affect boundaries and the surrounding plasma.

The comet-solar wind interaction region can also be observed remotely, due to resonance fluorescence processes occurring in common ions such as CO^+ and H_2O^+. The structures observed in the ion coma and tail reveals the spatial distribution and motion of cometary ions, e.g., *Figure 14*. Coma and near-tail ions will be observable with *Comet Interceptor* cameras, providing complementary observations of ion structures and their dynamics, especially during the approach to the comet. The rate of motion and relative densities of these structures can be compared to the *in-situ* observations, providing ground truth data for remote plasma observations from Earth.

2.4 Proposed measurements with *Comet Interceptor*

The multiple spacecraft structure of Comet Interceptor means that the comet will be observed from different angles during the flyby, building up a 3D picture of the nucleus, coma, and interaction with the solar wind. This will allow differences in time (e.g., due to the changing activity of the comet) and in space (e.g., due to inhomogeneities in the outgassing pattern) to be separated, which has not been possible in any previous flyby mission, or even with Rosetta, which could only sample one area of the coma at a time.

In this section we summarise the broad categories of measurement relevant for nucleus and coma environment science and unique capabilities that *Comet Interceptor* will provide. Details of the requirements and flow down to specific measurements are given in Section 3.

Concerning nucleus science, *Comet Interceptor* will:

- measure the size, shape, and rotation rate of the target comet nucleus.
- return resolved images of the surface that reveal its morphology.
- constrain the nucleus composition directly via remote sensing observations (imaging, spectroscopy, and polarimetry).
- measure directly, for the first time at a comet, nucleus thermal properties via thermal infrared imaging.

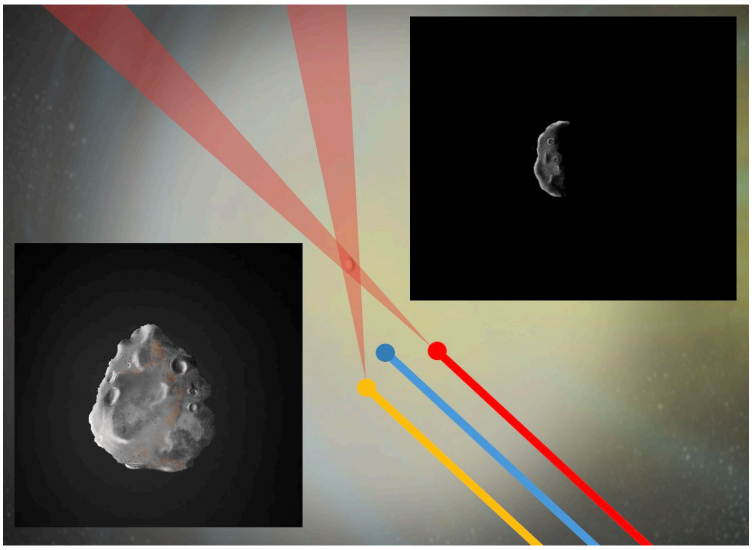

Figure 15: The remote sensing instruments aboard all three platforms will return complementary views of the nucleus from different directions.

Visible and near-infrared images of the nucleus will be returned from three different viewpoints, as illustrated in *Figure 15*: from the main spacecraft (A) and both probes. The highest resolution images are expected to have a resolution of ~10 m / pixel, comparable to previous comet flyby missions, and allowing direct comparison of an LPC with the more evolved short period comet nuclei imaged previously. The highest resolution images will come from the CoCa instrument on Spacecraft A, which will track the nucleus through the flyby. Probe B1 will have both narrow- and wide-angle visible cameras to image the nucleus and its surroundings from a fixed orientation during closest approach, and the OPIC instrument, on probe B2, will return resolved images of the nucleus and the inner coma from a different angle shortly before closest approach. Composition information will come from multi-colour imaging (four broadband filters in the visible range in CoCa; a tuneable hyperspectral imager in the 0.9 - 1.7 µm near-infrared region and fixed narrowband filters between 8.9 and 21.6 µm in MIRMIS) and point spectroscopy in the 2.5 - 5 µm range (MIRMIS/MIR). Unique insights into the physical properties of the surface layers (particle sizes, thermal inertia) will come from visible wavelength polarimetry measurements (EnVisS) and thermal-infrared temperature measurements (MIRMIS).

Data will be captured through the flyby from a wide range of phase angles, further allowing the reflectance properties of the nucleus (and different resolved regions on it) to be assessed. The variety of viewpoints, and the possibility to constrain the unilluminated portions of the nucleus through a combination of thermal imaging and imaging of its silhouette against the background coma, will give good constraints on the size and shape of the entire nucleus, even if, due to the flyby nature of the mission, detailed imaging can only be returned from one side. The nucleus rotation rate will be constrained by both resolved imaging and images of the unresolved nucleus in the days before and after the flyby by CoCa.

A mission to a relatively pristine LPC will be an important advance in cometary science as a whole, as direct measurements of the coma composition can be related to nucleus ices with a very different processing history, and the distribution of active areas can be studied. Mapping the distribution of neutral gasses in the coma will give information on bulk composition and nucleus inhomogeneity and will probe coma chemistry. Measuring the composition of the coma at different distances from the nucleus will provide information for coma chemistry models. Remote sensing of the large-scale distribution of different species will be combined with *in situ* sampling to derive production rates of the individual volatile species for the time of the flyby (for comparison to ground-based observations). Identification of parent and daughter neutral and ion species will enable an assessment of their relationship in the coma. All of these individual elements will combine to give a comprehensive picture of the similarities and differences between comets with different evolutionary histories. The spacecraft measurements are critical: while we have ground-based observations of many comets of different classes, it is unclear what differences are evolutionary versus inherent. Comparison of the direct inner coma measurements at an LPC and with previous JFC missions, in particular *Rosetta*, will help disentangle coma processes and long-term evolutionary trends.

Comet Interceptor will detect small-scale structures within the coma, <1 km in scale for a slow flyby, through *in situ* measurements of dust flux (DISC sensor within DFP on both spacecraft A and probe B2) and gas density (MANiaC), along with remote sensing imaging from cameras on all platforms (CoCa, MIRMIS, WAC, NAC, OPIC, EnVisS). Such an analysis, combined with nucleus shape observations, will supply information about the complex coma–nucleus relationship. For a bright LPC, measurements of even larger-scale spatial distribution of species in the coma will be possible from ground-based observatories and will provide, for the very first time, a clear link between the features observed from the ground and the nucleus of a comet.

Mapping of the dust and neutral gas jets both near to and far from the nucleus, especially on approach and post-encounter, where dust jet and shell structuring can constrain the time history of nucleus activity, will reveal more active locations and periodicities in the ejection rate of material. The jets should be mappable to their source locations, tying into high resolution images of the nucleus. The composition of the gas jets can also reveal a considerable amount about the active regions, such as determining whether all active regions have the same composition, and whether or not the relative abundances of different ices vary across the body. Observations in the IR will isolate jet emission by H_2O, CO_2, and CO, but also typically less abundant species such as methane, ethane, and methanol. Spectral information about the coma, and, better still, spectral imaging, will be highly beneficial. The spatial distribution of neutral hydrogen would provide a time history of activity in the comet; this could be achieved with imaging of the Lyman-α line in the UV range. The composition of the coma can be measured directly using *in situ* observations by a mass spectrometer. Coverage of masses up to a few hundred Daltons (amu) would be particularly beneficial. More direct inferences about surface activity can be made using thermal maps of the nucleus. For these, the surface would need to be resolved to better than ~300 m for a 3 km-wide body.

Measuring *in situ* absolute densities of major neutral gasses (MANiaC) and comparing with ground-based observations will allow coma models used to deduce production rates from ground-based observations to be tested and constrained. This is crucial to interpret the wealth of ground-based data using a common baseline. These measurements will also allow *Comet Interceptor* will help investigate the contribution of distributed sources and the pathways leading to different gas species and their complex relation with the bulk composition. MANiaC mass spectroscopy will also reveal minor constituents of the gas coma, and isotopic ratios of D/H if the gas production rate is sufficiently high (and possibly the most abundant isotopes of O, C, and S), allowing detailed comparison of composition differences and/or similarities between a less evolved comet and results from *Rosetta* at 67P.

The EnVisS camera will provide unique, simultaneous all-sky brightness and polarimetric curves, allowing us to study the observed phase function curve and the degree of linear polarisation from the same data set, including the important forward- and back-scattering regimes. The combination of both datasets will yield key constraints for the physical properties of the dominant population of dust particles in the coma, alongside the dust mass distribution measured along two different trajectories by DFP/DISC.

A detailed characterisation of the plasma environment of a comet requires measurements of the magnetic and electric field strength and direction, the electron and ion distribution functions (density, temperature, and flow velocity vector), and the ion composition, in the different comet-solar wind interaction regions (e.g., solar wind, diamagnetic cavity) and at their boundaries.

Comet Interceptor will assess, through DFP sensors on spacecraft A and B2, and the B1 Plasma Suite, the energy, mass, and momentum transfer in the cometary environment, through the coma and across boundaries. Multi-point measurements of ions, magnetic fields, and nm- to mm-scale dust will elucidate the physics behind mass transfer and the consequences for both the coma and tail. Unprecedented ENA observations will help us to understand the role of charge exchange collisions in the transfer of energy and momentum from the solar wind to the coma. Solar wind and cometary ion and electron dynamics will enable the assessment of the amount of electrically-charged material impacting the (pristine) comet surface.

For the three magnetometers on this mission, the bow shock (or bow wave), the field-line draping pattern around the inner coma, and the diamagnetic cavity, are of specific interest, amongst other features. Using the spatial separation of the three spacecraft and their magnetometer measurements, one can deduce the three-dimensional shape of the magnetic field, and study the differences in magnetic activity. The magnetic field measurements also play a defining role in analysing the internal structure and type of the plasma boundaries.

Given the possibly high flyby speed, the planned high cadence measurements of the most prominent plasma properties (ion and electron density, electron temperature) are essential to capture as much as possible of the detailed spatial and temporal structure of the plasma. This will help in particular in studying the internal structure of the boundaries (shape, spatial extent, etc.). The ion coma and ion tail in its vicinity will be observed by the visible light cameras CoCa, WAC/NAC, OPIC and EnVisS on all three platforms.

3 Scientific requirements

The overall goal of the Comet Interceptor mission is to provide the first investigation of an LPC, and to sample different regions of the coma simultaneously. The scientific requirements that need to be met to achieve this goal can be conveniently divided into two Science Themes: Firstly, measurement of the properties of the cometary nucleus that will allow to compare an LPC with Short-period comet nuclei investigated by previous missions. Secondly, investigation of the coma, its connection to the nucleus (cometary activity) and its interaction with the solar wind will take advantage of the multi-point perspective through three spacecraft.

The two science themes are first broken down into top level Science Objectives (Level 0) that describe the properties of the target to be investigated. In the next step, each Science Objective is split in a series of Science Requirements (Level 1) that quantitatively describe the features, characteristics and processes that need to be measured to achieve the Science Objective. Finally, Level 2 Requirements describe the measurements by each instrument that contribute to meeting the Level 1 requirements.

The tables below list the Science Objectives and the Level 1 Science Requirements. The Level 2 Science Requirements are described in the Science Requirements Document (ESA-COMET-SCI-RS-001).

Science Theme	Level 0 – Science Objective
Comet Nucleus Science - What is the surface composition, shape, morphology, and structure of the target object?	Comet Interceptor shall characterise the target shape, size and rotation state.
	Comet Interceptor shall characterise the target morphology.
	Comet Interceptor shall assess the bulk composition of the target surface.
Comet Environment Science - What is the composition of the coma, its connection to the nucleus (activity) and the nature of its interaction with the solar wind?	Comet Interceptor shall characterise and map the bulk neutral composition of the coma and determine any local structure and connection to the nucleus.
	Comet Interceptor shall determine the isotopic composition of the coma.
	Comet Interceptor shall characterise the structure of the dust environment of the coma and determine any connection to the nucleus.
	Comet Interceptor shall characterise the coma dust properties, including reflectance and polarimetric properties and determine dust fluxes.
	Comet Interceptor shall determine motion and evolution of ion rays and other coma and tail features including dust and gas.
	Comet Interceptor shall characterise the plasma environment around the target, determine any resulting boundaries and assess energy, mass and momentum transfer.

Table 1: Science Objectives of Comet Interceptor

Level 0 – Science Objective	**Level 1 – Science Requirement**
Comet Interceptor shall characterise the target shape, size and rotation state.	*Comet Interceptor* shall establish the size and shape of the directly illuminated portion of the target to an accuracy of < 60 m.
	Comet Interceptor shall establish the size and shape of the unilluminated (potentially indirectly illuminated by backscattered sunlight) portion of the target to an accuracy of < 600 m.
	Comet Interceptor shall determine existence and location of any non-surface bound boulders with sizes > decametres in the vicinity of the nucleus.
	Comet Interceptor shall assess the rotation rate and angular momentum orientation with an accuracy of 1%.
Comet Interceptor shall characterise the target morphology	*Comet Interceptor* shall establish the existence and characterise surface features on the directly illuminated surface to an accuracy of < 20 m.
	Comet Interceptor shall establish the existence and characterise surface features in unilluminated areas (potentially indirectly illuminated by backscattered sunlight) to an accuracy of < 300 m.
	Comet Interceptor shall determine the target phase curve by measuring the geometric albedo of the surface > 5 different phase angles (φ) where max phase angle should be least 90° and include measurement at φ < 5°.
	Comet Interceptor shall assess the bulk surface roughness via polarimetric observations.

Comet Interceptor shall assess the bulk composition of the target surface	*Comet Interceptor* shall determine the colour of the object and its colour diversity at visible wavelengths.
	Comet Interceptor shall determine the thermal and spectral characteristics of the surface.

Table 2: Science Requirements corresponding to the Science Objectives related to the cometary nucleus

Level 0 – Science Objective	**Level 1 – Science Requirement**
Comet Interceptor shall characterise and map the bulk neutral composition of the coma and determine any local structure and connection to the nucleus.	*Comet Interceptor* shall map coma volatiles including H_2O, CO and CO_2 with an accuracy of 300 m
	Comet Interceptor shall determine absolute and relative densities of volatiles (e.g., H_2O, CO, and CO_2) along the fly-by trajectory.
	Comet Interceptor shall detect minor species (e.g., O_2) and potential distributed sources.
	Comet Interceptor shall make Hydrogen Lyman-alpha observations of the coma
	Comet Interceptor shall determine the large-scale gas coma activity, morphology and any variability therein.
Comet Interceptor shall determine the isotopic composition of the coma.	*Comet Interceptor* shall determine D/H and $^{18}O/^{16}O$ ratios in H_2O.
	Comet Interceptor shall investigate isotopes in other species including $^{34}S/^{32}S$ and $^{13}C/^{12}C$.
Comet Interceptor shall characterise the structure of the dust environment of the coma and determine any connection to the nucleus.	*Comet Interceptor* shall determine the large-scale dust coma activity, morphology and any variability therein.
	Comet Interceptor shall determine the inner dust coma brightness distribution to potentially capture evidence of non-$1/r^2$ particle distributions resulting from processes such as acceleration, sublimation, and/or fragmentation.
	Comet Interceptor shall establish evidence for (and any variation of) dust emission from the surface by measuring reflected light from dust in the vicinity of the nucleus.
	Comet Interceptor shall determine the existence (or not) of local dust structures in the coma.
Comet Interceptor shall characterise the coma dust properties, including reflectance and polarimetric properties and determine dust fluxes.	*Comet Interceptor* shall measure the mass and fluence of dust in the range 1-200 μm, where possible with multipoint measurements.
	Comet Interceptor shall search for the existence of, and if found characterise, dust particles in the range centimetre – decimetre (chunks and snowballs).
	Comet Interceptor shall determine the compositional diversity of the dust within the comet coma.
	Comet Interceptor shall determine coma dust reflectance and polarimetric properties at visible wavelengths.
Comet Interceptor shall determine motion and evolution of ion rays and other coma and tail features including dust and gas.	*Comet Interceptor* shall produce maps of ion rays via wide field imaging of the coma
	Comet Interceptor shall determine the existence (or not) of in-situ plasma signatures correlating to features observed through wide field imaging of coma.
Comet Interceptor shall characterise the plasma environment around the target, determine any resulting boundaries and assess energy, mass and momentum transfer.	*Comet Interceptor* shall determine the electron, ion, ENA, E and B field environment around the comet.
	Comet Interceptor shall assess and quantify coupling between neutral, dust and plasma, including potential assessment of dust charging.
	Comet Interceptor shall identify plasma structures and boundaries and characterise, where possible, with multipoint measurements.
	Comet Interceptor shall characterise the plasma wave environment ($\lambda \geq 2$ km) to constrain energy and momentum transfer across the coma.

Table 3: Science Requirements related to the cometary coma environment.

4 Payload

The Comet Interceptor payload was selected to fulfil the mission Science Objectives. For the Nucleus Theme, the Comet Camera (CoCa) on Spacecraft A will determine the physical properties of the nucleus with high resolution images, while the Infrared spectra taken by the Modular InfraRed Molecules and Ices Sensor (MIRMIS) will provide information about the composition and the thermal properties. They will be supported by the Narrow Angle Camera (NAC) on probe B1 and the Optical Periscope Imager for Comet (OPIC) on Probe B2, which will image the nucleus from perspectives different from those of Spacecraft A, providing stereo views and increasing the fraction of the surface that can be investigated by the flyby.

For the Comet Environment Theme, the coma composition will be measured *in situ* by the Mass Analyzer for Neutrals in a Coma (MANiaC), including measurement of isotopic ratios. Gas composition measurements through remote sensing will be performed by MIRMIS. In addition, the Hydrogen Imager (HI) on probe B1 will monitor the cometary water production rate from months before the flyby until end of its operations. The spatial distribution of dust will be investigated from three different viewpoints by CoCa on Spacecraft A, the Wide Angle Camera (WAC) on Probe B1, and OPIC and the all-sky imager Entire Visible Sky (EnVisS) on probe B1. EnVisS will additionally constrain dust properties through polarimetric measurements, and the Dust Impact Sensor and Counter (DISC), part of the Dust, Fields, and Plasma (DFP) instrument, will measure the mass distribution of dust particle colliding with both Spacecraft A and Probe B2. For the investigation of cometary plasma and its interaction with the solar wind, the magnetic field will be measured simultaneously by magnetometers on all three spacecraft, and plasma properties will be derived from measurements of three spectrometers as part of DFP and an ion mass spectrometer as part of the Plasma Suite (PS) onboard Probe B1.

The following subsections provide an overview of the Comet Interceptor scientific instruments.

4.1 Spacecraft A

4.1.1 COmet CAmera (CoCA)

The camera system on-board Spacecraft A, CoCa, is required to provide detailed imaging of the nucleus and the innermost coma of the target. The design uses previous heritage to establish a baseline performance that surpasses that of previous fly-by missions to comets. The instrument is based upon two elements. Firstly, it uses the telescope of the Colour and Stereo Surface Imaging System (CaSSIS) that is successfully operating at Mars on the European Space Agency's ExoMars Trace Gas Orbiter (TGO). Secondly, the CoCa design uses the detector system of the JANUS instrument from ESA's JUICE mission. By integrating these two elements, CoCa can achieve an angular scale of 8 µrad px^{-1}, which is nearly a factor of three superior to that of the Halley Multicolour Camera on-board *Giotto*. The detector system uses a rolling shutter technique to allow rapid image read-out with a minimum possible exposure time of 220 µs to avoid motion smear at closest approach for even the highest velocity fly-bys. A major difference here is that, unlike *Giotto* which was a spinning spacecraft, *Comet Interceptor* is a three-axis stabilised system implying that the exposure times can be selected. The detector allows saturation of the nucleus without blooming of charge. This, in turn, implies that the exposure times of selected images can be programmed to provide high signal to noise observations of the dust coma while saturating on the nucleus. This capability will increase the flexibility of the mission if targets are eventually found that have only weak dust emission.

CoCa will be equipped with four selectable interference filters covering the sensitivity range of the detector (roughly 400 nm to 1000 nm). The filters will be around 150 nm in bandwidth and optimised to have approximately equal signal to noise ratio in all images of the nucleus. Low spectral resolution is not a disadvantage here as previous observations have shown that visible spectra are mostly featureless with a constant reflectivity gradient. Subtle broadband colour differences were seen by the *Rosetta* camera OSIRIS: the high signal to noise ratio being emphasized by the CoCa team would be of benefit in identifying similar colour variations across the surface of the target comet. The filters are mounted in a filter mechanism that has been designed to switch filters accurately and quickly. This is to ensure minimum changes in phase angle between adjacent images to facilitate registration. A goal of 1 second between images, including a filter change, has been set. The detector and read-out electronics can provide two images per second if the filter is not changed. In most cases the change in phase angle for adjacent observations will be <1°. The passage through closest approach and imaging at high cadence will also provide a data set for establishing the 3D spatial distribution of dust in the inner coma using post-processing tomography techniques.

The instrument is capable of acquiring around 2500 images during the encounter. Data compression (using a JPEG algorithm used extensively on CaSSIS) and sub-framing are foreseen to ensure that the on-board storage produces no practical limit to the flexibility of the data acquisition. It is intended that the instrument will be set into a "mode" by command and will continue imaging in this mode until there is a mode change or until CoCa is told to stop. This has the advantage that CoCa operates autonomously with pre-defined modes that can be programmed in flight and therefore adjusted to the properties of the final target post-launch. Failure detection and recovery is also foreseen within the flight software in the event that an upset occurs during the encounter sequence. The system at this stage still allows for real-time downlink if this is considered feasible following detailed spacecraft design.

During the proposal phase, it was established that an instrument based on extensive heritage could meet all of the scientific objectives of an imaging system on *Comet Interceptor* Spacecraft A. The current instrument design will

- Determine the size, shape, and albedo of the nucleus
- Identify features on the nucleus at <20 metres resolution (assuming a nominal 1000 km fly-by) and allow comparison with similar observations of the surfaces of short-period comets
- Establish the reflectivity spectral gradient of the nucleus and of sub-regions on the nucleus
- Search for evidence of surface ices for comparison with *Rosetta* and *Deep Impact* observations of SPCs.
- Determine the spatial distribution of dust emission from the nucleus (including the dayside/nightside emission ratio, which may have implications for the presence of super-volatiles such as CO)
- Investigate and constrain the properties of the acceleration region of the inner coma by studying dust column density profiles
- Constrain the rotation of the nucleus through, as a minimum, observation of dust coma structures
- Establish the direction and relative magnitudes of jet-like structures for correlation with dust impact events on the spacecraft
- Provide pointing information including determination of the fly-by geometry
- Identify impact events on the spacecraft by providing evidence of uncontrolled Spacecraft Attitude changes.

The CoCa design is shown in *Figure 16.* The Camera Support Unit (CSU) has numerous elements. The open structure in *Figure 16* is a 13.5 cm diameter 4-mirror off-axis telescope with a focal length of 880 mm following the design for the CaSSIS telescope on TGO. The structure is carbon-fibre reinforced plastic (CFRP). Following the CaSSIS experience, a small change to the internal baffling at the intermediate stop (between mirror M2 and M3) has been made and improved front baffle has been designed. Otherwise, the design is unchanged. The mirrors are silver coated, providing a field of view that is larger than the active area of the detector in the focal plane. The open structure ensures low mass and will finally be wrapped in multi-layer insulation to produce a light-tight unit. The telescope is mounted on a baseplate that also supports the detector and filter wheel assembly. The detector is a spare of the development for JANUS, the imaging system on JUICE. The sensor is a back-side illuminated (BSI) CMOS device from e2v with 1504 x 2000 pixels and 7μm pitch, a peak quantum efficiency exceeding 90% and a full-well of 27000 e^-. A radiator will be used to reduce the sensor temperature, with -30°C being the goal, although nominal operation can be achieved at 0°C. Combined with the telescope system, the detector provides a field of view of 0.69° x 0.92°. The filters (*Figure 17*) will use fused silica substrates with standard interference coatings, designed for high throughput with sharp cut-offs and high out-of-band rejection. The baseplate isolates the CSU from the spacecraft using isostatic mounts in order to limit the thermo-elastic influence of the spacecraft on the instrument. The PEU houses the proximity electronics for the detector and is mounted close to the CSU. The ELU provides power conversion, instrument control, and data management.

Considerable effort has been invested in protecting CoCa from hyper-velocity dust impacts during the fly-by. It is to be recalled that HMC was damaged severely during the 1P/Halley encounter despite being mostly behind the Whipple shield of the spacecraft. In the case of *Comet Interceptor*, a rotating mirror assembly (RMA) has been developed which will allow CoCa to be mounted behind the protection shield while still providing a continuous view of the nucleus.

The RMA has two elements (*Figure 18*) - the SMA (Scan Mirror Assembly) and the SME (Scan Mirror Electronics). The SMA is a mechanism holding the folding mirror and that will rotate this mirror in order to orient the field of view of CoCa towards the comet during encounter. It is based on a brushless DC motor moving the mirror via a gear system and an optical position sensor in order to allow closed loop control. The mechanism will be driven by the SME that will take care of powering the motor to position the folding mirror based on encounter parameters provided by the spacecraft platform combined with the read-out of the position sensor. The SMA includes a protection system that will hide the mirror from incoming dust particles during the most critical part of the encounter, when the spacecraft is closest to the nucleus.

The CoCa and RMA system will be provided by a highly experienced team from Switzerland, Germany, Hungary, Spain, and Belgium. Furthermore, a clear hand-over of Instrument Lead Scientist responsibilities has been defined for CoCa at the time of instrument delivery to the spacecraft.

Instrument pixel scale	8 µrad/px
Field of View	0.69° x 0.92°
Detector	CIS115 Back-side illuminated CMOS image sensor
Pixels	1504 x 2000
Pixel size	7 x 7 um
Exposure times	220 µs (fly-by) to 15 min (identification), rolling shutter
Imaging rate multi-colour	≥ 1 frame per second
Imaging rate single colour	≥ 2 frames per second
Filters	475 nm (Δλ=150 nm) BLU 675 nm (Δλ=100 nm) ORG 775 nm (Δλ=100 nm) RED 900 nm (Δλ=150 nm) NIR
Mass	13.5 kg (3 units)
Power	19 W average
Volume	CSU: 350 x 460 x 550 mm^3; PEU: 210 x 160 x 70 mm$^{3;}$ ELU: 120 x 240 x 180 mm^3
Data I/F	Spacewire
Instrument memory (holding science data)	2 x 128Gbit
Max data volume	128Gbit uncompressed

Table 4: The main characteristics of the CoCa instrument.

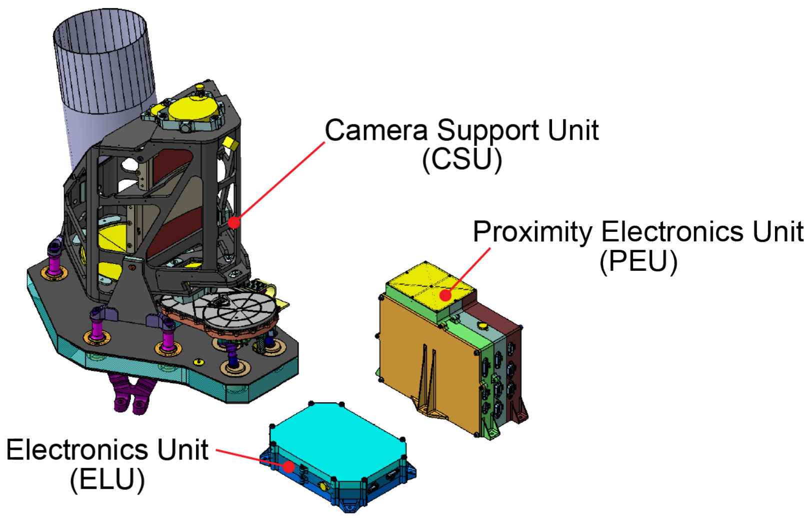

Figure 16: CAD/CAM of the CoCa instrument. Left: The Camera Support Unit (CSU). Right: The Electronics Unit (ELU). Centre: The Proximity Electronics Unit (PEU).

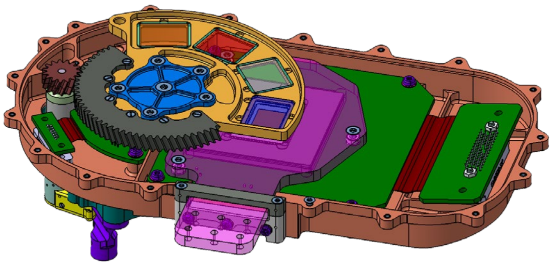

Figure 17: The filter wheel assembly with four filters. The detector is shown in pink below one of the filters. The filter wheel includes a launch lock to prevent motion during launch.

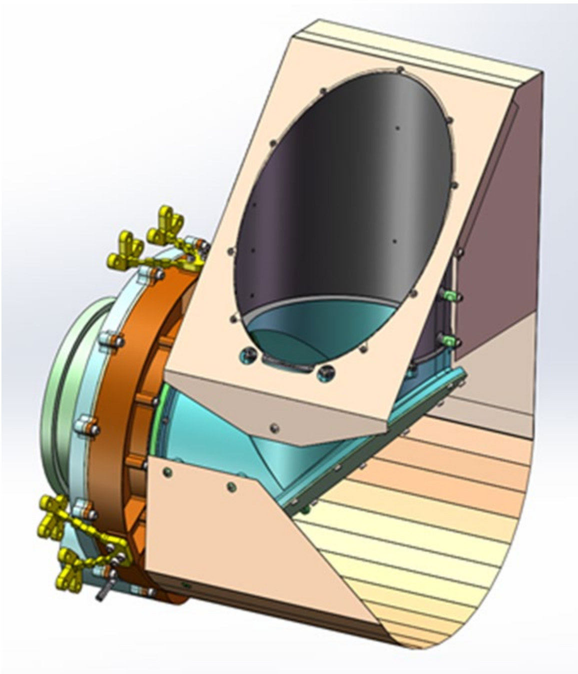

Figure 18: CAD/CAM drawing of the RMA showing the opening and the fold mirror mount (turquoise colour) and the mounting feet.

4.1.2 Modular InfraRed Molecules and Ices Sensor (MIRMIS)

4.1.2.1 MIRMIS Introduction

MIRMIS is the multispectral and hyperspectral imaging system for *Comet Interceptor* and is mounted on Spacecraft A. With its wide (0.9 – 25 µm) spectral range and mapping capability MIRMIS, as part of the wider *Comet Interceptor* payload, is designed to meet the mission's top-level science goal of understanding the diversity of comets by mapping the composition and temperature of the nucleus and coma.

The MIRMIS instrument directly addresses four of the top-level science questions in the *Comet Interceptor* science requirements document [ESA-COMET-SCI-RS-001] (Section 3):

MIRMIS comprises two modules that contain a multi-spectral thermal (6-25 µm) infrared imager (MIRMIS/TIRI), a near infrared (0.9 – 1.6 µm) hyperspectral imager (MIRMIS/NIR) and a mid-infrared (2.5 -5 µm) point spectrometer (MIRMIS/MIR) with an integrated command and data handling unit (*Figure 19*, *Table 5*).

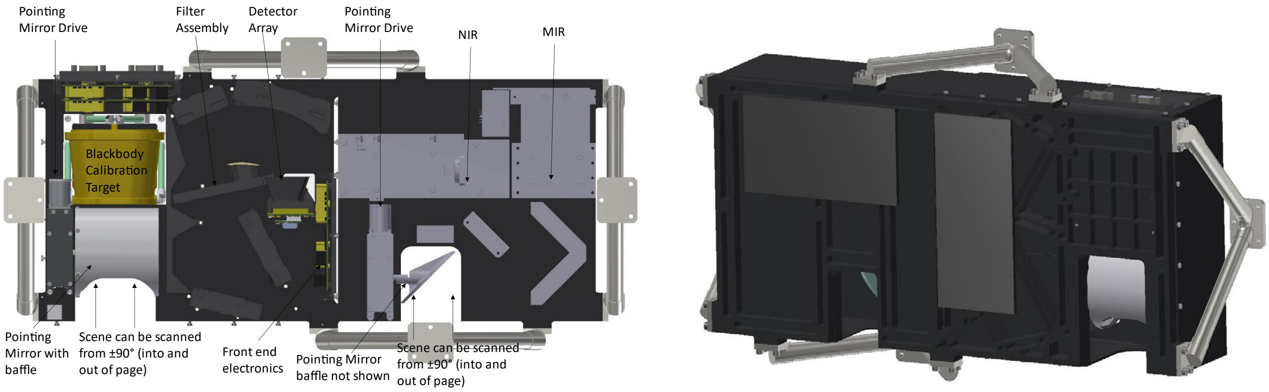

Figure 19: (Left) MIRMIS TIRI/MIR/NIR mounted on a common optical bench. Total module volume: 548.5 mm (x) x 282.0 mm (y) x 126.8 mm (z). (Right) instrument cover showing instrument and MIR detector radiators.

Scientific performance summary	Spectral range 0.9 to > 25 µm using three channels: • MIRMIS NIR - hyperspectral camera 0.9 to 1.7 µm • MIRMIS MIR - single-point spectrometer ~2.5 – 5.0 µm • MIRMIS TIRI – Multispectral Thermal Imager ~6 – 25 µm
Key instrument numbers	**TIRI:** FoV = 9 x 7 degrees (7 µm diffraction limit)**,** IFoV = 0.26 mrad **NIR**: FoV = 6.7 x 5.4 degrees, iFoV = 0.18 mrad **MIR:** FoV = 2-degree circular (TBC) **Total Mass** (CBE): 8.8 kg with margin Standby average: 8.3 W Standby average with detector thermal control: 9.9 W Average science operating mode (Nucleus pointing): 11.2 W Average science operating mode (Coma monitoring): 9.7 W Total module Volume: 548.5 mm (x) x 282.0 mm (y) x 126.8 mm (z)

Table 5: MIRMIS instrument summary table.

4.1.2.2 MIRMIS Scientific Goal Summary.

Measurements of the spatial distribution of ices, minerals, gases (e.g., H_2O, CO_2, CH_4 etc.) and surface temperature are essential to constrain the formation, evolution of the *Comet Interceptor* target nucleus and coma. Mapping of the compositional diversity and thermal physical variation (via the thermal inertia) could indicate whether the nucleus is a rubble pile object with different evolutionary histories, or a uniform body formed as a single process.

By covering the spectral range 0.9 to 25 µm MIRMIS will map the ice mineral, and gas composition of the target nucleus and coma (*Figure 20*) and the distribution of surface temperatures on the nucleus.

4.1.2.3 MIRMIS Measurement Principle.

MIRMIS' integrated modules (NIR, MIR and TIRI) provide near-IR-mid-IR spectroscopy of the coma and thermal-IR multispectral mapping of the nucleus. For measurements of the coma's volatile inventory MIRMIS (NIR and MIR) will target the bright molecular fluorescence emission at (e.g.) 2.5 to 5 µm (*Figure 20*), including spectral regions that are sensitive to e.g., CO_2 that are unobservable from the ground. Spatially resolved mapping of coma fluorescence with MIRMIS (NIR) and point measurements (MIR) will measure the spatial distribution of the primary volatile molecules, identify trace gas species, characterize coma chemistry inhomogeneities and determine chemical abundance variations that can be traced to nucleus regions that are indicative of bursts. MIRMIS will also be able to measure nuclear ices and mineral compositions by targeting silicate mineral features (e.g., 1 and 2 µm), water ice absorption features (e.g., 2.7 – 3.0 µm), organics (3.0 – 3.6 µm), CO_2-ice (4.3 µm) and CO-ice (4.7 µm). MIRMIS' thermal infrared module (TIRI) will provide unique information on the temperature distribution on the nucleus and surface composition (*Figure 20*). By measuring the nucleus' diurnal response at multiple > 6 µm wavelengths, MIRMIS will provide key information on the surface and near sub-surface thermal physical properties (e.g., cold traps, boulders/powdered regolith). MIRMIS-TIRI uses multiple infrared spectral channels to determine the nucleus' composition and a broadband imaging capability to measure its temperature. Spatially resolved temperature maps provide information on potential volatile source regions.

4.1.2.4 Scientific Performance Summary

MIRMIS achieves the scientific goals (Section 0) by making measurements using three integrated modules contained in a single compact (*Table 5*) high heritage instrument (*Figure 19*).

The MIRMIS modules (NIR/MIR/TIRI, *Table 5*) share a common mechanical, thermal, and electrical interface to the spacecraft. MIRMIS instrument command and data handling unit (CDHU) is designed to allow independent operation (via a preloaded command table and on-board data storage) during the encounter with the *Comet Interceptor* target body. Each module is described below.

4.1.2.5 TIRI module design

The Thermal Infrared Imager (TIRI) module (*Figure 19*, left) is a high spatial resolution (~260 m from 1000 km closest approach), multichannel, thermal imaging radiometer optimized for *Comet Interceptor*.

TIRI uses gold-coated all reflective optics with f/1.4 and a 50-mm aperture. The optical design is derived from the TechDemoSat-1 CMS instrument modified to accommodate a larger array with higher pixel density.

A pointing mirror is used to direct the field of view onto the target object, a black body calibration target or a space view. Calibrations using the black body and space view will be performed immediately before and after each observation sequence. A two-mirror telescope directs the incoming infrared radiation onto a filter assembly used to define multiple spectral channels. This filter assembly is re-imaged onto an uncooled microbolometer array using a three-mirror relay.

Figure 21 shows the nominal arrangement of filters which are mapped onto the 640x480 pixel microbolometer array. The central portion of the array is used for broad band thermal imaging and narrow band filter strips (*Table 6*) can be used in pushbroom-like mode to build up images targeting mineralogical and detailed thermal investigations.

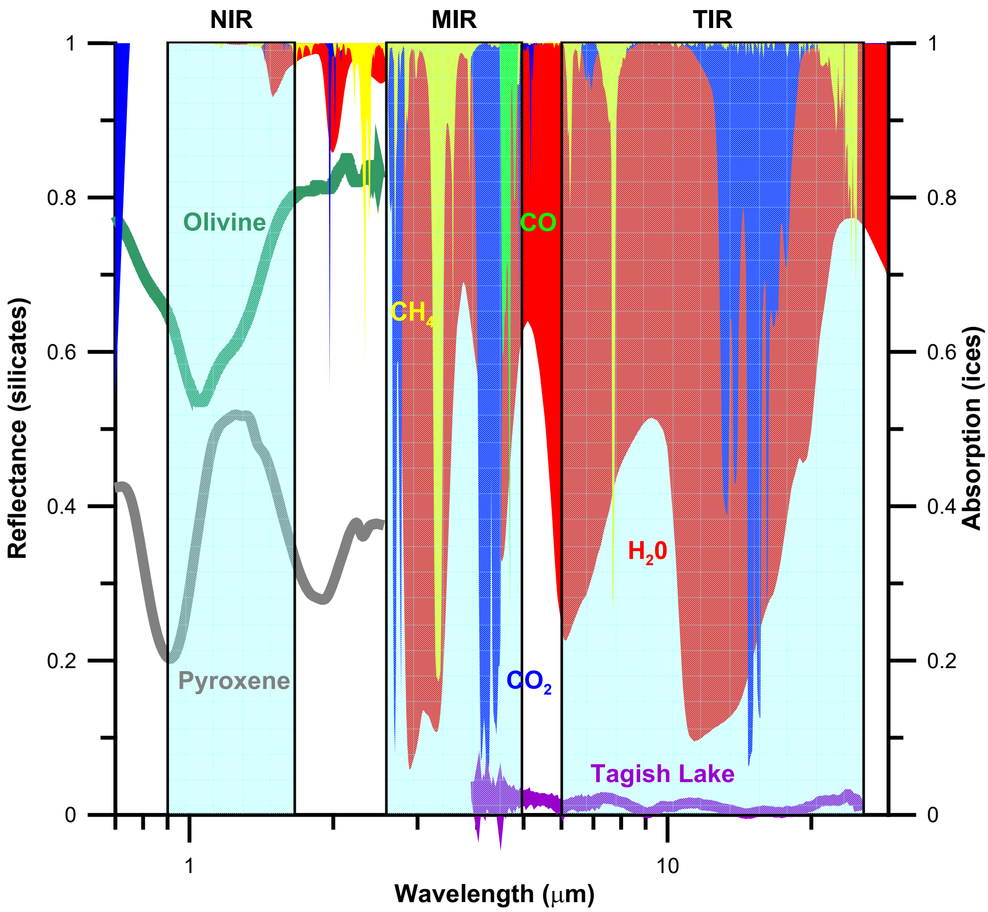

Figure 20: Spectral range and main compositional species covered by the MIRMIS instrument's spectral range.

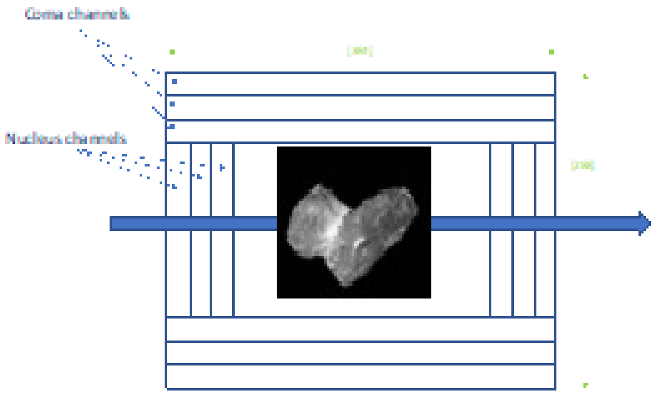

Figure 21: TIRI Field of View. Scale dependent on target and distance.

Centre (microns)	Half width
7.7	0.2
8.9	0.2
10.4	0.2
12.0	0.2
13.9	0.2
16.1	0.5
18.7	0.5
21.6	0.5
7-25	Broadband

Table 6: TIRI filter bandpass positions.

4.1.2.6 NIR module design

MIRMIS-NIR will provide information on the mineralogical properties of the nucleus, as well as nucleus shape information.

The NIR module (*Figure 22,* left) is a spectral imager capable of taking 2D images at freely selectable wavelengths at 0.9 - 1.7 µm region. The imager operation is based on a tuneable Fabry-Perot Interferometer, which is used as an adjustable bandpass filter. The filter is combined with a commercial-off-the-shelf InGaAs Focal Plane Assembly (FPA). The spectral datacube is formed by taking a sequence of multiple images at different wavelengths. The Field of View is ca. 6.7 x 5.4 degrees with 640 x 512 pixels.

The design is based on refractive optics, based on design utilized in the ASPECT imager on the MILANI CubeSat for ESA's HERA mission. Prototype of the NIR channel has been flying in low Earth orbit since November 2018 on-board the Reaktor Hello World nanosatellite.

4.1.2.7 MIR module design

The basic principle of the MIR channel (*Figure 22*, right) is the same as in the NIR channel. The difference is that in the MIR channel, the detector array is replaced with a single HgCdTe (MCT) photodiode. This simplifies the optics significantly, and only one lens is needed for the photodiode.

The preliminary field of view for MIR is ca. 2-degree circular, but this can be later adjusted to the scientific mission needs.

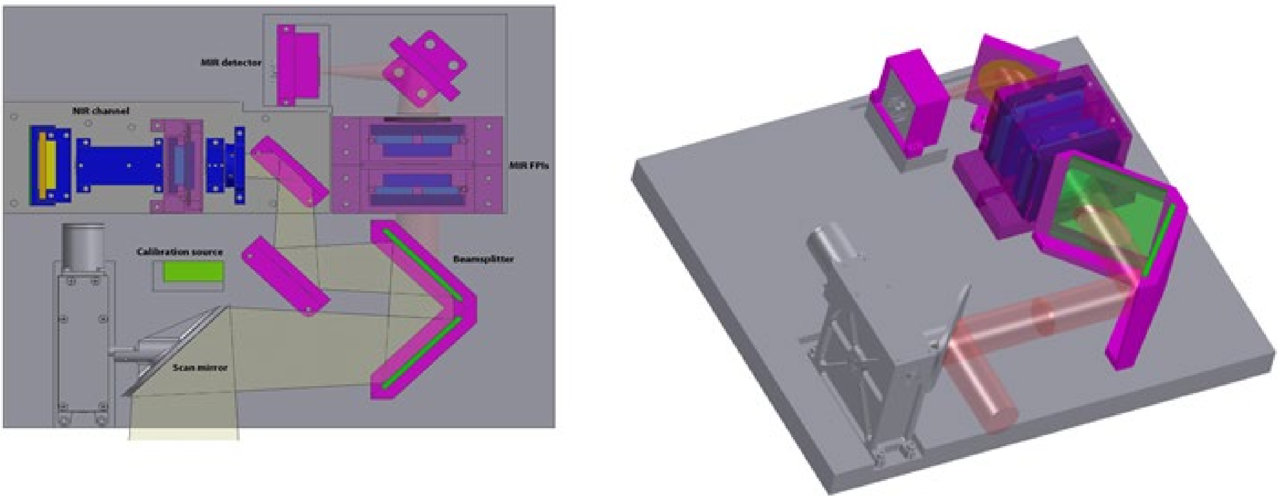

Figure 22: (left) MIRMIS NIR-MIR channel layout; (right) 3D model of the MIR channel, showing the beamsplitter, the FPI cascade and the detector.

4.1.3 Mass Analyzer for Neutrals in a Coma (MANiaC)

Comets that visited the inner solar system for the first time have thus far only been observed remotely by Earth and space-based telescopes. *Comet Interceptor*, and with it the Mass Analyzer for Neutrals in a Coma (MANiaC), will for the first time observe *in situ*, the composition of an LPC, or possibly a more primitive DNC, or even an IO or IC.

MANiaC is located on Spacecraft A and dedicated to the *in-situ* measurement of the neutral gas coma. MANiaC consists of two instruments, a time-of-flight mass spectrometer and a neutral density gauge. The mass spectrometer obtains the relative abundances of the major and a subset of minor volatiles. The neutral density gauge measures the total gas density. Combining the measurements of both instruments yields the absolute densities of a suite of volatile species along the fly-by trajectory.

From these measurements, elemental, molecular, and isotope abundances of the gas will be derived. Depending on the gas and dust activity of the comet, the combined measurements will address the following science questions:

- Monitoring the major volatiles H_2O, CO, and CO_2 in the coma to study the target's activity and associated gas mass loss rate. These results may also be combined and compared with Earth-based remote sensing observations.
- Deriving the D/H ratio in H_2O to study the provenience of the water ice in the comet and to investigate potential sources of the water on Earth.
- Assessing the amounts of key volatiles such as O_2 and other highly volatile species. Are there more highly volatiles compared to a comet that visited the inner solar system already multiple times?
- Obtaining an inventory of (complex) organic molecules and other species possibly relevant in pre-biotic chemistry.
- Measurement of icy grains' composition and abundance should some be collected in the ion source.

MANiaC is split into three units as shown in *Figure 23*: the Sensor Head Unit (SHU), the Bayard-Alpert style Neutral Density Gauge (NDG), and the ELectronic Unit (ELU). The SHU is based on the Neutral Gas Mass Spectrometer built for the Roskosmos Luna-Resurs mission (Wurz et al., 2012) and both SHU and NDG draw heritage from the *Rosetta* ROSINA Reflectron-type Time-Of-Flight (RTOF) mass spectrometer (Scherer et al. 2006) and the COmet Pressure Sensor (COPS) (Balsiger et al., 2007). Since the fly-by velocity in the range of 10 to 70 km/s will be much larger than the neutral gas speed (~1 km/s) MANiaC will be mounted on the spacecraft such that the aperture is always pointing in the direction of relative motion of the spacecraft.

To cope with the large range of possible fly-by velocities, both the SHU and the NDG contain antechambers for the thermalization of the incoming gas. Afterwards, the neutral gas entering the ion source will be ionized by impacting 70 eV electrons emitted by a hot filament. In the NDG, the resulting ions are measured as a current by a sensitive electrometer and in proportion to the gas density inside the antechamber and hence the surrounding coma. In the SHU, the newly formed ions are accelerated by a sharp extraction voltage pulse into the drift section. After passing the reflectron, i.e., an opposing electric field, the ions cross the drift section again before impinging on the Micro Channel Plate detector. Since the voltage pulse provides the same energy to all extracted ions, their arrival time on the detector can be converted into a mass/charge ratio. Hence after the extraction pulse a fast ADC records 65536 channels of 0.5 ns each. This corresponds to a range in time-of-flight between 0 and 32.768 μs and converts to a mass/charge range from

0 to ~1000 Da/e^-. Extractions are repeated every 100 µs, i.e., at 10 kHz, and the channels are histogrammed (summed) to a selectable number of extractions, resulting in a single mass-per-charge spectrum. The SHU is designed for a mass resolution of $m/\Delta m > 800$ for mass/charge > 40 Da/e^- and a density range of 10^{-6} to 10^{-14} mbar. Both the SHU and the NDG (density range of 10^{-5} to 10^{-11} mbar) will be operating continuously during the fly-by and measurements far from the comet will be used to assess the spacecraft background (see Schläppi et al. 2010). An adjustable measurement integration time between 0.05 and 100 s per spectrum (SHU) and pressure reading (NDG) is implemented to cope with the large range of possible fly-by velocities. After the fly-by the locally stored mass spectra will be compressed for later downlink.

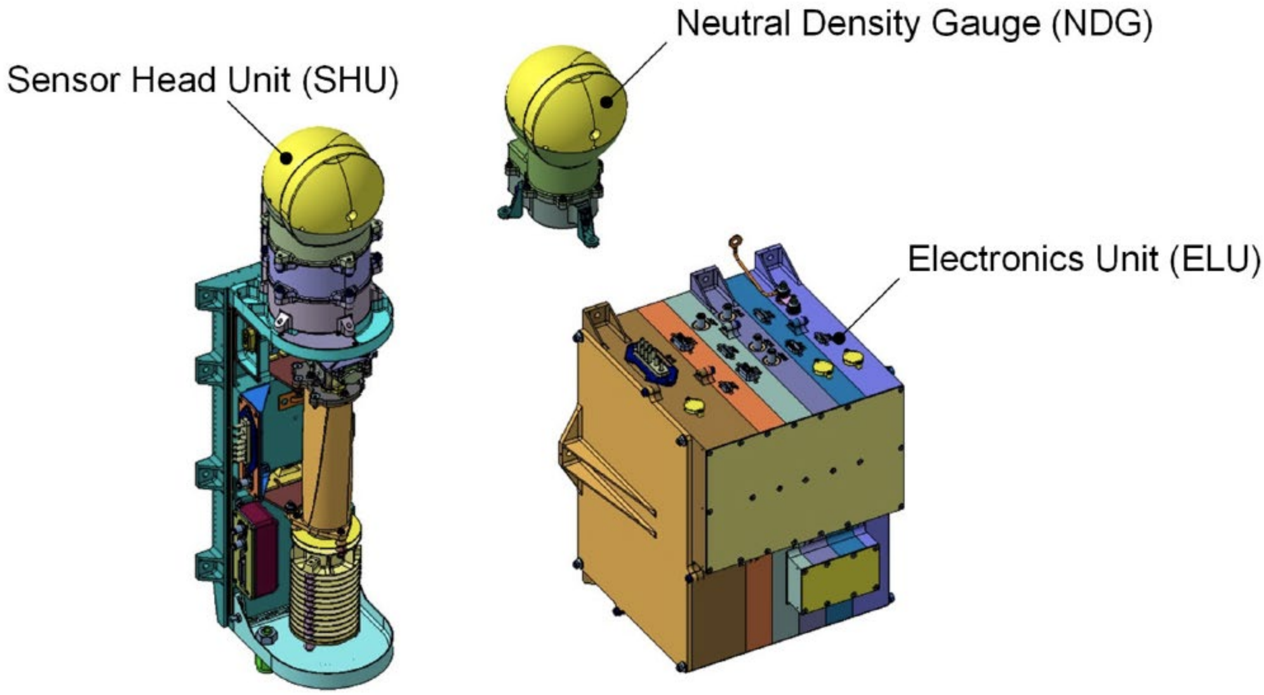

Figure 23: MANiaC consisting of a time-of-flight mass spectrometer (SHU, Sensor Head Unit), the Neutral Density Gauge (NDG), and the ELectronic Unit (ELU). For reference the long axis of the SHU corresponds to ~470 mm. Only the antechamber spheres of both the NDG and the SHU (marked yellow) are exposed to the gas and dust flow of the coma and are covered by dedicated dust shields. The rest is enclosed and protected inside the spacecraft.

MANiaC is being built by an international consortium formed by the Instituto de Astrofísica de Andalucía (IAA Granada, Spain), the Institut für Weltraumforschung (IWF Graz, Austria), the Institut de Recherche en Astrophysique et Planétologie (IRAP Toulouse, France), and Creotech Instruments S.A. (Piaseczno, Poland) under the lead of the University of Bern (Switzerland).

4.1.4 Dust, Fields, and Plasma (DFP-A)

The Dust Field and Plasma (DFP) package is a combined experiment dedicated to the multi-point *in situ* study of the multi-phased ionized and dusty environment in the coma of the target dynamically new comet and its interaction with the surrounding space environment and the Sun (*Figure 24*). The DFP will measure the magnetic field, electric field, plasma parameters (density, temperature, and speed), the distribution functions of electrons, ions, and energetic neutrals, spacecraft potential, and the cometary dust. in order to:

- Identify boundaries and regions in the cometary environment of a comet and its interaction with the Sun and the solar wind (e.g., bow shock, diamagnetic cavity) and to assess their structure.

- Map the dust and plasma phases around the target dynamically new comet.

- Assess the mass, momentum, and energy transfer in the cometary environment.

- Provide simultaneous magnetic field, plasma, and dust measurements to identify the interplay between the ionized and dusty phases around a comet and characterize dusty plasma properties.

- Map the solar wind – coma interaction.

- Describe and map the (i) electron, (ii) negative and positive ion, and (iii) energetic neutral atom distribution functions in the vicinity of the comet and in the interaction region with the solar wind.

- Identify the electron and ion kinetic processes that mediate the solar wind-comet interactions from ion kinetic scales down to electron scales.

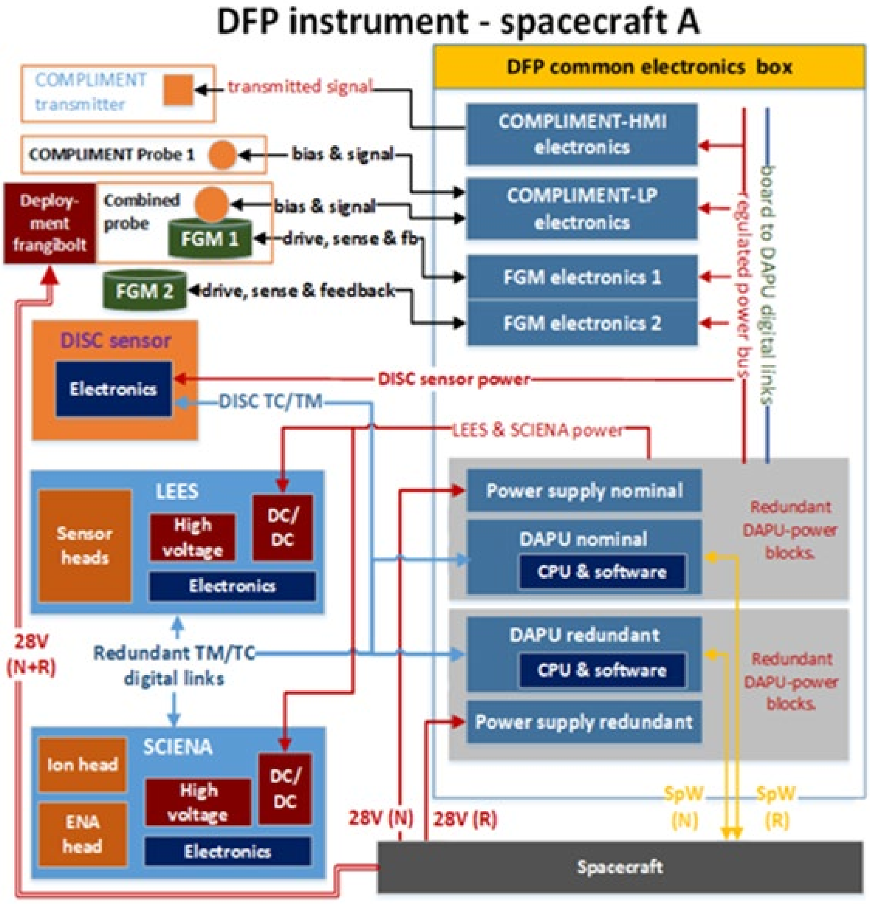

Figure 24: The configuration of the DFP instrument on Spacecraft A.

To enable these multipoint measurements, five instrumental sensors, common data processing unit DAPU, and power supply system PSU will be constructed and placed on Spacecraft A, and two sensors with the respective DAPU and PSU will be present on Probe B2 (see Section 4.3.3).

4.1.4.1 *DISC*

The Dust Impact Sensor and Counter (DISC) will be provided in two identical units: one will be mounted on SC/A and a second on S/C B2 (*Figure 25*). DISC is the DFP sensor devoted to the "*in situ*" characterization of cometary dust, in particular to count the dust particles populating the coma and to determine the mass of individual dust particles. DISC design is a direct heritage of the GIADA, an instrument on-board the *Rosetta* mission. DISC is a monitoring instrument with event driven acquisitions that will provide an in-situ characterization of dust particles in the coma of the comet for particles with masses in the range 10^{-15}–10^{-8} kg (for particles with mass > 10^{-8}kg, the dust particle count will be provided).

From the individual particle momentum measurement, knowing the relative speed between the S/Cs and the dust particles will be possible to determine the mass of individual impacting particles in particular for individual dust particles of the cometary coma impacting on the aluminium plate, mass distribution, count, impact duration, density structure. The expected range of particles momentum is between 3×10^{-11} and 2×10^{-03} kg*m/s, similar to the GIADA Impact Sensor wide measurement range.

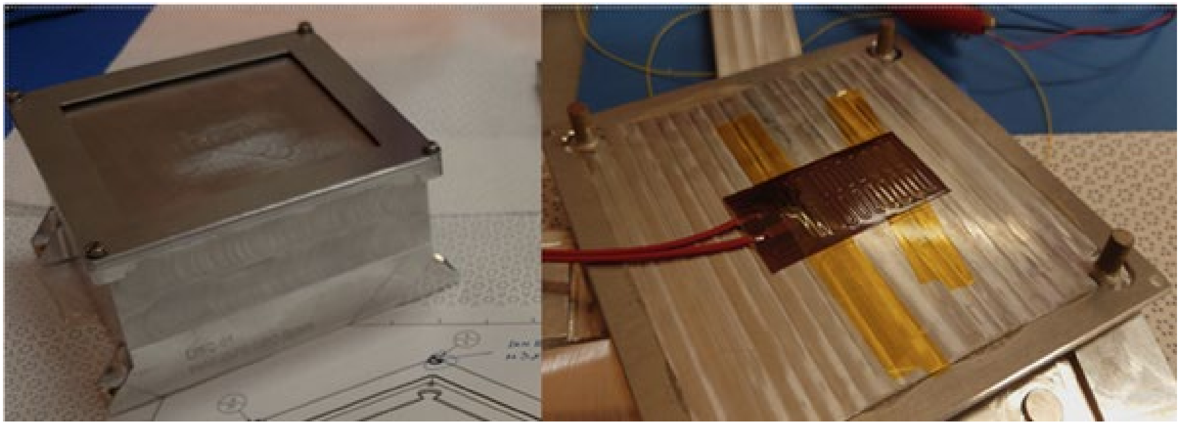

Figure 25: DISC Unit: left panel) assembled DISC breadboard; right panel) Sensing plate with glued PZTs at 3 corners DISC Unit: left panel) assembled DISC breadboard; right panel) Sensing plate with glued PZTs at 3 corners

4.1.4.2 *FGM-A*

The Fluxgate Magnetometer on Spacecraft A (FGM-A) will perform 3D magnetic field measurements for boundary detection & characterisation and for resolving structure inside the boundary. Furthermore, FGM-A will measure the magnetic field simultaneously with magnetic field experiments on-board probes B1 and B2 in order to resolve various wave modes (e.g., ion cyclotron waves, mirror modes). Its main properties are shown in *Table 7*.

Operation range	± 16000 nT (configurable)
Digital Resolution	2 pT
Noise	< 10 pT/sqrt(Hz) at 1 Hz
Absolute accuracy	± 1 nT (goal), ± 2 nT (requirement)
Mass	1.8 kg boom with sensors, 0.5 kg electronics
Power	1.2 W total
Temperature range	[-80; +60] °C (both survival and operation). No heaters installed.

Table 7: FGM-A properties.

The FGM-A fluxgate magnetometer is composed of two sensors (outboard and inboard) mounted on a deployable boom (with heritage from *Venus Express* and *Kompsat-2A*) and their electronic front-ends, which are hosted in the DFP CEBOX. The fluxgate outboard sensor has been merged with the COMPLIMENT Spherical Probe. The combined sensor consists of a hollow spherical Langmuir probe that harbours a fluxgate magnetometer at its centre. Special precautions have been taken to minimize the possible interference between both whiles at the same time being very lightweight.

4.1.4.3 *COMPLIMENT*

The COMetary Plasma Light InstruMENT unit (COMPLIMENT) will provide the following measurements: electric field and waves (one component), high cadence independent ion and electron densities, electron temperature(s), S/C potential, integrated EUV flux, nanodust impacts (signal processed by DAPU) in order to address the structure and dynamics of the ionized and dusty cometary environment and its interactions with the escaping cometary atmosphere.

COMPLIMENT (*Table 8, Figure 26*) is composed of three sensors: two electric spherical probes (8 cm), one of which is a merged Electro-magnetic sensor (COMPLIMENT + FGM-A), mounted on booms and a transmitter, two electronic boards (LP and HMI) for signal generation, reception, and treatment, plus dedicated software hosted on the DAPU.

Electric field component $\delta E(t)$	1 Hz-1.4 MHz2 V/m/sqrt(Hz)(>500Hz)
Electron density	10^2-10^5 cm^{-3}, <1 Hz
Density fluctuation $\delta n/n$	DC-10 kHz
Ion density N_i	10^2-10^5 cm^{-3} , <1 Hz
Electron Temperature T_e	0,01-30 eV , <1 Hz
S/c potential U_{sc}	<100 Hz
Integrated solar flux	<1 Hz

Table 8: COMPLIMENT properties

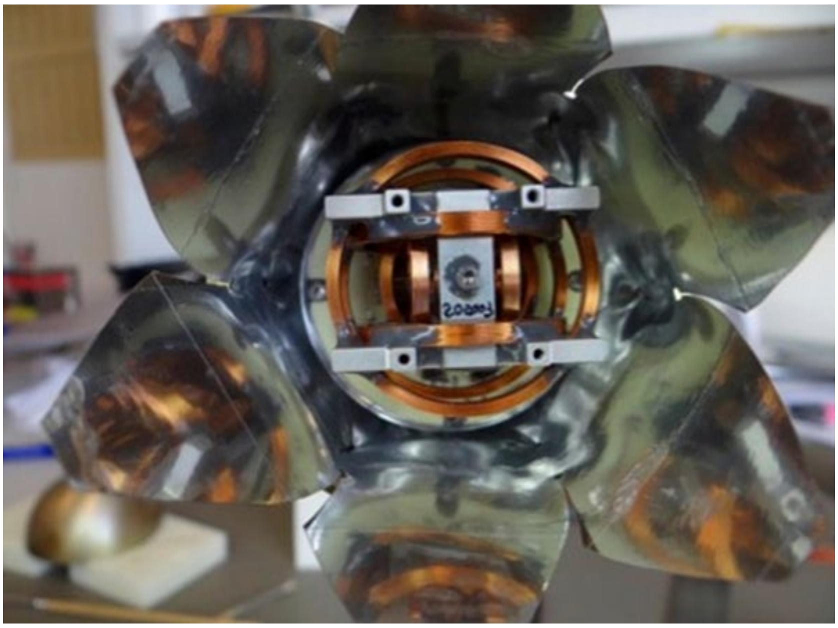

Figure 26: Integration of merged probe COMPLIMENT+FGM-A.

4.1.4.4 *SCIENA*

The Dust, Field, and Plasma Solar wind and Cometary Ions and Energetic Neutral Atoms (DFP-SCIENA) is an instrument to measure energetic particles of solar wind and cometary origin, both with and without charge (*Table 9, Figure 27*). The ion observational capabilities allow for direct detection of solar wind and cometary ions, providing energy, direction, and a rough mass estimate. These measurements are necessary to see the three-dimensional flow of plasma in the comet magnetosphere in order to assess the mass, momentum, and energy flow and transfer between different plasma regions, identification of plasma boundaries such as the bow shock, solar wind void and similar. The energetic neutral atom (ENA) measurement capability allows us to study the direct interaction of the solar wind with the neutral atmosphere, providing continuous monitoring of the dynamic pressure of the solar wind, an estimate of the position of the regions of strongest interaction between the solar wind and the coma as well as the coupling between the coma and the cometary ions. The ENA measurements are thus needed to understand energy transfer in the coma environment, boundary formation, and to disentangle temporal and spatial effects and thus obtain a true 3D picture of the coma environment.

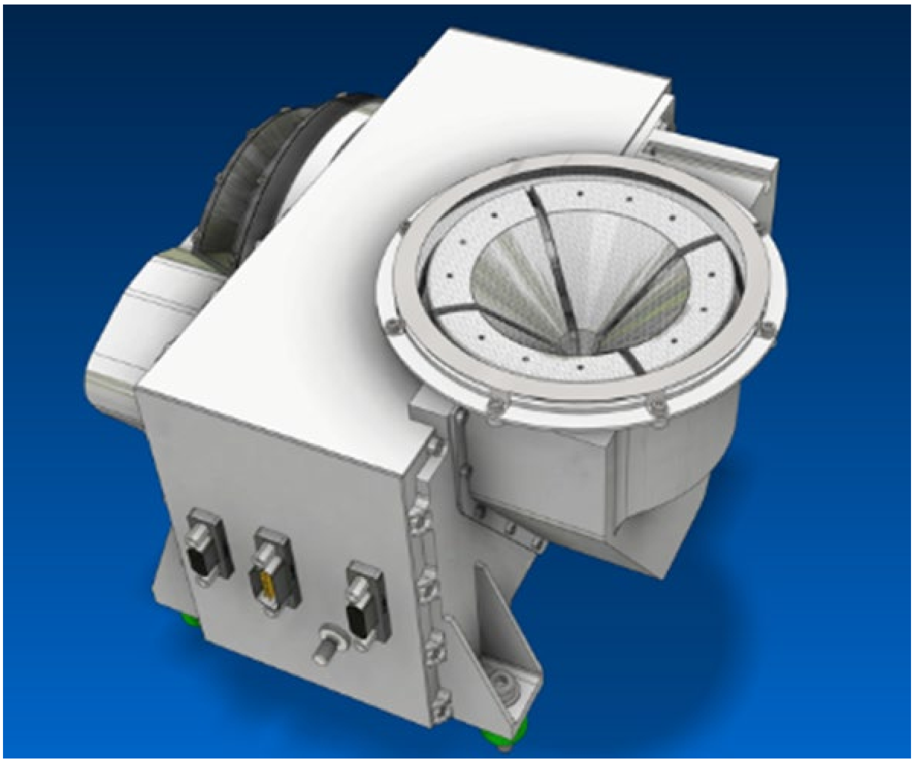

Figure 27: The SCIENA instrument with the ENA sensor to the left and the ions sensor to the right.

	Ions	ENA
Energy range	10 eV – 15 keV	300 eV – 3 keV
Angular coverage	Near 2 π	~ 30° x 150°
Mass resolution	1,2,4,8,16,32 amu	1, heavy
Time resolution	1 s / energy spectra 20-50 s / full distribution	1-10 s / energy spectra 5 – 50 s / full scan

Table 9: SCIENA properties.

4.1.4.5 *LEES*

The Dust, Field and Plasma Low-Energy Electron Spectrometer (LEES) is an instrument to determine the thermal and suprathermal electron densities, temperatures, and velocity distribution functions of the local plasma environment of both the solar wind and coma (*Table 10*). LEES will also measure the local properties of negatively charged ions, dust, and detect photoelectrons resulting from neutral-plasma interactions in order to infer the magnetic connectivity between the cometary environment and the spacecraft. The LEES measurements are needed to understand the ionization sources of the cometary neutral gas as well as to infer the plasma boundaries of the induced magnetosphere of the comet.

Energy range	1-1000 eV
Energy resolution	0.1
Elevation resolution, deg.	2.5
Elevation range	$-40^\circ \div +70^\circ$
Azimuth sector, deg.	22
Azimuth range	360°

Table 10: LEES properties.

4.1.4.6 *DAPU-A*

The Dust And data Processing Unit (DAPU) is a central data processing unit of the DFP instrument suite both on Spacecraft A and B2 . It is a computer board serving as a common digital interface between the spacecraft and the DFP instruments and sensors. On Spacecraft A, DAPU also performs detection of dust impacts in COMPLIMENT probe voltage data. DAPU will:

- Perform last stage processing, compression and buffering of all science data,
- Store the data from the entire flyby in its large flash memory (as a backup copy in case),
- Manage common DFP suite modes, instrument commanding and configuration.
- On DFP-A, DAPU will also count dust particle impacts linked to the plasma cloud from the evaporated dust grains, allowing to detect of small dust particles down to less than 100 nanometres in diameter.

4.1.4.7 *PSU-A*

The Power Supply Units (*Table 11*) shall generate, condition, control, monitor, and distribute electrical power to the DFP units from two unregulated 28 V buses, to fulfil the instrument power demands throughout all mission phases. The instrument power interfaces toward the spacecraft have been designed to prevent any single point failure, which could lead to a short circuit. The PSU modules include current and voltage monitoring, soft-start circuits, over-current protection (OCP), over-voltage protection (OVP), and under-voltage lock-out circuitry (UVLO) for the protection of the DFP units and subsystems.

Parameter	PSU-A
Supply Voltage (unregulated) [V]	24 – 34
Power [W]	22
Redundancy	YES (NOM/RED)
Mass [kg]	0.5 (NOM+RED)
Secondary output voltages	3.7V, +/-5V, +/-12V

Table 11: PFU-A characteristics.

The current design of the PSU units is based on previous and ongoing instrument power supply designs that have been implementing isolated DC/DC converters with embedded logic for switching control, protection, and HK monitoring. The designs have heritage from instruments built in CBK that were mainly used for radio and plasma diagnostics i.e.: Chronograph Control Block for *PROBA-3* (for ESA) and *RELEC* (for Russia) – FM delivered.

4.2 Spacecraft B1

4.2.1 Hydrogen Imager (HI)

4.2.1.1 *A short description of the science or measurement objectives*

Hydrogen Imager (HI) will measure the spatial distribution of Hydrogen Ly-alpha (121.6 nm) brightness of the comet coma through the "image mode" and "light-curve mode". The former mode takes the Lyman-alpha maps of the whole coma with its field of view of 4° × 4° and its spatial resolution of 0.02-0.1°. The latter mode takes emission profile of Hydrogen Lyman-alpha along the trajectory of the B1 probe (the line of sight is perpendicular to the velocity vector) during the closest approach phase.

The activity of the comet such as water production rate and its spatial variation can be calculated from the radial profile of hydrogen deduced from these data. The asymmetric structure and its temporal variation will also be measured, which may in turn link to the surface structure and rotation period of nucleus.

Observation before the closest approach phase will lead to the full image of the coma (10^6-10^7 km). The data generated is 130 kB per image, with a 256×256 matrix. The frequency and number of images which HI will take depends on the operation plan.

During the closest approach phase, the line of sight of HI will be perpendicular to the B1 probe velocity. The count rates will be measured for 4 or 9 regions of interest in order to obtain light curves across the nucleus. Measuring the characteristics of hydrogen, including the isotope ratio and temperature are also science objectives.

4.2.1.2 *An outline of the instrument*

HI is a Cassegrain-type UV imager (121.6 nm, Hydrogen Lyman-alpha) with bandpass filters *(Figure 28*). The specifications are summarized in *Table 12*. The 1st and 2nd mirrors are coated with Al/MgF_2 to achieve high reflectivity to Lyman-alpha and high durability during ground operations against elements such as water vapour in the surrounding environment. The baseline of the optical design is to use aspheric mirrors (such as parabolic mirror) to achieve high spatial resolution. The possibility of using a spherical mirror instead of aspherical ones is also considered to reduce manufacturing costs and time.

A bandpass filter made of 2.0 mm-thick MgF_2 is installed on the light axis to reject incoming light other than Lyman-alpha. The band centre of the filter is set to 122 nm, with a transmittance of about 10%; the band width is around 10 nm (FWHM).

A combination of an Image Intensifier (I.I.) and CMOS sensor with around 50 fps (flame per second) is used as a 2D photon detector. The CsI photocathode is used for the I.I. and the backside of the I.I. is illuminated by the electron clouds generated through the micro channel plates. The fibre optic plate (FOP) connects the I.I. with CMOS images sensor. The concept of the detector is shown in Murakami et al. (2016). For the lightcurve mode, the CMOS image sensor is used to calculate the number of incident photon per flame. For the imaging mode, the main processor of HI will calculate the centre of masses of photon events for each flame and integrates on the 256×256 matrix.

HI is also equipped with two additional gas filters on the light axis. Both filters consist of glass cell filled with hydrogen and deuterium. By heating up the gases with a tungsten filament installed inside the cell, the Hydrogen Lyman-alpha (121.567 nm) and Deuterium (121.534 nm) are resonantly absorbed. In addition, the absorption width can be modified by controlling the filament temperature. This means that the gas filter is able to deduce the hydrogen to deuterium ratio, and also their temperatures. It should be noted that the accuracy of those measurement depends strongly on the geometric conditions of the target and B1 probe.

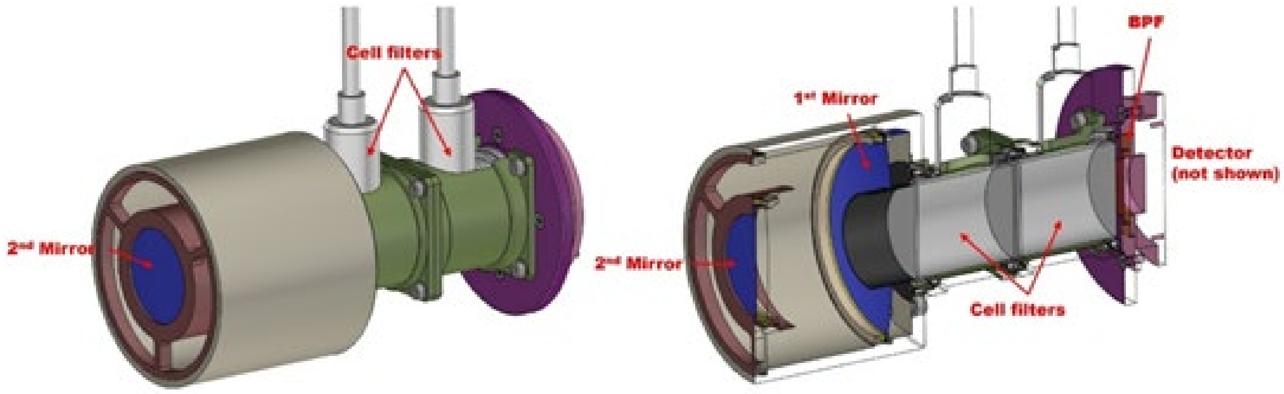

Figure 28: Design overview of HI.

Parameters	Values	Note
Mass, size	<2.5 U[2], <2 kg	w/baffle, electronics
Field of view	4° × 4°	256×256 matrix, spot diameter ~ 0.02°
Aperture	Φ60 mm	Al/MgF_2 coating, F/4-5
Bandpass filter	122+/-10 nm	Transmittance = 5-10 %
Effective area	2×10^{-3} cm^2	Geometrical: 3-5 cm^2 (w/ baffle)
Count rate	0.012 cps/pix/kR	800 cps/all/kR
Ly-alpha filters (opt.)	Φ35 mm Length=40 mm	Gas filters with H_2 and D_2

Table 12: The specifications of the HI instrument.

4.2.2 Plasma Suite (PS)

PS consists of an ion mass spectrometer and a 3-axis magnetometer. It provides velocity distribution functions of individual ion species of the low-energy coma plasma, as well as the DC and low-frequency AC magnetic field data.

The main science objectives addressed by PS are:

- Characterisation of the plasma environment around the target, determination of any resulting boundaries and assessment of energy, mass, and momentum transfer.
- Determination of motion and evolution of ion rays and other coma and tail features including dust and gas.
- Characterisation of the bulk neutral composition of the coma and determination of any local structure and connection to the nucleus (PS does not measure neutral particles, but ion composition measurements provide information on the neutral composition and its spatial heterogeneity).

The ion mass spectrometer has a 2-pi steradian field of view. The magnetometer shall be mounted on top of a boom to avoid the spacecraft magnetic noise. They are controlled by a common electronics board.

The ion sensor consists of an electrostatic analyser and time-of-flight mass analyser (TOF). The incident energy and direction of each incoming ion are determined by the electrostatic analyser. Ions are then introduced to the TOF sector, where mass-per-charge is measured by the linearly increasing electric field. A large field-of-view (entire hemisphere if there is no exterior interference) is achieved by an entrance deflector in the electrostatic analyser unit.

[2] 1 U = 10x10x10cm

The PS magnetometer is based on the fundamental mode orthogonal fluxgate (FM-OFG) technique (Figure 29). FM-OFG adopts an amorphous wire sensor core driven with a unique excitation method where AC current is superposed on DC bias current. It enables low-noise detection of magnetic field with compact and light-weight sensor design.

The design of PS is based on the MSA instrument on-board the MMX spacecraft (Yokota et al., 2021). Its heritage is extensively utilised here, while some modification for the ion sensor structure is introduced to allow it to be accommodated in a much smaller spacecraft.

The key performance aspects of PS are summarised in Table 13

The magnetometer is accommodated on the top of an extensible boom for magnetic cleanliness of the measurements (*Figure 30*). The boom is stowed during the launch and deployed during the commissioning phase after the launch. The release of the launch lock will be conducted by spacecraft A with the interface designated in the interface requirements document. The extension is then driven by the motor powered by probe B1.

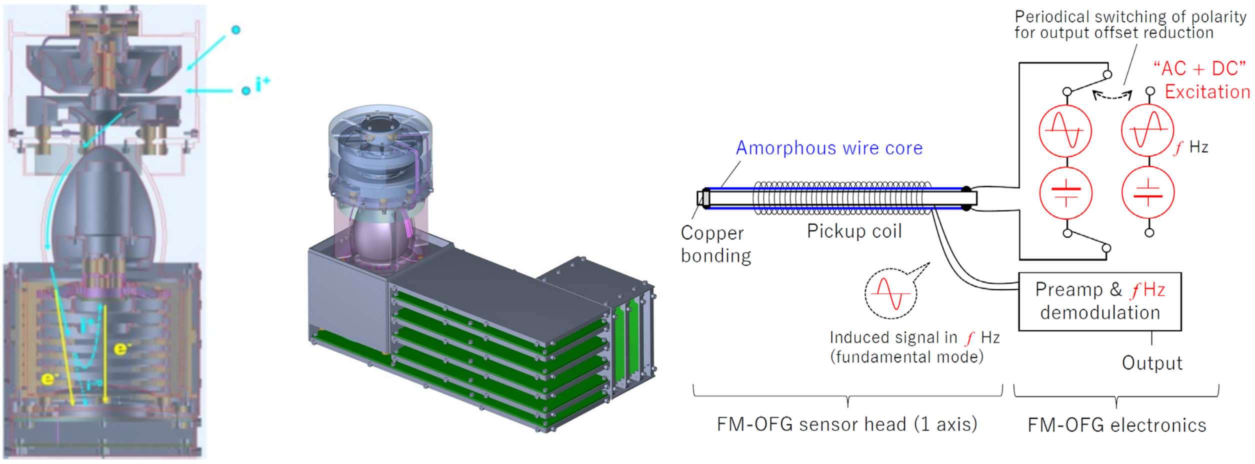

Figure 29: Schematic diagrams for (left) the ion sensor optics, (centre) PS structure including electronics boxes, and (right) the FM-OFG magnetometer sensor.

PS sensor	Expected performance
Ion mass spectrometer: Instantaneous 3-D distribution of ions, with mass discrimination	Energy: 10 – 20,000 eV/q, ΔE/E ~ 10% Mass: M/ΔM ~ 30 Field-of-view: Hemispheric
Magnetometer: DC and low-frequency AC magnetic field	Absolute accuracy: 1 nT@±512 nT Range Directional accuracy: < 5 degrees Noise level: ~12 pT/Hz$^{1/2}$ @1 Hz ~6 pT/Hz$^{1/2}$ @10 Hz

Table 13: Expected performance of PS.

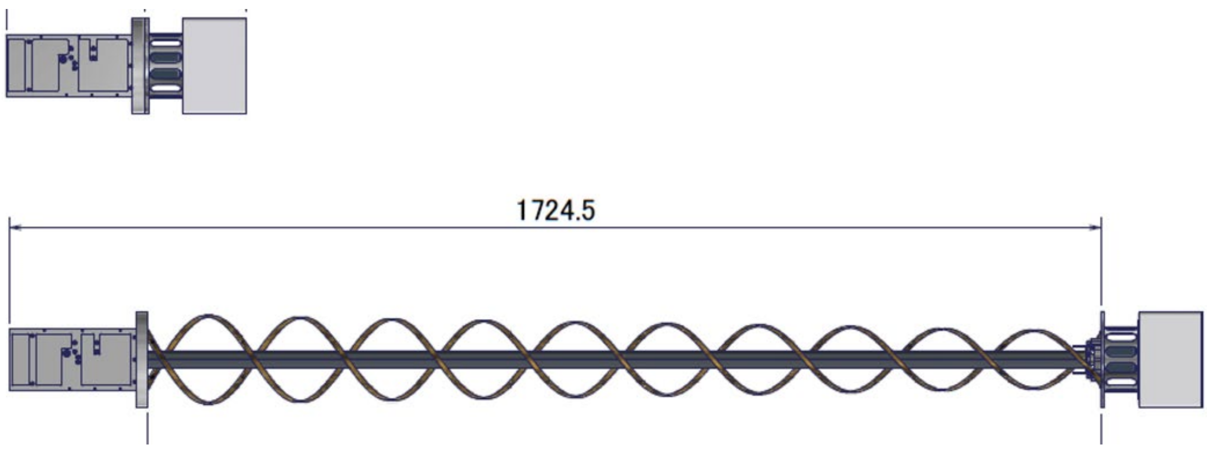

Figure 30: An extensible boom of stowed (top) and deployed (bottom) states.

4.2.3 Narrow Angle Camera (NAC) and Wide Angle Camera (WAC)

The Narrow Angle Camera (NAC) is an optical telescopic camera. NAC will obtain optical images of the target nucleus with high solar phase angle, to address the nucleus science. Science objectives of NAC are:

- Observing the size and global shape of the target nucleus.
- Characterising the surface morphology of the target nucleus.
- Characterising the spin state of the target nucleus.

The spatial resolution of the NAC is about 40 m/pix or better at a closest approach distance of 850 km. The field of view is enough wide to observe the entire nucleus. The cometary nucleus shape and its surface morphology are modified by the solar heating. The high solar phase angle region is expected to be less heated than other parts of the nucleus, so that the NAC is aimed at the polar regions of permanent low insolation to reveal the most primordial regions of the long period comet.

The Wide Angle Camera (WAC) is also an optical camera with wide field-of-view. The main purpose of WAC is:

- Evaluating the coma structure around the nucleus.

The field of view of the WAC is 90 x 90 degrees. The instantaneous field of view is roughly 40 times wider than that of the NAC.

Both cameras are utilized not only for the scientific objectives, but also for the optical navigation (or attitude control) of the B1 probe. During the fly-by, the NAC and the WAC acquire images of the target continuously. These data are used for the lightcurve analysis and for structural evolution of the coma, as well as the optical navigation source data. At closest approach, the NAC carries out resolved imaging of the nucleus to determine the shape and surface morphology of the target, jointly with the images by CoCa.

The NAC/WAC system (*Figure 31*) consists of:

(1) Electronics box with control function of the cameras and interface to the bus system

(2) Narrow angle camera sensor and optics

(3) Wide angle camera sensor and optics

The electronics box and narrow angle camera sensor will be developed based on the telescopic camera TENGOO on-board Martian Moon Explorer MMX (Kameda et al., 2021). Some additional functions are installed, including a flash memory storage, WAC control function, and image processing.

Table 14 summarises the specifications of the NAC and the WAC. The NAC is equipped with a CCD sensor. In contrast, the WAC sensor will be CMOS because of the restricted volume, mass, and power available. At a closest approach of 850 km, the spatial resolutions are 15.6 m/pix and 540 m/pix for the NAC and the WAC. These cameras have panchromatic filters covering 0.4 to 0.75 μm in wavelength.

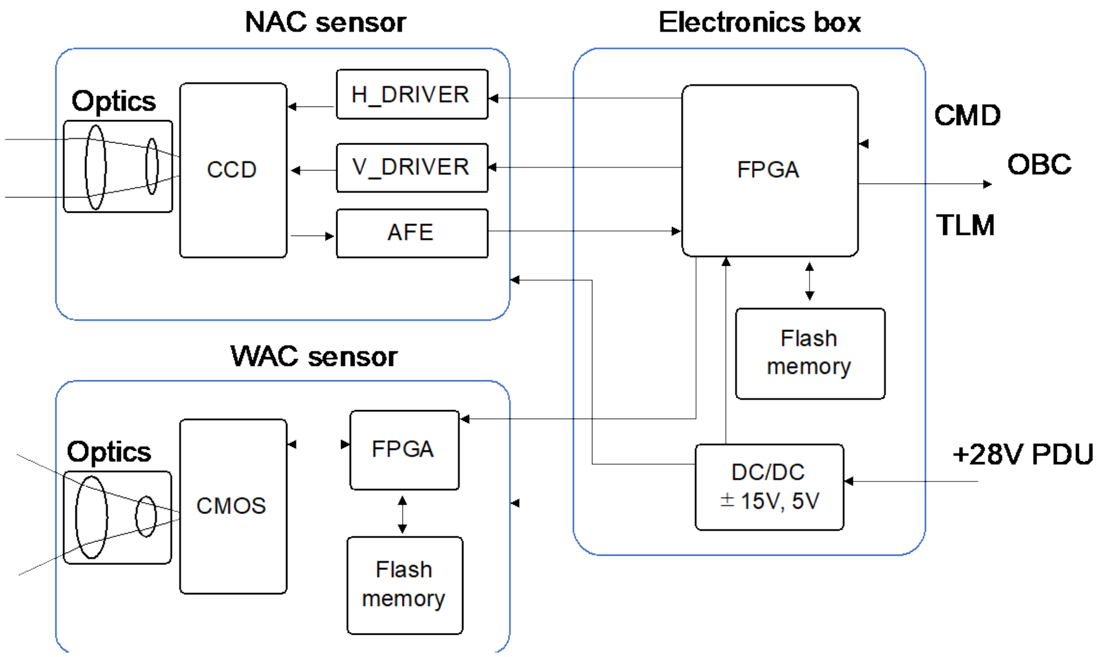

Figure 31: Block diagram of the NAC/WAC.

	Narrow Angle Camera	Wide Angle Camera
Sensor	CCD	CMOS
Pixel number	3296 x 2472 pix	2048 x 2048 pix
Focal length	300 mm	8.6 mm
F-Number	6.0	2.8
FOV	3.5 deg x 2.6 deg	90 deg x 90 deg
iFOV	0.018 mrad	0.77 mrad
Filter	0.4 – 0.75 µm (TBD)	0.4 – 0.75 µm (TBD)
Size	10 x 10 x 40 cm	10 x 10 x 10 cm
Weight	~ 4 kg	~ 1 kg

Table 14: Preliminary designs of the NAC and the WAC.

4.3 Spacecraft B2

4.3.1 Entire Visible Sky (EnVisS)

4.3.1.1 *EnVisS Measurement principle and objective*

The EnVisS camera has been conceived to study the comet dust environment, including its polarimetric properties, in the visible wavelength range from 550-800 nm. The FoV of the instrument is designed to allow the entire sky to be acquired thanks to the rotation of the B2 spacecraft.

EnVisS will feature a flexible push-broom/push-frame imaging technique, thus acquiring slices of the sky, while the probe rotates (see *Figure 32*); the slices acquired will be stitched together, on-ground, to form a whole sky image.

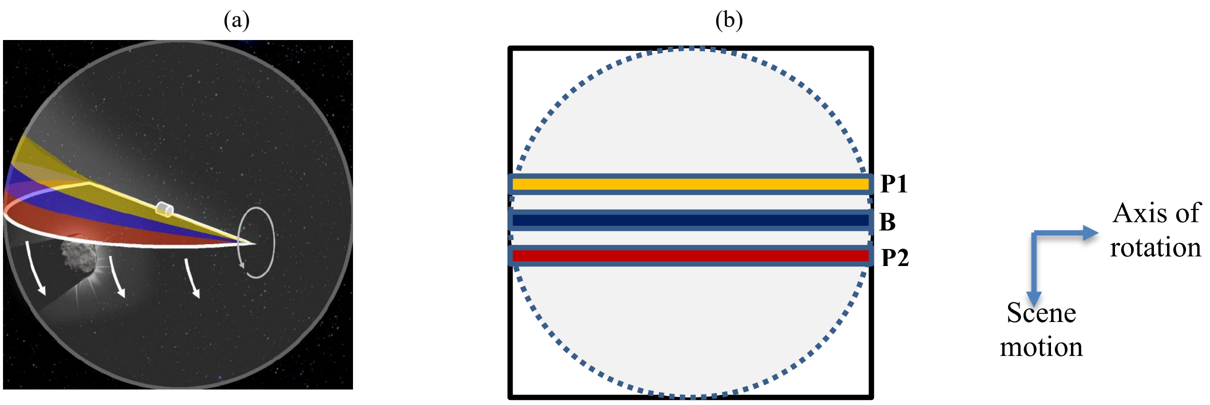

Figure 32: In (a) we show an illustration of the EnVisS full sky imaging scanning concept. In (b) we show the schematics of the filter strip images on the 2kx2k detector.

EnVisS will map the intensity, the degree of linear polarisation and polarisation angle orientation of the light scattered by the dust particles in the comet coma with a full 180° phase angle coverage. Such a measurement is unique, it has never been carried out in space. HOPE, on-board the *Giotto* spacecraft, could only observe a very narrow angle FoV in the direction opposite to the motion of the spacecraft.

The coma investigation will be conducted throughout the full fly-by of the comet from an advantageous point inside the coma itself. The probe spin-axis will be pointed at the comet nucleus for most of the time, except at closest approach when the comet nucleus will fall inside the camera FoV (see *Figure 33* for the expected geometry of the fly-by and the EnVisS placement on the B2 probe).

Depending on the target object activity, the map of the coma will be taken with different spatial resolution (i.e., smearing and pixel binning) in order to achieve the desired SNR. The minimum resolution element is 0.2°.

4.3.1.2 *EnVisS: Instrument Design*

The EnVisS instrument features a fish-eye lens coupled to a commercial space-qualified detector from 3D-Plus company and ad-hoc power and data handing units and software (see *Figure 34*).

The design solution adopted for the filters in EnVisS, i.e., filter strips mounted as near as possible to the detector, allows for a compact, low mass and low complexity camera.

Three broad band filters, all working in the same wavelength range, are foreseen for the camera:

- one broadband filter positioned to be centred on the detector (see *Figure 32*, blue central strip B).
- two polarimetric filters with transmission axis angles oriented at 45° one to the other (see *Figure 32* the yellow and red strips P1 and P2).

The EnVisS optical head will have a 3.45 mm focal length with an MTF of 70% at 45 lp/mm to match a 2x2 pixel resolution element. The full FoV of the instrument will be 180° in the direction of the spin axis, i.e., across-track direction, and 45° in the plane of rotation and motion of the scene, i.e., along-track direction. The full EnVisS characteristics are summarized in *Table 15*.

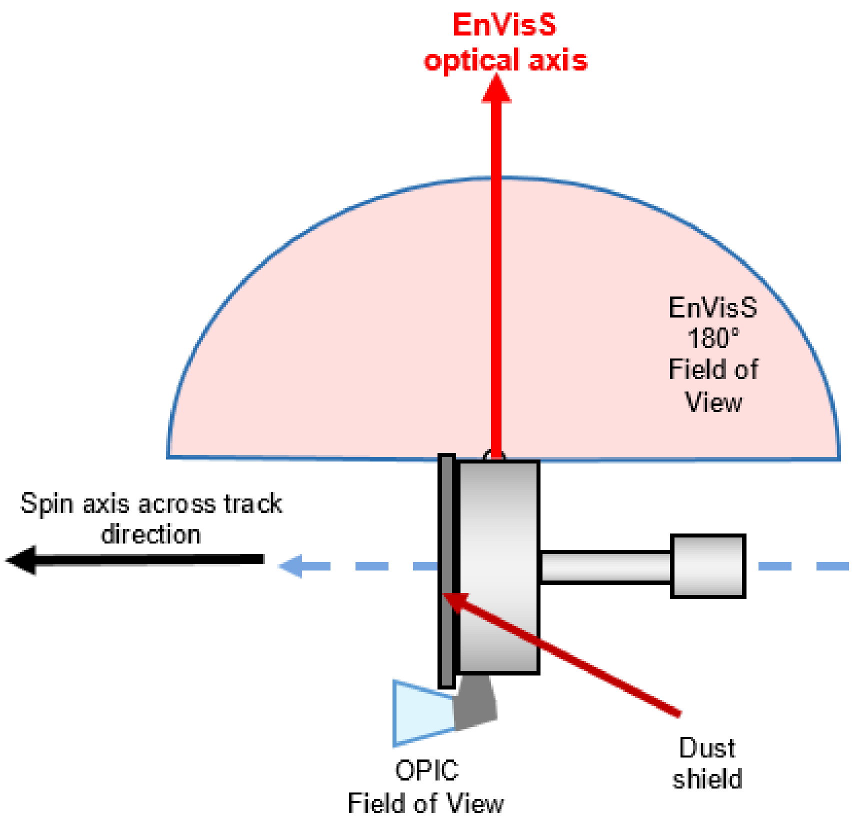

Figure 33: The placement of the EnVisS camera on the B2 probe.

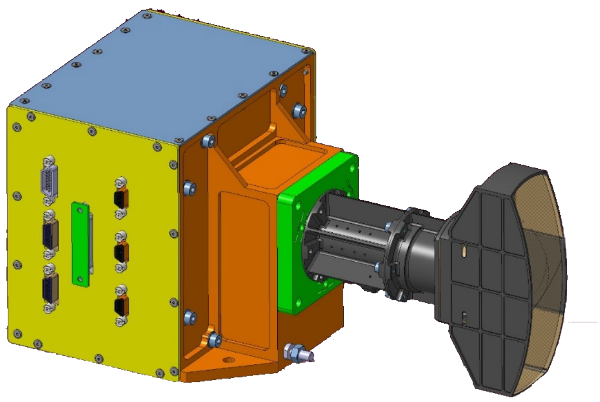

Figure 34: EnVisS instrument present mechanical layout (Courtesy of MSSL-UK and Leonardo SpA-IT)

The direction of apparent motion of the scene due to the S/C B2 rotation is parallel to the vertical direction in *Figure 33*, while the horizontal direction corresponds to the direction of the spin axis.

Wavelength coverage	550-800 nm 1 broad band filter (B) and 2 polarimetric filters (P1 and P2)
Instrument FoV	180°x45° (fixed) 180°x360° (dynamic)
Entrance aperture (F#)	1.23 mm (2.8)
Detector	CMOS 2kx2k 5.5-micron px size
Scale factor	0.1°/px
MTF	>70% @ 45 lp/mm
Distortion and telecentricity	<8% (f-theta distortion law) and <4° (at the FoV edges)

Table 15: Summary of EnVisS characteristics

A flexible approach has been devised to allow a SNR of 10 to be obtained in the case of broadband images and of 100 for the polarimetric images. The signal from the coma in the direction of the apparent motion of the scene is not expected to show big changes, so a high spatial resolution is not needed from a scientific point of view. The integration time for each filter strip can be tuned, allowing for some smearing in the along-track direction. The spatial resolution can be retained in the across-track direction to assure a sampling of the comet phase function every 0.2°. This strategy will also allow for an adjustment of the exposure time if the radiance of the coma is different to the expected.

Should the signal be extremely low, further pixel binning on-board, or co-adding, on-ground, of the images over different rotations, could be considered.

4.3.2 Optical Periscope Imager for Comets (OPIC)

Optical Periscopic Imager for Comets (OPIC), situated on the probe B2 and looking over the edge of its dust shield, is an automated camera system for taking images during the fly-by of the target's near environment and of the target itself (*Figure 35, Figure 36*). It consists of an automated camera head (3D Plus 3DCM734-1 SS), imaging optics (lens assembly and baffled periscope) and interface electronics.

It has a 2048 x 2048-pixel CMV4000 sensor and an integrated ProAsic3 FPGA. OPIC's field-of-view is ≈18.2 x 18.2 degrees.

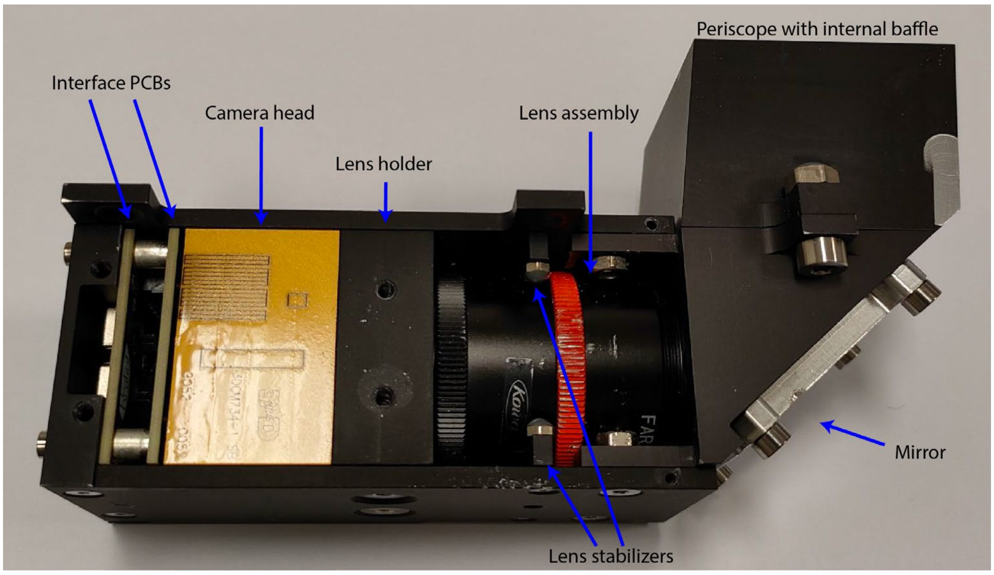

Figure 35: OPIC engineering model with internals exposed.

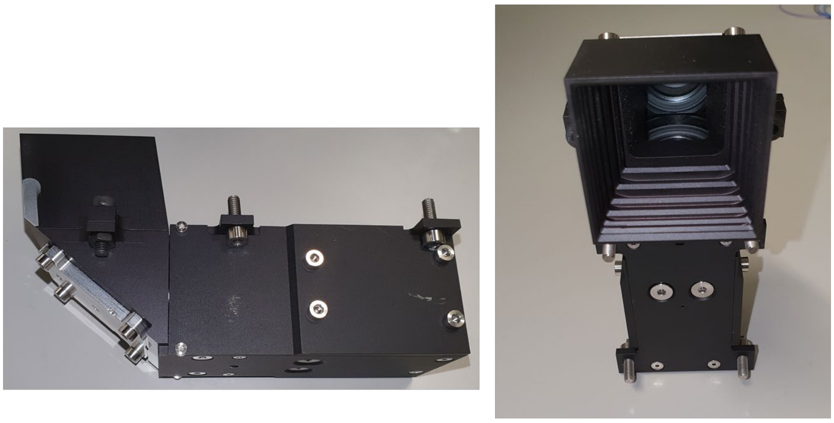

Figure 36: OPIC engineering model external view (representative of flight model).

When the B2 probe is far from the nucleus, OPIC will take long exposure images of the area around the nucleus (see *Figure 37* for a simulated image). At this distance, the nucleus is not resolvable and will only be a dot on the image. These images will show how much gas and dust is in the viewing direction of OPIC and its spatial distribution. The data can be also used to constrain the trajectory and rotation state of B2 after B2-A separation.

Figure 37: A qualitative OPIC image at a long distance from the target. This also simulates longer exposures needed to capture stars and the induced motion blur. This is a simulation from the SISPO project (Pajusalu et al. 2022).

When the B2 probe gets closer to the target, the nucleus will become resolvable *(Figure 38)*. Images will be taken automatically and processed on-board before transmission to Spacecraft A and onward to the Earth. The images will show the low-resolution structure of the nucleus and of the gas and dust immediately around it, including potential satellites and fragmentations. This can be combined with imagery from the A and B1 spacecraft to generate a more detailed and less ambiguous 3D model of the target, as each spacecraft will only travel in a line and so will have a limited range of viewing angles to the target.

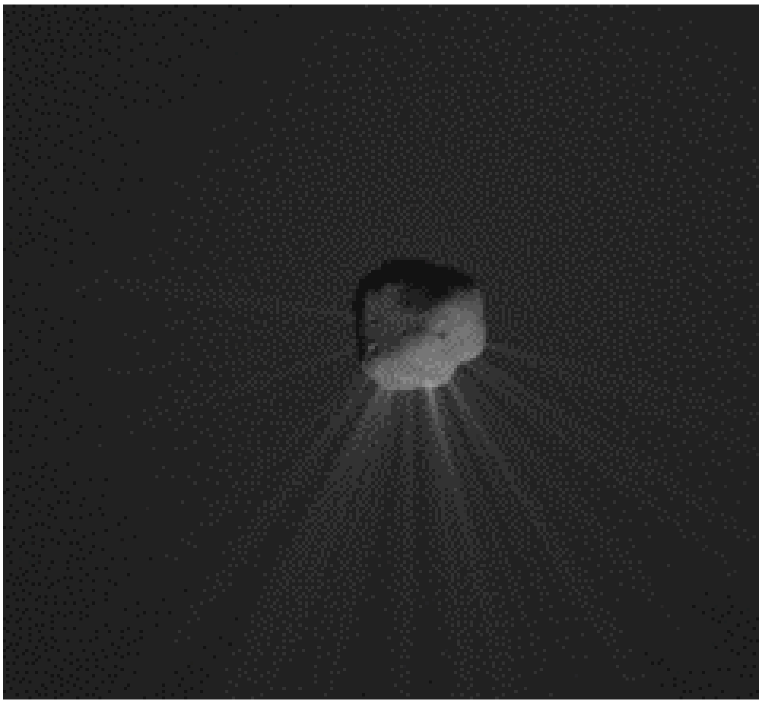

Figure 38: Simulated image of the nucleus and its immediate surroundings, cropped (200 x 200 pixels) from a full simulated OPIC frame (2048 x 2048 pixels). This is a simulation from the SISPO project (Pajusalu et al. 2022)

OPIC also can provide images that can later be stitched together, potentially complemented by EnVisS images (*Figure 39*).

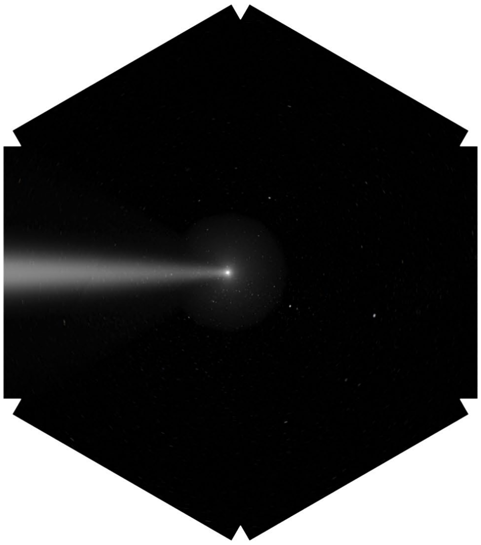

Figure 39: Stitched OPIC images to form a full cone image. This is a simulation from the SISPO project (Pajusalu et al., 2022).

OPIC is expected to have multiple different imaging modes:

1. Full frame images far from the nucleus.

Exposure times can be set to either prioritise seeing fainter features and collecting navigation data, or to avoid overexposure of the coma. The images will probably include motion blur far from the nucleus, but can be used for near- and far environment studies. It is expected that full frame images can be downlinked.

2. Nucleus and very near environment images.

Close to the nucleus, OPIC imaging is limited mainly by the data budget, meaning that it is probable that images will have to be heavily cropped and/or downscaled to fit in the communications budget. For closest approach during fly-by, an algorithm will be implemented that detects automatically whether or not the target is in the field of view and then crops a predetermined area around it for transmission. This functionality can be useful for studying surface activity, such as jets, in conjunction with CoCa.

3. Full frame images near the nucleus.

These images can only be transmitted after fly-by. Images taken near the nucleus could be used to image fainter features, or dust.

4.3.3 Dust, Fields, and Plasma (DFP-B2)

The Dust Field and Plasma (DFP) on spacecraft A and B2 probe (*Figure 40*) is a combined experiment dedicated to the multi-point study *in situ* of the multi-phased ionized and dusty environment in the coma of the target dynamically new comet and its interaction with the surrounding space environment and with the Sun. The DFP on probe B2 will measure the magnetic field and the cometary dust in order to:

- Identify boundaries and regions in the cometary environment of a comet and its interaction with the Sun and with the solar wind (e.g., bow shock, diamagnetic cavity) and to assess their structure.
- Map the dust and plasma phases around the target dynamically new comet.
- Assess the mass, momentum, and energy transfer in the cometary environment.
- Provide simultaneous magnetic field, plasma, and dust measurements to identify the interplay between the ionized and dusty phases around a comet and characterize dusty plasma properties.
- Map the solar wind – coma interaction.

To enable these multipoint measurements, two instrumental sensors, DISC, and FGM-B2, common data processing unit DAPU and power supply system PSU will be constructed and placed on probe B2.

4.3.3.1 *DISC*

The Dust Impact Sensor and Counter (DISC) on Probe B2 is identical to that on Spacecraft A (see Section 4.1.4.1).

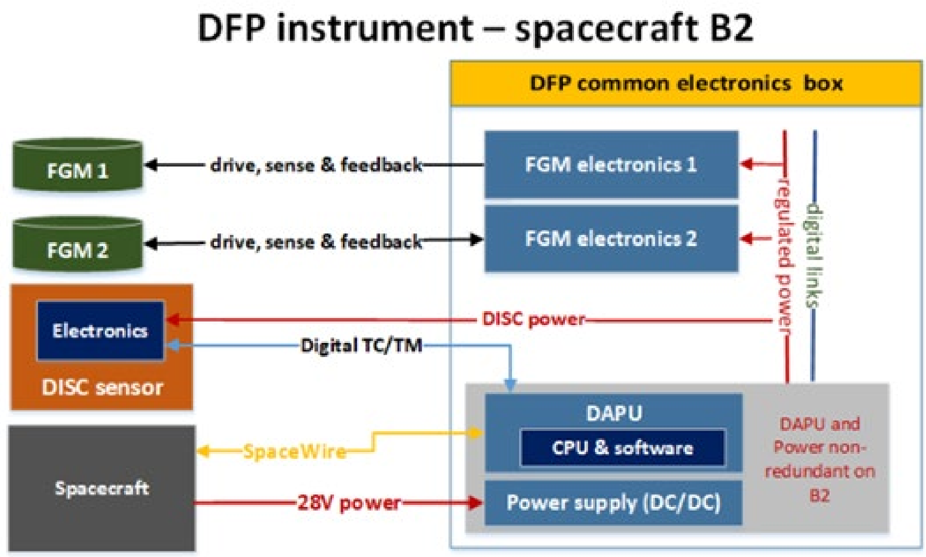

Figure 40: Design of the DFP instrument on Probe B2.

4.3.3.2 *FGM- B2*

FGM-B2 (BFG for short) will measure the 3D magnetic field vector. Its dataset will be used to identify field boundaries and regions and assess their nature (*Figure 41*). These result from the interaction of the solar wind with the cometary plasma and include the bow shock and the diamagnetic cavity, whose origin is still under debate. FGM-B2 will also detect various wave modes, such as mirror modes and ion cyclotron waves.

Operation range	± 1020 nT (configurable)
Digital Resolution	31 pT
Noise	< 10 pT/sqrt(Hz) at 1 Hz
Absolute accuracy	± 1 nT (goal), ± 2 nT (requirement)
Mass	180 g (two sensors), 410 g (electronics)

Power	1.8 W total
Temperature range	[-80; +60] °C (both survival and operation). No heaters installed.

Table 16: FGM-B2 performance.

Magnetometers are the only instruments present on all three spacecraft. This multi-point capability will allow assessment of the 3D structure of the field boundaries and energy transfer through waves across boundaries. The FGM-B2 fluxgate magnetometer is composed of two sensors (outboard and inboard) mounted on a rigid boom and their electronic front-ends, which are hosted in the DFP CEBOX. Whilst both sensors and electronics have a strong heritage (e.g., *Rosetta*/Philae, *Venus Express*, and *THEMIS* for the sensors and *MMS*, *Geo-KOMPSAT-2A*/SOSMAG for the electronics), their mass and power consumption have been optimised for the resource-constrained Probe B2.

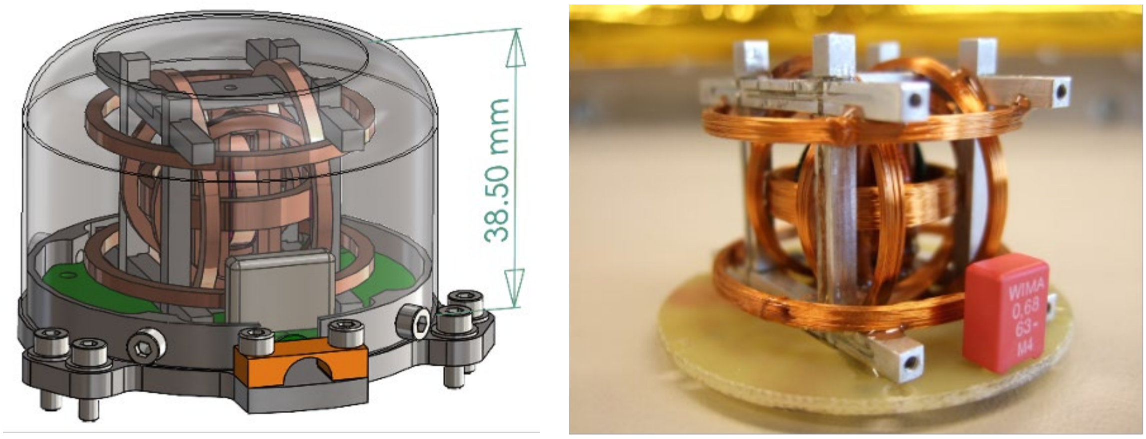

Figure 41: CAD rendering of one FGM-B2 sensor (left) and picture of its sensing elements (right).

4.3.3.3 *DAPU B2*

The Dust and Data Processing Unit (DAPU) is the central data processing unit of the DFP instrument suite, both on Spacecraft A and on B2. It is a computer board, serving as a common digital interface between the spacecraft and the DFP instruments and sensors. It:

- Performs the last stage of processing, compression and buffering of all science data,
- Stores the data from the entire flyby in its large flash memory (as a backup copy in case of transmission problems), and
- Manages common DFP suite modes, instrument commanding and configuration.

4.3.3.4 *PSU-B2*

The Power Supply Units will generate, condition, control, monitor, and distribute electrical power to the DFP units from two unregulated 28 V buses, to fulfil the instrument power demands throughout all mission phases (*Table 17*). The instrument power interfaces toward the spacecraft have been designed to prevent any single point failure, which could lead to a short circuit. The PSU modules include current and voltage monitoring, soft-start circuits, over-current protection (OCP), over-voltage protection (OVP), and under-voltage lock-out circuitry (UVLO) for the protection of the DFP units and subsystems.

The current design of the PSU units is based on previous and ongoing instrument power supply designs that have been implementing isolated DC/DC converters with embedded logic for switching control, protection, and HK monitoring.

Parameter	PSU-B2
Supply Voltage (unregulated) [V]	28V
Power [W]	10
Redundancy	NO
Mass [kg]	0.25
Secondary output voltages	3.4V, ±5V,

Table 17: The parameters of the PSU-B2 unit.

5 Mission design

5.1 Mission analysis

The *Comet Interceptor* mission aims to intercept an LPC, ideally a DNC that is approaching the inner solar system for the first time, or even an interstellar body, in a close-approach fly-by scenario using three elements: a mother spacecraft, S/C A, and probes B1 and B2 carried as payloads until the fly-by and delivered to different fly-by trajectories. This will allow the gathering of multi-point observations of the comet and its coma.

LPC objects are typically discovered as they reach the inner Solar System, no more than a few years before perihelion passage and therefore their orbits are not known in advance. As a result, the *Comet Interceptor* mission calls for an innovative and flexible mission concept. By waiting in an orbit around SEL2, typically for up to 3 years before being targeted, the probability of finding a suitable LPC that can be reached in time is considerably increased.

The likelihood of discovering a LPC during the waiting period will be greatly increased soon by the availability of the LSST, with which it is expected that during its routine operations, much earlier LPC discoveries, at heliocentric distances ~20 AU will be achieved, giving warning times of > 5 years before targeting. This might even be early enough to know the target comet before launch, although not before the mission and spacecraft designs have to be frozen.

Comet Interceptor will transfer using its on-board propulsion system to a single fly-by of the target during which all science measurements will occur. Science data from the probes B1 and B2 will be transmitted to S/C A and stored on-board. The downlink to Earth of the science data obtained will take place in the months immediately following the comet fly-by. In the unlikely event that no other suitable target is identified, *Comet Interceptor* will transfer to a backup target from a list of known short-period comets.

The *Comet Interceptor* Science Consortium has endorsed this mission design as the most efficient to provide the science return.

5.1.1 Target comet population

The characterization of the LPC population is based on numerical studies of the evolution of these objects and comparisons with observational data, in particular from the Pan-STARRS1 survey (Wiegert & Tremaine, 1999, Boe et al., 2019). The *Comet Interceptor* Science Consortium provided a set of 1699 LPCs with perihelion inside 2 AU, which has been used to derive statistical distributions for the orbit parameters of the LPC population. The cumulative distribution functions (CDF) for the perihelion distance, eccentricity and inclination are illustrated in *Figure 42*. The orbits of LPCs are quasi-parabolic with probability of eccentricity peaking steeply very close to 1 (the minimum eccentricity in the set is 0.9504), and more likely to be retrograde (64% probability of inclination > 90º). The rest of the orbital elements follow statistical distributions that are very well described by a uniform distribution. Correlations between orbital elements are neglected for the simulations carried out in the context of *Comet Interceptor*.

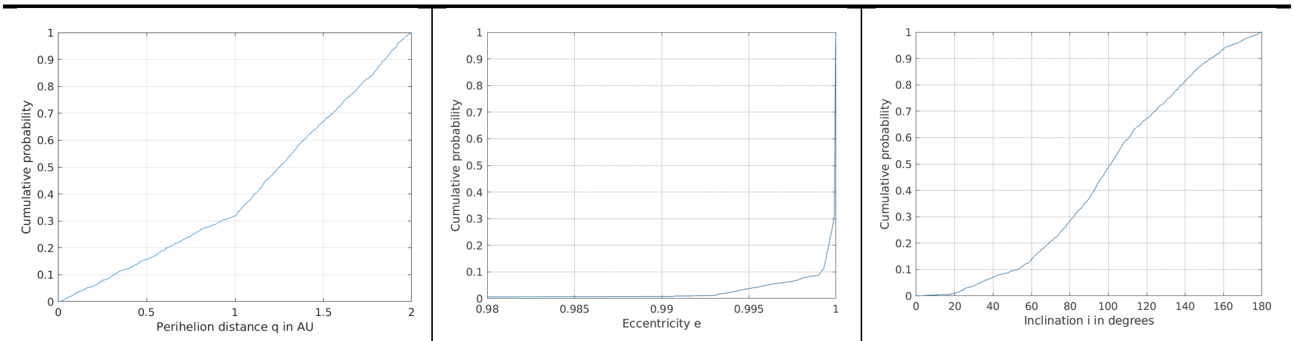

a) Perihelion distance b) Eccentricity c) Inclination

Figure 42: Empirical CDFs of LPCs with perihelion < 2 AU.

5.1.2 Launch, transfer to SEL2 and waiting phase at SEL2

Comet Interceptor is scheduled to launch in 2029 in a shared launch with the ESA mission ARIEL on an Ariane 62. The launch configuration envisages the use of the Ariane 6 short fairing (TBC) and the Dual Launch Structure, with *Comet Interceptor* as the upper passenger and ARIEL as the lower.

The injection orbit for *Comet Interceptor* will be a 9-deg inclined high-apogee, nearly parabolic orbit with perigee/apogee altitudes at 180 km and 1.5 million km, respectively. The Ariane 62 will use a direct ascent strategy, with a single boost of the upper stage's Vinci engine. An additional biasing boost between both spacecraft separations will be implemented in order to reach slightly different SEL2 transfer trajectories, unbiased for *Comet Interceptor* and biased for ARIEL. This launch scenario results in a total wet launch mass for *Comet Interceptor* limited to approximately 975 kg, excluding the mass of any required launch adapter.

A large amplitude quasi-Halo orbit is selected for *Comet Interceptor* on the basis of the following arguments:

- Compatibility with ARIEL also targeting a large amplitude SEL2 orbit.
- Minimization of Delta-V required for the transfer and no need for an insertion manoeuvre.
- Mitigation of eclipses during transfer and in the orbit around SEL2.

A sample direct transfer to a large SEL2 quasi-Halo and waiting phase around SEL2 are depicted in *Figure 43* in order to show possible orbit features and geometry.

The transfer geometry and amplitude of the achievable quasi-Halo orbit will depend on the launch date and time. Assuming that a single Ariane 62 flight program is used, the natural variation of the perigee velocity over the launch window will have to be corrected with a manoeuvre 2 days into the mission. This manoeuvre will be combined with the correction of launcher injection errors.

Additional trajectory correction manoeuvres are planned at days 5 and 20 to achieve an accurate manoeuvre-free transfer into the quasi-Halo orbit. Including the deterministic and the stochastic parts, 50 m/s are allocated overall, for the trajectory corrections during this part of the mission. The overall duration of the transfer is around 3-4 months from launch. During this time, commissioning activities for the Spacecraft and probes will be carried out.

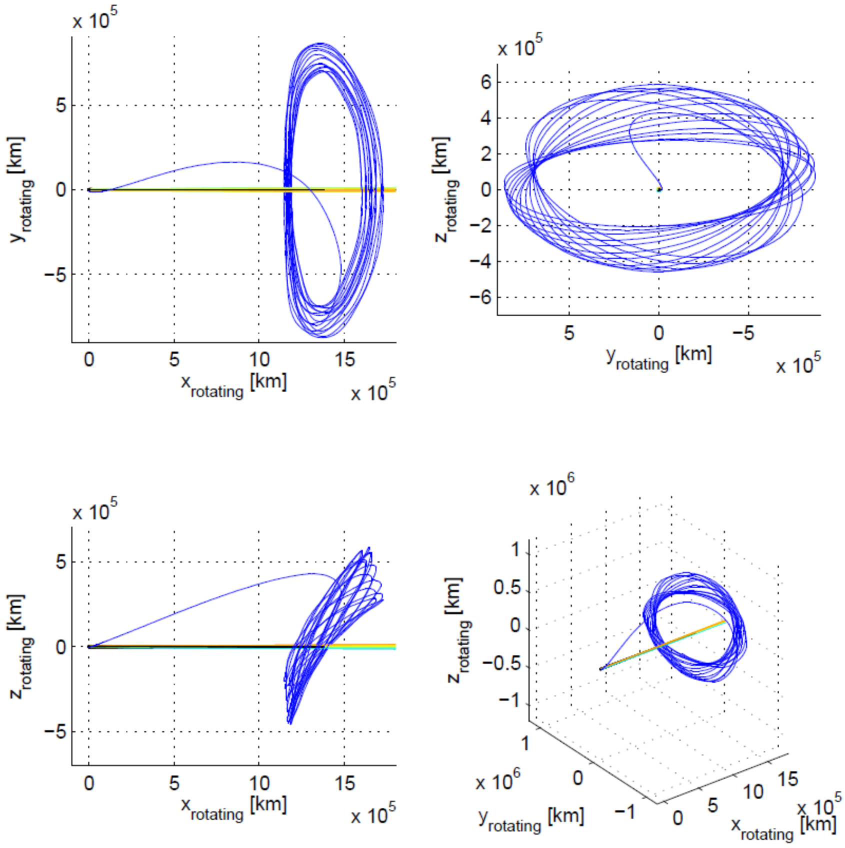

Figure 43: Sample transfer to SEL2 quasi-Halo orbit and waiting phase in the Sun-Earth rotating frame.

Comet Interceptor will spend an unknown time orbiting around SEL2, typically between few months to 4 years. It is during this waiting time that Earth-based observatories are expected to discover one or more potential targets for the mission if one was not found prior to launch. Following target selection, *Comet Interceptor* will remain near SEL2 waiting for the right conditions to start the transfer towards the target comet.

Quasi-Halo orbits around SEL2, up to an amplitude of ~1 million km, have a period of roughly 180 days. These orbits are inherently unstable; any small perturbation will lead to an exponential deviation from the reference orbit, hence periodic station keeping manoeuvres are planned. The frequency and size of these manoeuvres depends on the spacecraft's ability to reduce velocity perturbations and dynamic noise. The current plan considers station keeping manoeuvres every 28 days and allocates 2.3 m/s per year to stay at the SEL2.

5.1.3 Transfer from SEL2 to encounter

Newly detected potential targets will be monitored continuously from Earth, and the possible transfer trajectories and encounter/post-encounter profiles will be studied in detail for each candidate a minimum of 6 months in advance of initiating the transfer. Once the comet target is selected, or a decision is made to go to the backup, the spacecraft will wait until the optimum time to depart from the orbit around SEL2.

An optimal transfer trajectory avoids costly out-of-plane Delta-V manoeuvres and stays close to the Ecliptic plane. As a result, the target comet has to be intercepted at one of its nodal crossings of the Ecliptic, hence the location of the encounter can be defined by just 2 parameters: the heliocentric distance at encounter Rc and the phase angle of Earth at encounter θ, measured as the Comet-Sun-Earth angle. Analysed by 2-body dynamics under solar gravity, the transfer orbit needs to have the perihelion and/or the aphelion distance adjusted in such a way that Rc can be reached, together with an orbital period such that the phase drift, ahead or behind Earth, that leads to the desired angle θ in a given transfer time. Typically, this requires as much as 2 trajectory manoeuvres, though in few cases the addition of a third manoeuvre can be beneficial.

At the beginning of the transfer, when the spacecraft leaves the vicinity of SEL2, the gravity effect of Earth has a significant impact on the trajectory. Extensive analysis leads to two different strategies being envisaged:

1) Direct Transfer. The spacecraft performs a manoeuvre to leave parking orbit around SEL2 in order to exit the gravitational pull of the Earth-Moon system and is injected into a heliocentric orbit drifting towards encounter. A second deep-space manoeuvre, at a given time during the transfer orbit to the comet might be necessary to adjust the orbit or the phasing. These transfers can be Exterior, when the spacecraft leaves directly towards the outside of the Sun-Earth direction, or Interior, when the spacecraft leaves towards the Earth, performing a first high-altitude Earth fly-by before leaving in the SEL1 direction. The complex dynamics of the interior case can exploit multiple loops around the Earth and/or an Earth fly-by to reduce the transfer Delta-V.

2) Moon Gravity Assist. The dynamics of the SEL2 manifold towards Earth allow a Moon fly-by to be performed, after which the spacecraft can escape from Earth with a velocity at infinity of about 1 to 1.4 km/s and direction approximately opposite to the Earth's velocity vector. This is an efficient way to reach heliocentric orbits with perihelion below 1 AU and favours targets with negative phase angle at encounter (θ<0, ahead of Earth). The Moon fly-by allows Delta-V savings, but introduces additional operational complexity.

The reachable domain of comet encounters for each strategy, as illustrated by *Figure 44* is driven by a trade between transfer time and Delta-V. It is observed that direct transfers favour Rc>1 AU and θ>0 (behind Earth), while the opposite occurs for transfers with Moon gravity assist, whereas a region of overlap exists in which both strategies are feasible. Increasing the transfer time impacts significantly the reachable domain.

Figure 45 illustrates sample transfer trajectories to one of the identified backup targets. Two transfer trajectories are shown: one optimised for minimum Delta-V, requiring 37 m/s and 847 days, and one optimised for minimum transfer time with a Delta-V cap at 570 m/s that reduces the transfer duration to 529 days. In both cases the exterior direct transfer strategy is used, and the transfer requires 2 manoeuvres, one to depart from SEL2 and one deep space manoeuvre during the cruise towards the comet encounter.

It is likely that *Comet Interceptor* will be able to adjust slightly the transfer trajectory in order to fly-by a suitable non-active minor body. Such a fly-by would be a good opportunity for an engineering test of the spacecraft systems and operational procedures required for the comet fly-by in a similar scenario, i.e., the optical navigation cameras and autonomous tracking. This would add valuable experience to increase the mission robustness and probability of success of the actual science fly-by.

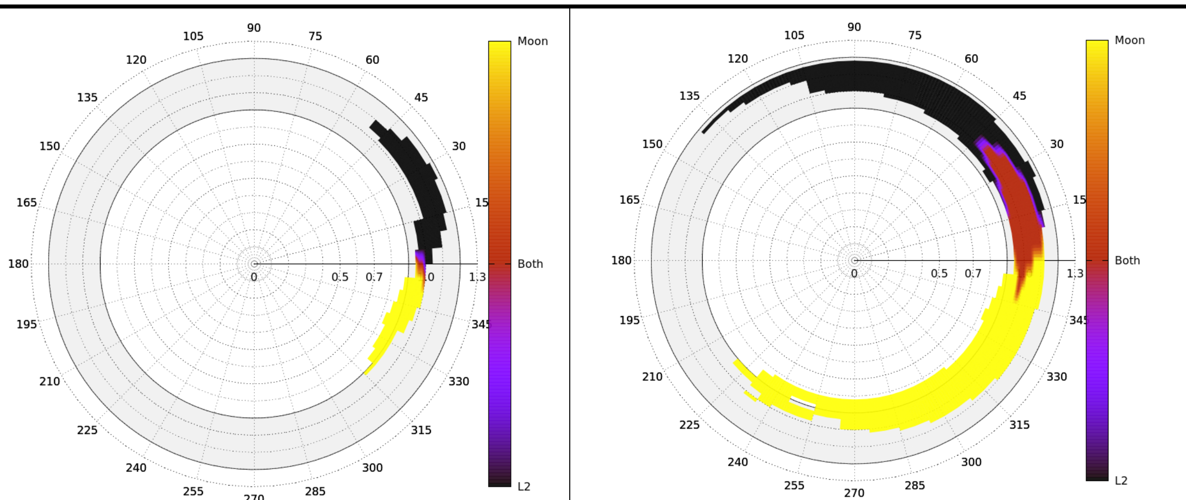

a) Transfer Time: 1 year

b) Transfer Time: 3 years

Figure 44: Reachable Rc-θ regions with 750 m/s for sample transfer times of 1 and 3 years.

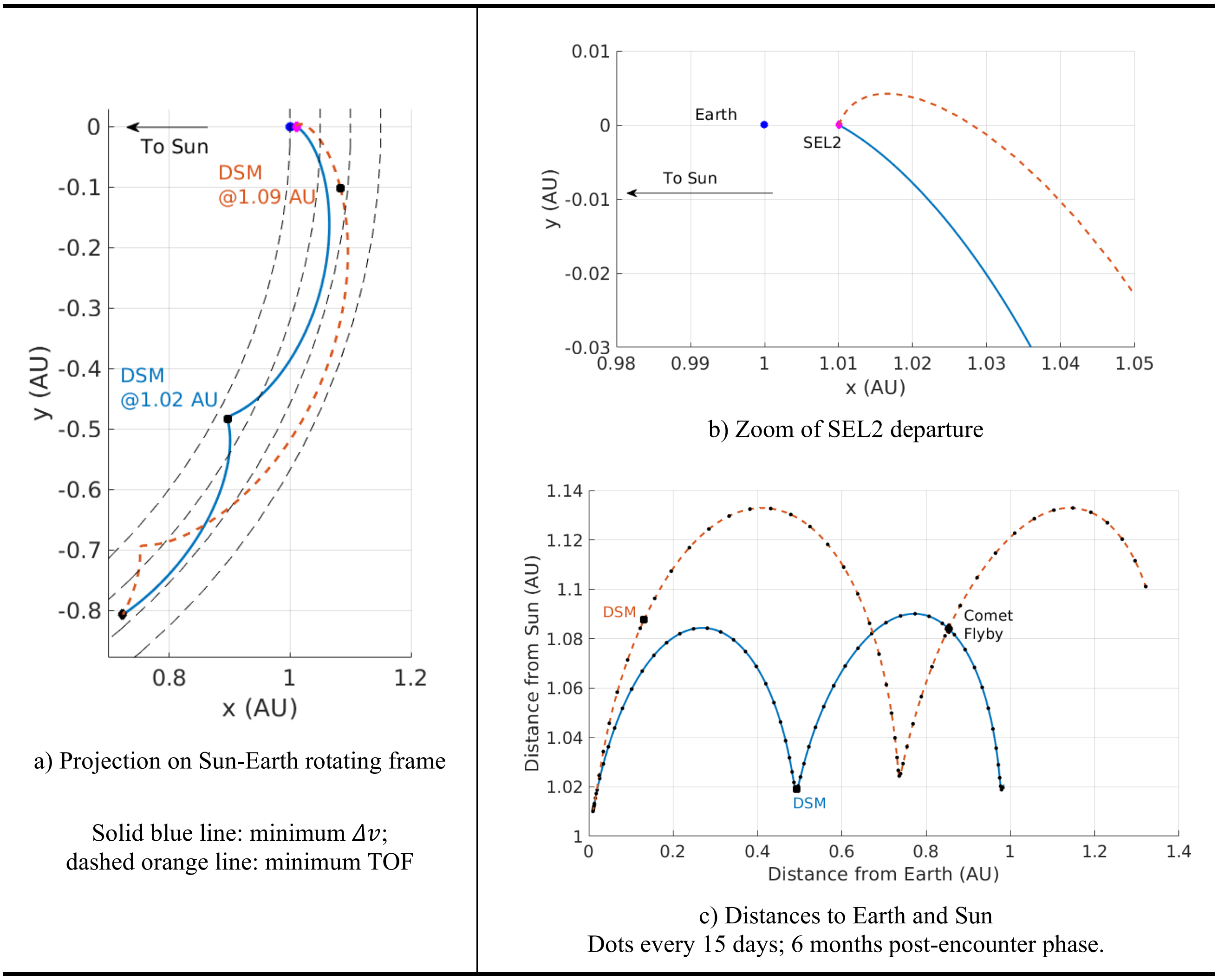

a) Projection on Sun-Earth rotating frame

Solid blue line: minimum Δv;
dashed orange line: minimum TOF

b) Zoom of SEL2 departure

c) Distances to Earth and Sun
Dots every 15 days; 6 months post-encounter phase.

Figure 45: Geometry of sample transfers to backup comet target 26P.

5.1.4 Probabilistic reachability analysis and statistics of key mission parameters

The results presented in this section have been obtained using a Monte Carlo tool that simulates possible *Comet Interceptor* missions, modelling from the target detection process to the transfer and comet encounter and the following post-encounter phase. The simulations consider a rate of 14 LPCs per year with perihelion inside 2 AU originating from the comet population of Section 5.1.1. This underlying assumption is consistent with the historical observations of 21 new LPCs in the 2010-2019 decade with nodal crossings in the accessible [0.9, 1.25] AU range.

The probability of finding at least one feasible LPC target within the given set of constraints and mission requirements is used as a figure of merit. *Figure 46* shows how the mission duration and the transfer ΔV impact this probability. With the current allocations of 600 m/s for the transfer and 6 years overall mission duration the probability is 80% (30% of single target plus 50% of multiple targets). Excluding the transfer option with the Moon gravity assist reduces the probability significantly down to 63%.

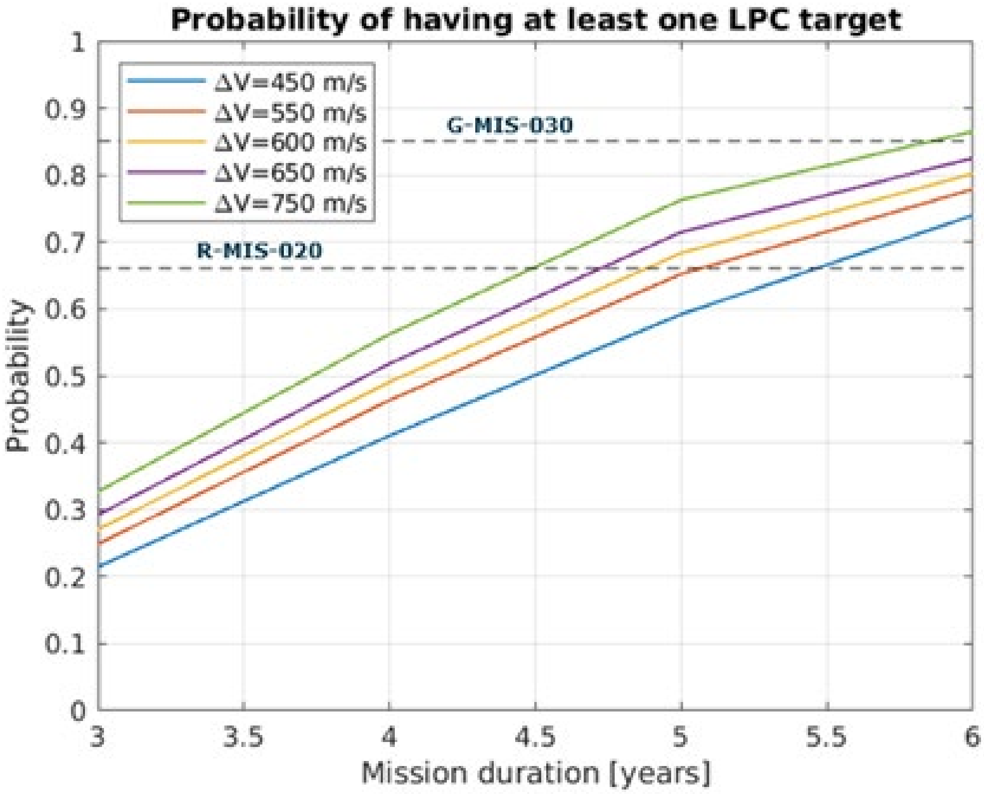

Figure 46: Influence of Delta-V and mission duration on the probability of at least one LPC target. Time between launch and target detection < 2 years, mission duration includes 6 months post-encounter phase.

A Monte Carlo mission simulator has been used to extract some statistical information on durations relevant to the mission. We have to consider that missions finding multiple feasible targets might choose to favour a given parameter, thus two limiting cases are studied. The main results are summarised in *Figure 47* in which the case of the mission eventually intercepting a backup comet target has been disregarded. The median waiting time at SEL2 is observed to be in the range between 1 and 2 years, while waiting times longer than 4 years rarely occur (<5% of cases).

As far as the transfer duration from SEL2 to the comet is concerned, when aiming for the shortest transfer there is a preference for heliocentric transfers favouring durations close to an integer number of years, rather than intermediate durations. Aiming for the longest transfer tends to smooth out the peaks and to result in more uniform distribution. The median of this parameter lies between 1.5 and 2.5 years.

For the mission duration from launch to comet encounter (limited to 5.5 years assuming 6 years maximum overall duration, minus 6 months of post-encounter activities), the statistics show an increasing probability density followed by a flat region for durations above 4 years. The median is observed around 3.5 years and the 90-percentile at about 5 years.

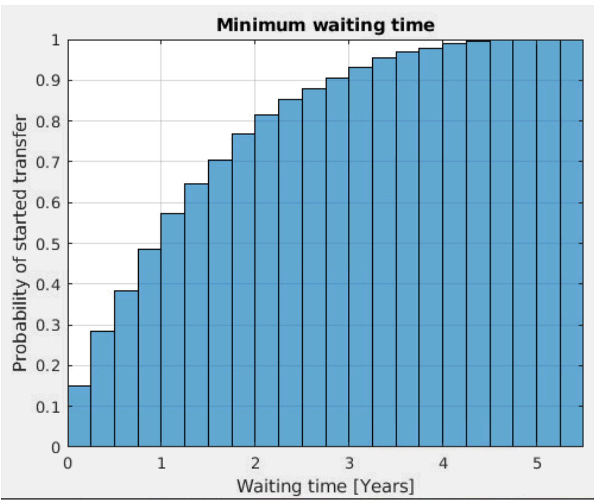

a) Shortest waiting at SEL2

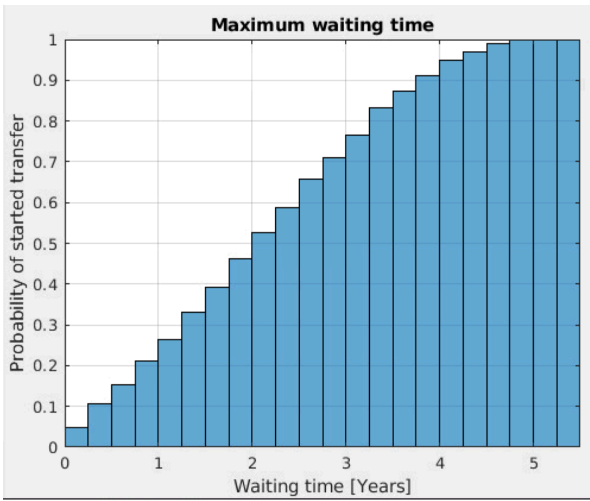

b) Longest waiting at SEL2

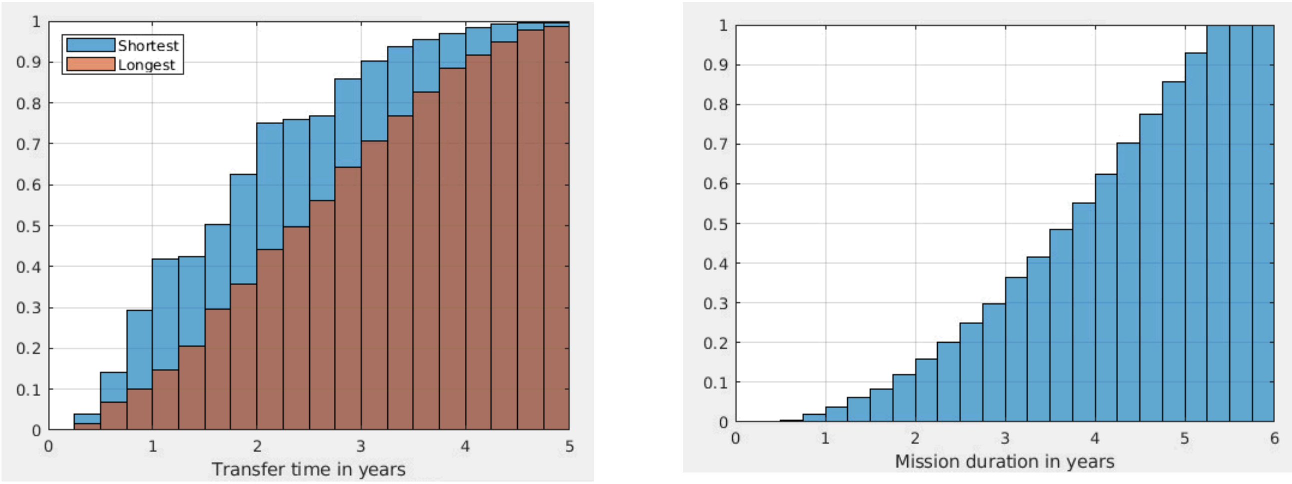

c) Transfer time from SEL2 to the comet encounter. d) Duration from launch to comet encounter.

Figure 47: Statistics of time parameters relevant for the mission.

5.1.5 Comet Encounter

Figure 48 shows the distribution of the modulus of the encounter relative velocity, $\vec{v}_{rel} = \vec{v}_{SC} - \vec{v}_{comet}$, and the fly-by solar aspect angle (the angle between the Comet-Sun vector and $\vec{v}_{rel}$), for simulated feasible encounters obtained from the population of LPCs. The relative velocity is biased towards higher values and peaks around 60 km/s. The fly-by solar aspect angle shows a symmetrical distribution around 90 degrees. Constraining the encounter parameters has an impact on the availability of targets: having a 60 km/s maximum velocity would remove 33% of possible targets, while the baselined 70 km/s requirement removes only 8.5%. On the other hand, the requirement that constrains the fly-by solar aspect angle to 90±45 degrees removes approximately 7.5% of the targets.

In addition, it must be pointed out that the orbital mechanics of the encounter with an LPC at a given heliocentric distance, from 0.9 to 1.2 AU, constrain the feasible combinations of relative velocity and fly-by solar aspect angle, as depicted in *Figure 49.* The fly-by solar aspect angle provides information directly as to whether the encounter is on the inbound or the outbound leg of the comet's orbit, with the angle being > 90º or < 90º, respectively.

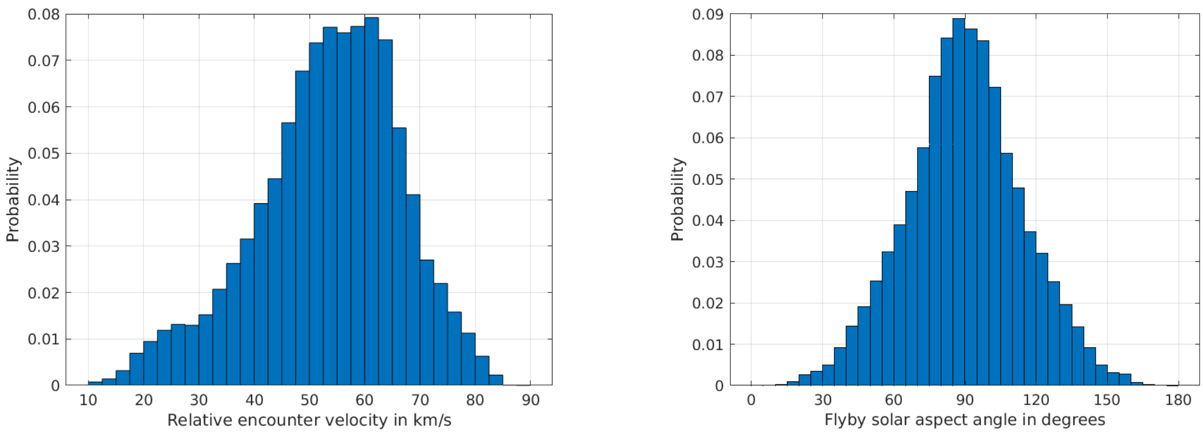

a) Relative velocity b) Fly-by solar aspect angle

Figure 48: Relative encounter velocity and fly-by solar aspect angle for reachable LPCs (0.7 AU < Rc < 1.3 AU).

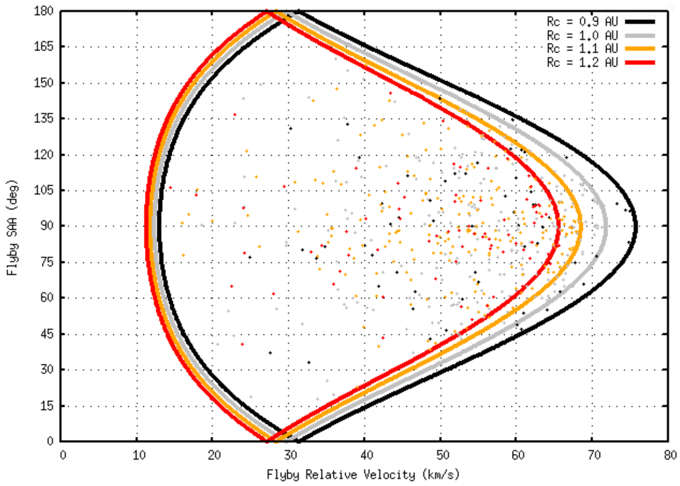

Figure 49: Allowed regions of relative velocities and fly-by solar aspect angles.

The approach to encounter phase is assumed to be defined as the last 60 days before the comet fly-by. By trajectory design there will be no need for a deterministic manoeuvre during this phase, hence operations can focus on the navigation required to reach the comet. This navigation will rely on ground-based measurements of the comet's position, radio tracking of the spacecraft using the ESTRACK DSA and, most importantly, on the optical data from the NAVCAM. The optical observations have the strength to directly relate the states of Spacecraft and target comet improving the accuracy of the prediction of the fly-by location and time, and allowing to perform critical trajectory correction manoeuvres (TCMs).

The fly-by targets are defined in the B-plane, which is the plane perpendicular to the relative velocity $\vec{v}_{rel}$ and passes through the comet centre. Two perpendicular directions are defined: the T vector is defined by the orthogonal projection of the Sun-to-target vector onto the B-plane, and the R vector completes an orthogonal right-handed triad with S=$\vec{v}_{rel}$ and T. The B-plane targets for Spacecraft and probes are defined by the closest approach distance and the angle θ, with the T-axis measured in the direction towards the R-axis.

From -3 days onwards, the final approach operations will take place according to the timeline illustrated in *Figure 50*, which is still subject of refinement and optimisation in future phases of the mission design.

- The NAVCAM will be used continuously to improve the determination of the nucleus position and the accuracy of the fly-by. A ground turn-around time of 12 h (seen as the data cut-off time before each TCM) is considered necessary to downlink the last image, perform the on-ground processing, orbit determination and next manoeuvre and/or separation planning, and to uplink the telecommands. Therefore, the input data cut-off for each TCM is 12 hours beforehand.
- The *Comet Interceptor* spacecraft composite (A+B1+B2) is assumed to be targeted at the B1 aim point, with a closest approach of 850 km and $\theta = 135°$, thanks to the navigation during the approach phase.
- A stochastic TCM @ -44 hours to the fly-by will target the composite precisely at the B1 aim point, making use of the most updated optical observations.
- Separation of Probe B1 will occur 2 hours later, following a post-TCM tranquilisation phase and a slew of the composite to the separation attitude.
- TCM @ 30 hours to the fly-by will target the composite (A+B2) towards the aim point of Probe B2 at closest approach of 400 km and $\theta = 180°$. This TCM will combine a deterministic part of roughly 6 m/s with a stochastic correction.
- Separation of Probe B2 occurs 6 hours later.
- The diversion manoeuvre of S/C A occurs -20 hours to the fly-by. It targets a greater closest approach distance of 1000 km and $\theta = 180°$. The deterministic part of the diversion manoeuvre is 8.5 m/s.

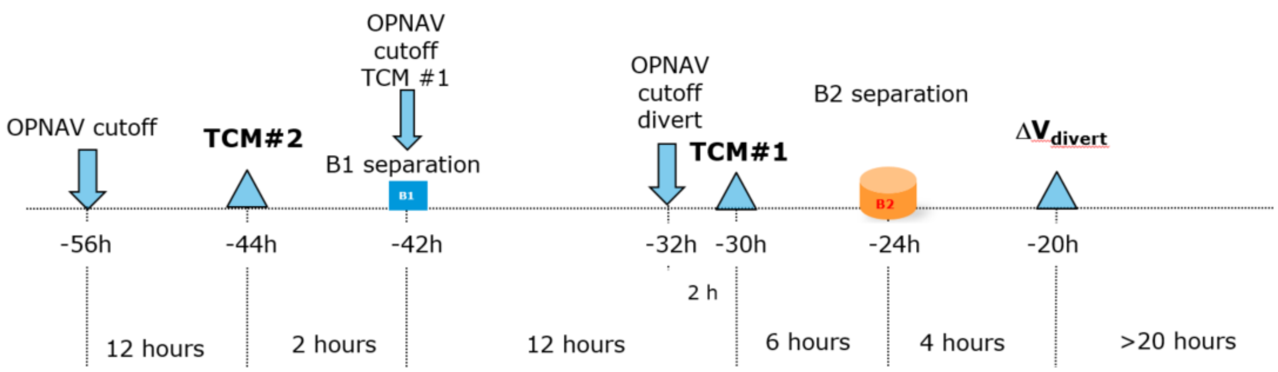

Figure 50: Timeline of operations for the comet fly-by.

5.1.6 Back-up targets

It is critical for the success of *Comet Interceptor* that the availability of a backup target for any launch date is ensured. This has been investigated for a down-selected list of 11 comet candidates provided by the Science Consortium and for the 4-year launch timeframe 2029-2032. The analysis identified 4 backup targets compatible with a transfer ΔV allocation of 600 m/s and an overall mission duration of 6 years, chronologically as follows:

1. From 2029-03-24 to 2030-05-18: 15P/Finlay
2. From 2030-05-18 to 2030-12-14: 289P/Blanpain
3. From 2030-12-14 onwards: 300P/Catalina

A potential encounter with 26P/Grigg-Skjellerup in Q1 of 2029 is now not regarded as feasible, as the ARIEL launch is currently scheduled for late in Q4 of 2029. *Figure 51* shows a summary of the backup target selection. Taking as example launch on January 1st, 2030, the backup target is comet 15P/Finlay and the latest selection of a primary LPC target needs to occur before about 3 years after launch. Otherwise, a transfer to 15P will be used, which requires departure about 3.5 years after launch and arrives in September 2034; 6 months later, or 5.2 years after launch, the mission will be finished.

We observe that more than 3 years are provided consistently from launch until the decision to go to the backup target. Only relatively short periods, in Q1-Q2 2030 and May 2032, provide shorter decision cut-off times of between 2.5 and 3 years.

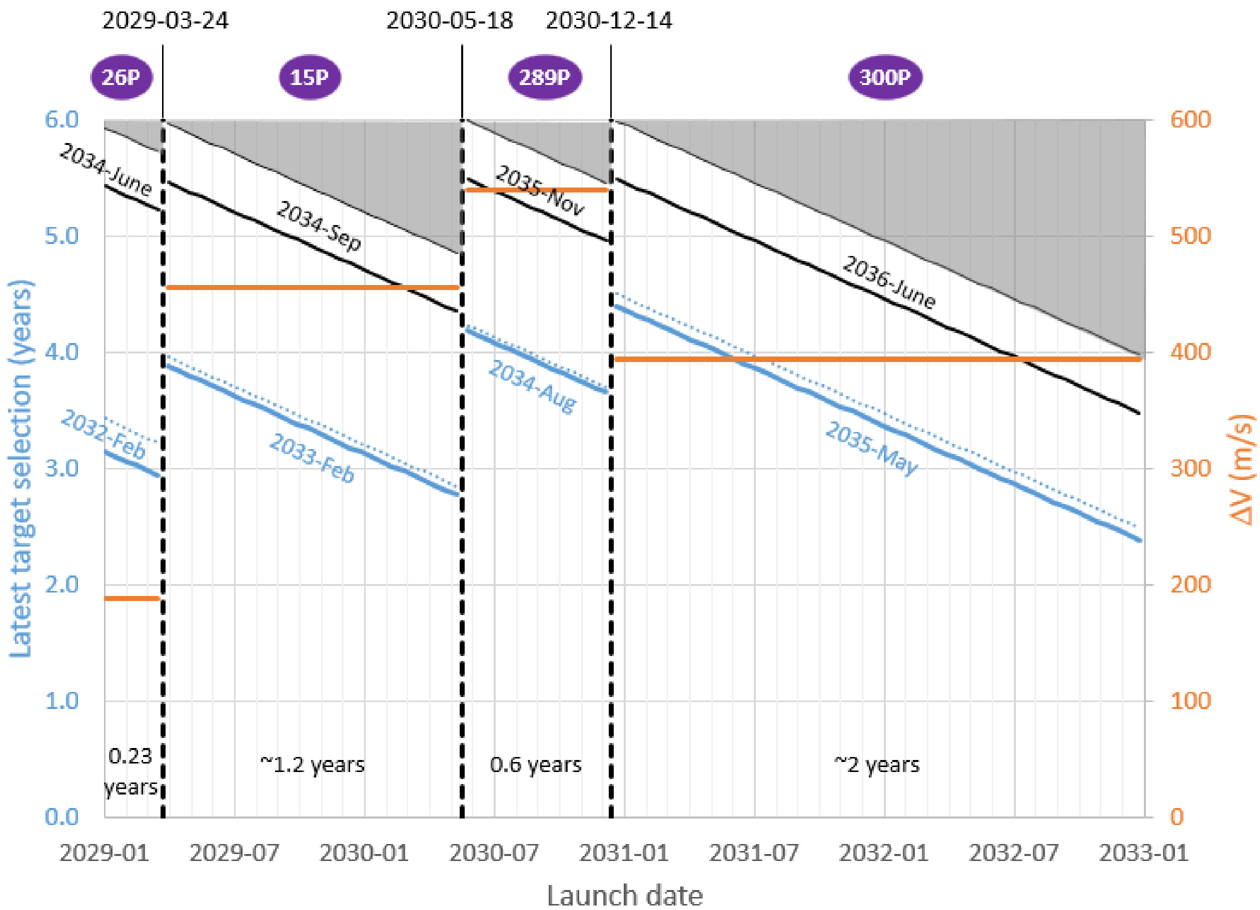

Figure 51: Summary of backup target selected as a function of the launch date.

5.2 Spacecraft design drivers

The *Comet Interceptor* mission design is driven by the key objective of performing multi-point observations during a high relative velocity fly-by with a target which will be identified after the finalisation of the S/C design. The main design drivers of *Comet Interceptor* Spacecraft A and probe B2 are summarised in *Table 18*.

Design driver	Main implications
Dual launch with ARIEL on A62	Max launch mass limited to 975 kg.
Multi-point observation principle	Additional probes to be carried by the main S/C.
Large payload complement	Accommodation of several *in-situ* and remote sensing units on S/C A and Probe B2.
Target defined at late stage	S/C design compatible with range of possible targets, of encounter conditions and Sun-Earth-Target geometries.
Maximise probability to reach a suitable target	Maximise Delta-V capability. Navigation & Target tracking capabilities to remain compatible with multiple targets. High maximum fly-by relative velocity (range 10 to 70 km/s).
Interplanetary mission	S/C operating at ~ 1-2 AU from Earth.
Measurements performed during a high relative velocity fly-by	"One shot" science. Data downlinked to Earth after the closest approach.
Comet environment	Capability to survive the micrometeoroid and dust environment for a variety of possible targets.
Programmatic constraints as from F-Mission call.	Cost at completion boundaries. Fast development track. Incompatibility with dedicated technology developments and need to rely on existing, flight qualified solutions.

Table 18: Main design drivers for the Comet Interceptor spacecraft.

At the time of writing, the project is completing the definition phase (phase A/B) and preparing for the satellite level Preliminary Design Review, with two candidate prime contractor consortia working in parallel (respectively an OHB-IT led consortium and a TAS-UK led consortium). The respective designs are represented in *Figure 52* and *Figure 53*. The selection of the prime contractor is expected shortly after PDR and mission adoption, in Q3-2022.

Given the fast development approach followed by *Comet Interceptor*, both design solutions must rely on existing platform heritage, minimizing the need for qualification/delta-qualification activities. The total CI spacecraft mass, including propellant and margins is limited to 975 kg by the presently estimated launcher performance (for a dual launch with Ariel). The overall dimensions of the stowed S/ C (without considering appendages) are approximately 2000 mm x 2000 mm x 2500 mm.

The configuration of the S/C A is similar for both contractors, including:

- a cuboid shape, hosting all platform equipment and accommodating payload and probes.
- the AOGNC subsystem, responsible for Attitude, Orbit, Guidance and Navigation Control, including different sensors (Coarse Sun Sensor, Gyro, Star Trackers, Navigation Cameras) and actuators (Reaction Wheels and Reaction Control System).
- a chemical propulsion system with a large Delta-V capability.
- a communication system based on a fixed High Gain Antenna operating in X band and including an inter-satellite link operating in S band.
- two deployable solar arrays.
- a thermal control system, based on a classic passive design.
- a dust shield protecting S/C A and probes during the encounter phase on the ram face.
- two probes accommodated on the same S/C side.

The chemical propulsion system is designed to provide, within the maximum allowed launch mass, a minimum transfer Delta-V capability of 600 m/s (see section 5.1.4); in addition, should the Ariane 6.2 performance improve by the time of the Comet Interceptor launch, the capability to load additional propellant, thus exceeding the minimum required Delta-V performance, is requested.

It is noted that during the fly-by the target is maintained in the field of view of the high-resolution camera CoCa via a dedicated rotating mirror (Rotating Mirror Assembly), while the S/C maintains inertial attitude, maintaining the dust shield in the direction of the relative velocity.

Probe B2 is a small craft, with axisymmetric shape, gyroscopically stabilised and without propulsion and attitude control capability, deployed from S/C A via a dedicated separation system. Probe B2 hosts a subset of scientific instruments and transmits data to the main spacecraft via a dedicated inter-satellite link. The total probe mass is approx. 35 kg, with a typical diameter of approximately 0.5 m. The configuration of the probe (Probe B2) is similar for both contractors and includes:

- Axisymmetric shape compatible with the spin stabilisation.
- Power system based on a primary battery.
- Communication system working in S-band.
- Dust shield protecting the probe during the encounter.
- Operational lifetime of approximately 30 hr.

Probe B1 is a small craft, with cuboid shape, 3-axis stabilised, without propulsion capability, deployed from S/C A via a dedicated separation system (see *Figure 54*). Probe B1 hosts a subset of scientific instruments and transmits data to the main spacecraft via a dedicated inter-satellite link. The total probe mass is approx. 35 kg, with a typical size of approximately 0.5 m. The configuration of Probe B1 includes:

- A flat, cuboid shape compatible.
- Dedicated Attitude, Guidance and navigation sub-system using P/L units
- Electrical power system based on deployable solar arrays and a secondary battery.
- Communication system working in S-band.
- Dust shield protecting the probe during the encounter.

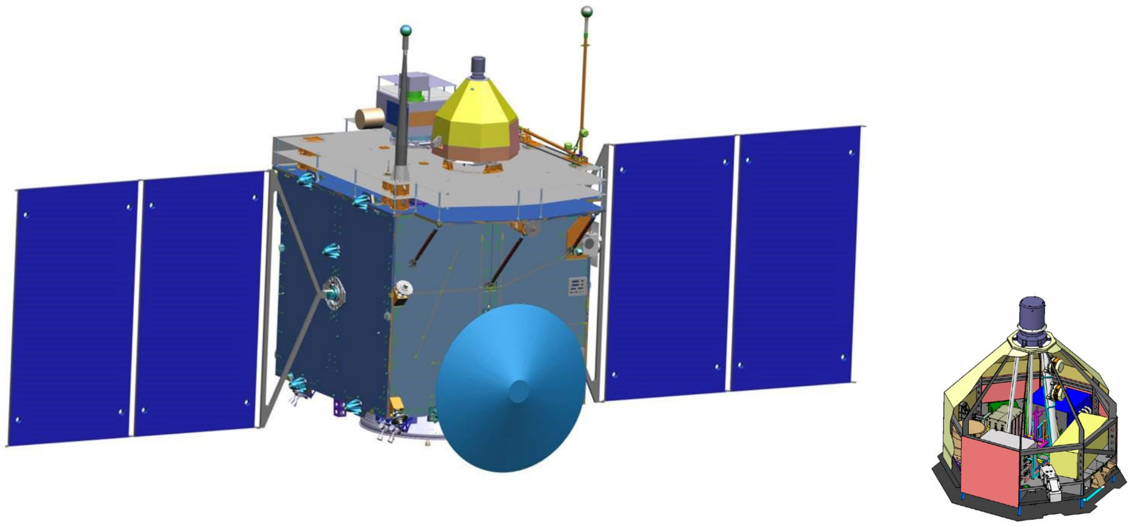

Figure 52: Comet Interceptor spacecraft – OHB.

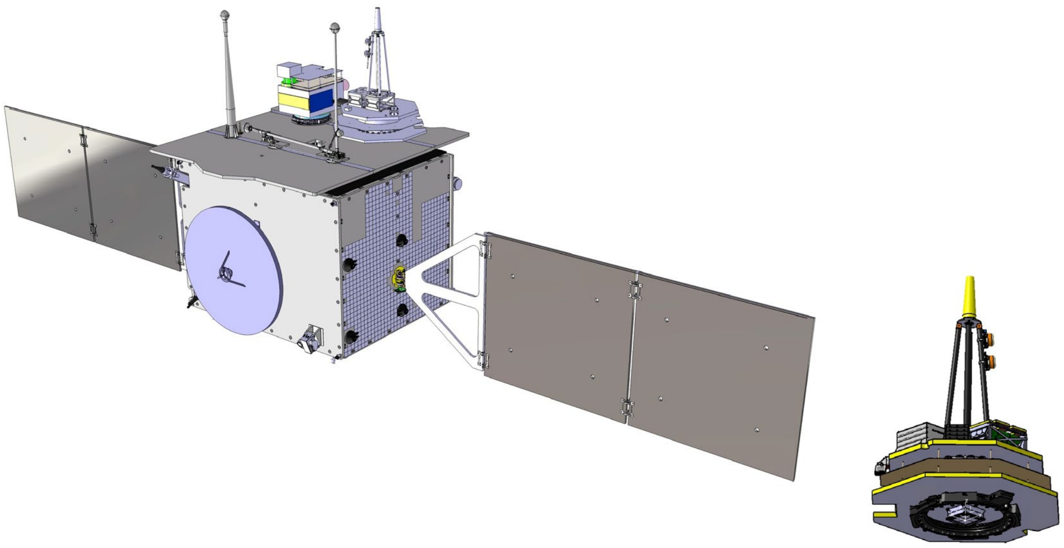

Figure 53: Comet-I spacecraft – TAS.

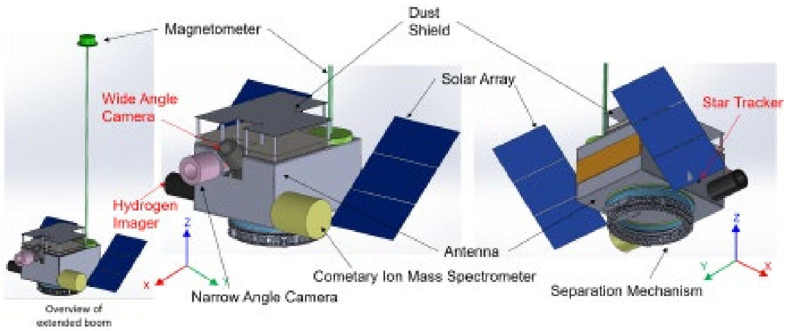

Figure 54: Comet-I probe B1 after separation from S/C A (JAXA).

5.3 Integration and testing

The Assembly, Integration and Testing (AIT) approach of the *Comet Interceptor* Spacecraft is based on a simplified model philosophy and on an incremental integration and test approach.

The spacecraft level model philosophy is defined to be consistent with the existing design heritage and is expected to include:

1) Structural Qualification Model

2) Electrical Functional Model

3) Proto-Flight Model

The scientific payload and the probe providers are required to contribute to spacecraft level test models by providing structurally representative units and electrical functional models. The corresponding delivery dates have been defined in order to respect the overall project plan. In particular, testing on SQM and EFM are expected to be started before the satellite level Critical Design Review. Units to be integrated on Probe B2 are the first to be delivered, so as to allow the completion of probe level tests before delivery to the main S/C integrator.

Testing will follow an incremental approach, including:

1) qualification and/or acceptance level tests at unit level

2) qualification and/or acceptance level tests of the scientific instruments

3) qualification and/or acceptance tests at probe level

4) qualification and/or acceptance tests at main spacecraft level. Thermal tests at spacecraft level will be performed at PFM level.

It is noted that instruments calibration activities will be performed before delivery to the S/C prime contractor, since, in line with the F-mission boundaries, no calibration or science performance test is possible at spacecraft level.

6 Ground Segment

6.1 Ground Segment Architecture

The overall architecture and data flow of *Comet Interceptor* is shown in *Figure 55*.

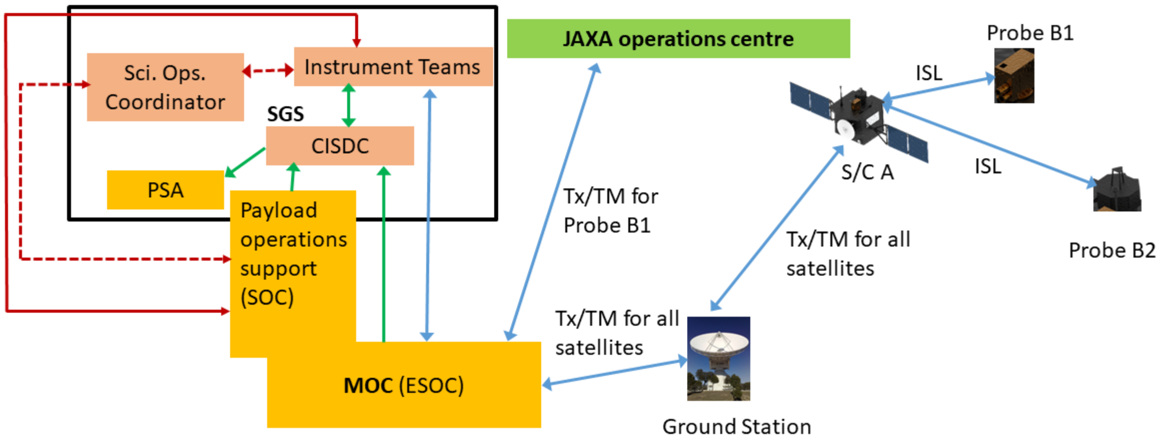

Figure 55: Mission elements and interfaces on Comet Interceptor. Red lines represent uplink interfaces, green lines downlink, and blue lines both uplink and downlink. Yellow boxes are ESA entities, dark orange represent ESA member state (and Japanese in case of Instrument Teams) contributions, and green JAXA centre.

All telemetry data are transmitted by S/C A to the MOC located at ESOC. The main spacecraft communicates with the two probes through inter-satellite links.

ESOC is responsible for the operations of Spacecraft A and probes. JAXA is responsible for definition of operations of Probe B1. After separation the two probes will operate autonomously from S/C A, following a pre-loaded operations timeline.

The high-level operations plan is proposed to the SWT by the Science Operations Coordinator, funded by ASI, in close cooperation with the instrument teams and supported by the Science Operations Component (SOComp) at ESAC. As *Comet Interceptor* is a small mission and the science phase is a single fast fly-by, uplink of payload data goes through a direct interface between instrument teams (JAXA Operations Centre, or the instrument teams for probe B1) and MOC, without involving an interface to SOComp. SOComp on *Comet Interceptor* does provide limited payload operations support, closely associated with the MOC for planning of the comet fly-by.

For downlink, instrument data are distributed from MOC to instrument teams and to the *Comet Interceptor* Science Data Centre (CISCD), hosted by the Belgium User Support and Operations Centre (BUSOC). Auxiliary data (e.g., Spacecraft and comet orbit and attitude) and certain spacecraft data will also be distributed to the SOComp for creating a SPICE dataset. Data processing will be performed by the CISDC and the instrument teams. At the end of post operations, all data will be transferred from the CISDC to ESA's Planetary Science Archive (PSA) and the corresponding Japanese archiving authority for long-term archiving.

6.2 Mission Operations

Mission operations will be managed, developed, and conducted by the Operations Directorate (OPS) of ESA with the Mission Operations Centre located at the European Space Operations Centre (ESOC) in Darmstadt, Germany.

The approach taken for mission operations will be similar to the one already adopted for other ESA interplanetary missions, with all the specific adaptations required by the mission profile and by the very constrained budget linked to an F-Class mission.

Given the very specific mission profile, which includes:

- shared launch with ARIEL,
- transfer to L2 and wait for selection of target comet, if not already made prior to launch
- interplanetary transfer from L2 to target comet,
- approach and fly-by, with actual science measurements concentrated over few days,

An extremely slim approach for science operations planning has been assumed, where all will be coordinated by the MOC, without the establishment of a Science Operations Centre, rather having science operations expertise from the Science Directorate embedded in the MOC team for the fly-by planning.

The MOC architecture (*Figure 56*) will be the same as the one adopted for other interplanetary missions, except for a direct line with the instrument teams for the planning of operations, a scheme almost identical to the one conceived for science operations of the Juice mission during the cruise towards Jupiter.

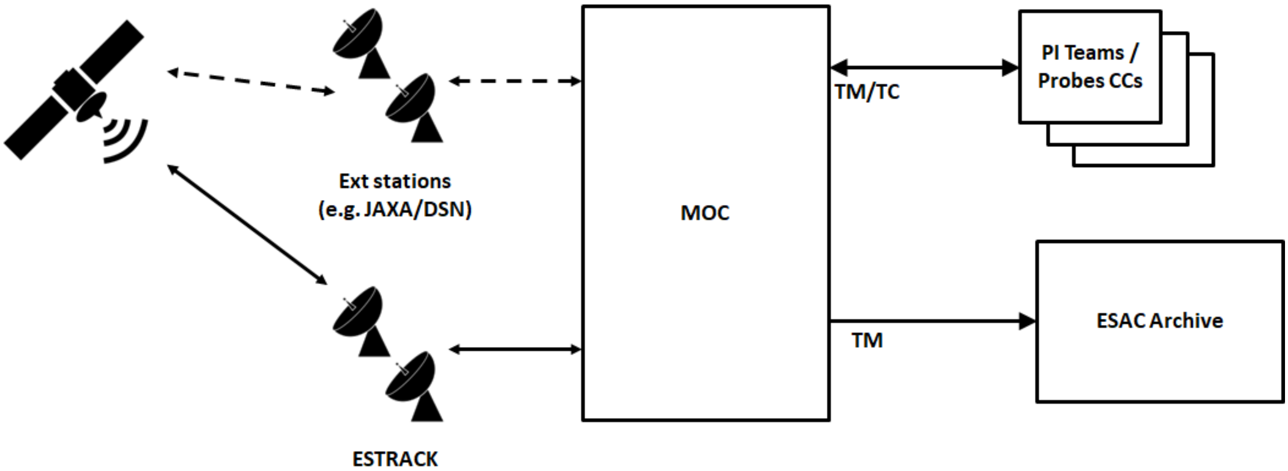

Figure 56: Mission Operations concept for Comet Interceptor.

The intended approach for spacecraft monitoring and control is based on a standardised set of operation interface requirements and related on-board services and functions to be implemented in the on-board software, which would allow implementation of the vast majority of operations by means of a time-tagged queue of commands, with the possibility of controlling/affecting execution by means of ancillary functions like parameter monitoring, reaction to events, on-board control procedures (OBCPs), etc.

Mission planning will be conducted offline, with the generation of command sequences based on operations requirements and validated against agreed mission rules and constraints.

The most challenging activities will be the navigation towards the target, requiring optical navigation techniques on top of the traditional radiometric data, and the unique fly-by opportunity, when the reliability and availability of the spacecraft have to be maximised. Both operations will be largely based on the experience accumulated in the frame of the *Rosetta* asteroid fly-bys (Steins in 2008 and Lutetia in 2010), which had an almost identical profile. The final approach was based on optical navigation and autonomous on-board guidance initialised to optimise pointing towards the target during closest-approach by compensating the along-track navigation error (which was the dominating factor).

Separation of the probes will put a not negligible delta on the criticality of the final approach activities; in this case, experience from the release of the *Rosetta Philae* lander will prove to be valuable.

6.3 Science Operations, Data Handling and Archiving

The Science Operations are described in detail in the Science Operations Concept Document (COMET-ESA-SOC-OD-001). A summary is given here.

6.3.1 Components of the Science Ground Segment

6.3.1.1 *Science Operations Component (SOComp)*

A standard Science Operations Centre approach, located at ESAC (as implemented for M and L class missions) is out of scope, given the nature of the F class constraints, and the very short duration of the main mission science operations. Hence, we refer instead to a Science Operations Component (SOComp). This approach considers a close association of the SOComp with the MOC.

The SOComp is responsible for the science operations of the ESA-funded part of the *Comet Interceptor* Science Ground Segment.

The responsibility for the SGS tasks and activities are distributed and shared between SOComp and the Consortium SGS (CSGS) and comprise the SGS architecture, mission planning, instrument operations and calibration, data processing, and archiving.

The responsibility for the design, implementation, and operation of the SOComp rests with ESA/ESAC.

The main tasks of the SOComp are:

- Responsibility for the scientific operations of the mission,
- Interface with MOC for reception of selected spacecraft telemetry (e.g., solar panel orientation) and auxiliary files for SPICE kernel creation
- Support of the high-level planning and payload operations. The reception of correctly formatted science and auxiliary data for the archive from CISDC.

6.3.1.2 *ESA Member State Contributions to the SGS*

6.3.1.2.1 Comet Interceptor Science Data Centre

The Belgian User Support and Operations Centre (B.USOC) will host the *Comet Interceptor* Science Data Centre (CISDC).

The tasks of CISDC will depend on the phase of the mission. During the mission phases C and D, CISDC will iterate with SOComp and instrument teams to define interfaces and set up data management and visualisation tools. In Phase E, it will continue to work on interfacing with instrument teams on science data and calibration pipelines. The CISDC will serve this data, in archive format, to the members of the Science Working Team and eventually deliver to the archive at SOComp (PSA). The delivery schedule will be according to the data policy of the mission (Section 7.5)

The following provides a more detailed view of the activities for the CISDC.

- The CISDC will serve all the science data from the ESA spacecraft and the JAXA spacecraft, as this facilitates and supports the raison d'etre of the CISDC, being able to implement the full calibration of the data and in particular develop multi-spacecraft data products.
- Instrument teams and CISDC are responsible for providing PSA compliant data for the archive.
- Auxiliary data of spacecraft and comet trajectory and attitude data (provided by MOC FD and by SOComp as SPICE kernels) will be distributed as well. The CISDC will also provide coordinated data from multiple instruments, for instance in data combinations that are relevant for particular science themes. CISDC will host and provide documentation regarding the instruments and data products. The CISDC offers to serve data from Earth-based campaigns of candidate target objects on a case-by-case basis.

The CISDC has no component in the uplink, only in downlink. The responsibility for the instrument calibration pipelines remains with the Instrument Lead Scientists (ILSs). The CISDC (in coordination with the SOComp archive scientist and ESA PS) will coordinate with all ILSs the data that they are planning to provide and the data that they need themselves to do their processing (e.g., from other sensors to obtain a better calibration, or inter-calibration). The CISDC will interact with the science community, should these be interested in specific combinations of data or graphs (e.g., quick look plots). The CISDC sets up inter-calibration activities. It plays the role of facilitator; the Science Team remains responsible for providing cross-calibrated data based on lower-level data produced by the instrument teams and auxiliary data provided by the CISDC.

In the post operations phase all the data (at the various processing levels) and documentation is transferred from CISDC to ESAC.

The CISDC will interact with SOComp specifically for the provision of auxiliary data (position, attitude, possibly data regarding spacecraft subsystems). Throughout all of this the CISDC interacts with SOComp, primarily via the ESA PS to manage the whole process.

6.3.1.2.2 Science Operations Coordinator

The Science Operations Coordinator leads science planning and harmonisation across teams, in close communication with the ESA Project Scientist, to build a single science operations plan for the fly-by. This includes balancing different scientific priorities from the whole science team, interacting with the instrument teams on necessary resources (e.g., data volume, power) and operational requirements/constraints, and aligning plans between the three spacecraft. The instruments operations timeline for the fly-by will be based on inputs from the whole science team, through the Science Working Team. Final decisions on the timeline will be made by the project scientist, following the advice of the SWT, based on input from Science Operations Coordinator and of the MOC.

6.3.1.2.3 Target Identification team

The main goal of the mission is to characterise an LPC. LPCs have historically been identified from a few years to a few months prior to their perihelion, too short a period to enable a mission to be planned and launched. *Comet Interceptor* will achieve its goal by waiting at the Sun-Earth L2 point while the search for a suitable target is made. The Target IDentification Team (TIDT), as a Working Group supporting the Comet Interceptor Science Working Team, is responsible for finding suitable targets for the mission. In the case a suitable target is not identified in the allotted time, a Back-Up Comet Target (BUCT) will have already been assigned linked to the launch date.

6.3.1.2.4 Instrument teams

The Instrument teams are one of the major components of the SGS. Instrument teams are responsible for:

- Instrument development, testing, calibration, performance assessment and preparation of the related documentation and in particular, the preparation of a detailed Instrument User Manual.
- Instrument maintenance, in particular for the development, update, test and documentation of the on-board flight software.
- Instrument calibration: perform calibration, organize, and communicate to ESA any calibration campaigns deemed necessary on ground and in-flight, development of calibration algorithms and maintenance of calibration files.
- Supporting the preparation of instruments timelines as agreed and in coordination with the science operations coordination activity.
- Supporting verification and validation of the instruments' timeline and resulting command sequences prepared for uploading to spacecraft.
- Participation in the analysis and verification of the raw data and reporting of any anomaly.
- Development and maintenance of algorithms, numerical codes and databases needed for data processing, quick-look analysis, and calibration.
- Providing to CISDC calibration files and algorithms/routines needed for data processing/and or/ providing calibrated data via their pipelines and software to the CISDC for archive data product generation.
- Monitoring of the instrument operations, in particular by analysis of the telemetry for instrument housekeeping data to assess the instrument's health and report any anomaly to ESA.
- Communicating to ESA SOComp and MOC any required change in instrument configuration (new resource profiles, operational constraints etc.)
- Participate in ground segment reviews, in particular support the archive review.

6.3.2 Science Ground Segment tasks and activities

6.3.2.1 *Overall SGS architecture*

To achieve the mission objectives science operations is divided into two paths, from the ground segment to the *Comet Interceptor* spacecraft commonly classified as uplink path and from the *Comet Interceptor* spacecraft to the ground segment, commonly classified as the downlink path.

6.3.2.2 *Science Mission Planning and Instrument Operations (uplink)*

Comet Interceptor is a fly-by mission. As such, science mission planning is focused about a short < 1-week time period, around closest approach. Based on a Master Science Plan produced by the SWT, and inputs from the instrument teams and members of the science teams, the SOCoord will propose high level instrument operations timelines for all spacecraft to the SWT, well in advance of the encounter phase. The timelines include resource allocations (currently, the only resources to consider are data volume, and, for probe B2, energy). The proposal is discussed by the SWT, and a recommendation issued to the Project Scientist for final approval. While, for some scenarios of comet selection and flyby, the actual timelines need to be created relatively quick (a few months), the process is to be rehearsed either with a flyby of a Backup Target Comet and with a simulated flyby of a Long-period Comet. Based on the approved timelines, the Instrument Teams will create Telecommand Sequences (Payload Operations Requests) and deliver them to the MOC. MOC will check them for consistency with resource availability and mission constraints and the SOCoord and the ESA Project Scientist, supported by an Operations Engineer, for agreement with the approved timeline. As such, the SOComp dedicated to instrument operations will be closely linked to MOC.

Some science operations outside of the encounter phase may be possible (to support target characterisation and activity monitoring) and will be carried out via the SOComp, following approval by the PS advised by the SWT and SOCoord, Instrument calibration and check out are PI-MOC interactions.

6.3.2.3 *Data Processing and calibrations (Downlink)*

Following downlink via the OGS, raw data will arrive to the Instrument teams. It is expected that the total raw data volume of the mission will be ~ 200 GB. The CISDC will work with the Instrument teams who will deliver raw data and calibration pipelines or, in special cases, calibrated data products. CISDC will also support utilisation of multi-spacecraft measurements to improve calibration. CISDC will centrally serve raw and calibrated data to the science team for science use and validation. Those data will be provided in archive format immediately, to facilitate more rapid interactions and avoid the overhead of conversion issues when eventually delivering to the archive (ESDC) during post operations. Close interaction between the CISDC and the European Science Data Centre (ESDC), in particular with the archive scientist, is a necessity.

6.3.2.4 *Data Archive*

The main activity of the ESAC-based archive team (ESDC) will be to support the CISDC in ensuring appropriate implementation and use of archive compliant data formatting and eventual reception of that data for ingestion. CISDC will serve science and HK data to the science teams in the appropriate archive format (e.g., PDS4). This will avoid transition and translation issues when the data is finally transferred to the ESDC in the mission post operations phase. While there is no proprietary period on Comet Interceptor, access to the data will be restricted to the Science Team for a calibration and validation period of maximum 6 months.

All data (S/C A, B1 and B2) are served via CISDC and eventually the ESA archive. Data will be delivered in archive format (PDS version 4) and documented according to archive standards.

6.3.3 Science Operations evolution with mission phases

6.3.3.1 *Overview of mission phases*

The mission phases and durations are driven by the Spacecraft and payload development and in-orbit operation with exception of the post-operations phase. The phases are marked as 0/A/B (B1/B2)/C/D/E (E1/E2)/F with the following descriptions for the F class:

- 0: Feasibility phase (swift assessment of the proposed mission, identifying major mission drivers and concept design)
- A: Assessment study phase (feasibility, preliminary configuration, and system design)
- B1/B2: Definition study phase (requirements, SRR end of B1, with consolidation up to PDR (end B2) and mission adoption)
- C: Implementation phase (detailed design, until CDR)
- D: Implementation phase (AIV, until QAR/FAR)
- E1: Implementation phase (launch & Near-Earth commissioning, until NECR)
- E2: Nominal operations
- F: Post-Operations (including decommissioning and spacecraft disposal)

The science operations phases are tagged in a different way than the above listed overall mission phases. Phases C and D are grouped as “Development phase”, E1 and E2 are grouped as “Operational phase”, and F remains the “Post-Operations phase”. Dedicated Ground Segment reviews are planned to monitor progress during both the development and operations phases. Due to the small size of the SOComp, the review schedule follows that of the MOC.

Phase E1 of the operational phase can be further divided into LEOP and commissioning phase driven by mission operations activities. Phase E2 starts with the performance verification phase, which transitions seamlessly into routine science operations. SGS activities comprise different tasks and interactions during these phases and are therefore split out. Any mission extensions to routine science operations will also fall under phase E2.

Phase F starts after routine science operations and any mission extensions and is dedicated to SGS activities. Nevertheless, during the first few months of phase F also the S/C disposal and MOC rundown are happening in parallel.

6.3.3.2 *Development phase*

The TIDT will continually monitor observations and provide any viable targets to ESA (MOC) for further analysis. The SOCoord will begin working on science operations coordination to put together sample high level science operations plans, in particular focusing on science priorities and related instrument operations. SOComp and the Science Operations Coordinator will coordinate with the Instrument teams to ensure that telecommand sequences sent to MOC will reflect the agreed science operations plan. CISDC and Instrument teams will agree on interfaces, and CISDC will install its data management system. This may include visualisation tools.

Closer to launch, (L-2) an archive scientist will start activities, predominantly focused on interfacing with CISDC and Instrument teams and ensuring archive format compliance for the data products. At around L-1 an operations engineer will become available as well as SPICE support, which will enable more detailed examination of science operations timelines and geometry. Around launch, a science operations engineer will begin working with the Instrument teams to support them in converting the high-level time science operations timeline, provided by the science operations coordination via SOCoord, to telecommand/instrument commands for transmission to the spacecraft by MOC. Mechanisms to check compatibility of these commands with the approved high-level science priorities and plan will be developed at this stage. Given the one-off nature of the mission profile, operational quick look products are not considered necessary.

During this phase, target selection and confirmation criteria will be consolidated and implemented by the TIDT and SWT. Target confirmation will be under the authority of the SWT, supported by MOC.

6.3.3.3 *Operational phases*

6.3.3.3.1 LEOP and Commissioning Phase

This phase is fully under MOC control with SOComp in listening/support mode with instrument teams as appropriate. Following a successful Near-Earth Commissioning Review (NECR) the handover of the responsibility over the mission from the ESA Project Manager to the ESA Project Scientist (in the function of Mission Manager) is completed. The spacecraft is transferred to L2 during this phase.

6.3.3.3.2 Waiting at L2 and reaction to target identification.

During this phase, once a target has been identified, a rehearsal fly-by may be implemented if a reachable target (most likely an asteroid) is found. It allows all operations procedures to be refined and checked, in particular considering the actual encounter trajectory information, The SOCoord will update any relevant priorities depending on the nature of the actual flyby target (based on activity estimates and other properties).

During this period, CISDC will be setting up interfaces to receive instrument pipelines and calibrated data and setting up visualisation tools, in close collaboration with the instrument teams and the ESA archive team. This may include ground-based data of potential targets and the eventual selected mission target.

6.3.3.3.3 Encounter and Post Encounter Science Operations Phase

During cruise to the target, trajectory updates and updated information about the target will enable refinement of the science operations plan. Where possible, navigation measurements with respect to the comet, in combination with ground-based data, will provide valuable information on the activity of the comet.

CISDC will finalise preparations for data reception during the encounter and subsequent data processing and provision to the science team. In addition, CISDC will monitor the completeness and quality of the archive products.

The focus of SOComp activity will be in supporting instrument operations (including any updates on SC A trajectories from MOC and their translation to SPICE) and the implementation of the SWT endorsed operations plan.

The post encounter phase (maximum 6 months, but with a duration depending on the actual distance of SC A from Earth) will be the main encounter downlink phase, followed by end of mission and post operations. The uplink part of the SOComp will be run down during the post-encounter phase.

6.3.3.3.4 Post-Operations Phase

SOComp activities will focus on supporting the CISDC in the timely delivery of data to the archive. CISDC will process and provide science and auxiliary data to the science team, including support for the trajectory and attitude reconstruction of the B1 and B2 probes. By the end of the post-operations phase, the CISDC will have delivered all science and associated housekeeping and auxiliary (SPICE) data, and documentation to ESA for archiving in the Planetary Science Archive. The delivery will be evaluated in the archive review, which may result in a redelivery. Afterwards, further updates to science data will be provided directly by instrument teams to ESDC.

7 Management

7.1 Procurement scheme

The procurement scheme followed by the *Comet Interceptor* project follows the typical scheme for ESA science missions, with the Agency being responsible for the procurement of the main spacecraft, Probe B2, launch services and mission operations, while the scientific payload is developed by the Member States. The overview of the different mission elements is provided in *Figure 57*.

The tender for the procurement of the Comet-I S/C covers both the definition phase (A/B – up to and including PDR, parallel competitive) and the implementation phase (C/D/E1, up to and including the in-flight commissioning review). The procurement is based on a single tendering action, with the down-selection of the prime contractor performed at the end of Phase A/B. The definition phase activities include a number of preparatory activities, proposed by each competing contractor for de-risking critical technical areas.

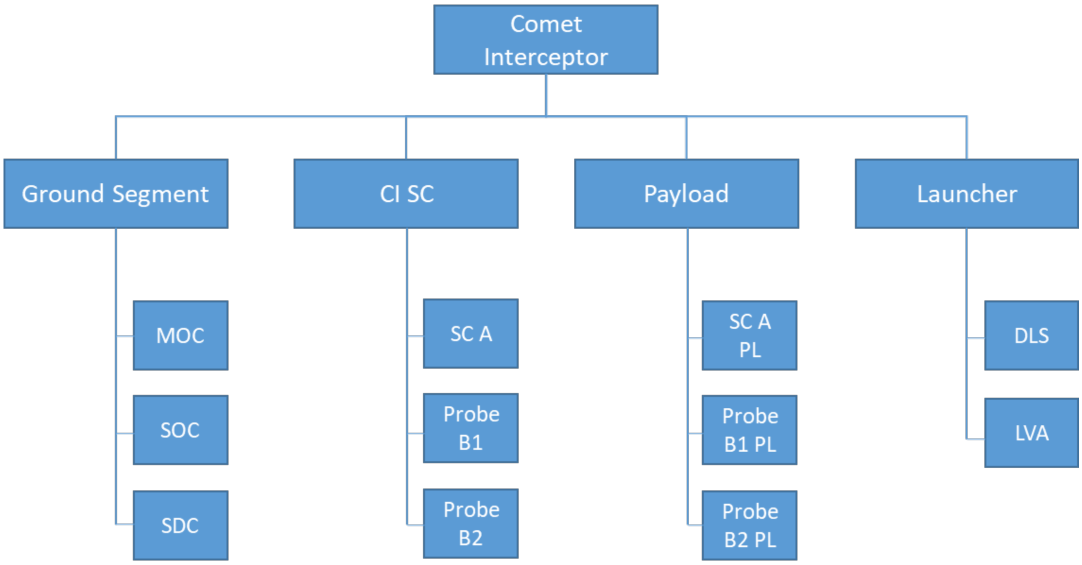

Figure 57: Mission elements.

The selection of the prime contractor, responsible for the development of Spacecraft A, Probe B2 and the integration of both Probe B1 and of the science payload, is planned after the satellite PDR and after mission adoption by SPC. In order to remain within the F-mission boundaries, during phase A/B ESA has promoted a Design-To-Cost approach, aiming to identify an optimum mission solution in terms of cost and science return. This approach has led to an incremental revision of the ESA requirements in areas driving cost, while preserving the science objectives. The requirements baseline evolution has been reflected in the release of an updated Mission and System Requirements Document, shortly after PRR and SRR.

Comet Interceptor will be launched together with ARIEL on an Ariane 62, in a dual launch configuration. The procurement of the launch services is part of the ARIEL cost at completion.

The procurement of the *Comet Interceptor* payload follows the ESA science traditional approach with instruments funded and developed nationally, and delivered formally by ESA to the prime contractor. In order to de-risk the instrument procurement approach, ESA has implemented a number of measures resulting from recent lessons learned and agreements reached in a joint ESA-SPC working group. In particular ESA has provided funding to address lower TRL instrument units and to maintain work continuity at the scientific institutes during the definition phase. .Member States are also responsible for supporting payload safety, maintenance and operations throughout the mission and provision of contributions to the SGS, including the CISDC.

A Multi-Lateral Agreement (MLA) will be established between ESA and the Funding Agencies to formalise the commitments, responsibilities, and deliverables of all parties.

Comet Interceptor includes international cooperation with JAXA, who are responsible for the development and delivery of Probe B1 to ESA. During Phase A/B, the ESA and JAXA teams have interacted with the objective of defining and consolidating the interfaces between Probe B1 and S/C A. These are documented in a related Interface Requirements Document. ESA and JAXA have interacted too to establish a joint project plan. The cooperation scheme aims at decoupling as much as possible the development of Probe B1 from the rest of the project by defining as early as possible a set of 'clean-and-clear' interface requirements, which enable the two agencies to progress with a limited number of interdependencies. After separation from the main S/C, probe B1 will operate autonomously, following a pre-loaded sequence of telecommands defined by JAXA, while data are relayed to S/C A via the Inter Satellite Link (ISL). The ISL is procured by ESA, including the unit to be installed on Probe B1.

7.2 Project management

The overarching responsibility for the *Comet Interceptor* mission rests with ESA's Directorate of Science. ESA responsibilities cover the mission architecture, the development and procurement of S/C A and Probe B2, the satellite integration and test activities, the launch services procurement (dual launch with ARIEL), the mission and science operations. The overall CI mission management scheme is summarised in *Figure 58*.

During the development and commissioning phases, an ESA-appointed Project Manager will be responsible for implementing and managing ESA's activities. After a successful Near-Earth commissioning review, a Mission Manager will take over the responsibility for the mission throughout its nominal and any extended phases.

The *Comet Interceptor* mission relies on the cooperation with JAXA, providing the Probe B1 and associated payload, within the remit of an ESA-JAXA Memorandum of Understanding (MoU).

The ESA ground segment includes the Mission Operation Centre (MOC), the Science Operation Component (SOComp) and a number of Ground Stations (G/S) used in the different mission phases. The Science Ground Segment (SGS) is formed by the SOComp (which includes the Planetary Science Archive), and the Comet Interceptor Science Data Centre (CISDC), which is part of the Belgian User Support and Operations Centre (BUSOC) (see Section 6 for further details).

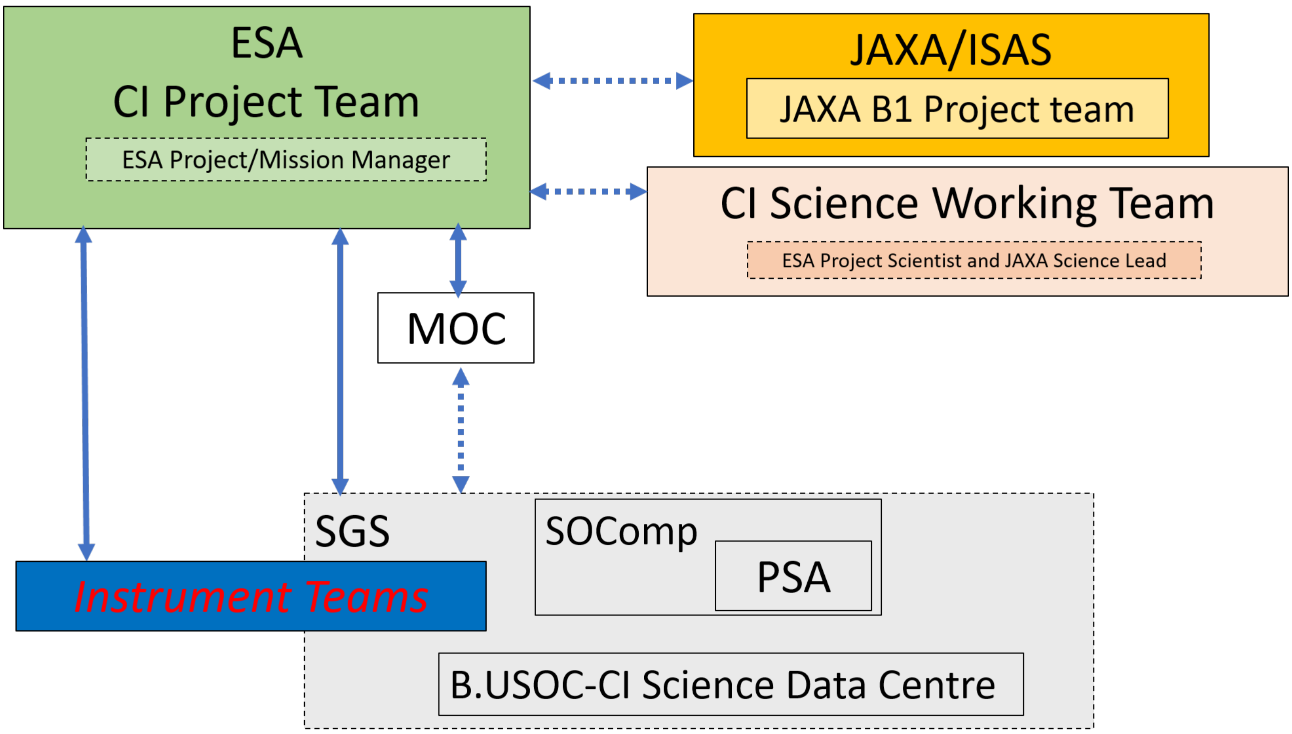

Figure 58: Overview of the Comet Interceptor Mission Management scheme

7.3 Science Management

A *Comet Interceptor* Science Working Team (SWT) will be appointed by ESA after the mission has been adopted. The ESA Project Scientist (PS), in coordination with the JAXA Science Lead (SL) will chair the SWT.

The SWT will advise ESA on all aspects of the mission potentially affecting its scientific performance. It will assist the ESA PS and the JAXA SL in maximising the overall scientific return of the mission within the established boundary conditions. It will act as a focus for the interests of the scientific community in *Comet Interceptor*.

The SWT members will have the data access and rights as indicated in Section 7.5

Members of the SWT are expected to contribute to monitor and to give advice on all aspects of the *Comet Interceptor* mission which affect its scientific performance. They may perform specific scientific and/or technical tasks, as needed during development and operations.

Based on the inputs provided by the Science Operations Coordinator (see Section 6.3.1.2.2), the operations timeline for the fly-by will be recommended by the SWT. Final approval and responsibility for the mission operations remain with ESA.

Based on the inputs provided by the TIDT (see Section 6.3.1.2.3), the SWT will advise ESA on the target selection, as well as on related target navigation aspects.

A more detailed description of the science management approach and the SWT composition will be reported in the Science Management Plan.

7.4 Schedule

The key dates for the *Comet Interceptor* high level schedule are given in *Table 19.* Compared to L- or M-class missions, the schedule is highly compressed, with 3 years of study phase (0, A, B) from SPC selection in June 2019 to adoption in June 2022, and 6 years of development phase (C, D) from adoption to launch readiness mid-2028. Launch is scheduled for December 2029, together with ARIEL.

Milestone	**Date**
Selection of *Comet Interceptor* as F1 mission	June 2019
PDR	Q2 2022
Mission Adoption	June 2022
Prime selection	Q4 2022
Start of phase C/D	Jan 2023
CDR	July 2023 (Instruments) Q4 2024 (System)
Delivery of payload flight units	Q4 2025 (probe B2), Q1 2026 (S/C A)
QAR	Dec 2027
Launch ready	Mid-2028
Launch (L)	Dec. 2029 (shared with ARIEL)
Arrival at L2	L + 4 months
Waiting at L2	Maximum ~5 years
Transfer to target Comet	
Comet fly-by	Latest ~L + 5.5 years
End of Operations	Latest L + 6 years

Table 19: The key dates for the Comet Interceptor high level schedule.

7.5 Data rights

All raw data will be provided by ESA to the Instrument Lead Scientists (ILSs) and to the CISDC, as soon as they will be received on the ground, together with the trajectory, attitude, and relevant spacecraft status information; these data will be archived in the CISDC.

After reception of the raw data, the ILSs and CISDC will have maximum of six months to calibrate and validate the data and to create calibrated data. Immediately afterwards, the CISDC will make the calibrated data publicly available, together with the raw data. To facilitate analysis of multi-instrument data, all data will be shared among the Instrument Lead Scientists (ILSs) and through them with the instrument Co-Investigators (Co-Is),), and with the members of the Science Working Team (SWT) upon creation by the pipeline. Any use of data for publication before the end of the six months period needs agreement by the respective ILS and requires immediate public release of the relevant data. During the calibration and validation period, selected data products will be released for outreach purposed by ESA, in coordination with JAXA and the relevant ILSs and data providers.

High-level science data (Level 5 data) may be produced by the instrument teams, the CISDC, members of the SWT and/or other scientists. Once published, Level 5 data may also be archived in the CISDC.

By the end of the post-operations phase, the CISDC will deliver all data and associated documentation to the European Science Data Centre (ESDC) for long-term archiving in the Planetary Science Archive (PSA).

8 Communication and outreach

Since ancient times, comets have always fascinated people. While they were historically considered bad omens, today the visibility of a comet in the night sky still carries fascination. Communications activities related to cometary missions can build on this interest in those bodies, as demonstrated by ESA's *Giotto* and *Rosetta* missions.

Until launch, outreach activity will be focussed on key hardware deliveries, the launch campaign, and possibly the detection of potential target objects. For potential targets, and in particular the finally selected target, continued release of information will allow the public to follow the characterisation of the comet. After launch, and, in particular, after the comet fly-by, a regular flow of science results from the mission will be prepared in a manner suitable for communication and public outreach purposes. Such outreach activity necessitates the timely availability of suitably processed data and the full involvement of the instrument teams.

ESA will have overall responsibility for the science communications, educational and outreach activities related to *Comet Interceptor*. ESA and JAXA will have the right to use any data acquired by *Comet Interceptor* for outreach purposes, in coordination with the holders of the data rights as applicable.

Approximately one year before the satellite Qualification and Acceptance Review, a public outreach coordination group will be established in close collaboration between ESA, JAXA, the relevant bodies funding the provision of the scientific payload in the Member States and other institutions involved in the mission, in particular the Scientific Consortium. Interactions between these parties will have to coordinate the outreach effort and to guarantee consistency between all applicable documents and policies.

Formal dedicated agreements regarding public outreach activities will be established between ESA, the relevant funding authorities, and other institutions involved in the mission. The terms and conditions contained in these agreements will be applicable on the relationships between the funding authorities and the various scientific investigators. These agreements will take account of any necessary project-specific science-to-public-outreach balance. The implementation of such agreements will be tracked by the SWT and as part of the standard project reviews.

9 References

A'Hearn M. F., Belton M. J. S., Delamere W. A., Kissel J., Klaasen K. P., McFadden L. A., Meech K. J., Melosh H. J., Schultz P. H., Sunshine J. M., Thomas P. C., Veverka J., Yeomans D. K., Baca M. W., Busko I., Crockett C. J., Collins S. M., Desnoyer M., Eberhardy C. A., Ernst C. M., Farnham T. L., Feaga L., Groussin O., Hampton D., Ipatov S. I., Li J.-Y., Lindler D., Lisse C. M., Mastrodemos N., Owen W. M., Richardson J. E., Wellnitz D. D., White R. L., Deep Impact: Excavating Comet Tempel 1, Science, 310, 258 (2005).

A'Hearn M. F., Belton M. J. S., Delamere W. A., Feaga L. M., Hampton D., Kissel J., Klaasen K. P., McFadden

L. A., Meech K. J., Melosh H. J., Schultz P. H., Sunshine J. M., Thomas P. C., Veverka J., Wellnitz D. D., Yeomans D. K., Besse S., Bodewits D., Bowling T. J., Carcich B. T., Collins S. M., Farnham T. L., Groussin O., Hermalyn B., Kelley M. S., Kelley M. S., Li J.-Y., Lindler D. J., Lisse C. M., McLaughlin S. A., Merlin F., Protopapa S., Richardson J. E., Williams J. L., EPOXI at Comet Hartley 2, Science, 332, 1396 (2011).

Adams F. C., The Birth Environment of the Solar System, Annual Review of Astronomy and Astrophysics, 48, 47 (2010).

Alfven H., On the theory of comet tails., Tellus, 9, 92 (1957).

Alho M., Simon Wedlund C., Nilsson H., Kallio E., Jarvinen R., Pulkkinen T. I., Hybrid modeling of cometary plasma environments. II. Remote-sensing of a cometary bow shock, Astronomy and Astrophysics, 630, A45 (2019).

Alho M., Jarvinen R., Simon Wedlund C., Nilsson H., Kallio E., Pulkkinen T. I., Remote sensing of cometary bow shocks: modelled asymmetric outgassing and pickup ion observations, Monthly Notices of the Royal Astronomical Society, 506, 4735 (2021).

Altwegg K., Balsiger H., Bar-Nun A., Berthelier J. J., Bieler A., Bochsler P., Briois C., Calmonte U., Combi M., De Keyser J., Eberhardt P., Fiethe B., Fuselier S., Gasc S., Gombosi T. I., Hansen K. C., Hässig M., Jäckel A., Kopp E., Korth A., LeRoy L., Mall U., Marty B., Mousis O., Neefs E., Owen T., Rème H., Rubin M., Sémon T., Tzou C.-Y., Waite H., Wurz P., 67P/Churyumov-Gerasimenko, a Jupiter family comet with a high D/H ratio, Science, 347, 1261952 (2015).

Altwegg K., Balsiger H., Bar-Nun A., Berthelier J.-J., Bieler A., Bochsler P., Briois C., Calmonte U., Combi

M. R., Cottin H., De Keyser J., Dhooghe F., Fiethe B., Fuselier S. A., Gasc S., Gombosi T. I., Hansen K. C., Haessig M., Ja ckel A., Kopp E., Korth A., Le Roy L., Mall U., Marty B., Mousis O., Owen T., Reme H., Rubin M., Semon T., Tzou C.-Y., Waite J. H., Wurz P., Prebiotic chemicals--amino acid and phosphorus--in the coma of comet 67P/Churyumov-Gerasimenko, Science Advances, 2, e1600285 (2016).

Altwegg K., Balsiger H., Berthelier J. J., Bieler A., Calmonte U., De Keyser J., Fiethe B., Fuselier S. A., Gasc S., Gombosi T. I., Owen T., Le Roy L., Rubin M., Sémon T., Tzou C.-Y., D₂O and HDS in the coma of 67P/Churyumov-Gerasimenko, Philosophical Transactions of the Royal Society of London Series A, 375, 20160253 (2017a).

Altwegg K., Balsiger H., Berthelier J. J., Bieler A., Calmonte U., Fuselier S. A., Goesmann F., Gasc S., Gombosi T. I., Le Roy L., de Keyser J., Morse A., Rubin M., Schuhmann M., Taylor M. G. G. T., Tzou C.-Y., Wright I., Organics in comet 67P - a first comparative analysis of mass spectra from ROSINA-DFMS, COSAC and Ptolemy, Monthly Notices of the Royal Astronomical Society, 469, S130 (2017b).

Altwegg K., Balsiger H., Fuselier S. A., Cometary Chemistry and the Origin of Icy Solar System Bodies: The View After Rosetta, Annual Review of Astronomy and Astrophysics, 57, 113 (2019).

Altwegg K., Balsiger H., Hänni N., Rubin M., Schuhmann M., Schroeder I., Sémon T., Wampfler S., Berthelier J.-J., Briois C., Combi M., Gombosi T. I., Cottin H., De Keyser J., Dhooghe F., Fiethe B., Fuselier S. A., Evidence of ammonium salts in comet 67P as explanation for the nitrogen depletion in cometary comae, Nature Astronomy, 4, 533 (2020).

Asphaug E., Benz W., Size, Density, and Structure of Comet Shoemaker-Levy 9 Inferred from the Physics of Tidal Breakup, Icarus, 121, 225 (1996).

Bagnulo S., Cellino A., Kolokolova L., Nežič R., Santana-Ros T., Borisov G., Christou A. A., Bendjoya Ph. & M. Devogèle, Unusual polarimetric properties for interstellar comet 2I/Borisov, Nature Communications, 12, 1797 (2021)

Bardyn A., Baklouti D., Cottin H., Fray N., Briois C., Paquette J., Stenzel O., Engrand C., Fischer H., Hornung K., Isnard R., Langevin Y., Lehto H., Le Roy L., Ligier N., Merouane S., Modica P., Orthous-Daunay F.-R., Rynö J., Schulz R., Silén J., Thirkell L., Varmuza K., Zaprudin B., Kissel J., Hilchenbach M., Carbon-rich dust in comet 67P/Churyumov-Gerasimenko measured by COSIMA/Rosetta, Monthly Notices of the Royal Astronomical Society, 469, S712 (2017).

Barkan A., Merlino R. L., D'Angelo N., Laboratory observation of the dust-acoustic wave mode, Physics of Plasmas, 2, 3563 (1995).

Barucci M. A., Filacchione G., Fornasier S., Raponi A., Deshapriya J. D. P., Tosi F., Feller C., Ciarniello M., Sierks H., Capaccioni F., Pommerol A., Massironi M., Oklay N., Merlin F., Vincent J.-B., Fulchignoni M., Guilbert-Lepoutre A., Perna D., Capria M. T., Hasselmann P. H., Rousseau B., Barbieri C., Bockelée-Morvan D., Lamy P. L., De Sanctis C., Rodrigo R., Erard S., Koschny D., Leyrat C., Rickman H., Drossart P., Keller

H. U., A'Hearn M. F., Arnold G., Bertaux J.-L., Bertini I., Cerroni P., Cremonese G., Da Deppo V., Davidsson

B. J. R., El-Maarry M. R., Fonti S., Fulle M., Groussin O., Güttler C., Hviid S. F., Ip W., Jorda L., Kappel D., Knollenberg J., Kramm J.-R., Kührt E., Küppers M., Lara L., Lazzarin M., Lopez Moreno J. J., Mancarella F., Marzari F., Mottola S., Naletto G., Pajola M., Palomba E., Quirico E., Schmitt B., Thomas N., Tubiana C., Detection of exposed H_2O ice on the nucleus of comet 67P/Churyumov-Gerasimenko. as observed by Rosetta OSIRIS and VIRTIS instruments, Astronomy and Astrophysics, 595, A102 (2016).

Bauer J. M., Grav T., Fernández Y. R., Mainzer A. K., Kramer E. A., Masiero J. R., Spahr T., Nugent C. R., Stevenson R. A., Meech K. J., Cutri R. M., Lisse C. M., Walker R., Dailey J. W., Rosser J., Krings P., Ruecker K., Wright E. L., NEOWISE Team, Debiasing the NEOWISE Cryogenic Mission Comet Populations, The Astronomical Journal, 154, 53 (2017).

Belton M. J. S., Thomas P., Li J.-Y., Williams J., Carcich B., A'Hearn M. F., McLaughlin S., Farnham T., McFadden L., Lisse C. M., Collins S., Besse S., Klaasen K., Sunshine J., Meech K. J., Lindler D., The complex spin state of 103P/Hartley 2: Kinematics and orientation in space, Icarus, 222, 595 (2013).

Bernhardt P. A., Roussel-Dupre R. A., Pongratz M. B., Haerendel G., Valenzuela A., Gurnett D. A., Anderson R.R., Observations and theory of the AMPTE magnetotail barium releases, Journal of Geophysical Research, 92, 5777 (1987).

Bertini I., La Forgia F., Tubiana C., Güttler C., Fulle M., Moreno F., Frattin E., Kovacs G., Pajola M., Sierks H., Barbieri C., Lamy P., Rodrigo R., Koschny D., Rickman H., Keller H. U., Agarwal J., A'Hearn M. F., Barucci M. A., Bertaux J.-L., Bodewits D., Cremonese G., Da Deppo V., Davidsson B., Debei S., De Cecco M., Drolshagen E., Ferrari S., Ferri F., Fornasier S., Gicquel A., Groussin O., Gutierrez P. J., Hasselmann P. H., Hviid S. F., Ip W.-H., Jorda L., Knollenberg J., Kramm J. R., Kührt E., Küppers M., Lara L. M., Lazzarin M., Lin Z.-Y., Moreno J. J. L., Lucchetti A., Marzari F., Massironi M., Mottola S., Naletto G., Oklay N., Ott T., Penasa L., Thomas N., Vincent J.-B., The scattering phase function of comet 67P/Churyumov-Gerasimenko coma as seen from the Rosetta/OSIRIS instrument, Monthly Notices of the Royal Astronomical Society, 469, S404 (2017)

Beth A., Altwegg K., Balsiger H., Berthelier J.-J., Calmonte U., Combi M. R., De Keyser J., Dhooghe F., Fiethe B., Fuselier S. A., Galand M., Gasc S., Gombosi T. I., Hansen K. C., Hässig M., Héritier K. L., Kopp E., Le Roy L., Mandt K. E., Peroy S., Rubin M., Sémon T., Tzou C.-Y., Vigren E., First in-situ detection of the cometary ammonium ion NH_4^+ (protonated ammonia NH_3) in the coma of 67P/C-G near perihelion, Monthly Notices of the Royal Astronomical Society, 462, S562 (2016).

Beth A., Altwegg K., Balsiger H., Berthelier J.-J., Combi M. R., De Keyser J., Fiethe B., Fuselier S. A., Galand M., Gombosi T. I., Rubin M., Sémon T., ROSINA ion zoo at Comet 67P, Astronomy and Astrophysics, 642, A27 (2020).

Bieler A., Altwegg K., Balsiger H., Bar-Nun A., Berthelier J.-J., Bochsler P., Briois C., Calmonte U., Combi M., de Keyser J., van Dishoeck E. F., Fiethe B., Fuselier S. A., Gasc S., Gombosi T. I., Hansen K. C., Hässig M., Jäckel A., Kopp E., Korth A., Le Roy L., Mall U., Maggiolo R., Marty B., Mousis O., Owen T., Rème H., Rubin M., Sémon T., Tzou C.-Y., Waite J. H., Walsh C., Wurz P., Abundant molecular oxygen in the coma of comet 67P/Churyumov-Gerasimenko, Nature, 526, 678 (2015).

Bieler A., Altwegg K., Balsiger H., Berthelier J.-J., Calmonte U., Combi M., De Keyser J., Fiethe B., Fougere N., Fuselier S., Gasc S., Gombosi T., Hansen K., Hässig M., Huang Z., Jäckel A., Jia X., Le Roy L., Mall U. A., Rème H., Rubin M., Tenishev V., Tóth G., Tzou C.-Y., Wurz P., Comparison of 3D kinetic and hydrodynamic models to ROSINA-COPS measurements of the neutral coma of 67P/Churyumov- Gerasimenko, Astronomy and Astrophysics, 583, A7 (2015).

Biermann L., Brosowski B., Schmidt H. U., The interactions of the solar wind with a comet, Solar Physics, 1, 254 (1967).

Biver N., Bockelée-Morvan D., Paubert G., Moreno R., Crovisier J., Boissier J., Bertrand E., Boussier H., Kugel F., McKay A., Dello Russo N., DiSanti M. A., The extraordinary composition of the blue comet C/2016 R2 (PanSTARRS), Astronomy and Astrophysics, 619, A127 (2018).

Blum J., Gundlach B., Krause M., Fulle M., Johansen A., Agarwal J., von Borstel I., Shi X., Hu X., Bentley

M. S., Capaccioni F., Colangeli L., Della Corte V., Fougere N., Green S. F., Ivanovski S., Mannel T., Merouane S., Migliorini A., Rotundi A., Schmied R., Snodgrass C., Evidence for the formation of comet 67P/Churyumov-Gerasimenko through gravitational collapse of a bound clump of pebbles, Monthly Notices of the Royal Astronomical Society, 469, S755 (2017).

Bockelée-Morvan D., Lis D. C., Wink J. E., Despois D., Crovisier J., Bachiller R., Benford D. J., Biver N., Colom P., Davies J. K., Gérard E., Germain B., Houde M., Mehringer D., Moreno R., Paubert G., Phillips T. G., Rauer H., New molecules found in comet C/1995 O1 (Hale-Bopp). Investigating the link between cometary and interstellar material, Astronomy and Astrophysics, 353, 1101 (2000).

Bodewits D., Noonan J. W., Feldman P. D., Bannister M. T., Farnocchia D., Harris W. M., Li J.-Y., Mandt K. E., Parker J. W., Xing Z.-X., The carbon monoxide-rich interstellar comet 2I/Borisov, Nature Astronomy, 4, 867 (2020).

Bodewits D., Lara L. M., A'Hearn M. F., La Forgia F., Gicquel A., Kovacs G., Knollenberg J., Lazzarin M., Lin Z.-Y., Shi X., Snodgrass C., Tubiana C., Sierks H., Barbieri C., Lamy P. L., Rodrigo R., Koschny D., Rickman H., Keller H. U., Barucci M. A., Bertaux J.-L., Bertini I., Boudreault S., Cremonese G., Da Deppo V., Davidsson B., Debei S., De Cecco M., Fornasier S., Fulle M., Groussin O., Gutiérrez P. J., Güttler C., Hviid S. F., Ip W.-H., Jorda L., Kramm J.-R., Kührt E., Küppers M., López-Moreno J. J., Marzari F., Naletto G., Oklay N., Thomas N., Toth I., Vincent J.-B., Changes in the Physical Environment of the Inner Coma of 67P/Churyumov-Gerasimenko with Decreasing Heliocentric Distance, The Astronomical Journal, 152, 130 (2016)

Boehnhardt H., Tozzi G. P., Bagnulo S., Muinonen K., Nathues A., Kolokolova L., Photometry and polarimetry of the nucleus of comet 2P/Encke, Astronomy and Astrophysics, 489, 1337 (2008).

Boehnhardt H., Bibring J.-P., Apathy I., Auster H. U., Ercoli Finzi A., Goesmann F., Klingelhöfer G., Knapmeyer M., Kofman W., Krüger H., Mottola S., Schmidt W., Seidensticker K., Spohn T., Wright I., The Philae lander mission and science overview, Philosophical Transactions of the Royal Society of London Series A, 375, 20160248 (2017).

Britt D. T., Boice D. C., Buratti B. J., Campins H., Nelson R. M., Oberst J., Sandel B. R., Stern S. A., Soderblom L. A., Thomas N., The morphology and surface processes of Comet 19/P Borrelly, Icarus, 167, 45 (2004).

Brownlee D., The Stardust Mission: Analyzing Samples from the Edge of the Solar System, Annual Review of Earth and Planetary Sciences, 42, 179 (2014).

Cambianica P., Cremonese G., Fulle M., Simioni E., Naletto G., Pajola M., Lucchetti A., Penasa L., Massironi M., Frattin E., Güttler C., Sierks H., Tubiana C., Long-term measurements of the erosion and accretion of dust deposits on comet 67P/Churyumov-Gerasimenko with the OSIRIS instrument, Monthly Notices of the Royal Astronomical Society, 504, 2895 (2021).

Chernova G. P., Kiselev N. N., Jockers K., Polarimetric Characteristics of Dust Particles as Observed in 13 Comets: Comparisons with Asteroids, Icarus, 103, 144 (1993)

Chesley S. R., Belton M. J. S., Carcich B., Thomas P. C., Pittichová J., Klaasen K. P., Li J.-Y., Farnham T. L., Gillam S. D., Harris A. W., Veverka J., An updated rotation model for Comet 9P/Tempel 1, Icarus, 222, 516 (2013).

Choi Y.-J., Cohen M., Merk R., Prialnik D., Long-Term Evolution of Objects in the Kuiper Belt Zone—Effects of Insolation and Radiogenic Heating, Icarus, 160, 300 (2002).

Choukroun M., Keihm S., Schloerb F. P., Gulkis S., Lellouch E., Leyrat C., von Allmen P., Biver N., Bockelée-Morvan D., Crovisier J., Encrenaz P., Hartogh P., Hofstadter M., Ip W.-H., Jarchow C., Janssen M., Lee S., Rezac L., Beaudin G., Gaskell B., Jorda L., Keller H. U., Sierks H., Dark side of comet 67P/Churyumov- Gerasimenko in Aug.-Oct. 2014. MIRO/Rosetta continuum observations of polar night in the southern regions, Astronomy and Astrophysics, 583, A28 (2015).

Choukroun M., Altwegg K., Kührt E., Biver N., Bockelée-Morvan D., Drążkowska J., Hérique A., Hilchenbach M., Marschall R., Pätzold M., Taylor M. G. G. T., Thomas N., Dust-to-Gas and Refractory-to- Ice Mass Ratios of Comet 67P/Churyumov-Gerasimenko from Rosetta Observations, Space Science Reviews, 216, 44 (2020).

Ciarniello M., Capaccioni F., Filacchione G., Raponi A., Tosi F., De Sanctis M. C., Capria M. T., Erard S., Bockelee-Morvan D., Leyrat C., Arnold G., Barucci A., Beck P., Bellucci G., Fornasier S., Longobardo A., Mottola S., Palomba E., Quirico E., Schmitt B., Photometric properties of comet 67P/Churyumov- Gerasimenko from VIRTIS-M onboard Rosetta, Astronomy and Astrophysics, 583, A31 (2015).

Ciarniello M., Fulle M., Tosi F., Capaccioni F., Filacchione G., Raponi A., Rinaldi G., Rotundi A., Mottola S., De Sanctis M. C., Bockelée-Morvan D., Formisano M., Magni G., Longobardo A., Capria M. T., Modeling the Seasonal Evolution of 67P/Churyumov-Gerasimenko Water Loss Rate, 52nd Lunar and Planetary Science Conference, 2031 (2021).

Ciarniello M., Fulle M., Raponi A., Filacchione G., Capaccioni F., Rotundi A., Rinaldi G., Formisano M., Magni G., Tosi F., De Sanctis M. C., Capria M. T., Longobardo A., Beck P., Fornasier S., Kappel D., Mennella V., Mottola S., Rousseau B., Arnold G., Macro and micro structures of pebble-made cometary nuclei reconciled by seasonal evolution, Nature Astronomy, in press, (2022). Cleeves L. I., Bergin E. A., Alexander

C. M. O. 'D ., Du F., Graninger D., Öberg K. I., Harries T. J., The ancient heritage of water ice in the solar system, Science, 345, 1590 (2014).

Cleeves L. I., Bergin E. A., Alexander C. M. O. 'D ., Du F., Graninger D., Öberg K. I., Harries T. J., The ancient heritage of water ice in the solar system, Science, 345, 1590 (2014)

Cleeves L. I., Bergin E. A., O'D. Alexander C. M., Du F., Graninger D., Öberg K. I., Harries T. J., Exploring the Origins of Deuterium Enrichments in Solar Nebular Organics, The Astrophysical Journal, 819, 13 (2016).

Coates A. J., Mazelle C., Neubauer F. M., Bow shock analysis at comets Halley and Grigg-Skjellerup, Journal of Geophysical Research, 102, 7105 (1997).

Cottin H., Fray N., Distributed Sources in Comets, Space Science Reviews, 138, 179 (2008).

Davidsson B. J. R., Sierks H., Güttler C., Marzari F., Pajola M., Rickman H., A'Hearn M. F., Auger A.-T., El- Maarry M. R., Fornasier S., Gutiérrez P. J., Keller H. U., Massironi M., Snodgrass C., Vincent J.-B., Barbieri C., Lamy P. L., Rodrigo R., Koschny D., Barucci M. A., Bertaux J.-L., Bertini I., Cremonese G., Da Deppo V., Debei S., De Cecco M., Feller C., Fulle M., Groussin O., Hviid S. F., Höfner S., Ip W.-H., Jorda L., Knollenberg J., Kovacs G., Kramm J.-R., Kührt E., Küppers M., La Forgia F., Lara L. M., Lazzarin M., Lopez Moreno J. J., Moissl-Fraund R., Mottola S., Naletto G., Oklay N., Thomas N., Tubiana C., The primordial nucleus of comet 67P/Churyumov-Gerasimenko, Astronomy and Astrophysics, 592, A63 (2016).

Davidsson B. J. R., Gutiérrez P. J., Nucleus properties of Comet 67P/Churyumov Gerasimenko estimated from non-gravitational force modeling, Icarus, 176, 453 (2005).

Davidsson B. J. R., Gutiérrez P. J., Non-gravitational force modeling of Comet 81P/Wild 2. I. A nucleus bulk density estimate, Icarus, 180, 224 (2006).

Davidsson B. J. R., Gutiérrez P. J., Rickman H., Physical properties of morphological units on Comet 9P/Tempel 1 derived from near-IR Deep Impact spectra, Icarus, 201, 335 (2009).

Davidsson B. J. R., Gutiérrez P. J., Groussin O., A'Hearn M. F., Farnham T., Feaga L. M., Kelley M. S., Klaasen K. P., Merlin F., Protopapa S., Rickman H., Sunshine J. M., Thomas P. C., Thermal inertia and surface roughness of Comet 9P/Tempel 1, Icarus, 224, 154 (2013).

Davidsson B. J. R., Thermophysical evolution of planetesimals in the primordial disc, Monthly Notices of the Royal Astronomical Society, 505, 5654 (2021).

De Keyser J., Dhooghe F., Altwegg K., Balsiger H., Berthelier J.-J., Briois C., Calmonte U., Cessateur G., Combi M. R., Equeter E., Fiethe B., Fuselier S., Gasc S., Gibbons A., Gombosi T., Gunell H., Hässig M., Le Roy L., Maggiolo R., Mall U., Marty B., Neefs E., Rème H., Rubin M., Sémon T., Tzou C.-Y., Wurz P., Evidence for distributed gas sources of hydrogen halides in the coma of comet 67P/Churyumov-Gerasimenko, Monthly Notices of the Royal Astronomical Society, 469, S695 (2017).

De Sanctis M. C., Capria M. T., Coradini A., Thermal Evolution and Differentiation of Edgeworth-Kuiper Belt Objects, The Astronomical Journal, 121, 2792 (2001).

De Sanctis M. C., Capaccioni F., Ciarniello M., Filacchione G., Formisano M., Mottola S., Raponi A., Tosi F., Bockelée-Morvan D., Erard S., Leyrat C., Schmitt B., Ammannito E., Arnold G., Barucci M. A., Combi M., Capria M. T., Cerroni P., Ip W.-H., Kuehrt E., McCord T. B., Palomba E., Beck P., Quirico E., VIRTIS Team, Piccioni G., Bellucci G., Fulchignoni M., Jaumann R., Stephan K., Longobardo A., Mennella V., Migliorini A., Benkhoff J., Bibring J. P., Blanco A., Blecka M., Carlson R., Carsenty U., Colangeli L., Combes M., Crovisier J., Drossart P., Encrenaz T., Federico C., Fink U., Fonti S., Irwin P., Langevin Y., Magni G., Moroz L., Orofino V., Schade U., Taylor F., Tiphene D., Tozzi G. P., Biver N., Bonal L., Combe J.-P., Despan D., Flamini E., Fornasier S., Frigeri A., Grassi D., Gudipati M. S., Mancarella F., Markus K., Merlin F., Orosei R., Rinaldi G., Cartacci M., Cicchetti A., Giuppi S., Hello Y., Henry F., Jacquinod S., Rees J. M., Noschese R., Politi R., Peter G., The diurnal cycle of water ice on comet 67P/Churyumov-Gerasimenko, Nature, 525, 500 (2015).

Della Corte V., Rotundi A., Zakharov V., Ivanovski S., Palumbo P., Fulle M., Longobardo A., Dionnet Z., Liuzzi V., Salatti M., GIADA microbalance measurements on board Rosetta: submicrometer- to micrometer- sized dust particle flux in the coma of comet 67P/Churyumov-Gerasimenko, Astronomy and Astrophysics, 630, A25 (2019).

Della Corte V., Rotundi A., Fulle M., Gruen E., Weissman P., Sordini R., Ferrari M., Ivanovski S., Lucarelli F., Accolla M., Zakharov V., Mazzotta Epifani E., Lopez-Moreno J. J., Rodriguez J., Colangeli L., Palumbo P., Bussoletti E., Crifo J. F., Esposito F., Green S. F., Lamy P. L., McDonnell J. A. M., Mennella V., Molina A., Morales R., Moreno F., Ortiz J. L., Palomba E., Perrin J. M., Rietmeijer F. J. M., Rodrigo R., Zarnecki J. C., Cosi M., Giovane F., Gustafson B., Herranz M. L., Jeronimo J. M., Leese M. R., Lopez-Jimenez A. C., Altobelli N., GIADA: shining a light on the monitoring of the comet dust production from the nucleus of 67P/Churyumov-Gerasimenko, Astronomy and Astrophysics, 583, A13 (2015).

Dello Russo N., Kawakita H., Vervack R. J., Weaver H. A., Emerging trends and a comet taxonomy based on the volatile chemistry measured in thirty comets with high-resolution infrared spectroscopy between 1997 and 2013, Icarus, 278, 301 (2016).

Dones L., Weissman P. R., Levison H. F., Duncan M. J., Oort cloud formation and dynamics, Comets II, 153 (2004).

Dones L., Brasser R., Kaib N., Rickman H., Origin and Evolution of the Cometary Reservoirs, Space Science Reviews, 197, 191 (2015).

Drozdovskaya M. N., van Dishoeck E. F., Jørgensen J. K., Calmonte U., van der Wiel M. H. D., Coutens A., Calcutt H., Müller H. S. P., Bjerkeli P., Persson M. V., Wampfler S. F., Altwegg K., The ALMA-PILS survey: the sulphur connection between protostars and comets: IRAS 16293-2422 B and 67P/Churyumov- Gerasimenko, Monthly Notices of the Royal Astronomical Society, 476, 4949 (2018).

Drozdovskaya M. N., van Dishoeck E. F., Rubin M., Jørgensen J. K., Altwegg K., Ingredients for solar-like systems: protostar IRAS 16293-2422 B versus comet 67P/Churyumov-Gerasimenko, Monthly Notices of the Royal Astronomical Society, 490, 50 (2019).

Duncan M. J., Levison H. F., A scattered comet disk and the origin of Jupiter family comets, Science, 276, 1670 (1997).

Edberg N. J. T., Eriksson A. I., Odelstad E., Vigren E., Andrews D. J., Johansson F., Burch J. L., Carr C. M., Cupido E., Glassmeier K.-H., Goldstein R., Halekas J. S., Henri P., Koenders C., Mandt K., Mokashi P., Nemeth Z., Nilsson H., Ramstad R., Richter I., Wieser G. S., Solar wind interaction with comet 67P: Impacts of corotating interaction regions, Journal of Geophysical Research (Space Physics), 121, 949 (2016).

Edberg N. J. T., Alho M., André M., Andrews D. J., Behar E., Burch J. L., Carr C. M., Cupido E., Engelhardt I. A. D., Eriksson A. I., Glassmeier K.-H., Goetz C., Goldstein R., Henri P., Johansson F. L., Koenders C., Mandt K., Möstl C., Nilsson H., Odelstad E., Richter I., Simon Wedlund C., Stenberg Wieser G., Szego K., Vigren E., Volwerk M., CME impact on comet 67P/Churyumov-Gerasimenko, Monthly Notices of the Royal Astronomical Society, 462, S45 (2016).

Ekenbäck A., Holmström M., Barabash S., Gunell H., Energetic neutral atom imaging of comets, Geophysical Research Letters, 35, L05103 (2008).

El-Maarry M. R., Thomas N., Giacomini L., Massironi M., Pajola M., Marschall R., Gracia-Berná A., Sierks H., Barbieri C., Lamy P. L., Rodrigo R., Rickman H., Koschny D., Keller H. U., Agarwal J., A'Hearn M. F., Auger A.-T., Barucci M. A., Bertaux J.-L., Bertini I., Besse S., Bodewits D., Cremonese G., Da Deppo V., Davidsson B., De Cecco M., Debei S., Güttler C., Fornasier S., Fulle M., Groussin O., Gutierrez P. J., Hviid

S. F., Ip W.-H., Jorda L., Knollenberg J., Kovacs G., Kramm J.-R., Kührt E., Küppers M., La Forgia F., Lara

L. M., Lazzarin M., Lopez Moreno J. J., Marchi S., Marzari F., Michalik H., Naletto G., Oklay N., Pommerol A., Preusker F., Scholten F., Tubiana C., Vincent J.-B., Regional surface morphology of comet 67P/Churyumov-Gerasimenko from Rosetta/OSIRIS images, Astronomy and Astrophysics, 583, A26 (2015).

El-Maarry M. R., Thomas N., Gracia-Berná A., Pajola M., Lee J.-C., Massironi M., Davidsson B., Marchi S., Keller H. U., Hviid S. F., Besse S., Sierks H., Barbieri C., Lamy P. L., Koschny D., Rickman H., Rodrigo R., A'Hearn M. F., Auger A.-T., Barucci M. A., Bertaux J.-L., Bertini I., Bodewits D., Cremonese G., Da Deppo V., De Cecco M., Debei S., Güttler C., Fornasier S., Fulle M., Giacomini L., Groussin O., Gutierrez P. J., Ip W.-H., Jorda L., Knollenberg J., Kovacs G., Kramm J.-R., Kührt E., Küppers M., Lara L. M., Lazzarin M., Lopez Moreno J. J., Marschall R., Marzari F., Naletto G., Oklay N., Pommerol A., Preusker F., Scholten F., Tubiana C., Vincent J.-B., Regional surface morphology of comet 67P/Churyumov-Gerasimenko from Rosetta/OSIRIS images: The southern hemisphere, Astronomy and Astrophysics, 593, A110 (2016).

Feaga L. M., Protopapa S., Schindhelm R., Stern S. A., A'Hearn M. F., Bertaux J.-L., Feldman P. D., Parker

J. W., Steffl A. J., Weaver H. A., Far-UV phase dependence and surface characteristics of comet 67P/Churyumov-Gerasimenko as observed with Rosetta Alice, Astronomy and Astrophysics, 583, A27 (2015).

Feldman P. D., A'Hearn M. F., Bertaux J.-L., Feaga L. M., Parker J. W., Schindhelm R., Steffl A. J., Stern S. A., Weaver H. A., Sierks H., Vincent J.-B., Measurements of the near-nucleus coma of comet 67P/Churyumov-Gerasimenko with the Alice far-ultraviolet spectrograph on Rosetta, Astronomy and Astrophysics, 583, A8 (2015).

Fernández J. A., Gallardo T., Young J. D., The end states of long-period comets and the origin of Halley-type comets, Monthly Notices of the Royal Astronomical Society, 461, 3075 (2016).

Filacchione G., de Sanctis M. C., Capaccioni F., Raponi A., Tosi F., Ciarniello M., Cerroni P., Piccioni G., Capria M. T., Palomba E., Bellucci G., Erard S., Bockelee-Morvan D., Leyrat C., Arnold G., Barucci M. A., Fulchignoni M., Schmitt B., Quirico E., Jaumann R., Stephan K., Longobardo A., Mennella V., Migliorini A., Ammannito E., Benkhoff J., Bibring J. P., Blanco A., Blecka M. I., Carlson R., Carsenty U., Colangeli L., Combes M., Combi M., Crovisier J., Drossart P., Encrenaz T., Federico C., Fink U., Fonti S., Ip W. H., Irwin P., Kuehrt E., Langevin Y., Magni G., McCord T., Moroz L., Mottola S., Orofino V., Schade U., Taylor F., Tiphene D., Tozzi G. P., Beck P., Biver N., Bonal L., Combe J.-P., Despan D., Flamini E., Formisano M., Fornasier S., Frigeri A., Grassi D., Gudipati M. S., Kappel D., Mancarella F., Markus K., Merlin F., Orosei R., Rinaldi G., Cartacci M., Cicchetti A., Giuppi S., Hello Y., Henry F., Jacquinod S., Reess J. M., Noschese R., Politi R., Peter G., Exposed water ice on the nucleus of comet 67P/Churyumov-Gerasimenko, Nature, 529, 368 (2016).

Filacchione G., Capaccioni F., Ciarniello M., Raponi A., Rinaldi G., De Sanctis M. C., Bockelèe-Morvan D., Erard S., Arnold G., Mennella V., Formisano M., Longobardo A., Mottola S., An orbital water-ice cycle on comet 67P from colour changes, Nature, 578, 49 (2020).

Fitzsimmons A., Dahlgren M., Lagerkvist C.-I., Magnusson P., Williams I. P., A spectroscopic survey of D- type asteroids, Astronomy and Astrophysics, 282, 634 (1994).

Fornasier S., Dotto E., Hainaut O., Marzari F., Boehnhardt H., De Luise F., Barucci M. A., Visible spectroscopic and photometric survey of Jupiter Trojans: Final results on dynamical families, Icarus, 190, 622 (2007).

Fornasier S., Barucci M. A., de Bergh C., Alvarez-Candal A., DeMeo F., Merlin F., Perna D., Guilbert A., Delsanti A., Dotto E., Doressoundiram A., Visible spectroscopy of the new ESO large programme on trans- Neptunian objects and Centaurs: final results, Astronomy and Astrophysics, 508, 457 (2009).

Fornasier S., Hasselmann P. H., Barucci M. A., Feller C., Besse S., Leyrat C., Lara L., Gutierrez P. J., Oklay N., Tubiana C., Scholten F., Sierks H., Barbieri C., Lamy P. L., Rodrigo R., Koschny D., Rickman H., Keller

H. U., Agarwal J., A'Hearn M. F., Bertaux J.-L., Bertini I., Cremonese G., Da Deppo V., Davidsson B., Debei S., De Cecco M., Fulle M., Groussin O., Güttler C., Hviid S. F., Ip W., Jorda L., Knollenberg J., Kovacs G., Kramm R., Kührt E., Küppers M., La Forgia F., Lazzarin M., Lopez Moreno J. J., Marzari F., Matz K.-D., Michalik H., Moreno F., Mottola S., Naletto G., Pajola M., Pommerol A., Preusker F., Shi X., Snodgrass C., Thomas N., Vincent J.-B., Spectrophotometric properties of the nucleus of comet 67P/Churyumov- Gerasimenko from the OSIRIS instrument onboard the ROSETTA spacecraft, Astronomy and Astrophysics, 583, A30 (2015).

Fornasier S., Mottola S., Keller H. U., Barucci M. A., Davidsson B., Feller C., Deshapriya J. D. P., Sierks H., Barbieri C., Lamy P. L., Rodrigo R., Koschny D., Rickman H., A'Hearn M., Agarwal J., Bertaux J.-L., Bertini I., Besse S., Cremonese G., Da Deppo V., Debei S., De Cecco M., Deller J., El-Maarry M. R., Fulle M., Groussin O., Gutierrez P. J., Güttler C., Hofmann M., Hviid S. F., Ip W.-H., Jorda L., Knollenberg J., Kovacs G., Kramm R., Kührt E., Küppers M., Lara M. L., Lazzarin M., Moreno J. J. L., Marzari F., Massironi M., Naletto G., Oklay N., Pajola M., Pommerol A., Preusker F., Scholten F., Shi X., Thomas N., Toth I., Tubiana C., Vincent J.-B., Rosetta's comet 67P/Churyumov-Gerasimenko sheds its dusty mantle to reveal its icy nature, Science, 354, 1566 (2016).

Fougere N., Combi M. R., Tenishev V., Rubin M., Bonev B. P., Mumma M. J., Understanding measured water rotational temperatures and column densities in the very innermost coma of Comet 73P/Schwassmann- Wachmann 3 B, Icarus, 221, 174 (2012).

Fougere N., Combi M. R., Rubin M., Tenishev V., Modeling the heterogeneous ice and gas coma of Comet 103P/Hartley 2, Icarus, 225, 688 (2013).

Fray N., Bardyn A., Cottin H., Baklouti D., Briois C., Engrand C., Fischer H., Hornung K., Isnard R., Langevin Y., Lehto H., Le Roy L., Mellado E. M., Merouane S., Modica P., Orthous-Daunay F.-R., Paquette J., Rynö J., Schulz R., Silén J., Siljeström S., Stenzel O., Thirkell L., Varmuza K., Zaprudin B., Kissel J., Hilchenbach M., Nitrogen-to-carbon atomic ratio measured by COSIMA in the particles of comet 67P/Churyumov- Gerasimenko, Monthly Notices of the Royal Astronomical Society, 469, S506 (2017).

Fulle M., Water and deuterium-to-hydrogen ratio in comets, Monthly Notices of the Royal Astronomical Society, 505, 3107 (2021).

Fulle M., Blum J., Green S. F., Gundlach B., Herique A., Moreno F., Mottola S., Rotundi A., Snodgrass C., The refractory-to-ice mass ratio in comets, Monthly Notices of the Royal Astronomical Society 482, 3326 (2019).

Fulle M., Blum J., Rotundi A., Gundlach B., Güttler C., Zakharov V., How comets work: nucleus erosion versus dehydration, Monthly Notices of the Royal Astronomical Society, 493, 4039 (2020a).

Fulle M., Blum J., Rotundi A., CO-driven activity constrains the origin of comets, Astronomy and Astrophysics, 636, L3 (2020b).

Fulle M., Della Corte V., Rotundi A., Weissman P., Juhasz A., Szego K., Sordini R., Ferrari M., Ivanovski S., Lucarelli F., Accolla M., Merouane S., Zakharov V., Mazzotta Epifani E., López-Moreno J. J., Rodríguez J., Colangeli L., Palumbo P., Grün E., Hilchenbach M., Bussoletti E., Esposito F., Green S. F., Lamy P. L., McDonnell J. A. M., Mennella V., Molina A., Morales R., Moreno F., Ortiz J. L., Palomba E., Rodrigo R., Zarnecki J. C., Cosi M., Giovane F., Gustafson B., Herranz M. L., Jerónimo J. M., Leese M. R., López-Jiménez

A. C., Altobelli N., Density and Charge of Pristine Fluffy Particles from Comet 67P/Churyumov-Gerasimenko, The Astrophysical Journal, 802, L12 (2015).

Fulle M., Leavsseur-Regourd A.C., McBride N., Hadamcik E., In situ dust measurements from within the coma of 1P/Halley, The Astronomical Journal, 119, 1968 (2000)

Fulle M., Water and deuterium-to-hydrogen ratio in comets, Monthly Notices of the Royal Astronomical Society, 505, 3107 (2021)

Furuya K., Aikawa Y., Depletion of Heavy Nitrogen in the Cold Gas of Star-forming Regions, The Astrophysical Journal, 857, 105 (2018).

Fuselier S. A., Altwegg K., Balsiger H., Berthelier J. J., Beth A., Bieler A., Briois C., Broiles T. W., Burch J. L., Calmonte U., Cessateur G., Combi M., De Keyser J., Fiethe B., Galand M., Gasc S., Gombosi T. I., Gunell H., Hansen K. C., Hässig M., Heritier K. L., Korth A., Le Roy L., Luspay-Kuti A., Mall U., Mandt K. E., Petrinec S. M., Rème H., Rinaldi M., Rubin M., Sémon T., Trattner K. J., Tzou C.-Y., Vigren E., Waite J. H., Wurz P., Ion chemistry in the coma of comet 67P near perihelion, Monthly Notices of the Royal Astronomical Society, 462, S67 (2016).

Galand M., Feldman P. D., Bockelée-Morvan D., Biver N., Cheng Y.-C., Rinaldi G., Rubin M., Altwegg K., Deca J., Beth A., Stephenson P., Heritier K. L., Henri P., Parker J. W., Carr C., Eriksson A. I., Burch J., Far- ultraviolet aurora identified at comet 67P/Churyumov-Gerasimenko, Nature Astronomy, 4, 1084 (2020)

Gardner E., Lehto H. J., Lehto K., Fray N., Bardyn A., Lönnberg T., Merouane S., Isnard R., Cottin H., Hilchenbach M., The Cosima Team, The detection of solid phosphorus and fluorine in the dust from the coma of comet 67P/Churyumov-Gerasimenko, Monthly Notices of the Royal Astronomical Society, 499, 1870 (2020).

Giovane F., Eichhorn G., McKisson J., Weinberg J.L., Weisenberger A., Lamy P., Llebaria A., Detaille M., Levasseur-Regourd A.C. & Le Blanc J. M., 1991, Applied Optics 30(18), pp. 2579-2591

Glassmeier K.-H., Interaction of the solar wind with comets: a Rosetta perspective, Philosophical Transactions of the Royal Society of London Series A, 375, 20160256 (2017).

Goetz C., Koenders C., Richter I., Altwegg K., Burch J., Carr C., Cupido E., Eriksson A., Güttler C., Henri P., Mokashi P., Nemeth Z., Nilsson H., Rubin M., Sierks H., Tsurutani B., Vallat C., Volwerk M., Glassmeier K.- H., First detection of a diamagnetic cavity at comet 67P/Churyumov-Gerasimenko, Astronomy and Astrophysics, 588, A24 (2016).

Goetz C., Koenders C., Hansen K. C., Burch J., Carr C., Eriksson A., Frühauff D., Güttler C., Henri P., Nilsson H., Richter I., Rubin M., Sierks H., Tsurutani B., Volwerk M., Glassmeier K. H., Structure and evolution of the diamagnetic cavity at comet 67P/Churyumov-Gerasimenko, Monthly Notices of the Royal Astronomical Society, 462, S459 (2016).

Goetz C., Glassmeier K.-H., Volwerk M., Richter I., Plasma at comet 67P/Churyumov-Gerasimenko: implications for cometary activity, 42nd COSPAR Scientific Assembly, 42, B1.1-16-18 (2018).

Groussin O., Sunshine J. M., Feaga L. M., Jorda L., Thomas P. C., Li J.-Y., A'Hearn M. F., Belton M. J. S., Besse S., Carcich B., Farnham T. L., Hampton D., Klaasen K., Lisse C., Merlin F., Protopapa S., The temperature, thermal inertia, roughness and colour of the nuclei of Comets 103P/Hartley 2 and 9P/Tempel 1, Icarus, 222, 580 (2013).

Groussin O., Attree N., Brouet Y., Ciarletti V., Davidsson B., Filacchione G., Fischer H.-H., Gundlach B., Knapmeyer M., Knollenberg J., Kokotanekova R., Kührt E., Leyrat C., Marshall D., Pelivan I., Skorov Y., Snodgrass C., Spohn T., Tosi F., The Thermal, Mechanical, Structural, and Dielectric Properties of Cometary Nuclei After Rosetta, Space Science Reviews, 215, 29 (2019).

Gulkis S., Allen M., von Allmen P., Beaudin G., Biver N., Bockelée-Morvan D., Choukroun M., Crovisier J., Davidsson B. J. R., Encrenaz P., Encrenaz T., Frerking M., Hartogh P., Hofstadter M., Ip W.-H., Janssen M., Jarchow C., Keihm S., Lee S., Lellouch E., Leyrat C., Rezac L., Schloerb F. P., Spilker T., Subsurface properties and early activity of comet 67P/Churyumov-Gerasimenko, Science, 347, aaa0709 (2015).

Gundlach B., Fulle M., Blum J., On the activity of comets: understanding the gas and dust emission from comet 67/Churyumov-Gerasimenko's south-pole region during perihelion, Monthly Notices of the Royal Astronomical Society, 493, 3690 (2020).

Gunell H., Goetz C., Simon Wedlund C., Lindkvist J., Hamrin M., Nilsson H., Llera K., Eriksson A., Holmström M., The infant bow shock: a new frontier at a weak activity comet, Astronomy and Astrophysics, 619, L2 (2018).

Gunell H., Goetz C., Odelstad E., Beth A., Hamrin M., Henri P., Johansson F. L., Nilsson H., Stenberg Wieser G., Ion acoustic waves near a comet nucleus: Rosetta observations at comet 67P/Churyumov-Gerasimenko, Annales Geophysicae, 39, 53 (2021)

Guzmán V. V., Öberg K. I., Huang J., Loomis R., Qi C., Nitrogen Fractionation in Protoplanetary Disks from the $H^{13}CN/HC^{15}N$ Ratio, The Astrophysical Journal, 836, 30 (2017).

Güttler C., Mannel T., Rotundi A., Merouane S., Fulle M., Bockelée-Morvan D., Lasue J., Levasseur-Regourd

A. C., Blum J., Naletto G., Sierks H., Hilchenbach M., Tubiana C., Capaccioni F., Paquette J. A., Flandes A., Moreno F., Agarwal J., Bodewits D., Bertini I., Tozzi G. P., Hornung K., Langevin Y., Krüger H., Longobardo A., Della Corte V., Tóth I., Filacchione G., Ivanovski S. L., Mottola S., Rinaldi G., Synthesis of the morphological description of cometary dust at comet 67P/Churyumov-Gerasimenko, Astronomy and Astrophysics, 630, A24 (2019)

Hadamcik E., Levasseur-Regourd A. C., Imaging polarimetry of comet 73P/Schwassmann-Wachmann 3 main fragments during its 2006 apparition, Planetary and Space Science, 123, 51 (2016)

Haeberli R. M., Altwegg K., Balsiger H., Geiss J., Physics and chemistry of ions in the pile-up region of comet P/Halley., Astronomy and Astrophysics, 297, 881 (1995).

Hajra R., Henri P., Myllys M., Héritier K. L., Galand M., Simon Wedlund C., Breuillard H., Behar E., Edberg

N. J. T., Goetz C., Nilsson H., Eriksson A. I., Goldstein R., Tsurutani B. T., Moré J., Vallières X., Wattieaux G., Cometary plasma response to interplanetary corotating interaction regions during 2016 June-September: a quantitative study by the Rosetta Plasma Consortium, Monthly Notices of the Royal Astronomical Society, 480, 4544 (2018).

Hansen K. C., Altwegg K., Berthelier J.-J., Bieler A., Biver N., Bockelée-Morvan D., Calmonte U., Capaccioni F., Combi M. R., de Keyser J., Fiethe B., Fougere N., Fuselier S. A., Gasc S., Gombosi T. I., Huang Z., Le Roy L., Lee S., Nilsson H., Rubin M., Shou Y., Snodgrass C., Tenishev V., Toth G., Tzou C.-Y., Simon Wedlund C., Rosina Team, Evolution of water production of 67P/Churyumov-Gerasimenko: An empirical model and a multi-instrument study, Monthly Notices of the Royal Astronomical Society, 462, S491 (2016).

Harmon J. K., Nolan M. C., Ostro S. J., Campbell D. B., Radar studies of comet nuclei and grain comae, Comets II, 265 (2004).

Harmon J. K., Nolan M. C., Giorgini J. D., Howell E. S., Radar observations of 8P/Tuttle: A contact-binary comet, Icarus, 207, 499 (2010).

Harris A. W., The Rotation Rates of Very Small Asteroids: Evidence for 'Rubble Pile' Structure, Lunar and Planetary Science Conference, 27, 493 (1996).

Hartogh P., Lis D. C., Bockelée-Morvan D., de Val-Borro M., Biver N., Küppers M., Emprechtinger M., Bergin E. A., Crovisier J., Rengel M., Moreno R., Szutowicz S., Blake G. A., Ocean-like water in the Jupiter- family comet 103P/Hartley 2, Nature, 478, 218 (2011).

Hasselmann P. H., Barucci M. A., Fornasier S., Feller C., Deshapriya J. D. P., Fulchignoni M., Jost B., Sierks H., Barbieri C., Lamy P. L., Rodrigo R., Koschny D., Rickman H., A'Hearn M., Bertaux J.-L., Bertini I., Cremonese G., Da Deppo V., Davidsson B., Debei S., De Cecco M., Deller J., Fulle M., Gaskell R. W., Groussin O., Gutierrez P. J., Güttler C., Hofmann M., Hviid S. F., Ip W.-H., Jorda L., Keller H. U., Knollenberg J., Kovacs G., Kramm R., Kührt E., Küppers M., Lara M. L., Lazzarin M., Lopez-Moreno J. J., Marzari F., Mottola S., Naletto G., Oklay N., Pommerol A., Thomas N., Tubiana C., Vincent J.-B., The opposition effect of 67P/Churyumov-Gerasimenko on post-perihelion Rosetta images, Monthly Notices of the Royal Astronomical Society, 469, S550 (2017).

Hässig M., Altwegg K., Balsiger H., Bar-Nun A., Berthelier J. J., Bieler A., Bochsler P., Briois C., Calmonte U., Combi M., De Keyser J., Eberhardt P., Fiethe B., Fuselier S. A., Galand M., Gasc S., Gombosi T. I., Hansen K. C., Jäckel A., Keller H. U., Kopp E., Korth A., Kührt E., Le Roy L., Mall U., Marty B., Mousis O., Neefs

E., Owen T., Rème H., Rubin M., Sémon T., Tornow C., Tzou C.-Y., Waite J. H., Wurz P., Time variability and heterogeneity in the coma of 67P/Churyumov-Gerasimenko, Science, 347, aaa0276 (2015).

Heritier K. L., Altwegg K., Balsiger H., Berthelier J.-J., Beth A., Bieler A., Biver N., Calmonte U., Combi M. R., De Keyser J., Eriksson A. I., Fiethe B., Fougere N., Fuselier S. A., Galand M., Gasc S., Gombosi T. I., Hansen K. C., Hassig M., Kopp E., Odelstad E., Rubin M., Tzou C.-Y., Vigren E., Vuitton V., Ion composition at comet 67P near perihelion: Rosetta observations and model-based interpretation, Monthly Notices of the Royal Astronomical Society, 469, S427 (2017).

Hily-Blant P., Magalhaes V., Kastner J., Faure A., Forveille T., Qi C., Direct evidence of multiple reservoirs of volatile nitrogen in a protosolar nebula analogue, Astronomy and Astrophysics, 603, L6 (2017).

Hoppe P., Rubin M., Altwegg K., Presolar Isotopic Signatures in Meteorites and Comets: New Insights from the Rosetta Mission to Comet 67P/Churyumov-Gerasimenko, Space Science Reviews, 214, 106 (2018).

Huebner W. F., Benkhoff J., Capria M.-T., Coradini A., De Sanctis C., Orosei R., Prialnik D., Heat and Gas Diffusion in Comet Nuclei, Heat and Gas Diffusion in Comet Nuclei, (2006).

Isnard R., Bardyn A., Fray N., Briois C., Cottin H., Paquette J., Stenzel O., Alexander C., Baklouti D., Engrand C., Orthous-Daunay F.-R., Siljeström S., Varmuza K., Hilchenbach M., H/C elemental ratio of the refractory organic matter in cometary particles of 67P/Churyumov-Gerasimenko, Astronomy and Astrophysics, 630, A27 (2019).

Jewitt D. C., From cradle to grave: the rise and demise of the comets, Comets II, 659 (2004).

Jewitt D., Colour Systematics of Comets and Related Bodies, The Astronomical Journal, 150, 201 (2015).

Jewitt D., Kim Y., Mutchler M., Agarwal J., Li J., Weaver H., Cometary Activity Begins at Kuiper Belt Distances: Evidence from C/2017 K2, The Astronomical Journal, 161, 188 (2021).

Jorda L., Gaskell R., Capanna C., Hviid S., Lamy P., Ďurech J., Faury G., Groussin O., Gutiérrez P., Jackman C., Keihm S. J., Keller H. U., Knollenberg J., Kührt E., Marchi S., Mottola S., Palmer E., Schloerb F. P., Sierks H., Vincent J.-B., A'Hearn M. F., Barbieri C., Rodrigo R., Koschny D., Rickman H., Barucci M. A., Bertaux

J. L., Bertini I., Cremonese G., Da Deppo V., Davidsson B., Debei S., De Cecco M., Fornasier S., Fulle M., Güttler C., Ip W.-H., Kramm J. R., Küppers M., Lara L. M., Lazzarin M., Lopez Moreno J. J., Marzari F., Naletto G., Oklay N., Thomas N., Tubiana C., Wenzel K.-P., The global shape, density and rotation of Comet 67P/Churyumov-Gerasimenko from preperihelion Rosetta/OSIRIS observations, Icarus, 277, 257 (2016).

Jutzi M., Benz W., Toliou A., Morbidelli A., Brasser R., How primordial is the structure of comet 67P?. Combined collisional and dynamical models suggest a late formation, Astronomy and Astrophysics, 597, A61 (2017).

Kameda, S., Ozaki, M., Enya, K. et al. Design of telescopic nadir imager for geomorphology (TENGOO) and observation of surface reflectance by optical chromatic imager (OROCHI) for the Martian Moons Exploration (MMX). Earth Planets Space 73, 218 (2021). https://doi.org/10.1186/s40623-021-01462-9

Karlsson T., Eriksson A. I., Odelstad E., André M., Dickeli G., Kullen A., Lindqvist P.-A., Nilsson H., Richter I., Rosetta measurements of lower hybrid frequency range electric field oscillations in the plasma environment of comet 67P, Geophysical Research Letters, 44, 1641 (2017)

Keihm S., Tosi F., Kamp L., Capaccioni F., Gulkis S., Grassi D., Hofstadter M., Filacchione G., Lee S., Giuppi S., Janssen M., Capria M., Interpretation of combined infrared, submillimeter, and millimeter thermal flux data obtained during the Rosetta fly-by of Asteroid (21) Lutetia, Icarus, 221, 395 (2012).

Keller, H. U., 1990. The nucleus. In: Physics and chemistry of comets. Ed. W. F. Huebner, Springer-Verlag, Berlin, Heidelberg, New York, London, Paris, Tokyo, Hong Kong, Barcelona, Astrophysics and Space Science Library. Ser. Eds.: M. Harwitt, et al., pp. 13-68.

Keller H. U., Arpigny C., Barbieri C., Bonnet R. M., Cazes S., Coradini M., Cosmovici C. B., Delamere W. A., Huebner W. F., Hughes D. W., Jamar C., Malaise D., Reitsema H. J., Schmidt H. U., Schmidt W. K. H., Seige P., Whipple F. L., Wilhelm K., First Halley Multicolour Camera imaging results from Giotto, Nature, 321, 320 (1986).

Keller H. U., Mottola S., Davidsson B., Schröder S. E., Skorov Y., Kührt E., Groussin O., Pajola M., Hviid S. F., Preusker F., Scholten F., A'Hearn M. F., Sierks H., Barbieri C., Lamy P., Rodrigo R., Koschny D., Rickman H., Barucci M. A., Bertaux J.-L., Bertini I., Cremonese G., Da Deppo V., Debei S., De Cecco M., Fornasier S., Fulle M., Gutiérrez P. J., Ip W.-H., Jorda L., Knollenberg J., Kramm J. R., Küppers M., Lara L. M., Lazzarin M., Lopez Moreno J. J., Marzari F., Michalik H., Naletto G., Sabau L., Thomas N., Vincent J.-B., Wenzel K.- P., Agarwal J., Güttler C., Oklay N., Tubiana C., Insolation, erosion, and morphology of comet 67P/Churyumov-Gerasimenko, Astronomy and Astrophysics, 583, A34 (2015).

Kelley M. S. P., Woodward C. E., Gehrz R. D., Reach W. T., Harker D. E., Mid-infrared spectra of comet nuclei, Icarus, 284, 344 (2017).

Kimura H., Hilchenbach M., Merouane S., Paquette J., Stenzel O., The morphological, elastic, and electric properties of dust aggregates in comets: A close look at COSIMA/Rosetta's data on dust in comet 67P/Churyumov-Gerasimenko, Planetary and Space Science, 181, 104825 (2020).

Kiselev N., Rosenbush V., Levasseur-Regourd A.-C., Kolokolova L., Comets, Polarimetry of Stars and Planetary Systems, 379 (2015).

Knight, M. M., Kokotanekova, R., & Samarasinha, N. H. “PHYSICAL PROPERTIES OF COMET NUCLEI FROM REMOTE OBSERVATIONS”, to appear in Comets III, eds. Meech, K., & Combi, M. University of Arizona press. (2022)

Koenders C., Glassmeier K.-H., Richter I., Motschmann U., Rubin M., Revisiting cometary bow shock positions, Planetary and Space Science, 87, 85 (2013).

Koenders C., Glassmeier K.-H., Richter I., Ranocha H., Motschmann U., Dynamical features and spatial structures of the plasma interaction region of 67P/Churyumov-Gerasimenko and the solar wind, Planetary and Space Science, 105, 101 (2015).

Koenders C., Perschke C., Goetz C., Richter I., Motschmann U., Glassmeier K. H., Low-frequency waves at comet 67P/Churyumov-Gerasimenko. Observations compared to numerical simulations, Astronomy and Astrophysics, 594, A66 (2016).

Koenders C., Goetz C., Richter I., Motschmann U., Glassmeier K.-H., Magnetic field pile-up and draping at intermediately active comets: results from comet 67P/Churyumov-Gerasimenko at 2.0 AU, Monthly Notices of the Royal Astronomical Society, 462, S235 (2016).

Kokotanekova R., Snodgrass C., Lacerda P., Green S. F., Lowry S. C., Fernández Y. R., Tubiana C., Fitzsimmons A., Hsieh H. H., Rotation of cometary nuclei: new lightcurves and an update of the ensemble properties of Jupiter-family comets, Monthly Notices of the Royal Astronomical Society, 471, 2974 (2017).

Kokotanekova R., Snodgrass C., Lacerda P., Green S. F., Nikolov P., Bonev T., Implications of the small spin changes measured for large Jupiter-family comet nuclei, Monthly Notices of the Royal Astronomical Society, 479, 4665 (2018).

Kramer T., Noack M., On the Origin of Inner Coma Structures Observed by Rosetta during a Diurnal Rotation of Comet 67P/Churyumov--Gerasimenko., The Astrophysical Journal, 823, L11 (2016).

Kuroda D., Ishiguro M., Watanabe M., Akitaya H., Takahashi J., Hasegawa S., Ui T., Kanda Y., Takaki K., Itoh R., Moritani Y., Imai M., Goda S., Takagi Y., Morihana K., Honda S., Arai A., Hanayama H., Nagayama T., Nogami D., Sarugaku Y., Murata K., Morokuma T., Saito Y., Oasa Y., Sekiguchi K., Watanabe J.-. ichi ., Optical and Near-infrared Polarimetry for a Highly Dormant Comet 209P/LINEAR, The Astrophysical Journal, 814, 156 (2015).

Lacerda P., Fornasier S., Lellouch E., Kiss C., Vilenius E., Santos-Sanz P., Rengel M., Müller T., Stansberry J., Duffard R., Delsanti A., Guilbert-Lepoutre A., The Albedo-Colour Diversity of Transneptunian Objects, The Astrophysical Journal, 793, L2 (2014).

Lamy P. L., Toth I., Fernandez Y. R., Weaver H. A., The sizes, shapes, albedos, and colours of cometary nuclei, Comets II, 223 (2004).

Langevin Y., Merouane S., Hilchenbach M., Vincendon M., Hornung K., Engrand C., Schulz R., Kissel J., Ryno J., Optical properties of cometary particles collected by COSIMA: Assessing the differences between microscopic and macroscopic scales, Planetary and Space Science, 182, 104815 (2020).

Lara L. M., Lin Z.-Y., Rodrigo R. & Ip W.-H., 67P/Churyumov-Gerasimenko activity evolution during its last perihelion before the Rosetta encounter, A&A, 525 A36 (2011)

Lee S., von Allmen P., Allen M., Beaudin G., Biver N., Bockelée-Morvan D., Choukroun M., Crovisier J., Encrenaz P., Frerking M., Gulkis S., Hartogh P., Hofstadter M., Ip W.-H., Janssen M., Jarchow C., Keihm S., Lellouch E., Leyrat C., Rezac L., Schloerb F. P., Spilker T., Gaskell B., Jorda L., Keller H. U., Sierks H., Spatial and diurnal variation of water outgassing on comet 67P/Churyumov-Gerasimenko observed from Rosetta/MIRO in August 2014, Astronomy and Astrophysics, 583, A5 (2015).

Levasseur-Regourd A.-C., Agarwal J., Cottin H., Engrand C., Flynn G., Fulle M., Gombosi T., Langevin Y., Lasue J., Mannel T., Merouane S., Poch O., Thomas N., Westphal A., Cometary Dust, Space Science Reviews, 214, 64 (2018).

Levasseur-Regourd A. C., Renard J.-B., Hadamcik E., Lasue J., Bertini I. & Fulle M., Interpretation through experimental simulations of phase functions revealed by Rosetta in 67P/Churyumov-Gerasimenko dust coma, A&A 630 A20 (2019)

Levasseur-Regourd A.-C., Renard J.-B., Shkuratov Y., Hadamcik E., Laboratory studies, Polarimetry of Stars and Planetary Systems, Edited by L. Kolokolova, J. Hough, and A. Levasseur-Regourd. ISBN: 978-1-107- 04390-9. Cambridge University Press. p.35 (2015).

Levison H. F., Comet Taxonomy, Completing the Inventory of the Solar System, 107, 173 (1996).

Levison H. F., Duncan M. J., From the Kuiper Belt to Jupiter-Family Comets: The Spatial Distribution of Ecliptic Comets, Icarus, 127, 13 (1997).

Levison H. F., Duncan M. J., Dones L., Gladman B. J., The scattered disk as a source of Halley-type comets, Icarus, 184, 619 (2006).

Leyrat C., Blain D., Lellouch E., von Allmen P., Keihm S., Choukroun M., Schloerb P., Biver N., Gulkis S., Hofstadter M., Search for regional variations of thermal and electrical properties of comet 67P/CG probed by MIRO/Rosetta, AAS/Division for Planetary Sciences Meeting Abstracts #47, 47, 413.05 (2015).

Lippi M., Villanueva G. L., Mumma M. J., Faggi S., Investigation of the Origins of Comets as Revealed through Infrared High-resolution Spectroscopy I. Molecular Abundances, The Astronomical Journal 162, 74 (2021).

Lis D. C., Bockelée-Morvan D., Güsten R., Biver N., Stutzki J., Delorme Y., Durán C., Wiesemeyer H., Okada Y., Terrestrial deuterium-to-hydrogen ratio in water in hyperactive comets, Astronomy and Astrophysics, 625, L5 (2019).

Longobardo A., Palomba E., Capaccioni F., Ciarniello M., Tosi F., Mottola S., Moroz L. V., Filacchione G., Raponi A., Quirico E., Zinzi A., Capria M. T., Bockelee-Morvan D., Erard S., Leyrat C., Rinaldi G., Dirri F., Photometric behaviour of 67P/Churyumov-Gerasimenko and analysis of its pre-perihelion diurnal variations, Monthly Notices of the Royal Astronomical Society, 469, S346 (2017).

Lowry S., Duddy S. R., Rozitis B., Green S. F., Fitzsimmons A., Snodgrass C., Hsieh H. H., Hainaut O., The nucleus of Comet 67P/Churyumov-Gerasimenko. A new shape model and thermophysical analysis, Astronomy and Astrophysics, 548, A12 (2012).

Lowry S. C., Weissman P. R., CCD observations of distant comets from Palomar and Steward Observatories, Icarus, 164, 492 (2003).

Luspay-Kuti A., Hässig M., Fuselier S. A., Mandt K. E., Altwegg K., Balsiger H., Gasc S., Jäckel A., Le Roy L., Rubin M., Tzou C.-Y., Wurz P., Mousis O., Dhooghe F., Berthelier J. J., Fiethe B., Gombosi T. I., Mall U., Composition-dependent outgassing of comet 67P/Churyumov-Gerasimenko from ROSINA/DFMS. Implications for nucleus heterogeneity?, Astronomy and Astrophysics, 583, A4 (2015).

Luspay-Kuti A., Mousis O., Lunine J. I., Ellinger Y., Pauzat F., Raut U., Bouquet A., Mandt K. E., Maggiolo R., Ronnet T., Brugger B., Ozgurel O., Fuselier S. A., Origin of Molecular Oxygen in Comets: Current Knowledge and Perspectives, Space Science Reviews, 214, 115 (2018).

Mannel T., Bentley M. S., Boakes P. D., Jeszenszky H., Ehrenfreund P., Engrand C., Koeberl C., Levasseur-Regourd A. C., Romstedt J., Schmied R., Torkar K., Weber I., Dust of comet 67P/Churyumov-Gerasimenko collected by Rosetta/MIDAS: classification and extension to the nanometer scale, Astronomy and Astrophysics, 630, A26 (2019).

Mall U., Altwegg K., Balsiger H., Bar-Nun A., Berthelier J.-J., Bieler A., Bochsler P., Briois C., Calmonte U., Combi M. R., Dabrowski B., De Keyser J., Dhooghe F., Fiethe B., Fuselier S. A., Galli A., Garnier P., Gasc S., Gombosi T. I., Hansen K. C., Hässig M., Hoang M., Jäckel A., Kopp E., Korth A., Le Roy L., Magee B., Marty B., Mousis O., Rème H., Rubin M., Sémon T., Tzou C.-Y., Waite J. H., Wurz P., High-Time Resolution In-situ Investigation of Major Cometary Volatiles around 67P/C-G at 3.1 - 2.3 AU Measured with ROSINA- RTOF, The Astrophysical Journal, 819, 126 (2016).

Markkanen J., Agarwal J., Väisänen T., Penttilä A., Muinonen K., Interpretation of the Phase Functions Measured by the OSIRIS Instrument for Comet 67P/Churyumov-Gerasimenko, The Astrophysical Journal, 868, L16 (2018)

Marschall R., Markkanen J., Gerig S.-B., Pinzón-Rodríguez O., Thomas N., Wu J.-S., The dust-to-gas ratio, size distribution, and dust fall-back fraction of comet 67P/Churyumov-Gerasimenko: Inferences from linking the optical and dynamical properties of the inner comae., Frontiers in Physics, 8, 227 (2020).

Marshall D., Groussin O., Vincent J.-B., Brouet Y., Kappel D., Arnold G., Capria M. T., Filacchione G., Hartogh P., Hofstadter M., Ip W.-H., Jorda L., Kührt E., Lellouch E., Mottola S., Rezac L., Rodrigo R., Rodionov S., Schloerb P., Thomas N., Thermal inertia and roughness of the nucleus of comet 67P/Churyumov- Gerasimenko from MIRO and VIRTIS observations, Astronomy and Astrophysics, 616, A122 (2018).

Marty B., Avice G., Sano Y., Altwegg K., Balsiger H., Hässig M., Morbidelli A., Mousis O., Rubin M., Origins of volatile elements (H, C, N, noble gases) on Earth and Mars in light of recent results from the ROSETTA cometary mission, Earth and Planetary Science Letters, 441, 91 (2016).

Masoumzadeh N., Oklay N., Kolokolova L., Sierks H., Fornasier S., Barucci M. A., Vincent J.-B., Tubiana C., Güttler C., Preusker F., Scholten F., Mottola S., Hasselmann P. H., Feller C., Barbieri C., Lamy P. L., Rodrigo R., Koschny D., Rickman H., A'Hearn M. F., Bertaux J.-L., Bertini I., Cremonese G., Da Deppo V., Davidsson B. J. R., Debei S., De Cecco M., Fulle M., Gicquel A., Groussin O., Gutiérrez P. J., Hall I., Hofmann M., Hviid S. F., Ip W.-H., Jorda L., Keller H. U., Knollenberg J., Kovacs G., Kramm J.-R., Kührt E., Küppers M., Lara L. M., Lazzarin M., Lopez Moreno J. J., Marzari F., Naletto G., Shi X., Thomas N., Opposition effect on comet 67P/Churyumov-Gerasimenko using Rosetta-OSIRIS images, Astronomy and Astrophysics, 599, A11 (2017).

Mazelle C., Belmont G., Glassmeier K.-H., Le Quéau D., Rème H., Ultra low frequency waves at the magnetic pile-up boundary of comet P/Halley, Advances in Space Research, 11, 73 (1991)

Meech K. J., Svoren J., Using cometary activity to trace the physical and chemical evolution of cometary nuclei, Comets II, 317 (2004).

Meech K. J., Kleyna J. T., Hainaut O., Micheli M., Bauer J., Denneau L., Keane J. V., Stephens H., Jedicke R., Wainscoat R., Weryk R., Flewelling H., Schunová-Lilly E., Magnier E., Chambers K. C., CO-driven Activity in Comet C/2017 K2 (PANSTARRS), The Astrophysical Journal, 849, L8 (2017).

Meier P., Glassmeier K.-H., Motschmann U., Modified ion-Weibel instability as a possible source of wave activity at Comet 67P/Churyumov-Gerasimenko, Annales Geophysicae, 34, 691 (2016).

Mennella V., Ciarniello M., Raponi A., Capaccioni F., Filacchione G., Suhasaria T., Popa C., Kappel D., Moroz L., Vinogradoff V., Pommerol A., Rousseau B., Istiqomah I., Bockelee-Morvan D., Carlson R. W., Pilorget C., Hydroxylated Mg-rich Amorphous Silicates: A New Component of the 3.2 μm Absorption Band of Comet 67P/Churyumov-Gerasimenko, The Astrophysical Journal, 897, L37 (2020).

Merlino R. L., Current-driven dust ion-acoustic instability in a collisional dusty plasma, IEEE Transactions on Plasma Science, 25, 60 (1997).

Migliorini A., Piccioni G., Capaccioni F., Filacchione G., Bockelée-Morvan D., Erard S., Leyrat C., Combi M. R., Fougere N., Crovisier J., Taylor F. W., De Sanctis M. C., Capria M. T., Grassi D., Rinaldi G., Tozzi G. P., Fink U., Water and carbon dioxide distribution in the 67P/Churyumov-Gerasimenko coma from VIRTIS- M infrared observations, Astronomy and Astrophysics, 589, A45 (2016).

Morbidelli A., Nesvorny D., Laurenz V., Marchi S., Rubie D. C., Elkins-Tanton L., Wieczorek M., Jacobson S., The timeline of the lunar bombardment: Revisited, Icarus, 305, 262 (2018).

Moreno F., Guirado D., Muñoz O., Bertini I., Tubiana C., Güttler C., Fulle M., Rotundi A., Della Corte V., Ivanovski S. L., Rinaldi G., Bockelée-Morvan D., Zakharov V. V., Agarwal J., Mottola S., Toth I., Frattin E., Lara L. M., Gutiérrez P. J., Lin Z. Y., Kolokolova L., Sierks H., Naletto G., Lamy P. L., Rodrigo R., Koschny D., Davidsson B., Barucci M. A., Bertaux J.-L., Bodewits D., Cremonese G., Da Deppo V., Debei S., De Cecco M., Deller J., Fornasier S., Ip W.-H., Keller H. U., Lazzarin M., López-Moreno J. J., Marzari F., Shi X., Models of Rosetta/OSIRIS 67P Dust Coma Phase Function, The Astronomical Journal, 156, 237 (2018)

Müller D. R., Altwegg K., Berthelier J.-J., Combi M. R., De Keyser J., Fuselier S., Hänni N., Pestoni B., Rubin M., Schroeder I. R. H. G., Wampfler S. F., High D/H ratios in water and alkanes in comet 67P/Churyumov-Gerasimenko measured with the Rosetta/ROSINA DFMS, arXiv e-prints, arXiv:2202.03521 (2022).

Muñoz O., Moreno F., Gómez-Martín J. C., Vargas-Martín F., Guirado D., Ramos J. L., Bustamante I., Bertini I., Frattin E., Markannen J., Tubiana C., Fulle M., Güttler C., Sierks H., Rotundi A., Della Corte V., Ivanovski S., Zakharov V. V., Bockelée-Morvan D., Blum J., Merouane S., Levasseur-Regourd A. C., Kolokolova L., Jardiel T., Caballero A. C., Experimental Phase Function and Degree of Linear Polarization Curves of Millimeter-sized Cosmic Dust Analogs, The Astrophysical Journal Supplement Series, 247, 19 (2020)

Myers R. V., Nordsieck K. H., Spectropolarimetry of comets Austin and Churyumov-Gerasimenko, Icarus, 58, 431 (1984)

Nesvorný D., Vokrouhlický D., Dones L., Levison H. F., Kaib N., Morbidelli A., Origin and Evolution of Short-period Comets, The Astrophysical Journal, 845, 27 (2017).

Nesvorný D., Vokrouhlický D., Bottke W. F., Levison H. F., Evidence for very early migration of the Solar System planets from the Patroclus-Menoetius binary Jupiter Trojan, Nature Astronomy, 2, 878 (2018).

Neubauer F. M., Giotto magnetic-field results on the boundaries of the pile-up region and the magnetic cavity, Astronomy and Astrophysics, 187, 73 (1987).

Neubauer F. M., Glassmeier K. H., Acuña M. H., Mariani F., Musmann G., Ness N. F., Coates A. J., Giotto magnetic field observations at the outbound quasi-parallel bow shock of comet Halley., Annales Geophysicae, 8, 463 (1990).

Nilsson H., Gunell H., Karlsson T., Brenning N., Henri P., Goetz C., Eriksson A. I., Behar E., Stenberg Wieser G., Vallières X., Size of a plasma cloud matters. The polarisation electric field of a small-scale comet ionosphere, Astronomy and Astrophysics, 616, A50 (2018).

Nilsson H., Stenberg Wieser G., Behar E., Simon Wedlund C., Gunell H., Yamauchi M., Lundin R., Barabash S., Wieser M., Carr C., Cupido E., Burch J. L., Fedorov A., Sauvaud J.-A., Koskinen H., Kallio E., Lebreton J.-P., Eriksson A., Edberg N., Goldstein R., Henri P., Koenders C., Mokashi P., Nemeth Z., Richter I., Szego K., Volwerk M., Vallat C., Rubin M., Birth of a comet magnetosphere: A spring of water ions, Science, 347, aaa0571 (2015).

Nilsson H., Wieser G. S., Behar E., Gunell H., Wieser M., Galand M., Simon Wedlund C., Alho M., Goetz C., Yamauchi M., Henri P., Odelstad E., Vigren E., Evolution of the ion environment of comet 67P during the Rosetta mission as seen by RPC-ICA, Monthly Notices of the Royal Astronomical Society, 469, S252 (2017).

Oberst J., Giese B., Howington-Kraus E., Kirk R., Soderblom L., Buratti B., Hicks M., Nelson R., Britt D., The nucleus of Comet Borrelly: a study of morphology and surface brightness, Icarus, 167, 70 (2004).

Odelstad E., Eriksson A. I., Johansson F. L., Vigren E., Henri P., Gilet N., Heritier K. L., Vallières X., Rubin M., André M., Ion Velocity and Electron Temperature Inside and Around the Diamagnetic Cavity of Comet 67P, Journal of Geophysical Research (Space Physics), 123, 5870 (2018).

Oort J. H., The structure of the cloud of comets surrounding the Solar System and a hypothesis concerning its origin, Bulletin of the Astronomical Institutes of the Netherlands, 11, 91 (1950).

Paganini L., Mumma M. J., Villanueva G. L., DiSanti M. A., Bonev B. P., Lippi M., Boehnhardt H., The Chemical Composition of CO-rich Comet C/2009 P1 (Garradd) at R_h = 2.4 and 2.0 AU before Perihelion, The Astrophysical Journal, 748, L13 (2012).

Pajusalu M., Iakubivskyi I., Schwarzkopf G. J., Knuuttila O., Väisänen T., Bührer M., Palos M. F., Teras, H., Le Bonhomme G., Praks J., Slavinskis A., SISPO: Space Imaging Simulator for Proximity Operations, PLoS ONE 17(3) (2022).

Parker R. J., The birth environment of planetary systems, Royal Society Open Science, 7, 201271 (2020).

Peixinho N., Delsanti A., Guilbert-Lepoutre A., Gafeira R., Lacerda P., The bimodal colours of Centaurs and small Kuiper belt objects, Astronomy and Astrophysics, 546, A86 (2012).

Pfalzner S., Vincke K., Cradle(s) of the Sun, The Astrophysical Journal, 897, 60 (2020).

Pirani S., Johansen A., Bitsch B., Mustill A. J., Turrini D., Consequences of planetary migration on the minor bodies of the early solar system, Astronomy and Astrophysics, 623, A169 (2019).

Pirani S., Johansen A., Mustill A. J., How the formation of Neptune shapes the Kuiper belt, Astronomy and Astrophysics, 650, A161 (2021).

Poch O., Istiqomah I., Quirico E., Beck P., Schmitt B., Theulé P., Faure A., Hily-Blant P., Bonal L., Raponi A., Ciarniello M., Rousseau B., Potin S., Brissaud O., Flandinet L., Filacchione G., Pommerol A., Thomas N., Kappel D., Mennella V., Moroz L., Vinogradoff V., Arnold G., Erard S., Bockelée-Morvan D., Leyrat C., Capaccioni F., De Sanctis M. C., Longobardo A., Mancarella F., Palomba E., Tosi F., Ammonium salts are a reservoir of nitrogen on a cometary nucleus and possibly on some asteroids, Science, 367, aaw7462 (2020).

Pravec P., Harris A. W., Michalowski T., Asteroid Rotations, Asteroids III, 113 (2002).

Preusker F., Scholten F., Matz K.-D., Roatsch T., Hviid S. F., Mottola S., Knollenberg J., Kührt E., Pajola M., Oklay N., Vincent J.-B., Davidsson B., A'Hearn M. F., Agarwal J., Barbieri C., Barucci M. A., Bertaux J.-L., Bertini I., Cremonese G., Da Deppo V., Debei S., De Cecco M., Fornasier S., Fulle M., Groussin O., Gutiérrez

P. J., Güttler C., Ip W.-H., Jorda L., Keller H. U., Koschny D., Kramm J. R., Küppers M., Lamy P., Lara L. M., Lazzarin M., Lopez Moreno J. J., Marzari F., Massironi M., Naletto G., Rickman H., Rodrigo R., Sierks H., Thomas N., Tubiana C., The global meter-level shape model of comet 67P/Churyumov-Gerasimenko, Astronomy and Astrophysics, 607, L1 (2017).

Quirico E., Moroz L. V., Schmitt B., Arnold G., Faure M., Beck P., Bonal L., Ciarniello M., Capaccioni F., Filacchione G., Erard S., Leyrat C., Bockelée-Morvan D., Zinzi A., Palomba E., Drossart P., Tosi F., Capria

M. T., De Sanctis M. C., Raponi A., Fonti S., Mancarella F., Orofino V., Barucci A., Blecka M. I., Carlson R., Despan D., Faure A., Fornasier S., Gudipati M. S., Longobardo A., Markus K., Mennella V., Merlin F., Piccioni G., Rousseau B., Taylor F., Refractory and semi-volatile organics at the surface of comet 67P/Churyumov-Gerasimenko: Insights from the VIRTIS/Rosetta imaging spectrometer, Icarus, 272, 32 (2016).

Raeder J., Neubauer F. M., Ness N. F., Burlaga L. F., Macroscopic Perturbations of the IMF by p/ Halley as Seen by the Giotto Magnetometer, Astronomy and Astrophysics, 187, 61 (1987).

Raponi A., Ciarniello M., Capaccioni F., Mennella V., Filacchione G., Vinogradoff V., Poch O., Beck P., Quirico E., De Sanctis M. C., Moroz L. V., Kappel D., Erard S., Bockelée-Morvan D., Longobardo A., Tosi F., Palomba E., Combe J.-P., Rousseau B., Arnold G., Carlson R. W., Pommerol A., Pilorget C., Fornasier S., Bellucci G., Barucci A., Mancarella F., Formisano M., Rinaldi G., Istiqomah I., Leyrat C., Infrared detection of aliphatic organics on a cometary nucleus, Nature Astronomy, 4, 500 (2020).

Richardson J. E., Melosh H. J., Lisse C. M., Carcich B., A ballistics analysis of the Deep Impact ejecta plume: Determining Comet Tempel 1's gravity, mass, and density, Icarus, 190, 357 (2007).

Richter I., Koenders C., Auster H.-U., Frühauff D., Götz C., Heinisch P., Perschke C., Motschmann U., Stoll B., Altwegg K., Burch J., Carr C., Cupido E., Eriksson A., Henri P., Goldstein R., Lebreton J.-P., Mokashi P., Nemeth Z., Nilsson H., Rubin M., Szegö K., Tsurutani B. T., Vallat C., Volwerk M., Glassmeier K.-H., Observation of a new type of low-frequency waves at comet 67P/Churyumov-Gerasimenko, Annales Geophysicae, 33, 1031 (2015).

Rickman H., Masses and densities of comets Halley and Kopff., Comet Nucleus Sample Return Mission, 249, 195 (1986).

Rubin M., Altwegg K., van Dishoeck E. F., Schwehm G., Molecular Oxygen in Oort Cloud Comet 1P/Halley, The Astrophysical Journal, 815, L11 (2015).

Rubin M., Engrand C., Snodgrass C., Weissman P., Altwegg K., Busemann H., Morbidelli A., Mumma M., On the Origin and Evolution of the Material in 67P/Churyumov-Gerasimenko, Space Science Reviews, 216, 102 (2020).

Scarf F. L., Ferdinand V., Coroniti V., Kennel C. F., Gurnett D. A., Ip W.-H., Smith E. J., Plasma Wave Observations at Comet Giacobini-Zinner, Science, 232, 377 (1986).

Schleicher D. G., Bair A. N., The Composition of the Interior of Comet 73P/Schwassmann-Wachmann 3: Results from Narrowband Photometry of Multiple Components, The Astronomical Journal, 141, 177 (2011).

Schloerb F. P., Keihm S., von Allmen P., Choukroun M., Lellouch E., Leyrat C., Beaudin G., Biver N., Bockelée-Morvan D., Crovisier J., Encrenaz P., Gaskell R., Gulkis S., Hartogh P., Hofstadter M., Ip W.-H., Janssen M., Jarchow C., Jorda L., Keller H. U., Lee S., Rezac L., Sierks H., MIRO observations of subsurface temperatures of the nucleus of 67P/Churyumov-Gerasimenko, Astronomy and Astrophysics, 583, A29 (2015).

Schwartz S. R., Michel P., Jutzi M., Marchi S., Zhang Y., Richardson D. C., Catastrophic disruptions as the origin of bilobate comets, Nature Astronomy, 2, 379 (2018).

Sierks H., Barbieri C., Lamy P. L., Rodrigo R., Koschny D., Rickman H., Keller H. U., Agarwal J., A'Hearn

M. F., Angrilli F., Auger A.-T., Barucci M. A., Bertaux J.-L., Bertini I., Besse S., Bodewits D., Capanna C., Cremonese G., Da Deppo V., Davidsson B., Debei S., De Cecco M., Ferri F., Fornasier S., Fulle M., Gaskell R., Giacomini L., Groussin O., Gutierrez-Marques P., Gutiérrez P. J., Güttler C., Hoekzema N., Hviid S. F., Ip W.-H., Jorda L., Knollenberg J., Kovacs G., Kramm J. R., Kührt E., Küppers M., La Forgia F., Lara L. M., Lazzarin M., Leyrat C., Lopez Moreno J. J., Magrin S., Marchi S., Marzari F., Massironi M., Michalik H., Moissl R., Mottola S., Naletto G., Oklay N., Pajola M., Pertile M., Preusker F., Sabau L., Scholten F., Snodgrass C., Thomas N., Tubiana C., Vincent J.-B., Wenzel K.-P., Zaccariotto M., Pätzold M., On the nucleus structure and activity of comet 67P/Churyumov-Gerasimenko, Science, 347, aaa1044 (2015).

Simon Wedlund C., Kallio E., Alho M., Nilsson H., Stenberg Wieser G., Gunell H., Behar E., Pusa J., Gronoff G., The atmosphere of comet 67P/Churyumov-Gerasimenko diagnosed by charge-exchanged solar wind alpha particles, Astronomy and Astrophysics, 587, A154 (2016).

Simon Wedlund C., Alho M., Gronoff G., Kallio E., Gunell H., Nilsson H., Lindkvist J., Behar E., Stenberg Wieser G., Miloch W. J., Hybrid modelling of cometary plasma environments. I. Impact of photoionisation, charge exchange, and electron ionisation on bow shock and cometopause at 67P/Churyumov-Gerasimenko, Astronomy and Astrophysics, 604, A73 (2017).

Simon Wedlund C., Bodewits D., Alho M., Hoekstra R., Behar E., Gronoff G., Gunell H., Nilsson H., Kallio E., Beth A., Solar wind charge exchange in cometary atmospheres. I. Charge-changing and ionization cross sections for He and H particles in H₂O, Astronomy and Astrophysics, 630, A35 (2019a).

Simon Wedlund C., Behar E., Nilsson H., Alho M., Kallio E., Gunell H., Bodewits D., Heritier K., Galand M., Beth A., Rubin M., Altwegg K., Volwerk M., Gronoff G., Hoekstra R., Solar wind charge exchange in cometary atmospheres. III. Results from the Rosetta mission to comet 67P/Churyumov-Gerasimenko, Astronomy and Astrophysics, 630, A37 (2019b).

Simon Wedlund C., Behar E., Kallio E., Nilsson H., Alho M., Gunell H., Bodewits D., Beth A., Gronoff G., Hoekstra R., Solar wind charge exchange in cometary atmospheres. II. Analytical model, Astronomy and Astrophysics, 630, A36 (2019c).

Snodgrass C., Lowry S. C., Fitzsimmons A., Photometry of cometary nuclei: rotation rates, colours and a comparison with Kuiper Belt Objects, Monthly Notices of the Royal Astronomical Society, 373, 1590 (2006).

Snodgrass C., A'Hearn M. F., Aceituno F., Afanasiev V., Bagnulo S., Bauer J., Bergond G., Besse S., Biver N., Bodewits D., Boehnhardt H., Bonev B. P., Borisov G., Carry B., Casanova V., Cochran A., Conn B. C., Davidsson B., Davies J. K., de León J., de Mooij E., de Val-Borro M., Delacruz M., DiSanti M. A., Drew J. E., Duffard R., Edberg N. J. T., Faggi S., Feaga L., Fitzsimmons A., Fujiwara H., Gibb E. L., Gillon M., Green

S. F., Guijarro A., Guilbert-Lepoutre A., Gutiérrez P. J., Hadamcik E., Hainaut O., Haque S., Hedrosa R., Hines D., Hopp U., Hoyo F., Hutsemékers D., Hyland M., Ivanova O., Jehin E., Jones G. H., Keane J. V., Kelley M. S. P., Kiselev N., Kleyna J., Kluge M., Knight M. M., Kokotanekova R., Koschny D., Kramer E. A., López-Moreno J. J., Lacerda P., Lara L. M., Lasue J., Lehto H. J., Levasseur-Regourd A. C., Licandro J., Lin Z. Y., Lister T., Lowry S. C., Mainzer A., Manfroid J., Marchant J., McKay A. J., McNeill A., Meech K. J., Micheli M., Mohammed I., Monguió M., Moreno F., Muñoz O., Mumma M. J., Nikolov P., Opitom C., Ortiz J. L., Paganini L., Pajuelo M., Pozuelos F. J., Protopapa S., Pursimo T., Rajkumar B., Ramanjooloo Y., Ramos E., Ries C., Riffeser A., Rosenbush V., Rousselot P., Ryan E. L., Santos-Sanz P., Schleicher D. G., Schmidt M., Schulz R., Sen A. K., Somero A., Sota A., Stinson A., Sunshine J. M., Thompson A., Tozzi G. P., Tubiana C., Villanueva G. L., Wang X., Wooden D. H., Yagi M., Yang B., Zaprudin B., Zegmott T. J., The 67P/Churyumov-Gerasimenko observation campaign in support of the Rosetta mission, Philosophical Transactions of the Royal Society of London Series A, 375, 20160249 (2017).

Snodgrass C., Fitzsimmons A., Lowry S. C., Weissman P., The size distribution of Jupiter Family comet nuclei, Monthly Notices of the Royal Astronomical Society, 414, 458 (2011).

Solem J. C., Cometary breakup calculations based on a gravitationally-bound agglomeration model: the density and size of Shoemaker-Levy 9., Astronomy and Astrophysics, 302, 596 (1995).

Sosa A., Fernández J. A., Cometary masses derived from non-gravitational forces, Monthly Notices of the Royal Astronomical Society, 393, 192 (2009).

Stern S. A., Shull J. M., The influence of supernovae and passing stars on comets in the Oort cloud, Nature, 332, 407 (1988).

Stern S. A., The evolution of comets in the Oort cloud and Kuiper belt, Nature, 424, 639 (2003).

Thomas N., Davidsson B., El-Maarry M. R., Fornasier S., Giacomini L., Gracia-Berná A. G., Hviid S. F., Ip W.-H., Jorda L., Keller H. U., Knollenberg J., Kührt E., La Forgia F., Lai I. L., Liao Y., Marschall R., Massironi M., Mottola S., Pajola M., Poch O., Pommerol A., Preusker F., Scholten F., Su C. C., Wu J. S., Vincent J.-B., Sierks H., Barbieri C., Lamy P. L., Rodrigo R., Koschny D., Rickman H., A'Hearn M. F., Barucci M. A., Bertaux J.-L., Bertini I., Cremonese G., Da Deppo V., Debei S., de Cecco M., Fulle M., Groussin O., Gutierrez P. J., Kramm J.-R., Küppers M., Lara L. M., Lazzarin M., Lopez Moreno J. J., Marzari F., Michalik H., Naletto G., Agarwal J., Güttler C., Oklay N., Tubiana C., Redistribution of particles across the nucleus of comet 67P/Churyumov-Gerasimenko, Astronomy and Astrophysics, 583, A17 (2015).

Thomas P., A'Hearn M., Belton M. J. S., Brownlee D., Carcich B., Hermalyn B., Klaasen K., Sackett S., Schultz P. H., Veverka J., Bhaskaran S., Bodewits D., Chesley S., Clark B., Farnham T., Groussin O., Harris A., Kissel J., Li J.-Y., Meech K., Melosh J., Quick A., Richardson J., Sunshine J., Wellnitz D., The nucleus of Comet 9P/Tempel 1: Shape and geology from two flybys, Icarus, 222, 453 (2013).

Thomas P. C., A'Hearn M. F., Veverka J., Belton M. J. S., Kissel J., Klaasen K. P., McFadden L. A., Melosh H. J., Schultz P. H., Besse S., Carcich B. T., Farnham T. L., Groussin O., Hermalyn B., Li J.-Y., Lindler D. J., Lisse C. M., Meech K., Richardson J. E., Shape, density, and geology of the nucleus of Comet 103P/Hartley 2, Icarus, 222, 550 (2013).

Tiscareno M. S., Malhotra R., The Dynamics of Known Centaurs, The Astronomical Journal, 126, 3122 (2003).

Tosi F., Capaccioni F., Capria M. T., Mottola S., Zinzi A., Ciarniello M., Filacchione G., Hofstadter M., Fonti S., Formisano M., Kappel D., Kührt E., Leyrat C., Vincent J.-B., Arnold G., De Sanctis M. C., Longobardo A., Palomba E., Raponi A., Rousseau B., Schmitt B., Barucci M. A., Bellucci G., Benkhoff J., Bockelée- Morvan D., Cerroni P., Combe J.-P., Despan D., Erard S., Mancarella F., McCord T. B., Migliorini A., Orofino V., Piccioni G., The changing temperature of the nucleus of comet 67P induced by morphological and seasonal effects, Nature Astronomy, 3, 649 (2019).

Toth, I., 2017. Recalling VEGAs results on Comet Halley. In: Proc. of the Conference „From Giotto to Resetta: 30 years of cometary science from space and ground", 50th ESLAB Symposium held in Padova, Italy, October 27th to 29th, 2016, C. Barbieri, C. G. Someda (eds.), Padova, Presso la Sede Dell'Academia, ISBN 9-78-88- 98216-09-55, pp. 217-261.

Tremaine S., Dones L., On the Statistical Distribution of Massive Impactors, Icarus, 106, 335 (1993).

Verbiscer A. J., Helfenstein P., Buratti B. J., Photometric Properties of Solar System Ices, Astrophysics and Space Science Library, 356, 47 (2013).

Veverka J., Klaasen K., A'Hearn M., Belton M., Brownlee D., Chesley S., Clark B., Economou T., Farquhar R., Green S. F., Groussin O., Harris A., Kissel J., Li J.-Y., Meech K., Melosh J., Richardson J., Schultz P., Silen J., Sunshine J., Thomas P., Bhaskaran S., Bodewits D., Carcich B., Cheuvront A., Farnham T., Sackett S., Wellnitz D., Wolf A., Return to Comet Tempel 1: Overview of Stardust-NExT results, Icarus, 222, 424 (2013).

Vincent J.-B., Cometary topography and phase darkening, Astronomy and Astrophysics, 624, A5 (2019).

Vincent J.-B., Bodewits D., Besse S., Sierks H., Barbieri C., Lamy P., Rodrigo R., Koschny D., Rickman H., Keller H. U., Agarwal J., A'Hearn M. F., Auger A.-T., Barucci M. A., Bertaux J.-L., Bertini I., Capanna C., Cremonese G., da Deppo V., Davidsson B., Debei S., de Cecco M., El-Maarry M. R., Ferri F., Fornasier S., Fulle M., Gaskell R., Giacomini L., Groussin O., Guilbert-Lepoutre A., Gutierrez-Marques P., Gutiérrez P. J., Güttler C., Hoekzema N., Höfner S., Hviid S. F., Ip W.-H., Jorda L., Knollenberg J., Kovacs G., Kramm R., Kührt E., Küppers M., La Forgia F., Lara L. M., Lazzarin M., Lee V., Leyrat C., Lin Z.-Y., Lopez Moreno J. J., Lowry S., Magrin S., Maquet L., Marchi S., Marzari F., Massironi M., Michalik H., Moissl R., Mottola S., Naletto G., Oklay N., Pajola M., Preusker F., Scholten F., Thomas N., Toth I., Tubiana C., Large heterogeneities in comet 67P as revealed by active pits from sinkhole collapse, Nature, 523, 63 (2015).

Vincent J.-B., Böhnhardt H. & Lara L. M., A numerical model of cometary dust coma structures - Application to comet 9P/Tempel 1, A&A, 512, A60 (2010)

Vincent J.B., Farnham T., Kührt E., Skorov Y., Marschall R., Oklay N., El-Maarry M.R. & Keller H.U, Local Manifestations of Cometary Activity, Space Sci Rev, 215, 30 (2019)

Vincent J.-B., Lara L. M., Tozzi G. P., Lin Z.-Y. & Sierks H., Spin and activity of comet 67P/Churyumov-Gerasimenko, A&A, 549, A121 (2013)

Vincent J.-B., Oklay N., Pajola M., Höfner S., Sierks H., Hu X., Barbieri C., Lamy P. L., Rodrigo R., Koschny D., Rickman H., Keller H. U., A'Hearn M. F., Barucci M. A., Bertaux J.-L., Bertini I., Besse S., Bodewits D., Cremonese G., Da Deppo V., Davidsson B., Debei S., De Cecco M., El-Maarry M. R., Fornasier S., Fulle M., Groussin O., Gutiérrez P. J., Gutiérrez-Marquez P., Güttler C., Hofmann M., Hviid S. F., Ip W.-H., Jorda L., Knollenberg J., Kovacs G., Kramm J.-R., Kührt E., Küppers M., Lara L. M., Lazzarin M., Lin Z.-Y., Lopez Moreno J. J., Lowry S., Marzari F., Massironi M., Moreno F., Mottola S., Naletto G., Preusker F., Scholten F., Shi X., Thomas N., Toth I., Tubiana C., Are fractured cliffs the source of cometary dust jets? Insights from OSIRIS/Rosetta at 67P/Churyumov-Gerasimenko, Astronomy and Astrophysics, 587, A14 (2016).

Volwerk M., Glassmeier K.-H., Delva M., Schmid D., Koenders C., Richter I., Szegö K., A comparison between VEGA 1, 2 and Giotto flybys of comet 1P/Halley: implications for Rosetta, Annales Geophysicae, 32, 1441 (2014).

Volwerk M., Goetz C., Behar E., Delva M., Edberg N. J. T., Eriksson A., Henri P., Llera K., Nilsson H., Richter I., Stenberg Wieser G., Glassmeier K.-H., Dynamic field line draping at comet 67P/Churyumov- Gerasimenko during the Rosetta dayside excursion, Astronomy and Astrophysics, 630, A44 (2019).

Wang J.-H., Brasser R., An Oort Cloud origin of the Halley-type comets, Astronomy and Astrophysics, 563, A122 (2014).

Weibel E. S., Spontaneously Growing Transverse Waves in a Plasma Due to an Anisotropic Velocity Distribution, Physical Review Letters, 2, 83 (1959).

Weissman P., Morbidelli A., Davidsson B., Blum J., Origin and Evolution of Cometary Nuclei, Space Science Reviews, 216, 6 (2020).

Whipple F. L., A comet model. I. The acceleration of Comet Encke, The Astrophysical Journal, 111, 375 (1950).

Wirström E. S., Charnley S. B., Revised models of interstellar nitrogen isotopic fractionation, Monthly Notices of the Royal Astronomical Society, 474, 3720 (2018).

Wong I., Brown M. E., The Bimodal Colour Distribution of Small Kuiper Belt Objects, The Astronomical Journal, 153, 145 (2017).

Wurz P., Rubin M., Altwegg K., Balsiger H., Berthelier J.-J., Bieler A., Calmonte U., De Keyser J., Fiethe B., Fuselier S. A., Galli A., Gasc S., Gombosi T. I., Jäckel A., Le Roy L., Mall U. A., Rème H., Tenishev V., Tzou C.-Y., Solar wind sputtering of dust on the surface of 67P/Churyumov-Gerasimenko, Astronomy and Astrophysics, 583, A22 (2015).

Wyatt M. C., Bonsor A., Jackson A. P., Marino S., Shannon A., How to design a planetary system for different scattering outcomes: giant impact sweet spot, maximizing exocomets, scattered discs, Monthly Notices of the Royal Astronomical Society, 464, 3385 (2017).

Yokota, S., Terada N., Matsuoka A., Murata N., Saito Y., Delcourt D., Futaana Y., Seki K., Schaible M.J., Asamura K., Kasahara S., Nakagawa H., Nishino M.N., Nomura R., Keika K., Harada Y., Imajo S., "In situ observations of ions and magnetic field around Phobos: The Mass Spectrum Analyzer (MSA) for the Martian Moons eXploration (MMX) mission", Space Sci. Rev., doi:10.21203/rs.3.rs-130696/v1.

10 List of Acronyms

ABCL	As Built Configuration List
AC	Alternating Current
ADC	Analogue to Digital Converter
AFT	Abbreviated Functional Test
AIT	Assembly, Integration and Testing
AIV	Assembly, Integration and Verification
AKE	Attitude Knowledge Error
AMU	Atomic Mass Units
AOCS	Attitude and Orbit Control System
AOGNC	Attitude, Orbit, Guidance and Navigation Control
APE	Absolute Pointing Error
APS	Active Pixel Sensor
ASIC	Application Specific Integrated Circuit
ASPECT	Asteroid SPECTral imager
AU	Astronomical Unit
AVM	Avionics Validation Model
BCA	Baffle and Cover Assembly
BOL	Beginning of Life
BSI	Back Side Illuminated
BUCT	Back-Up Comet Target
BUSOC	Belgium User Support and Operations Centre
CaSSIS	Colour and Stereo Surface Imaging System
CCB	Configuration Control Board
CCD	Charge Coupled device
CCSDS	Consultative Committee for Space Data Systems
CDF	Cumulative Distribution Functions
CE	Cold Element
CFRP	Carbon Fibre Reinforced Plastic
CI	*Comet Interceptor*
CIDL	Configuration Item Data List
CISDC	*Comet Interceptor* Science Data Centre
CMOS	Complementary metal–oxide–semiconductor
CMS	Compact Modular Sounder (TechDemoSat-1)
CoCA	Comet CAmera

CoG	Centre of Gravity
Co-I	Co-Investigator
Co-ILS	Co-Instrument Lead Scientist
CoM	Centre of Mass
Comet-I	*Comet Interceptor*
COPS	COmet Pressure Sensor
CPU	Central Processing Unit
CSU	Camera Support Unit
DC	Direct Current
DCL	Declared Components list
DDV	Design Development Validation
DLP	Degree of Linear Polarisation
DMS	Data Management System
DNC	Dynamically New Comet
DPU	Digital Processing Unit
DSA	Deep Space Antennas
DTMM	Detailed Thermal Model
ECR	Engineering Change Request
ECSS	European Cooperation for Space Standardization
EFM	Electrical Functional Model
EGSE	Electrical Ground Support Equipment
EID	Experiment Interface Document
EIDP	End Item Data Package
ELDRS	Enhanced Low Dose rate Sensitivity
ELU	Electronics Unit
EMC	Electromagnetic Cleanliness/Compatibility
EMI	Electromagnetic Interference
ENA	Energetic Neutral Atom
EnVisS	Entire Visible Sky
EOL	End of Life (prior to encounter)
EPS	Electrical Power Subsystem
EQM	Electrical Qualification Model
ESA	European Space Agency
ESA	Electrostatic Analyser
ESD	Electro-Static Discharge
ESDC	ESA Science Data Centre
ESOC	European Space Operations Centre
ESTRACK	European Space Tracking network

EUV	Extreme Ultra-Violet
FC	Filament Controller
F-Class	ESA Fast Mission Class
FDIR	Failure Detection Isolation and Recovery
FEE	Front End Electronics
FEM	Finite Element Model
FFT	Full Functional Test
FM	Flight Model
FMEA	Failure Modes, Effects Analysis
FM-OFG	Fundamental Mode Orthogonal Fluxgate
FOP	Fibre Optic Plate
FoR	Field of Regard
FOSY	Factor of Safety - Yield
FOV, FoV	Field of View
FPA	Focal Plane Array
FS	Flight Spare
FWHM	Full Width Half Maximum
G/S	Ground Station
GAM	Gravity Assist Maneuver
GEM	*Giotto* Extended Mission
GIADA	Grain Impact Analyser and Dust Accumulator
GSE	Ground Support Equipment
H/W	Hardware
HE	Hot Element
HGA	High Gain Antenna
HI	Hydrogen Imager
HMC	Halley Multicolour Camera
HOPE	Halley Optical Probe Experiment
HSIA	Hardware Software Interaction Analysis
HTC	Halley-Type Comet
HV	High Voltage
HV-HPC	High Voltage High power Pulse Command
I/O	Input/Output
IAA	Instituto de Astrofísica de Andalucía
IC	Interstellar Comet
ICDR	Instrument Critical Design Review
ICE	International Comet Explorer
IDB	Instrument Data Base
IDS	Inter-Disciplinary Scientist
II	Image Intensifier

ILS	Instrument Line of Sight
ILS	Instrument Lead Scientist
IO	Interstellar Object
IPDR	Instrument Preliminary Design Review
iPiC	Implicit Particle in Cell
IR	InfraRed
IRAP	Institut de Recherche en Astrophysique et Planétologie
ISEE	International Sun Earth Explorer
ISL	Inter Satellite Link
ISM	InterStellar Medium
ISO	InterStellar Object
IWF	Institut für Weltraumforschung
JANUS	Jovis, Amorum ac Natorum Undique Scrutator
JAXA	Japan Aerospace Exploration Agency
JFC	Jupiter Family Comet
JUICE	JUpiter ICy moons Explorer
KBO	Kuiper Belt Object
KIP/MIP	Key/Major inspection point
L1	First Lagrange Point
L2	Second Lagrange Point
LCL	Latching Current Limiters
LEOP	Launch and Early Orbit Phase
LET	Linear Energy Transfer
LISN	Line Impedance Stabilization Network
LOS	Line Of Sight
LPC	Long Period Comet
LSST	Legacy Survey of Space and Time
LV	Low Voltage
MANiaC	Mass Analyzer for Neutrals in a Coma
MCU	Multiple Cell Upset
MGA	Medium Gain Antenna
MGSE	Mechanical Ground Support Equipment
MHD	Magnetohydrodynamic
MICD	Mechanical Interface Control Document
MIR	Mid-InfraRed
MIRMIS	Modular InfraRed Molecules and Ices Sensor
MLA	Multi-Lateral Agreement

MLI	Multi-Layer Insulation
MMX	Martian Moon Explorer
MOC	Mission Operations Centre
MoC	Matrix of Compliance
MOS	Metal Oxide Semiconductor
MoU	Memorandum of Understanding
MTL	Mission Time Line
NAC	Narrow Angle Camera
NASA	National Aeronautics and Space Administration
NAVCAM	NAVigation CAMera
NCR	Non-Conformance Report
NDG	Neutral Density Gauge
NECR	Near Earth Commissioning Review
NIC	Nearly Isotropic Comets
NIEL	Non-Ionizing Energy Loss
NIR	Near InfraRed
NPA	Non-Principal Axis
NPB	Negative Polarisation Branch
OBC	On Board Computer
OBCP	On-Board Control Proceedure
OCC	Oort Cloud Comet
OCP	Over-Current Protection
OGS	Operations Ground Segment
OHB-IT	Orbitale Hochtechnologie Bremen (Italia)
OPIC	Optical Periscope for Comets
OPS	ESA Operations Directorate
OTA	Optical telescope assembly
OTS	Off the Shelf
OVP	Over-Voltage Protection
PA	Product Assurance
PA	Principal Axis
PCDU	Power Conditioning and Distribution Unit
PDE	Pointing Drift Error
PDR	Preliminary Design Review
PEU	Proximity Electronics Unit
PFM	Proto-Flight Model
PI	Principal Investigator
PRR	Preliminary Requirement Review
PS	Plasma Suite
PS	Project Scientist
PSA	Planetary Science Archive

QA	Quality Assurance
QM	Qualification Model
RADLAT	Radiation Loat Acceptance Testing
RDM	Radiation Design Margin
RF	Radio Frequency
RFW	Request for Waivers
RHA	Radiation Hardness Assurance
RMA	Rotating Mirror Assembly
RMS	Radiated Magnetic Susceptibility
RPE	Relative Performance Error
RTOF	Reflectron-type Time-Of-Flight
RTU	Remote Terminal Unit
RVT	Radiation Verification Testing
S/C	Spacecraft
SCIENA	Solar wind and Cometary Ions and Energetic Neutral Atoms
SEB	Single Event Burnout
SEDR	Single Event Dielectric Rupture
SEE	Single Event Effect
SEFI	Single Event Functional Interrupt
SEGR	Single Event Gate Rupture
SEL	Single Event Latch-up
SEL1	Sun-Earth Lagrange Point 1
SEL2	Sun-Earth Lagrange Point 2
SET	Single Event Transient
SEU	Single Event Upset
SGS	Science Ground Segment
SHP	Standard High Power command
SHU	Sensor Head Unit
SICP	System Operations Validation
SL	(JAXA) Science Lead
SMA	Scan Mirror Assembly
SME	Scan Mirror Electronics
SMM	Structural Mathematical Model
SOComp	Science Operations Component
SOCoord	Science Operations Coordinator
SOP	Science Operations Phase
SOV	Spacecraft Operational Verification
SP	Short Period
SPC	ESA Science Programme Committee
SPC	Short Period Comet

SPICE	Spacecraft, Planet, Instrument, Camera-matrix, and Events
SpW	Space Wire
SQM	Structural Qualification Model
SRDB	System Requirement database
SRP	System Reference Point
SRR	System Requirements Review
SSC	Source Sequence Count
SSMM	Solid State Mass Memory
STA	Star tracker assembly
STM	Structural Thermal Model
STOH	Star tracker optical head
SVT	System Verification Test
SWT	Science Working Team
TAS-UK	Thales Alienia Space (UK)
TBC	To Be Confirmed
TBD	To Be Determined
TBW	To Be Written
TC/ TM	Telecommand / Telemetry
TCM	Trajectory Correction Manoeuvre
TCS	Thermal Control System
TENGOO	TElescopic Nadir imager for GeOmOrphology

TGO	Trace Gas Orbiter
TID	Total Ionizing Dose
TIDL	Total Ionizing Dose Level
TIDS	Total Ionizing Dose Sensitivity
TIDT	Target IDentification Team
TIRI	Thermal Infrared Imager
TM	Telemetry
TNIDL	Total Non-Ionizing Dose Level
TNIDS	Total Non-Ionizing Dose Sensitivity
TOF	Time of Flight
TRL	Technology Readiness Level
UFOV, UFoV	Unobscured Field of View
URF	Unit Reference Frame
URP	Unit Reference Point
UV	Ultra-Violet
UVLO	Under-Voltage Lock-Out circuitry
VCD	Verification Control Document
WAC	Wide Angle Camera
WBS	Work Breakdown Structure
WCA	Worst case analysis